Al-Mustansiriyah Journal of Science

ISSN 1814 - 635X

Vol. 27, No. 2, 2016

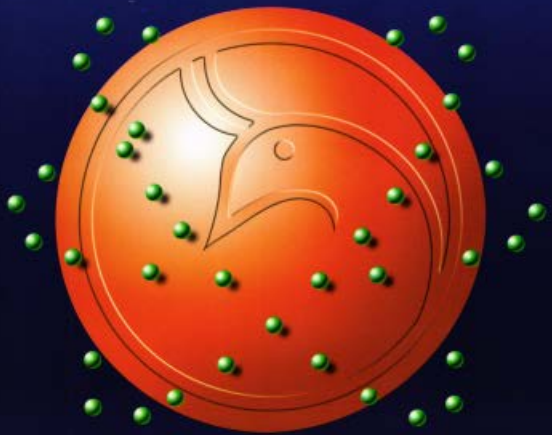

Issued by College of Science - Mustansiriyah University

Vol. 27
No. 2
2016

Al-Mustansiriyah Journal of Science

Issued by College of Science, Al-Mustansiriya University, Baghdad, Iraq

Editor in Chief
Prof. Dr. Saheb K. Al-Saiddy

Managing Editor
Assist. Prof. Dr. Salah Mahdi Al-Shukri

Technical Personnel
Maysaa' Nazar Mustafa
Shatha J. Mohammed

www.mjs-mu.com
E-mail: mustjsci@yahoo.com
Mobile: 07711184399
Number of Deposit at Iraqi National Library and Archives, 278, 1977

Al-Mustansiriyah Journal of Science

Editor in chief
Prof. Dr. Saheb K. Al-Saiddy
Department of Mathematics, College of Science,
Mustansiriyh University
E-mail : dr.saheb@yahoo.com

Editor Managing
Assist. Prof. Dr. Salah Mahdi Al-Shukri
Department of Chemistry, College of Science, Mustansiriyh University
salah_6@yahoo.com: E-mail

Editorial Board

Prof. Dr. Ibrahim R. Agool
Department of Physics, College of Science, Mustansiriyh University.
E-mail : ibrahim_agool@yahoo.com

Prof. Dr. Abd Aljabbar khalaf Atiyah
Department of chemistry, College of Science,
Mustansiriyh University
E-mail : abdel@yahoo.com

Prof. Dr. Hallah Mohamed Ragab
Engineering and Biotechnology Research
Division, National Research Center ,Cairo University,
Egypt
E-mail :hmragab@yahoo.com

Assist. Prof. Dr. Haider J. Ali
Department of Mathematics, College of Science,
Mustansiriyh University
E-mail :drhaid_20@yahoo.com

Prof. Dr. Dhai AL-Tarky
Department of Mathematics, University of Liverpool ,Uk
E-mail :Aljumeily@yahoo.com

Prof. Dr. Abdelfattah Bader
Department of BiosystematicBotany and Microbiology,College of Sciences , Helwan University, Egypt
E-mail : abadr_tanta@yahoo.com

Assist. Prof. Dr. Bidoor Yassin
Department of atmosphere, Mustansiriyh College of Science,
Mustansiriyh University
E-mail:bdor_humood@yahoo.come

Assist. Prof. Dr. Ali Hussein Alwan
Department of Biology, College of Science, Mustansiriyh University
E-mail :dr.alialameri72@yahoo.com

Assist. Prof.Dr. jameela harbi
Department of Computer Science, College of Science, Mustansiriyh University
E-mail :jameelahharbi@yahoo.com

Consultant Committee

Prof. Dr. Mahmoud Khalid Jassim
Department of Mathematics, College of Arts and Sciences, Nizwa University, Oman
E-mail :mkj602007@yahoo.com

Prof. Dr. Wael Mohamed El-Sayed
Department of parasitology, Medical Research Institute, Egypt
E-mail :waelotfy@yahoo.com

Prof. Nadia Kandile
Department of Chemistry, University of Ain Shams, Egypt
E-mail :nadiaghk@yahoo.com

Assist. Prof. Dr. Hadi Muhammad Ali
Department of Chemistry, Chairman of the Committee Dean of the College of Science, Nahrain University
Assist. Prof. Dr. Fadel Abid Rissan
Dean of thethe College of Science, Baghdad University

Prof. Dr.Tawfiq Abdel Khaliq Abbas
Department of Computer Science, Dean of the College of Information Technology, University of Babylon

Prof. Dr.Baher Abdul Khaliq Mahmoud
Department of Dairy Science and Technology, National Research Center, Egypt
E-mail :baher_effat@yahoo.com

Prof. Hanaa A. Hassan
Department of Chemistry, University of Ain Shams, Egypt
E-mail :drhanaahassan@yahoo.com

Assist. Prof. Dr. Mohammed Ali Nasser
Department of Mathematics, College of Education, University of Sanaa, Yemen

Assist. Prof. Dr. Abdulsada Abdul Abbas Rahe
Department of Biology, College of Science, University of Wasit

Instructions for Authors
Al-Mustansiriyah Journal of Science (MJS)

Manuscript text (first submission) should be double spaced on one side of high quality white A4 sheets (21.6×27.9 cm) with margins of one inch all around the page using Microsoft Word 2007 or 2010 using (doc.) type. The typing in Arabic or English must use (Times New Roman, font size of 14 pt). The sections should be arranged in the following order: Title Page, Abstract in English, Abstract in Arabic, Introduction, Materials and Methods (Experimental), Results and Discussion, Conclusion, Acknowledgment (if any), Abbreviations (if any) and list of References. The head of the sections should be capitalized, bolded and centered and font size of 16pt. **(e.g. ABSTRACT, INTRODUCTION, MATERIALS and METHODS (EXPERIMENTAL), RESULTS and DISCUSSION, CONCLUSION, ACKNOWLEDGMENTS, REFERENCES)**, and the others (sub-sections) should be in sentence case and bolded as well.

Title Page: Includes the title of the article, author's names with full names and affiliations. The affiliation should comprise the department, college, institution (University or Company), and should be typed as a footnote to the author's name. The e-mail address of the author responsible for correspondence (who is designated with an asterisk *) must be given at the first page under the name and affiliation of authors.

References: All references should be cited in using the appropriate Arabic numerals, which are enclosed in parenthesis (e.g. Polyurethane rigid foams are largely used as insulating materials for their combination of low density, low thermal conductivity and good mechanical properties [1-3].)

A list of references should be given in the end of the manuscript. References should be typed single-spaced and numbered sequentially in the order in which they are cited in the text. The number of the reference should be given between two brackets [ ].

❖ **Journal's paper**

[1]. Metallo S. J., Kane R. S., Holmlin R. E., Whitesides G. M., Journal of American chemical Society. 125, 5, 4534-4540, 2003.

❖ **Books:**

[2]. Edward M. Handbook of Adhesives and Sealants; McGraw-Hill: New York, 2000.

Tables: Tables should be created using the Table tool in MS Word using font size 9 point. Tables should be numbered with Arabic numerals and referred to by number in the Text (e.g., Table 1,2,3... etc.). Each Table should be typed with the legend above the Table.

Figures, Schemes and Diagrams should be numbered in a consecutive series of Arabic numerals in the order in which they are cited in the text (e.g., Figure 1 or Scheme 1).

CONTENTS

Al-Mustansiriyah Journal of Science
Vol. 27, No 2, 2016

journal homepage:www.mjs-mu.com

Synthesis and Characterization of Some New Metal Complexes of Ligand [N-(3-acetylphenylcarbamothioyl)-4-chlorobenzamide]

Basima M. Sarhan* Awf A.R. Ahmed** Enass J. Waheed*
*Department of Chemistry, College of Education for Pure Sciences, Ibn-AL-Haitham, University of Baghdad.
**Teacher, Ministry of Education- Iraq.

Articleinfo
Received
16/4/2015
Accepted
21/12/2015
Key Word:
3-Aminoaceto-phenon,
4-Chlorobenzoyl isothiocyanate,
complexes.

ABSTRACT

A new ligand [N-(3-acetylphenylcarbamothioyl)-4-chlorobenzamide] (CAD) was synthesized by reaction of 4-Chlorobenzoyl isothiocyanate with 3-amino acetophenone, The ligand was characterized by elemental micro analysis C.H.N. S., FT-IR, UV-Vis and ^{1}H,^{13}C- NMR spectra, some transition metals complexes of this ligand were prepared and characterized by FT-IR, UV-Vis spectra, conductivity measurements, magnetic susceptibility and atomic absorption, From obtained results the molecular formula of all prepared complexes were $[M(CAD)_2(H_2O)_2]Cl_2$ (M^{+2} =Mn, Co, Ni, Cu, Zn, Cd and Hg),the proposed geometrical structure for all complexes were octahedral.

الخلاصة

حضر الليكاند الجديد [N- (3- اسيتايل فنيل كاربامونايويل)-4- كلوروبنزمايد] (CAD) وذلك من مفاعله (4- كلوروبنزويل ايزوثايوسيانات) مع 3-امينو اسيتوفينون وبنسبة (1:1) وشخص بوساطة التحليل الدقيق للعناصر(S.N.H.C) والأشعة تحت الحمراء والأشعة فوق البنفسجية- المرئية وطيف الرنين النووي المغناطيسي, كما حضرت وشخصت معقدات أملاح بعض ايونات العناصر الانتقالية الثنائية التكافؤ(Mn, Co, Ni, Cu, Zn, Cd, Hg) مع الليكاند (CAD) وشخصت المعقدات المحضرة باستعمال الأشعة تحت الحمراء والأشعة فوق البنفسجية - المرئية والتوصيلية المولارية والحساسية المغناطيسية والامتصاص الذري واستنتج من الدراسات والتشخيصات إن المعقدات لها شكل ثماني السطوح حول الايون الفلزي مع اللكياند (CAD) ثنائي السن.

INTRODUCTION

3-Aminoacetophenone derived from aromatic amines have a wide variety and an important class of ligands in coordination chemistry and find extensive applications in different fields, e.g., biological, inorganic and analytical chemistry. Many biologically important acetophenone derivative have been reported in the literature possessing, antimicrobial antibacterial, antifungal, anti inflammatory antitumor and anti HIV activities[1-3].Synthesis ligand N-(2-2-[1-(3-aminophenyl) ethylidene] hydrazino-2-oxoethyl)benzamide(L) by the condensation N-benzoylglycine with 3-amino acetophenone, Complexes of Ni(II), Cu(II) and Cd(II) with ligand(L) have been prepared and characterized by elemental analysis, magnetic measurement, molar conductivity, IR, ^{1}HNMR and mass studies[4].Synthesis new Schiff base ligand 2,4-furyliminobenzylaceto phenone(FIAS) by the reaction 3-aminoacetophenone and furane-2-carbox aldehyde, Metal complexes of the ligand(FIAS) were prepared with chloride salts of Co(II), Ni(II) and Co(II) in ethanol[5]. Synthesis Co(II), Ni(II), Cu(II) and Zn(II) metal complexes from ligands L_1 and L_2 by the condensation of 3-aminoacetophenone, p-phenylenediamine and salicylaldehyde or 5-chlorosalicyl aldehyde[6].The aim of this work to prepare new ligand [N-(3-acetylphenyl carbamothioyl)-4-chlorobenzamide] (CAD),and it's metal complexes with Mn (II), Co(II), Ni(II), Cu(II), Zn(II), Cd(II) and Hg(II) ions.

Experimental

Chemicals

All reagents were analar or chemical pure grade by BDH, Merck and Fluka. All metal chloride salts and solvents purchased from Merk and Fluka com., and were used without purification.

Instruments

1H and 13C–NMR was recorded using Ultra Shield 300 MHz Switzerl and at University of Al al-Bayt, Jordan. Melting point was recorded by using Stuart- melting point apparatus. FT-IR spectra were recorded as KBr disc using 3800 Shimadzu in the range of (4000-400) cm-1. Electronic spectra were obtained using UV-160 Shimadzu spectrophotometer at 25℃ for 10-3M solution

DMSO with 1.000 ± 0.001 cm matched quartz cell. Molar Conductivity was measured at 25℃ for 10-3M solution of DMSO by using Philips PW. Digital. Elemental micro analyses(C.H.N.S) were performed using Acrlo Erba 1106 elemental analyzer. Magnetic susceptibility measurements were obtained by balance magnetic susceptibility by model MSB-MKI. Metal contents of the complexes were determined by atomic absorption technique by using Shimadzu(AA680G).

Synthesis of ligand(CAD)

The ligand was prepared by two steps:-

(A)- Synthesis of (4-Chlorobenzoyl isothiocyanate)

Mixture of 4-Chlorobenzoylchloride(3.33ml,1mmol) and ammonium thio cyanate (2g,1mmol) in (25 ml) of acetone was stirred under refluxed for 3hrs and then filtered, the filtrate was used for further reaction[7].

(B)-Synthesis of [N-(3-acetylphenylcarbamothioyl)-4-chlorobenzamide] (CAD)

(3.60g, 1mmol) of 3-aminoacetophenon in (20ml) acetone was rapidly added to 4-Chlorobenzoyl isothiocyanate and maintaining reflux. After refluxing for 6hrs, the resulting solid was collected, washed with acetone and recrystallization from ethanol, Yield(85%), (m.p=174-176)°C, C% found (57.47) calc.(57.75), H% found (3.56), calc.(3.91), N% found (8.38), calc.(8.42),S% found (9.92), calc.(9.62),as shown in scheme(1).

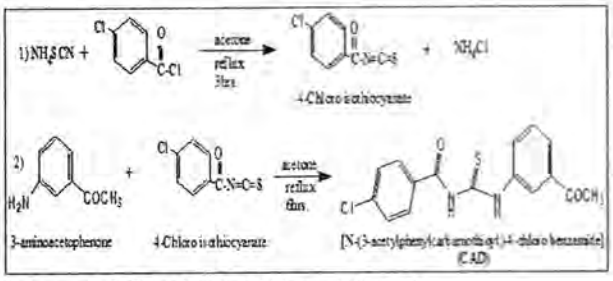

Scheme(1):Synthesis of ligand (CAD)

Synthesis of ligand (CAD) complexes

Synthesis of $[Ni(CAD)_2(H_2O)_2]Cl_2$ complex

A solution of (0.237g,1mmol) $NiCl_2 6H_2O$ in (10ml) ethanol was added to solution of (0.67g,2mmol) (CAD) in (10ml) ethanol. The mixture was stirred for 6 hrs at room temperature, the green solid was collected by filtration, washed with (1:1) mixture of water: ethanol, recrystallized from ethanol and dried in an oven(50°C).

Synthesis of $[Mn(CAD)_2(H_2O)_2]Cl_2$, $[Co(CAD)_2(H_2O)_2]Cl_2$, $[Cu(CAD)_2(H_2O)_2]Cl_2$, $[Zn(CAD)_2(H_2O)_2]Cl_2$, $Cd(CAD)_2(H_2O)_2]Cl_2$, $[Hg(CAD)_2(H_2O)_2]Cl_2$ complexes

A similar method to that mentioned for preparation of $[Ni(CAD)_2(H_2O)_2]Cl_2$ complex was used to prepare the complexes of [Mn^{+2},Co^{+2},Cu^{+2},Zn^{+2},$Cd^{+2}$and Hg^{+2}] ions (1mmol) with (CAD) (2mmol) ,Table (1) showed some physical properties of the prepared complexes.

Results and Discussion

FT-IR Spectrum of Ligand (CAD)

The FT-IR spectrum of the free ligand (CAD), Fig.(1) showed bands at(1672) cm^{-1},(1627)cm^{-1} and (1355)cm^{-1} due to υC=O(ketonic) ,υC=O(amidic) and υC=S respectively. While another absorption band at (3468)cm^{-1} could be explained as υN-H [8-10], The FT-IR spectral data of the free ligand were listed in Table(1).

FT-IR Spectra of ligand(CAD) complexes

These spectra exhibited marked difference between bands Fig.(2) belonging to the stretching vibration of υ(C=O amido) in the range between (1595-1587) cm^{-1} shifted lower frequencies by(40-32)cm^{-1} suggesting of the possibility of the coordination of ligand through the oxygen atom at the carbonyl group[11]while the band caused by υ(C=S) appeared between (1400-1436)cm^{-1} shifted to higher frequencies by (81-45)cm^{-1} which indicates to the coordination of ligand through the sulfur atom at the thion group to the central ion[12]. The stretching vibration band υ(C=O ketone) and υ(N-H) either show no change or very little in their frequencies (1674-1670)cm^{-1} and (3365-3209)cm^{-1} respectively there for indicating do not coordinate to the metal ion. Metal- oxygen and metal-sulfur bonds were confirmed by the presence of the stretching vibration of υ(M-O) and υ(M-S) around (478-472)cm^{-1} and (430-423)cm^{-1} respectively the spectra of complexes showed the appearance of bands in the range(850-838)cm^{-1} attributed to ρ(OH),These bands confirm the coordination of the water with metal [11],Table (1) describe the important bands and assignment for all prepared complexes.

UV-Vis Spectrum of Ligand (CAD)

The UV-Vis spectrum of the free ligand(CAD),Fig.(3) exhibits a high intense absorption peak at (34843)cm^{-1} which way attributed to electronic transition type $\pi \longrightarrow \pi^*$ [13,14].The data of electronic spectrum of the free ligand (CAD) were listed in Table (2).

UV-Vis Spectra of ligand(CAD) complexes

-$[Mn(CAD)_2(H_2O)_2]Cl_2$

The white complex of Mn(II) shows band at(35211)cm^{-1} due to ligand field and another bands at (11210)cm^{-1} and (10416)cm^{-1} which are caused by the electronic transfer $^6A_1g \longrightarrow {}^4T_1g_{(G)}$ and $^6A_1g \longrightarrow {}^4T_2g_{(G)}$ respectively, suggesting octahedral geometry around Mn(II) ion[15].

-$[Co(CAD)_2(H_2O)_2]Cl_2$

The spectrum of the blue complex gave four bands at (35087)cm^{-1}, (27027)cm^{-1}, (16286)cm^{-1} and (12269)cm^{-1} attributed to (L.F),C.T with $^4T_1g_{(F)} \longrightarrow {}^4T_1g_{(P)}$,

$^4T_{1g(F)} \longrightarrow {}^4A_2g$ and $^4T_{1g(F)} \longrightarrow {}^4T_2g_{(F)}$ respectively and the rachinter electronic repulsion parameter (B^-) was found to be $(433)cm^{-1}$, from the relation $\beta=B^- / B^*$, was found to be equal (0.45),these parameter are accepted to Co(II) octahedral complex[16].

-$[Ni(CAD)_2(H_2O)_2]Cl_2$

The spectrum of green complex of Ni(II) has revealed the following electronic transfer (L.F),C.T with $^3A_2g \longrightarrow {}^3T_1g_{(P)}$, $^3A_2g \longrightarrow {}^3T_2g_{(F)}$ $^3A_2g \longrightarrow {}^3T_1g_{(F)}$, , transition at $(36496)cm^{-1}$, $(27548)cm^{-1}$, $(14903)cm^{-1}$ and $(12406)cm^{-1}$ respectively, the(B^-) value found to be $(348)cm^{-1}$,while β was equal to (0.33) these are the characteristics for octahedral complexes of Ni(II)[17,18].

-[Cu $(CAD)_2(H_2O)_2]Cl_2$

The spectrum of yellow complex of Cu(II) , Fig.(4) show two bands at (36496) cm^{-1}, $(12360)cm^{-1}$ caused to (C.T),$^2Eg \longrightarrow {}^2T_2g$ transition respectively , which was a good agreement for distorted octahedral complex for Cu(II) ion[19,20].

-$[Zn(CAD)_2(H_2O)_2]Cl_2$,$[Cd(CAD)_2(H_2O)_2]Cl_2$ and $[Hg(CAD)_2(H_2O)_2]Cl_2$

Shows only charge transfer of (M→L) in range (35587-34965)cm^{-1}[21,22].All transition with their assignments are summarized in Table(2).

Physical properties of ligand (CAD) complexes

The solid complexes soluble in some common solvent such as dimethyl formamide, dimethylsulphoxide and relatively thermally stable. The molar conductivity values of all complexes in DMSO solvent in $10^{-3}M$ at 25°C(Table-3)indicated electrolyte nature with 1:2 ratio [23].The atomic absorption measurements for all complexes gave approximated values when its comparison with theoretical values, Table(3) includes the physical properties for the ligand and its complexes.

Magnetic moment of ligand(CAD) complexes

The values of measured magnetic susceptibility and effective magnetic moment (μeff) for the Mn(II), Co(II), Ni(II), Cu(II) complexes are shown in Table(3). Mn(II), Co(II), Ni(II) and Cu(II) complexes exhibit μeff (5.83, 5.25, 2.94, 1.76) B.M respectively ,which can be a normal values for high spin octahedral complexes[24].

NMR Spectra of Ligand (CAD)

^{1}H-NMR spectrum :-

^{1}H-NMR spectrum of free ligand (CAD),Fig.(5)which was recorded in DMSO-d_6 solvent showed the following signals: The singlet at δ(2.40)ppm refer to DMSO, singlet signal at δ(1.60)ppm due to (3H,CH_3CO), the singlet signal at δ(3.93)ppm due to(1H,NH sec amine),the multiplet signals at δ(6.09-7.95)ppm were attributed to aromatic protons, the singlet signal at δ(11.30)ppm refer to (1H,NH sec amide).

^{13}C-NMR spectrum

^{13}C-NMR spectrum of the free ligand (CAD),Fig.(6)showed chemical shift at δ(26.74)ppm refers(CH_3)for (CH_3CO) group. Chemical shifts at δ(38.38-41.36) ppm refer to DMSO. The chemical shifts at range δ(123.93-147.01)ppm due to aromatic carbons. while the signals at Fig.(2) showed the following signals at δ(171.06)ppm, δ(179.40)ppm and δ(197.22-197.47)ppm were attributed to (CONH),(C=S) and CO for (CH_3CO) group [25,26].

Suggested structures for complexes on the basis of molar conductivity, magnetic moment, spectroscopic studies (FT-IR,UV-Vis and atomic absorption) and (^{1}H,^{13}C-NMR for ligand(CAD)only) for the ligand and all prepared complexes, we suggested that the ligand (CAD) behaves as bidentate on coordination with Mn(II), Co(II), Ni(II), Cu(II), Zn(II), Cd(II) and Hg(II) ions via oxygen atom of (C=O) amido group and sulfer atom of (C=S) thion group, suggesting octahedral geometry around metal ions for all prepared complexes, as shown in Fig.(7).

Conclusions

The new ligand in this work has been readily prepared by reaction from 4-chlorobenzoyl isothiocyanate with 3-aminoacetophenone. The ligand was characterized by elemental micro analysis C.H.N.S, FT-IR, UV-Vis and ^{1}H,^{13}C-NMR spectra. The metal complexes of this ligand were prepared and characterized by FT-IR, UV-Vis spectra, conductivity measurements, magnetic susceptibility and atomic absorption, the proposed geometrical structure for all complexes were octahedral.

References

1. Rasheed, R.T.;"Synthesis of new metal complexes derived from 5-nitroso 8-hydroxyquinoline and salicylidene *P*-iminoacetophenone with Fe(II), Co(II), Ni(II) and Cu(II) ions", Journal of Al-Nahrain University; 15(4): 68-73, 2012.

2. Praveen, K.T. and Sulekh, C.; "Chromium(III) ion selective PVC membrane electrode based on a Schiff base ligand, 3-aminoacetophenonethiosemicarba zone", Anal. Bioanal. Electro Chem.; 3(2): 119-133, 2011.

3. Ahlatcioglu E., Senkal B., Bahire F. and Yesim G.; "Preparation and Poly merization of Chalcone substituted aniline and investigation of impedance properties", Materials Science in Semiconductor Processing; 28:50-103, 2014.

4. Promila T. and Lonibala R.; "Synthesis and Characterization of Divalent Ni, Co and Cd Complexes of N-(2-2-[1-(3-aminophenyl) ethylidene] hydrazino-2-oxoethyl) Benzamide", Oriental Journal of Chemistry; 30(4):2029-2035, 2014.

5. Jagvir S. and Prashant S. ; "Synthesis and Structural Properties of Co(II), Ni(II) and Co(II) Complexes with 2,4-Furyliminobenzylacetophenone", Journal of Biomedicine & Biotechnology; 12:1- 4, 2012.

6. Malathy M., Srividhya C. and Rajavel R. ; "Antimicrobial Activities of Co(II) ,Ni(II),Cu(II) and

Zn(II) Metal Complexes Derived from Tetradentate Schiff Base Ligands", The International Journal of Science & Technoledge; 2(5):157-165, 2014.
7. Kabbani, A.T.; Ramadan, H.; Hammuud, H.H and Hanuom, A.M.G; "Synthesis of some metal complexes of N-[(benzoyl amino)-thioxomethyl] amino acid (HL)", Journal of the University of Chemical Technology and Metallurgy; 40(4): 339-344, 2005.
8. Carey, F. A. "Organic Chemistry", 6th Ed., the McGraw-Hill Companies, Inc., New York, pp. 767, 2006.
9. Silverstein, R. M., Bassler, G. C., Morrill, T. C.. "Spectroscopic identification of organic compounds", 4th Ed. John Wiley & Sons, New York, 245-252, 1981.
10. March, J.; "Advanced Organic Chemistry", 4th Ed., J. Wiley and Sons, New York,329-332, 1991.
11.Nakamoto, K.; "Infrared spectra of inorganic and coordination compounds", 4th Ed., John Wily and Sons, New York,198-207,1996.
12.Al-Hashimi, S. M.; Sarhan, B.M. and Salman, A.W.; "Synthesis and characterization of N-acetyl –Dl – tryptophan with some metal ions", Iraq J. Chem.; 28:1-11, 2002.
13. Dyes, R.J.; "Application of absorption spectroscopy of organic compounds", Prentice –Hall, Inc., Englewood cliffs, N. J. London,Ch.4,47-56,1996.
14. Nicholas, D.; "Complexes and first-row transition elements Macmiloian chemistry", Text; 6(4):146, 1979.
15. Heidt, L.F.; Koster, G.F. and Johnson, A.M.; "Absorption spectrum of Mn(II) diethylenetriamine complexes", J. Am. Chem. Soc.; 80: 6471, 1958.
16. Lever, A. B.; "Inorganic electronic spectroscopy", Elsevier Publishing Company Amsterdam, London, New York, 2nd,276, 1968.
17. Jorgensen, C.K.; "Synthesis, characterization and antibacterial activity of Mn(II),Co(II),Ni (II)and Cu(II) complexes of U-carboxaldehyda phenyl hydrazone-1-phynyl-3-methyl-2-pyrazoline-5-one", Dran. Chem.Phys; 5(33),22-46,1963.
18. Juran, N.; Periesiuk, B.; Monojloriclniktic, S.R. and Cleap, M.B.; "Nitrogen-15 NMR coordination shifts of β –alanine and glycine in cobalt complexes", Inorg. Chem.;29: 1491-1495, 1990.
19. Al-Hashimi, S.M.; Sarhan, B.M. and Alwan, A.Y.; "Synthesis and characterization of same mixed-ligand complexes containing –N-acetyl glycine and pyridine with some metal ions", Ibn-AL-Haitham J. for Pure and Appl. Sci.; 18(4): 10-12, 2005.
20. Mukhlis, A. J.; Sarhan, B.M. and Rumez, R. M; "Synthesis and characteri- zation of novel metal complexes of (pentulose-γ-lactone-2,3-endibenzoate barbi turic acid with some metal ions", J.Baghdad for Sci,;10(3): 597-606, 2013.
21. Marcotrigiano, G.; Menabu, L.; Pellacani and Saladini, M.; "Structures of *bis*(U-amino pyridinium)tetrachlorocuprate mono hydrate", Inorganic Chimica Acta.; 32: 149-155, 1979.
22. Huheey, J.E.; "Inorganic chemistry, principles of structure and reactivity", 3th Ed. ,Harper international SI Edition; Maryland, 363-370,1983.
23. Diebbar-Sid, S., Benali- Baitich, O. and Deloume, J.P.; "Synthetic and Structural Studies of Some Bivalent Transition Metal Complexes with Oxygen and Nitrogen Containing Schiff Base" ; J. mol. Struct., 569:121, 2001.
24. Mulay, L. N., " Magnetic Susceptibility", John wiley and sons; New York; part1,vol(4), 25-31,1977.
25. Murugesan, C.; Asrar, A. A. and Mohamed S. M. ; "Synthesis, characteri- zation and antimicrobial activity of new mannich base", Pelagia Research Library; 5(1):18-21, 2014.
26. Popiolek, L.; kosikowska, U.; Mazur, L.; Dobosz, M. and Malam, A.; "Synthesis and antimicrobial evaluation of some novel 1,2,4-triazole and 1,3,4-thiadiazole derivatives ",Med. Chem. Res. ; 22 : 3134-3147, 2013.

Table (1): The characteristic bands of infrared spectra of ligand (CAD) and its metal complexes.

Compound	υ (N-H)	υ (C=O) Ketone	υ (C=O) Amide	υ (C=S)	ρ (O-H) of water	υ (M-O) of water	υ (M-O) of ν(C=O) Amide	υ (M-S)
Ligand (CAD)	3463(s)	1672 (s)	1627(s)	1355(s)	-	-	-	-
$[Mn(CAD)_2(H_2O)_2]Cl_2$	3338(s)	1674(s)	1589(s)	1428(m)	838(s)	465(w)	476(w)	423(w)
$[Co(CAD)_2(H_2O)_2]Cl_2$	3277(s)	1670(m)	1591(s)	1400(s)	850(s)	461(w)	476(w)	425(w)
$[Ni(CAD)_2(H_2O)_2]Cl_2$	3346(m)	1672(w)	1595(w)	1436(w)	840(m)	458(w)	474(w)	430(w)
$[Cu(CAD)_2(H_2O)_2]Cl_2$	3209(s)	1672(w)	1595(m)	1436(m)	852(m)	457(w)	475(w)	427(w)
$[Zn(CAD)_2(H_2O)_2]Cl_2$	3273(s)	1672(s)	1587(s)	1426(s)	839(s)	460(w)	478(w)	424(w)
$[Cd(CAD)_2(H_2O)_2]Cl_2$	3365(s)	1672(s)	1595(s)	1435(s)	842(s)	467(w)	472(w)	423(w)
$[Hg(CAD)_2(H_2O)_2]Cl_2$	3263 (w)	1674(s)	1595(s)	1436(w)	844(s)	459(w)	473(w)	423(w)

s=strong m=medium w=weak

Table (2): Electronic spectral data of ligand (CAD) and its complexes in DMSO solvent.

compounds	λ(nm)	ν(cm^{-1})	ABC	ε$_{max}$ molar^{-1} cm^{-1}	Transitions	Proposed structures
Ligand (CAD)	287	34843	2.367	2367	$\pi \longrightarrow \pi^*$	-
$[Mn(CAD)_2(H_2O)_2]Cl_2$	284 892 960	35211 11210 10416	1.989 0.023 0.023	1989 23 23	L.F $^6A_{1g} \longrightarrow {}^4T_{1g(G)}$ $^6A_{1g} \longrightarrow {}^4T_{2g(G)}$	oh
$[Co(CAD)_2(H_2O)_2]Cl_2$	285 370 614 815	35087 27027 16286 12269	2.427 1.692 0.697 0.014	2427 1692 697 14	L.F C.T mixed with $^2T_{1g(F)} \longrightarrow {}^4T_{1g(F)}$ $^4T_{1g(F)} \longrightarrow {}^4A_{2g}$ $^4T_{1g(F)} \longrightarrow {}^4T_{2g(F)}$	oh
$[Ni(CAD)_2(H_2O)_2]Cl_2$	274 363 671 806	36496 27548 14903 12406	2.153 1.497 0.026 0.022	2153 1497 26 22	L.F C.T mixed with $^3A_{2g} \longrightarrow {}^3T_{1g(F)}$ $^3A_{2g} \longrightarrow {}^3T_{1(F)}$ $^3A_{2g} \longrightarrow {}^3T_{2g(F)}$	oh
$[Cu(CAD)_2(H_2O)_2]Cl_2$	274 809	36496 12360	2.052 0.017	2052 17	C.T $^2E_g \longrightarrow {}^2T_{2g}$	oh
$[Zn(CAD)_2(H_2O)_2]Cl_2$	286	34965	2.425	2425	C.T	oh
$[Cd(CAD)_2(H_2O)_2]Cl_2$	281	35587	2.327	2327	C.T	oh
$[Hg(CAD)_2(H_2O)_2]Cl_2$	282	35460	2.375	2375	C.T	oh

C.T = Charge transfer

Table (3): Some physical properties and elemental microanalysis of (CAD) and its metal complexes .

Molecular formula	M.wt g.mol^{-1}	Color	M.P or dec.	M% Calculation (Found)	Molar Cond. Ohm^{-1} cm^2 Mol^{-1} in DMSO	μeff (B.M)
Ligand(CAD)	332.5	White	174-176 °C	–	3.7	–
$[Mn(CAD)_2(H_2O)_2]Cl_2$	827.94	White	220 D	6.63 (6.77)	69.70	5.83
$[Co(CAD)_2(H_2O)_2]Cl_2$	831.94	Violet	185-187 °C	7.08 (6.90)	82.68	5.25
$[Ni(CAD)_2(H_2O)_2]Cl_2$	831.71	Green	217 D	7.05 (7.26)	75.05	2.94
$[Cu(CAD)_2(H_2O)_2]Cl_2$	836.54	Yellow	213 D	7.59 (7.18)	77.73	1.76
$[Zn(CAD)_2(H_2O)_2]Cl_2$	838.38	White	196-198 °C	7.79 (7.90)	68.70	0
$[Cd(CAD)_2(H_2O)_2]Cl_2$	885.41	White	238 D	12.69 (12.39)	84.40	0
$[Hg(CAD)_2(H_2O)_2]Cl_2$	993.41	White	182-184 °C	20.19 (19.58)	70.60	0

dec. =decomposition

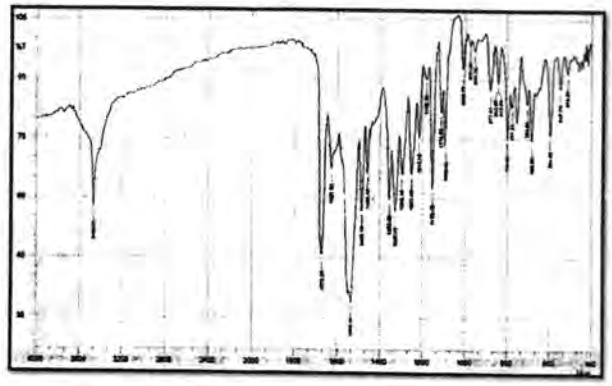

Fig.(1): Infrared spectrum of ligand (CAD)

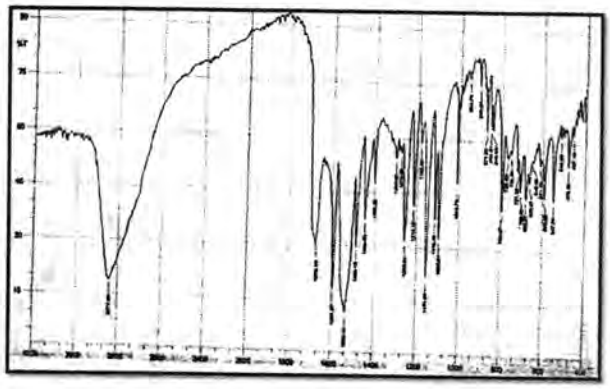

Fig.(2): Infrared spectrum of complex $[Co(CAD)_2(H_2O)_2]Cl_2$

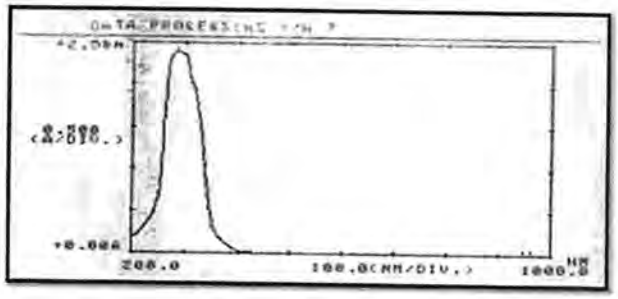

Fig. (3): Electronic spectrum of ligand (CAD)

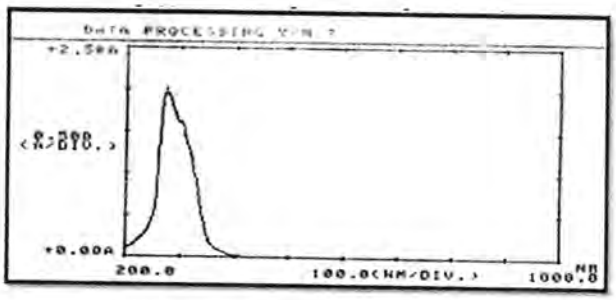

Fig. (4): Electronic spectrum of complex $[Cu(CAD)_2(H_2O)_2]Cl_2$

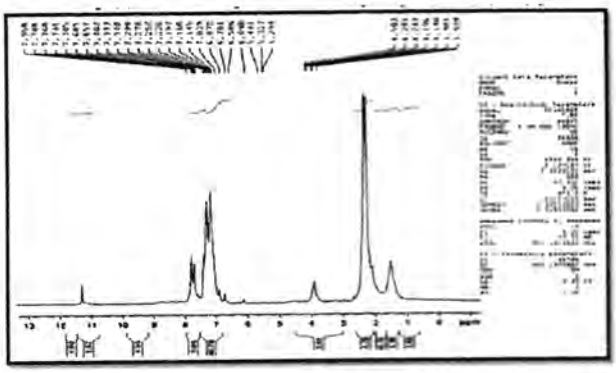

Fig. (5): ^{1}H-NMR spectrum of ligand (CAD)

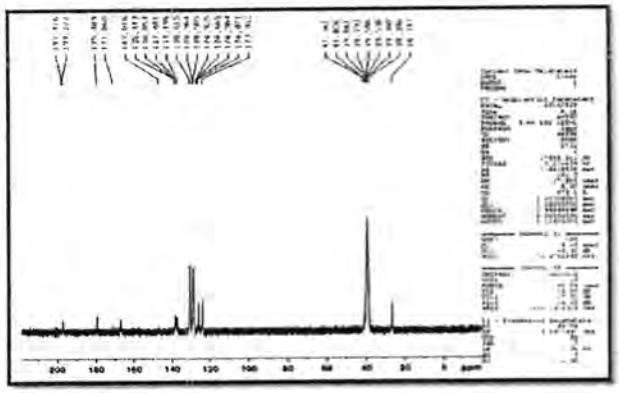

Fig. (6): ^{13}C-NMR spectrum of ligand (CAD)

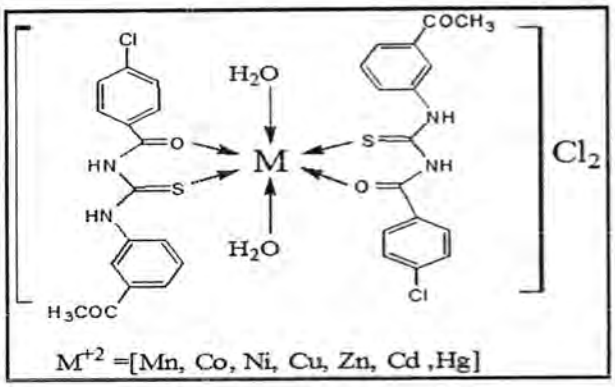

Fig.(7): Suggested geometrical structure of complexes $[M(CAD)_2(H_2O)_2]Cl_2$

Al-Mustansiriyah Journal of Science
Vol. 27, No 2, 2016

journal homepage:www.mjs-mu.com

Synthesis of some Heterocyclic Compounds Derived from(5,6 diphenyl-1,2,4-triazine-3-thiol)

Nisreen Kais Abood
Department of Chemistry, College of Science, Al-Mustansiriya University

Articleinfo

Received
1/9/2015
Accepted
16/11/2015

Keywords:
Triazine ,
Benzoxazole,
Thiozolidinone,
benzimidazole.

ABSTRACT

The present work describe the synthesis of new heterocyclic compounds starting from reaction 5,6 diphenyl-1,2,4-triazine 3-thiol with ethyl chloro acetate afforded compound (1),then treatment with thiourea or urea afforded compound (2,3). p-Bromo phenacyl bromide react with compounds (2,3) afforded compounds (4,5),treatment compound (1) with hydrazine hydrate to afforded 2-(5,6 di phenyl 1,2,4-triazin-3yl thio)aceto hydrazide compound (6) . Azomethines (7,8) were prepared through reaction of compound (6) with aromatic aldehyde, then (7,8) converted to thaizolidinone derivatives (9,10) after treatment with 2-mercapto acetic acid Reaction of compound (6) with phenyl iso thiocyanate to give compound(11) and the product (11)react with ethyl chloro acetate afforded compound (12) , then reaction (5,6 di phenyl1,2,4- triazin 3-thiol with chloro acetic acid gave compound (13)followed by refluxing (13) with ortho phenylenediamine gave compound (14). All compounds were confirmed by their melting point, FT-IR spectrum,^{1}HNMR spectrum for some of them.

الخلاصة

البحث الحالي يوضح تحضير مركبات حلقية غير متجانسة ,من تفاعل المركب الاساس (6,5 داي فنيل ترايازين 3-ثايول) مع اثيل كلورات لتكوين مركب (1) ,تفاعل المركب (1) مع ثايويوريا واليوريا اعطى مركبات جديدة(3,2) التي تفاعلت مع بارابروموفيناسيل بروماید لتعطي مشتقات جديدة (5,4).المركب (1)عند تفاعله مع الهيدرازين اللاماني اعطى مركب (6),مركبات ازوميثين (8,7) حضرت من تفاعل المركب (6) مع الالديهايدات الاروماتية ,ثم حولت المركبات(8,7)الى عدد من مشتقات ثايوزوليدنون (10,9) بعد تفاعلها مع 2-مركبتو حامض الخليك.تفاعل المركب (6) مع فنيل ايزوثايوسيانيت واثيل كلورو اسات فتكون المركبات (12,11) بالتتابع . تفاعل المركب الاساس (6,5 داي فنل ترايازين 3-ثايول) مع كلوروحامض الخليك اعطى المركب (13) وعند تسخين المركب (13) مع اورثو-امينوانيلين فاعطى المركب (14). شخصت هذه المركبات بقياس درجة الانصهار و الطرائق الطيفية (FT-IR) وبعضها شخص باطياف (^{1}HNMR).

INTRODUCTION

1,2,4-triazines and their condensed derivatives occupy a pivotal position in modern medicinal chemistry because of their high potential biological activities [1],the triazine structure is heterocyclic ring analogous to the six–membered benzene ring about with three carbons replaced by nitrogen . The three isomer of triazine are distinguished from each other by the position of their nitrogen atoms and are referred 1,2,3-triazine, 1,2,4-triazine , 1,3,5- triazine [2].1,2,4-triazine derivatives have been reported to posses aboard spectrum of bio activities including Anti-inflammatory[3],analgesic antihypertensive[4],cardiotonic[5], neuroletic nootropic [6], antihistaminergic[7], tuberculostatic[8], antiviral[9]. Thiazoles are important class of natural and synthetic compounds. Thiazole derivatives display a wide range of biological activities such as ,cardiotonic,fungicidal sedative ,anaesthetic, bactericidal and anti-inflammatory[10]. The synthesis of thiazole derivatives is important for their wide range of pharmaceutical and biological properties[11]. Oxazoles are a common structural motif found in numerous molecules that displayantiviral ,antifungal, antibacterial, and antiproliferative activities[12]. Benzimidazoles are an important class of heterocycles that are frequently used in drug and agrochemical discovery programs[13] Benzimidazole derivatives have a broad antifungal spectrum and display their antifungal activities by blocking the polymerization of and tubulin subunits1;2. Antitubulin agents, especially benzimidazoles, disrupt microtubule function in eucaryotic organisms such as fungi, protozoa and helminthes[14].

EXPERIMENTAL

The melting points were determined in open capillary tubes on a Gallen Kamp melting point apparatus and were uncorrected .The FT.IR Spectra of some prepared derivatives were taken on Shimadzu-2N,FTIR-8400 S.^{1}H-NMR Spectra of some prepared derivatives were recorded on a Varian-Mercury 300MHZ Spectrometer, d6-DMSO use as a solvent in^{1}H-NMR Spectra.

Preparation ethyl 2-(5,6 diphenyl-1,2,4-triazine-3yl thio)acetate (1)

Ethyl chloro acetate (1.1g,0.01 mol) was add dropwise to a stirred solution of 5,6 diphenyl-1,2,4-triazine-3thiol (2.6gm,0.01 mol) and KOH (0.56g,0.01mol) in 20 mL absolute ethanol. The reaction mixture was refluxed for 7 hrs., after that cooled filtered the product and recrystallized from chloroform. Table (1)

Preparation N-carbamothioyl-2- (5,6 diphenyl-1,2,4-triazine-3yl thio) acetamide(2), N-carbamoyl-2-(5,6 di phenyl-1,2,4-triazine-3yl thio) acetamide(3).

A mixture of ethyl 2-(5,6 di phenyl)1,2,4-triazine-3yl thio)acetate (1) (1.7 gm,0.005 mole) with (0.005mole) thiourea or urea respectively in 25mL absolute ethanol were refluxed for 5hrs. After cooling ,the product was filtered the product, and recrystallized from ethanol. Table (1)

Preparation N-4(4-bromophenyl)thiazle-2-yl-2-(5,6diphenyl-1,2,4-triazin-3ylthio)acetamide(4) and N-4(4-bromophenyl)oxazol-2-yl-2-(5,6diphenyl-1,2,4-triazin-3ylthio)acetamide(5)

A mixture of compounds(2 or 3)(0.002mole) and (0.002mole) of bromo phenacyl bromide were dissolved in 20ml absolute ethanol ,then refluxed for 8hrs.The mixture was cooled and neutralized with ammonium hydroxide solution ,the precipitated was filtered off and washed with water, recrystallized from ethyl acetate . Table (1)

Preparation 2-(5,6di phenyl)1,2,4-triazine-3yl thio)aceto hydrazide(6)

Ethyl 2-(5,6 di phenyl)1,2,4-triazine-3yl thio)acetate (1) (1.05,0.003mole) with hydrazine hydrate (0.15 g,0.003mole) in 30ml absolute ethanol ,then refluxed for (7-12) hrs.The precipitated solid was collected and recrystallized from ethanol. Table (1)

Preparation of Schiff bases (7,8)

To a stirring solution of compound(6)(2.7g,0.01mole)in absolute ethanol (15ml),an appropriated different aldehyde (0.01mole)was added with drops of glacial acetic acid, and then the mixture was refluxed 6hrs.Cooled at room temperature the precipitate was filtered and recrystallized from ethanol. Table (1)

Preparation of thiazolidenones (9,10)

A mixture of compound of Schiff bases(9 or10)(0.02mole)and 2-mercapto acetic acid (0.26ml,0.04mole)in dry benzene (30mL)was refluxed for 10hrs.The mixture was concentrated and recrystallized from methanol. Table 1

Preparation of 2-[2-(5,6diphenyl,1,2,4-triazine-3-ylthio)-N-phenyl hydrazinecarbothioamide (11).

A mixture of compound(6)(3.37 g,0.01mole) and phenyl iso thiocyanate (1.31ml,0.01mole),in absolute ethanol (20ml)was refluxed for 3hrs. The solid product was filtered and recrystallized from ethanol. Table 1

Preparation of 2-(5,6 diphenyl -1,2,4-triazine-3-ylthio)-N-(4-oxo-3-phenylthiazolidine-2-ylidene) aceto hydrazide (12).

Ethyl chloro acetate (0.49,0.004mole)was added dropwise to a stirring solution of compound(11) (1.89g,0.004mole)and anhydrous sodium acetate(0.004mole)in (20mL) absolute ethanol .The reaction mixture was refluxed for 6hrs.,the solid product was filtered and recrystallized from ethanol. Table 1

Preparation 2-(5,6 diphenyl -1,2,4-triazine-3-ylthio) acetic acid (13).

To (2.6 g, 0.01 mole)of 5,6-diphenyl -1,2,4-triazine 3-thiol in 20 ml of absolute ethanol ,(0.56,0.01 mole) of KOH was added followed by (0.095 g, 0.01 mole) of mono chloro acetic acid . The reaction mixture was heated under reflux for 8 hrs., the hot solution was evaporated under reduced pressure ,the solid was filtered washed with cold distilled water and recrysllaztion from ethanol. Table 1

Preparation of 2-[(5,6diphenyl-1,2,4-triazine-3-yl thio)methyl-3-1H-benzimidazol) (14).

Compound (13) (3.23 g, 0.01 mole)was refluxed for 10 hrs., with o-phenylenediamine (1.08 g, 0.01 mole)in 4N-hydro chloric acid (20mL). The mixture was neutralized with ammonia to precipitated the compound (14), the product was filtered and recrystallized from ethanol . Table 1.

SCHEME 1:

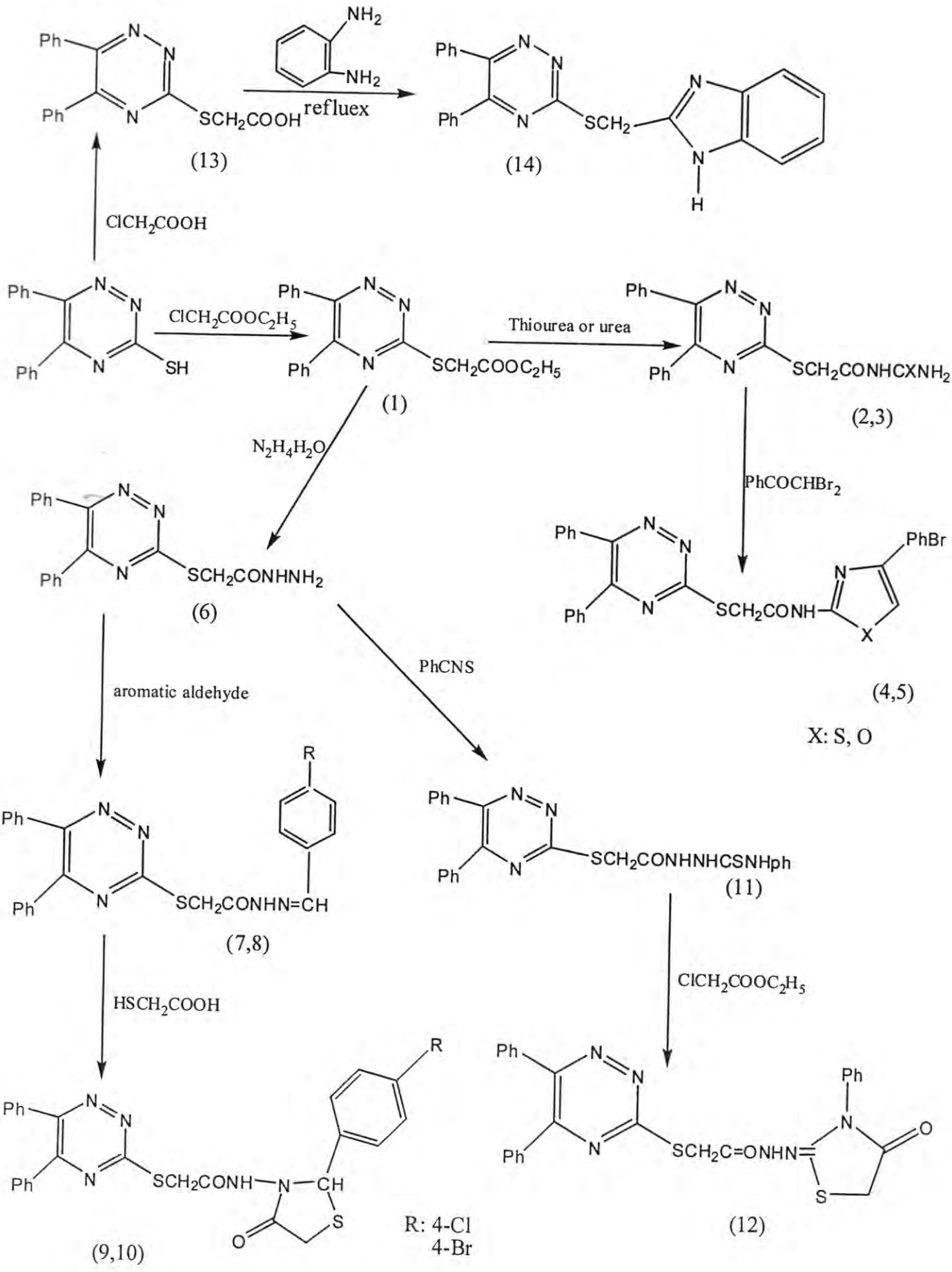
NH2
NH2
refluex
SCH2COOH
(13)
(14)
ClCH2COOH
ClCH2COOC2H5
SH
SCH2COOC2H5
(1)
Thiourea or urea
SCH2CONHCXNH2
(2,3)
N2H4H2O
PhCOCHBr2
SCH2CONHNH2
(6)
PhBr
SCH2CONH
X
(4,5)
X: S, O
aromatic aldehyde
PhCNS
R
SCH2CONHN=CH
(7,8)
SCH2CONHNHCSNHph
(11)
HSCH2COOH
ClCH2COOC2H5
SCH2CONH
CH
S
O
(9,10)
R: 4-Cl
4-Br
SCH2C=ONHN
(12)

Results and DISCUSSION

New derivatives of 5,6diphenyl-1,2,4-triazine-3-thiol containing another heterocyclic moiety were prepared following the reaction sequence depicted scheme **I**. Reaction 5,6 diphenyl-1,2,4-triazine -3-thiol with ethyl chloro acetate to form ethyl 2-(5,6 diphenyl-1,2,4-triazine-3ylthio) acetate **(1),**the FT-IR spectrum figure (1), show the appearance carbonyl of ester C=O 1730 cm^{-1} (table1), ^{1}H-NMR(DMSO_d_6)ppm of compound **(1)**:1.05(t,3H, $CH_2C\underline{H}_3$),4.15(s,2H,$C\underline{H}_2CH_3$),4.31 (s,2H,SCH_2) 7.7-7.8 CH aromatic protons (table 2) ,then condensation compond **(1)** with thiourea or urea to afford compound**(2,3),**the FT-IR spectra show disappearance carbonyl of ester and appearance the CONH stretching band at (1683,1678)cm^{-1} respectively (table 1),^{1}H-NMR(DMSO_d_6) ppm of compound **(2)**: 4.0(s,2H,$SC\underline{H}_2$), 7-7.9CH aromatic protons, 8.0 (s,1H,N$\underline{H}$), 9.53(s,2H,$N\underline{H}_2$) (table 2).Reaction compound **(2,3)** with bromo phenacyl bromide afforded compound **(4,5),**FT-IR spectra show the appearance carbonyl of amide (1672,1681)cm^{-1} table 1 .Condensation ethyl 2-(5,6 diphenyl-1,2,4-triazine-3yl thio)acetate**(1)** with hydrazine hydrat to afforded 2(5,6di phenyl-1,2,4-triazine-3ylthio)aceto hydrazide **(6),** FT-IR spectrum figure(3), show the disappearance carbonyl of ester and appearance carbonyl of amide CONH 1660cm^{-1}(table 1)^{1}H-NMR (DMSO _d_6)ppm of compound **6**: 4.0(s,2H,SCH_2) ,4.22(d,2H,NHN$\underline{H}_2$) ,7.3-7.9 CH aromatic protons,9.52(s,1H,N$\underline{H}NH_2$) (table 2) . Condensation hydrazide **(6)** with aromatic aldehydes to give **(7,8)** in absolute ethanol ,the formation of these Schiff bases was indicated by the presence in their FT-IR spectra which show azomethine CH=N stretching at (1623-1628)cm^{-1},treatment of Schiff bases **(7,8)** with 2-mercaptoacetic acid in dry benzene gave thiazolidenone derivatives **(9,10)** structure of these compounds were confirmed by the presence of C=O stretching band at (1720-1718)cm^{-1}due to thiazolidinone ring (table1).Treatment compound **(6)** with phenyl isothiocyanate afforded the corresponding thiosemicarbazide **(11)**, the FT-IR spectra show the appearance C=S stretching band at 1272cm^{-1} and NH stretching band at 3296cm^{-1} (table1), ^{1}H-NMR(DMSO_d_6) ppm of compound **11** : 2.12(s,1H,CONHNH) ,7.3-7.7 CH aromatic protons,10.08(s,1H,N$\underline{H}$ph), 12.52(s,1H,CON$\underline{H}$) (table2). Refluxing of compound **(11)** with ethyl chloro acetate afforded 4-thioazolidone derivatives **(12)** which was confirmed by the presence of C=O stretching band at 1695 cm^{-1} and C=N stretching band 1634cm^{-1}table 1. Condensation of 5,6 diphenyl-1,2,4-triazine-3-thiol with mono chloro acetic acid afforded compound **(13)** , FT-IR show the 3500 cm^{-1} band of OH ,carbonyl of acid 1695 cm^{-1} , 603 cm^{-1} band of C-S table 1, treatment compound (13) with o-phenylene diamine afforded compound (14). FT-IR show the appearance stretching band of NH 3306 cm^{-1} , 1620 C=N table 1.

TABLE 1:
PHYSICAL PRPOPERTIES AND SPECTRAL DATA OF COMPOUNDS

NO	formula	M.P. C°	Yield %	Color	Recrystallization Solvent	Infrared data cm^{-1}
1	$C_{19}H_{17}N_3O_2S$	223-225	66	White	Chloroform	1730C=Oester,2997-2922 CH alph ,3063 C-H arom.,1612C=N,1589 C=C arom. 671 C-S
2	$C_{18}H_{15}N_5OS_2$	166-168	60	White	Ethanol	1678 C=ONH,2924 C-H aliph ,3039 C-Harom.,3412-3398NH_2,, 610 C-S
3	$C_{18}H_{15}N_5O_2S$	190-192	55	White	Ethanol	1683C=ONH,2987 C-H aliph.,3062C-H arom.,3310,3248 NH_2, 603 C-S.
4	$C_{26}H_{18}Br\ N_5OS_2$	210-212	60	Yellow	Ethyl acetate	1681 C=O amide ,2978 C-H aliph.,3045 C-H arom. ,1649 C=N, 1597 C=C.
5	$C_{26}\ H_{18}BrN_5O_2S$	222-224	65	Brown	Ethyl acetate	1672 C=O amide, 2931-2810 C-H aliph.,3021C-H arom., 1638 C=N.1554 C=C.
6	$C_{17}H_{15}N_5OS$	198-200	70	White	Ethanol	1660 C=Oamide ,3269-3232 N-H_2 1595 C=C , 1616 C=N.
7	$C_{24}H_{19}ClN_5OS$	165-167	75	Orange	Ethanol	3308 N-H,3026 C-H arom.,1628 CH=N ,1006 C-Cl, 612 C-S.
8	$C_{24}H_{19}BrN_5OS$	178-180	77	Orange	Ethanol	3184 N-H,3024 C-H arom.,1623 CH=N ,610 C-Br
9	$C_{26}H_{20}ClN_5O_2S_2$	214-216	65	Dark yellow	Methanol	3290 N-H, 3093 C-H arom.,2895 C-H aliph.,1720 C=O, 1016 C-Cl.
10	$C_{26}H_{20}BrN_5O_2S_2$	224-226	60	Yellow	Methanol	3311 N-H, 3020 C-H arom., 2909 C-H aliph., 1718 C=O,643 C-Br, 1631 C=N.
11	$C_{24}H_{20}N_6OS_2$	200-202	60	Brown	Ethanol	3296-3180N-H,3080 C-H arom., 1272 C=S.
12	$C_{26}H_{20}N_6O_2S_2$	220-222	65	Brown	Ethanol	1695C=O,3210N-H,2920 C-H aliph. 1634 C=N.
13	$C_{17}H_{13}N_3O_2S$	121-123	60	Brown	Ethanol	3500 OH,3080 CH arom., 1695 CO,608 C-S.
14	$C_{23}H_{17}N_5S$	230-232	69	Yellow	Ethanol	3377,3306 NH, 3051 CH arom., 2960 CH aliph., 1620 C=N.

TABLE 2:
CHEMICAL SCHIFF'S ^{1}H-NMR SPECTRA.

No.	^{1}H-NMR (DMSO_d_6)δ ppm
1	1.05(t,3H, $CH_2\underline{CH_3}$),4.15(s,2H, $\underline{CH_2}CH_3$),4.31(s,2H,SCH_2), 7.7-7.8 CH aromatic protons
2	4.0(s,2H,$S\underline{CH_2}$), 7-7.9 CH aromatic protons, 8.0 (s,1H,N$\underline{H}$), 9.53(s,2H,$N\underline{H_2}$)
6	4.0(s,2H,SCH_2),4.22(d,2H,$NHN\underline{H_2}$) ,7.3-7.9 CH aromatic protons,9.52(s,1H,$N\underline{H}NH_2$)
11	2.12(s,1H,CONHNH), 7.3-7.7 CH aromatic protons,10.08(s,1H,N$\underline{H}$ph), 12.52(s,1H,CON$\underline{H}$)

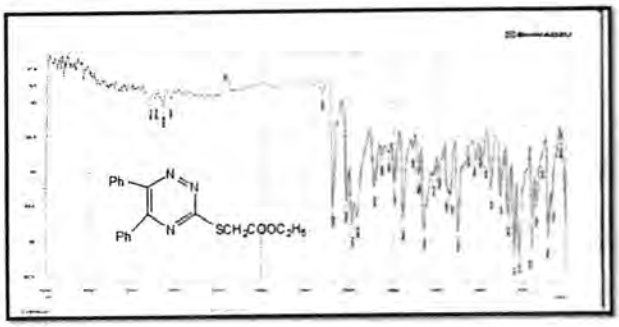

Figure1:FT-IR Spectrum of compound (1)

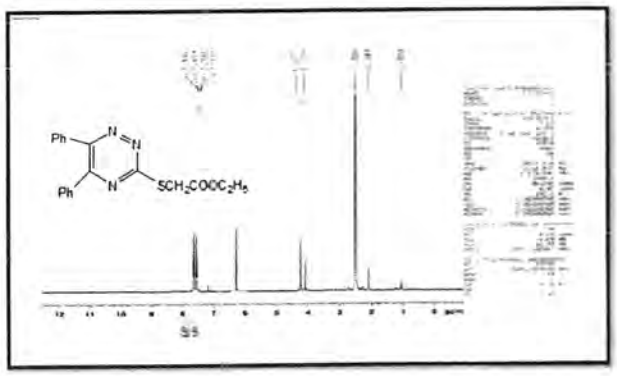

Figure 2:^{1}H-NMR Spectrum of compound (1)

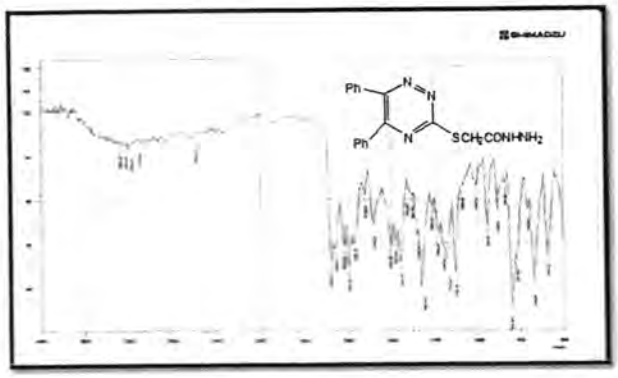

Figure 3:FT-IR Spectrum of compound (6)

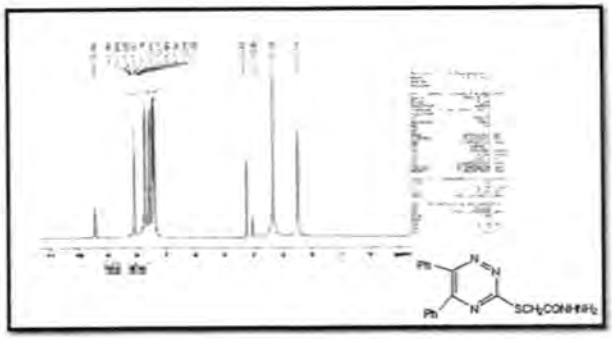

Figure 4:^{1}H-NMR Spectrum of compound (6)

REFREENCES :

1-B. S Holla, R. Gonsalves, S.Rao, S.Henoy,and H.N Gopalkrishna; Synthesis of some new biologically active bis-(thadiazolotriazines) and bia-(thiadiazolotriazinyl) alkanes: Farmaco 56, 899 (2001).

2- M.P Hay, F.B Prujin, S.A Gamage, H.D Liyanage, and W.R Wilson; Targeted 1,2,4-Benzotriazine 1,4-Dioxides: Potent Analogues of the Hypoxia-Selective Cytotoxin Tirapazamine: J. Med. Chem. 47, 475 (2004).

3- A .Baliani, G .J Bueno, M. L Stewart, V .Yardley, R. Brun, M. P Barrett,and I. H Gilbert; Design and synthesis of a series of melamine-based nitroheterocycles with activity against Trypanosomatid parasites: J. Med. Chem. 48, 5570–5579 (2005).

4- B .R Henke, T .G Consler, N. Go, R L Hale, D. R Hohman, S.A Jones, A T Lu, L .B Moore, J .T Moore, L A Orband-Miller, R G Robinett, J Shearin, P K Spearing, E L Stewart, P S Turnbull, S L Weaver, S P Williams, G B Wisely,and M H Lambert; A new series of estrogen receptor modulators that display selectivity for estrogen receptor beta: J. Med. Chem. 45, 5492–5505 (2002).

5- N. P Jensen, A. L Ager, R.A Bliss, C. J Canfield, B M Kotecka, K H Rieckmann, J. Terpinski, and D P Jacobus; Phenoxypropoxybiguanides, prodrugs of DHFR-inhibiting diaminotriazine antimalarials: J. Med. Chem. 44, 3925–3931 (2001).

6- A. Agarwal, K. Srivastava, S. K Puri, and P .M. S Chauhan; Syntheses of. 2,4,6-trisubstituted triazines as antimalarial agents: Bioorg. Med. Chem. Lett. 15, 531–533 (2005).

7- J.Salimon1 and N. Salih2 "Synthesis, characterization and biological activity of some new 1,2,4-triazine derivatives" Vol.2, No.2, pp 1041-1045,(2010).

8- T. Lubbers, P. Angehrn, H. Gmunder, S. Herzig, J. Kulhanek; Design, synthesis, and structure-activity relationship studies of ATP analogues as DNA gyrase inhibitors: Bioorg. Med. Chem. Lett. 10, 821–826 (2000).

9-V.V. Malwad, and J.M. Shirodkar; Synthesis and Antibacterial Activity of New Tetrazole Derivatives: Ind. J. Chem. 42B, 621–626(2003).

10- Y. Pandey, P. Kumar Sharma, N. Kumar,and A. Singh, "Biolgical Activities of Thiazolidine – A Review " International Journal of PharmTech Research,3(2), 980-985,(2011).

11- J.A Shiran, A. Yahyazadeh , M. Mamaghani , M. Rassa Regiose- lective"synthesis of novel 3-allyl-2-(substituted imino)-4-phenyl-3H-thiazole and 2,20-(1,3-phenylene)bis(3 -substituted-2-imino-4-phenyl-3H-thiazole) derivatives as antibacterial agents Journal of Molecular Structure 1039,113–118(2013).

12- V. Dabholkar and S. Ahmed Sabir"Synthesis of Novel oxazoles and their hydrazones"Rasayan J.Chem.,3(4);761-765(2010).

13- C. Chen , C. Chen , B. Li , J.Tao 1 and J. Peng "Aqueous Synthesis of 1-H-2-SubstitutedBenzimidazolesviaTransition-Metal-FreeIntramolecular Amination of Aryl Iodides" Molecules 17, 12506-12520(2012).

14- C. KUS "Synthesis of Some New Benzimidazole Carbamate Derivatives for Evaluation of Antifungal Activity", Turk J Chem27, 35 -39,(2003).

Al-Mustansiriyah Journal of Science
Vol. 27, No2, 2016

journal homepage:www.mjs-mu.com

A comparative Study of Adiponectin and Oxidative Stress (malondialdehyde and peroxynitrite) levels in Iraqi Patients with Acromegaly

Eiman A.Abass * Taghreed U.Mohammd* Baydaa Ahmed Abed** Sali Abed Zeghair**
*Chemistry Department, College of Education for Pure Science, Ibn Al-Haitam, Baghdad University
** National diabetes center al_mustansiria university

Articleinfo

Received
1/10/2015
Accepted
21/12/2015

Keywords:
acromegaly ,oxidative stress , adiponectin ,malondialdehyde, peroxynitrite.

ABSTRACT

The aim of this study is to find a relationship between oxidative stress and adiponectin in Iraqi patients with acromegaly. The present study included 30 patients with acromegaly disease attending at Al-Yarmuk teaching hospital , and 30 healthy individuals as a control group.The two groups with ages ranging (30-55) years. The results revealed a highly significant elevation in all parameters (GH,IGF-1 , adiponectin , malondialdehyde , and peroxynitrite) levels in sera of patients when compared with healthy control .It can be concluded that oxidative stress (malondialdehyde and peroxynitrite) may be valuable in detecting of endocrine diseases like acromegaly .

الخلاصة

هدفت هذه الدراسة لايجاد العلاقة بين الجهد التأكسدي وهرمون الاديبونكتين لدى المرضى العراقيين المصابين بتضخم الاطراف. وقد شملت هذه الدراسة (30) شخصا من المرضى الذين حضروا الى مستشفى اليرموك التعليمي وشخصوا من خلال قياس هرمون النمو GH والهرمون المشابه لهرمون النمو IGF-1 و(30) شخصا من الاصحاء كمجموعة ضابطة تتراوح اعمار المجموعتين ما بين 30 – 55 سنة ,بينت نتائج هذه الدراسة وجود ارتفاع معنوي في مستوى كلا من هرمون الاديبونكتين ، المالوندیهاید ،والبيروكسي نتريت في امصال المرضى العراقيين المصابين بتضخم الاطراف عند مقارنتهم مع المجموعة الضابطة . نستنتج من ذلك انه من الممكن استخدام الجهد التأكسدي المتمثل بالمالوندیهاید والبيروكسي نتريت مقياسا حيويا لمعرفة امراض الغدد الصماء مثل تضخم الاطراف .

INTRODUCTION

Acromegaly is due to excessive production of growth hormone (GH), generally by a pituitary GH-secreting adenoma. Its prevalence is estimated at 40-130 cases per million inhabitants [1]. It is characterized by slowly progressive acquired somatic disfigurement (mainly involving the face and extremities) and systemic manifestations. The diagnosis is confirmed by elevated serum GH concentrations that cannot be suppressed by an oral glucose load, and by increased levels of insulin-like growth factor 1 (IGF-1) [2].

Growth hormone (GH) and insulin-like growth factor-1 (IGF-1) most definitely play essential roles in growth in childhood, and continue to have important metabolic actions in [3].

It, as its name suggests, is implicated in postnatal growth. It is also used in replacement therapy for GH deficient children to induce linear growth . Indeed, it is well proven that pituitary GH deficiency or a defect in tissue GH receptor (GHR), result in dwarfism, whereas an excess of pituitary GH secretion results in gigantism in juveniles, or acromegaly in adults. The GH and insulin-like growth factor-I (IGF-I) axis is not only involved in the regulation of somatic growth, but also in glucose metabolism [4].

Adiponectin is exclusively secreted adipose tissues, and it plays a role in the suppression of the metabolic that may result in type 2 diabetes, obesity, atherosclerosis ,and an independent risk factor for metabolic syndrome [5]Adiponectin, an adipocyte-derived hormone, possesses insulin-sensitizing [6].

Oxidative stress can be identified as an imbalance between the oxidant materials (free radical and their metabolism outputs) and antioxidants. The cells contain oxidant materials more than antioxidants, which is lead to destroy the big vital molecules of the body. Oxidative stress happens when the level of oxidant compounds exceed the ability of antioxidants on removing it [7]. The formation of peroxynitrite is very toxic harmful for biomolecules and cells as it is interact with thiol leading

to lipid peroxidation [8], and attach cells membranes such as fat ,lipids,proteins, and nuclear acids causing many damages to different cells tissue and increases the oxidative stress [9].

Malondialdehyde (MDA) is reactive species which occurs naturally and it is used as a biomarker to measure the level of oxidative stress in an organism. [10]. Malondialdehyde (MDA) is an end product of lipid peroxidation. Reactive oxygen species degrade polyunsaturated fatty acid, forming Malondialdehyde (MDA). This compound is a reactive aldehydes and is one of the many reactive electrophilic species that causes toxic stress in cells and form covalent protein addicts which are referred to as advanced lipoxidation end products (ALE).[11].

Aim of study

This study aimd to find a relationship between oxidative stress and adiponectin in Iraqi patients with acromegaly.

Materials & Methods:

Subjects

Serum samples were obtained from 30 patients (18 women and 12 men) with non diabetic acromegaly disease and 30 healthy individuals as a control group(16 women and 14 men) with ages ranging from (30-55) years.The patients were diagnosed by GH,IGF,and abnormal growth of the hands and feet.This study was conducted in AL- Yarmuk teaching hospital,Baghdad,Iraq between January and June,2014.Serum samples were frozen at -20°C for subsequent analysis.

[

Determination of Serum GH, and IGF-1 (ng/ml)

Serum growth hormone and insulin-like growth factor-I levels were measured using immunoradiometric assay for the in vitro determination in human serum and plasma (GH IRMA kit, a Beckman Coulter Company,English)

Estimation of Serum Adiponectin Level (ng/ml)

Human adiponectin ELISA kit supplied by Human company is a solid-phase ELISA assay designed to measure the amount of total human adiponectin in cell culture separates, serum and plasma.

Estimations of Serum Peroxynitrite Level (µmol/L)

Serum peroxynitrite level was measured using the modified method of (vanuffelen.,1998) [12]. The principle of this determination is the radical peroxynitrite ($ONOO^-$) mediate nitration of phenol resulting in formation of nitrophenol which is detected spectrophotometrically at (412 nm).Concentration of nitrophenol refers to serum peroxynitrite level.

Determination of Serum Malondialdehyde (MDA) (mmol/L)

Serum level of malondialdehyde (MDA) was determined by the reaction of MDA with thiobarbituric acid(TBA) to form a color product of MDA- TBA_2 which is determined at 532 nm according to the modified method described by(Schmedes and Holmer.,1989) [13].

Statistical Analysis

Data were expressed as mean ± SD. The comparison between patients and control groups were analyzed using student t-test . Pearson 's correlation coefficient . P-value of < 0.001 and < 0.05 were considered highly significant and significant respectively.

Results & Discussion:

The levels of diagnostic parameters in patients and control groups are summarizes in table (1). The results which expressed as (mean± SD), showed a highly significant elevation ($p < 0.001$) in serum levels of GH and IGF of acromegaly patients when compared with control group .

Acromegaly is an endocrine diseases characterized by increased circulating growth hormone (GH) and insulin – like growth factor (IGF-1) levels , usually resulting from pituitary adenoma [14].Growth hormone causes the production of IGF-1. Together, excessive GH and IGF-1 can cause metabolic changes and soft tissue, bone, and organ enlargement. GH, or somatotropin, is responsible for the growth of almost all cells and tissues. [15].

The somatic growth and metabolic dysfunction associated with acromegaly result from excess secretion of GH and subsequent elevation of circulating and locally produced insulin-like growth factor-1 (IGF-1). In healthy individuals, GH secretion is under the dual regulation of growth hormone-releasing hormone (GHRH) and somatostatin, with variations in the secretion of somatostatin being the primary mode of regulation [16].

The collective results of the measured biochemical parameters are summarized in table (2). The result showed a highly significant increase ($p<0.001$) in serum level of adiponectin , peroxynitrite and malondialdehyde of acromegaly patients compared to healthy subjects. These results are agree with the finding of previous study [17-18].But they disagree with the results obtained by [19], who found that the serum levels of adiponectin was lower in acromegalic patients when compared to the control group.The difference in adiponectin levels in acromegalic patients depend on degree of insulin resistance in those subjects [20].

patients with active acromegaly have hypoadiponectinemia, which is reversible with GH-lowering therapies. Because adiponectin is known to have beneficial effects on insulin sensitivity, atherogenesis, and inflammation of the arterial wall, this reduction in adiponectin expression may contribute to the increased cardiovascular risk in patients with acromegaly. [21].Acromegalic patients present hypoadiponectinemia and a favorable bone marker profile. It has been reported that adiponectin and visfatin

could be a link between fat mass and bone in acromegaly. [22].

It has been found that the increased levels of IGF-I are associated with enhanced oxidative stress in rats and humans. In addition, increased ROS may play an important role in the complications and premature death in acromegaly. Some studies have shown increased oxidative stress and reduced antioxidant status in acromegaly [23].

Acromegaly is associated with increased levels of oxidative stress coupled by diminished antioxidant capacity and endothelial dysfunction indicated by the presence of decreased NO levels [24].

In fact, this is the first study which found the elevation in oxidative stress (peroxynitrite and malondialdehyde levels) in patients with acromegaly disease, which is a hormonal disorder that results from producing excessive amounts of GH in the body by pituitary .

In this study, the data show a negative correlation between adiponectin and peroxynitrite (r= - 0.160) figure(1) , while the data show a positive correlation between adiponectin and malondialdehyde (r = 0.172) figure (2) in acromegalic patients .

Conclusions

Finally , we can conclude that oxidative stress (malondialdehyde and peroxynitrite) may be of value in detection of endocrine diseases like acromegaly , and there were a negative and positive correlations between adiponectin with peroxynitrite and with malondialdehyde , respectively in acromegalic patients.

References

1. Chanson P, Salenave S, Kamenicky P , Acromegaly. Handbook of Clinical Neurology124:197-219 , 2014.
2. Vladimir V, Adrian D, Sabina Z and Albert B ,Management of acromegaly, F1000 Medicine Reports, 2:54, 2010.
3. Stochholm K, Juul S, Christiansen JS, Gravholt CH. Mortality and socioeconomic status in adults with childhood onset GH deficiency (GHD) is highly dependent on the primary cause of GHD. Eur J Endocrinol 167: 663-670 , 2012.
4. Davide C, Claudia N and Paula F, Growth Hormone, Acromegaly and Glucose Metabolism , Journal of Diabetes, Metabolic Disorders & Control, 1 (4), 2014.
5. Yamauchi,T.;Kamon,J.;Waki,H.;Terauechi,Y.;Kubo ta,N.;Hara,K.;and Moti,Y. The fat- derived hormone adiponectin reverses insulin resistance associated with both lipo-atrophy and obesity . Nat.Med.,7(8):941-946,2001.
6. Maeda N, Shimomura I, Kishida K, Nishizawa H, Matsuda M, Nagarentani H, Furuyama N, Kondo H, Takahashi M, Arita Y, Komuro R, Ouchi N, Kihara S, Tochino Y, Okutomi K , Horie M, Takeda S, Aoyama T, Funahashi S, Matsuzawa Y Diet-induced insulin resistance in mice lacking adiponectin/ACRP30. Nat Med 8:731–737, 2002.
7. Sekhon, L. H.; Gupta, S.; Kim, Y.; Agarwa, A. Female infertility and antioxidants current women's health Reviews, 6: 2, 2010.
8. Adachi,T.R.;Weisbrod,D.R,;Pimenetel,J.;Ying,J.;Vi ctor,S.and,Richard,A.C.S- glutathionation by peroxynitrite activates SERCA during arterial relaxation by nitric oxide.Net.Med.,10:1200-1007, 2004.
9. Pacher,P.; Beckman,J.S. and Liaudet ,L. "Nitric oxide and peroxynitrite in health and disease".Physiol.Rev.,87(1):315- 342,2007.
10. Del Rio D, Stewart AJ, Pellegrini N . "A review of recent studies on malondialdehyde as toxic molecule and biological marker of oxidative stress". Nutr Metab Cardiovasc Dis **15** (4): 316–328, 2005.
11. Meenakshi, T; and Dinesh, J; Adenosine Deaminase and Malondialdehyde Levels in Type-2 Diabetes Mellitus – a Short Study, Global Journal of Medical research ,14(4):758-787, 2014.
12. Vanuffelen,B.E.; Van Derzec, J.and Dekoster,B.M. Biochem.J.,330-719,1998. (Cited by Al-Zamely, O.M.; Al-Nimer, M.S.; Muslih, R.K. (2001). Detection the level of peroxy nitrite and related with antioxidant status in the serum of patient with acute myocardial infarction. Nat. J. Chem., **4**, 625-637).
13. Schmedes , A. and Holmer.G . A new thiobarbituric acid (TBA) method for determining free malondialdehyde (MDA) and hydroperoxides selective as a measure of lipid peroxidation. J.Am.Oil Chem Soc.,66(6):813-817, 1989.
14. Cigdem O, Alev E A, Ethem T C, Cagri Y, Asife S, Duygu S, Aylin S, Dincel, F, Balos T, Mujde A, Markers of early atherosclerosis, oxidative stress and inflammation in patients with acromegaly . Pitutary ,18(5):621-629 ,2015.
15. Jane JA Jr, Thapar K, Laws ER., Acromegaly: historical perspectives and current therapy. J Neurooncol. 54(2):129-137,2001.
16. Schneider HJ, Kosilek RP, Günther M, Roemmler J, Stalla GK, Sievers C, Reincke M, Schopohl J, Würtz RP.,A novel approach to the detection of acromegaly: accuracy of diagnosis by automatic face classification. J Clin Endocrinol Metab.96(7):2074-2080,2011.
17. Siemińska L, Lenart J, Cichoń-Lenart A, Niedziołka D, Marek B, Kos-Kudła B, Kajdaniuk D, Nowak M., Serum adiponectin levels in patients with acromegaly .UK journal , 19(112),514 – 516,2005.
18. Ronchi CL, Corbetta S, Cappiello V, Morpurgo PS, Giavoli C, Beck-Peccoz P, Arosio M, Spada A., Circulating adiponectin levels and cardiovascular risk factors in acromegalic patients . European Journal of Endocrinology , 150(5) : 663-669,2004.
19. Lam,K.S., Xu A.,Tan K.C., Wong LC, Tiu SC, Tam S.,Serum adiponectin is reduced in

acromegaly and normalized after correction of growth hormone excess .J.Clin.Endocrinol.Metab., 89(11),5448-5453,2004.

20. Hernandez-Morante JJ, Milagro FI, Lujan JA, Martinez JA, Zamora S, Garaulet M., Insulin effect on adipose tissue (AT) adiponectin expression is regulated by the insulin resistance status of the patients .Clin.Endocrinol.(Oxf) 69,412- 417,2008.
21. Karen Siu- Linglam, Aimin Xu, Kathryn Choon-Beng Tan, Lai-Ching wong, Sau-Cheung Tiu, and Sidney Tam Serum Adiponectin Is Reduced in Acromegaly and Normalized after Correction of Growth Hormone Excess. J Clin Endocrinol Metab, November, 89(11):5448 –5453,2004.
22. Nuria Sucunza, M. Jose´ Barahona, Eugenia Resmini, Jose-Manuel Ferna´ndez- Real, Wifredo Ricart, Jordi Farrerons, Jose´ Rodríguez Espinosa, Ana-María Marin, Teresa Puig, and Susan M. Webb . A Link between Bone Mineral Density and Serum Adiponectin and Visfatin Levels in Acromegaly , JClin Endocrinol Metab 94: 3889–3896, 2009.
23. Nishizawa H, Handayaningsih AE, Iguchi G, Cho Y, Takahashi M, Yamamoto M, Suda K, Kasahara K, Hakuno F, Yamanouchi K, Nishihara M, Seino S, _____ Takahashi S, Takahashi Y. , Enhanced oxidative stress in GH-transgenic rat and acromegaly in humans, Growth Hormone & IGF Research. 22(2), 64– 68,2012.
24. Anagnostis P., Efstathiadou Z.A., Gougoura S., Polyzos S.A., Karathanasi E., Dritsa P., Kita M., Koukoulis G.N. Oxidative Stress and Reduced Antioxidative Status, along with Endothelial Dysfunction in Acromegaly Horm Metab Res; 45(04): 314-318,2013.

Table (1): levels of diagnostic parameters in acromegaly patients and control groups

Groups / Parameters	Control	AC Patients	P-Value
GH (ng/ml)	2.77±0.67	25.76±1.22	p<0.001
IGF (ng/ml)	319.60 ± 78.31	817.00±153.90	p<0.001

Table(2): Levels of adiponectin, peroxynitrite ,and malondialdehyde in acromegaly patients and control groups

Groups / Parameters	Control	AC patients	P-Value
AD (ng/ml)	9.66±0.65	38.10±0.94	P<0.001
Peroxynitrite(µmol/L)	42.74±1.77	106.54±4.52	p< 0.001
MDA (mmol/L)	5.10±0.70	12.09±0.44	p<0.001

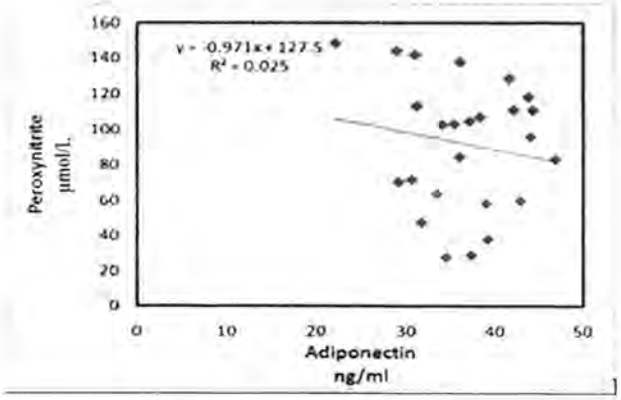

Figure (1): Correlation between adiponectin and peroxynitrite in acromegalic patients

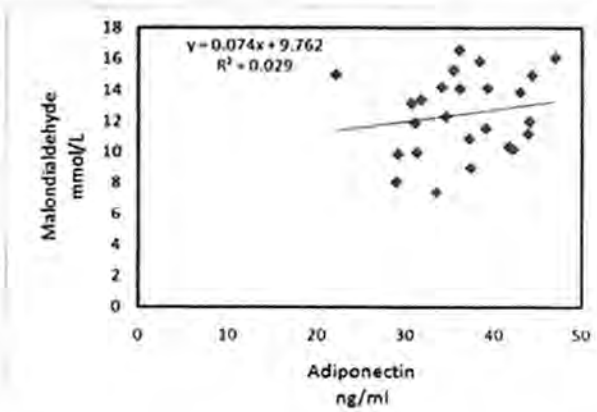

Figure (2) Correlation between adiponectin and malondialdehyde in acromegalic patients

Al-Mustansiriyah Journal of Science
Vol. 27, No 2, 2016

journal homepage:www.mjs-mu.com

Histopathological patterns in experimentally avian coccidiosis after treatment with Urtica dioica L. (Urticaceae)

Dunia Abid-Al Malik Al-ani[1] Enam Bader Falih[2] Amal Hasen Atyha[3]
[1]Minstry of Agriculture/ Office of Agriculture- research.
[2]Path.Depart.Coll. Vet. Med. / Univ. Baghdad / Iraq.
[3] Institute of medical Technology/Baghdad/ MTU

Articleinfo

Received
8/12/2015
Accepted
3/1/2016

Keywords: Urtica dioica L. (*Urticaceae*), Eimeria tenella, Broiler.Histopathology

ABSTRACT

This study was designed to investigate the effect of the herb type *Urtica dioica L* on the pathogenesis in chicken meat (Rose strain) were experimentally infected by 1500 oocyst of *Eimeria tenella* at 22 day old age. It divided randomly into three equal groups at 7 days. The first group represented the positive control, while the second and third groups were treated with herbs at a concentration of 1% and 5% in the feed and aqueous extract respectively, every day of the experiment. Histopathological examination of liver, spleen, intestines and brain of control group revealed hepatic cell necrosis; complete lymphoid depletion in splenic and bursal tissue associated with neuronal degeneration and accompanied by presence numerous degenerated merozoites in cecum. While the histopathological examination in treated groups showed well developed proliferation lesions mainly when treatment with water. Examination revealed major histopathological changes in fodder treatment group, vascular congestion and sinusoidal dilation with periodical MNCs infiltration, bursal epithelial hyperplasia with reactive lymphoid hyperplasia in splenic tissue together with pyers patches lymphoid depletion with evidence of cystic formation in neuronal tissues of infected chicks mainly at 48 old day.

الخلاصة

صممت هذه الدراسة لمعرفة تأثير عشبة القريص نوع *Urtica dioica L* على امراضية الاصابة التجريبية بالايميريا تينيلا في دجاج اللحم (سلالة روز) من خلال تجريعها بـ 1500 كيس بيضة متبوغ للطفيلي في اليوم 22من العمر . قسمت الافراخ عشوائيا إلى ثلاث مجاميع متساوية بعمر 7 أيام، مثلت المجموعة الاولى السيطرة الموجبة , في حين تم معالجة المجموعتين الثانية والثالثة بالعشبة على شكل مسحوق بتركيز 1% و 5% في العلف والمستخلص ماني للعشبة على التوالي طيلة ايام التجربة والذي بدء في اليوم السابع قبل الاصابة . أظهرالتشريح المرضي النسجي لنماذج من الكبد والطحال والامعاء والدماغ في مجموعة المعالجة بالماء درجات متفاوتة لافات نسجية مرضية واضحة مع تغيرات تنكسية ونخرية تضمنت نخر الخلايا الكبدية مصحوبا باستنزاف لخلايا الطحال وجراب فابريشا فضلا عن تنكس العصبونات ووجود العديد من مرحلة الاقسومة للطفيلي في الاعورين. كشف الفحص المجهري ، للملامح الرئيسية للتغيرات المرضية في المجموعة المعالجة بالعلف في اليوم 48 من العمر، عن احتقان الاوعية الدموية وتوسع جيبانيات الكبد يرافقه تكون بؤر تنكسية متعددة من الورم الحبيبي مكون من تجمع *الخلايا* البلعمية متعددة النوى وأظهرت المقاطع النسجية فرط تنسج لمفاوي في الطحال وجراب فابريشا وبقع باير كما لوحظ اختفاء الاقسومات (أحدى مراحل تطور الطفيلي) من الاعورين فضلا عن أدلة على وجود تطور لتنكس كيسي في نسيج الدماغ للدجاج المصاب.

INTRODUCTION

In the last decade plant extracts were widely investigated, medicinal plants stimulate and increase the secretion of digestive enzyme from liver and pancreas(1). Also, they were used for controlling avian coccidiosis and improving poultry performance worldwide, easy usage, non-side effects(2). And because of the development of coccidial resistance to the medical products and the potential harmful effects on human health, there is need to find out the safe alternatives for the control of avian coccidiosis and the use of herbal remedies in poultry diets has been proposed because of their natural stimulation of the immune system,enhanced growth performance and/or anticoccidial effects, anti-oxidant, anti-fungi and etc(1).

Since the *Urtica dioica* leaves containing high crude protein , amino acid , calcium and amino phosphorous and they have certain advantages for basic materials of formulate feed for livestock and poultry (3); also the nettle effects were create appetite stimulation and enhance digestive activity and protective effects against microorganism development ; stimulate the immunological response and had a relaxing effect and eliminated stress caused by environmental factors(4).The leave extract of *Urtica dioica* can cause a little increasing in the main morphometric indices of liver

such as area of hepatocyte , in the periportal zone liver and the other possibility for the hepatoprotective effects of *Urtica dioica* L. (*Urticaceae*) may be related to antioxidant activity to decrease and prevent liver damage , and lower liver enzyme depends on the antiflmmatory effect of *Urtica dioica* (5).

The aim of the present study was to investigate the effects of dried and aqueous extract *Urtica dioica* a medical plant as feed additive on histopathological lesions in broiler chickens organs(liver. spleen, bursal gland, cecum and brain) experimentally infected with *Eimeria tenella*, a highly pathogenic *Eimeria* species that causes caecal coccidiosis.

Materials and Methods

1- **Birds preparation** The environmental conditions of temperature and humidity

One hundred and fifty Ross chicks at one day old were fed with anticoccidial free feed. The environmental conditions were exactly same for all the groups. The temperature at about 3.7.3°c was maintained according to standard program . The birds were kept in 3 cages (5 × 5m). Each cage was equipped with feeders and drinkers. There was no mortalities recorded. To prevention of chickens against Newcastle and bursal infectious disease, all of the chicks were vaccinated at 11 and 14 days of age, respectively.

2 -**Preparation of herbal extracts.**

The dried parts of medicinal plants (leaves and stems) were used. Nettle was supplied from local market and has been ranked by the National Iraqi Institute for herbs in Abu Ghraib, cleaned and milled ,then stored in clean nylon bags. They were extracted according to Harbone and Mabray (6).

3- *Emeria tenella* challenge

Collected samples from cecum from broiler naturally infected with coccidiosis (local isolates of *E.tenella*) from different regions in the province of Baghdad after adding solution Potassium Dichromate concentration of 2.5% , and was purified by single oocysts infections by flotation methods (7). The isolation and increase parasite diagnosed oocysts parasite in laboratory branch parasites/college of veterinary medicine -University of Baghdad according to the method (8).The oocysts were preserved in 2.5% potassium dichromate solution to induce sporulation and kept in a refrigerator (3–5°C) until use(9). Each bird was challenged with 1500 oocysts /chicken of *E.tenella* at the age of 22nd day. (excepted control group).

4- **Experimental design**.

This experimental was conducted in poultry felid in College of Veterinary Medicine -University of Baghdad. experimental chicks were randomly divided into 3 groups (pen) of 50 birds each, from days 1 to 21, the birds were fed a starter diet and from days 22 to 48, a grower diet in mash were formulated using National Research Council (NRC) (10).Challenge of each bird was carried out by administering infected with *Eimeria tenella* at a dose rate of 1500 sporulated oocyte / ml in saline water per bird orally directly into the crop via an oral gavage on the 22nd day of age. The control group with no *Urtica dioica* supplement, no additives (control positive), The second group basal diet containing 1% of (*Urtica dioica* L.) at day 17 mixed with other ingredients, and 3rd group basal diet put water was containing aqueous extract of 0.5% of *Urtica dioica* at day 17 to end of experimental perio
d .

Histopathological examination

When the chicks reached 37, 48 days of age, were selected at random and killed for pathological examination, the liver, spleen, bursal glands, cecum and brain were isolated and the tissue samples were preserved in 10% neutral buffered formalin and were later processed using standard histopathological techniques.(11).

Results:

1-Control group at 37day old, the hall mark histopathological feature of liver showed sever vacuolar degeneration predominately fatty change with sinusoid dilation, (fig.1) together with per portal cellular infiltration consist mainly of MNCs. Also, the result showed destruction in splenic tissue characterized mainly by lymphoid depletion in white pulp (fig.2) as well as congestion of splenic red pulp with sinus congestion. However, sections at 48 day old, That showed sinusoid dilation and congestion associated with disrupted hepatic cord.(fig.4), and epithelial hepatic hyperplasia with cellular inflammatory infiltrate in sub capsular rejoin associated with slight fibrosis, individual cell necrosis of some hepatocytes(fig.5), as well as massive necrosis and congestion with hemorrhage in both splenic tissue associated with slight fibro muscular hyper atrophy of splenic tissuein.(fig.6 &7), also there was Sever distraction in the bursa follicles associated with sever necrotic changes in the medullary region and blood vesicles congestion in sub scapular layer. (fig. 8),but demonstrate sever epithelial ling distraction of sub mucosal glands associated with cellular infiltration in cecum.(fig.9).

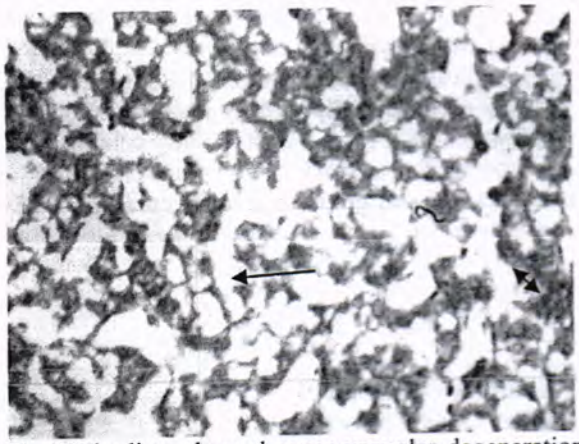

Fig.(1)The liver showed sever vacuolar degeneration of hepatic cords with sever sinusoid dilation( )and congestion( )at 37 day.(H&EstainX40)

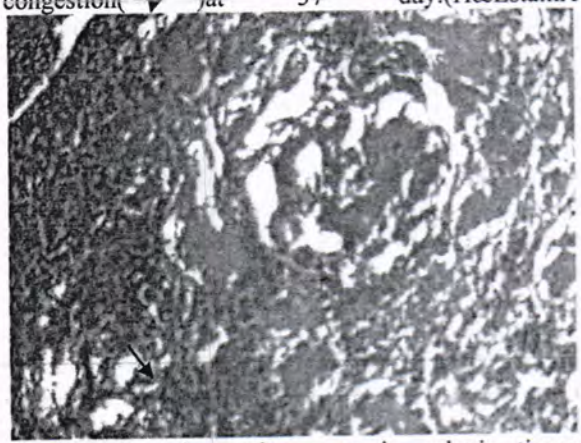

Fig(2)Similar observation seen in splenic tissue of infected control group that revel massive destruction in splenic tissue ( ) mainly characterized by lymphoid depletion white pulp. at 37 day (H&E stain,X40). and observed in bursal tissue associated with severs lose depletion bursal lymphoid follicles. both cortical and medullar lymphoid depletion.

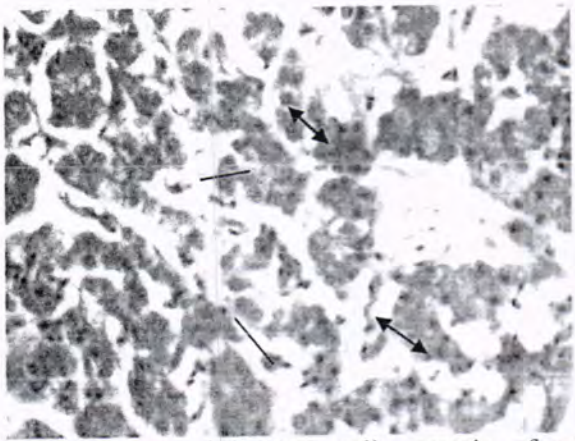

Fig(3)there was individual cell necrosis of some hepatocytes( )together with sinusoid dilation and congestion in liver associated ( )with disrupted hepatic cord, at 37 day (H& E stain, X40).

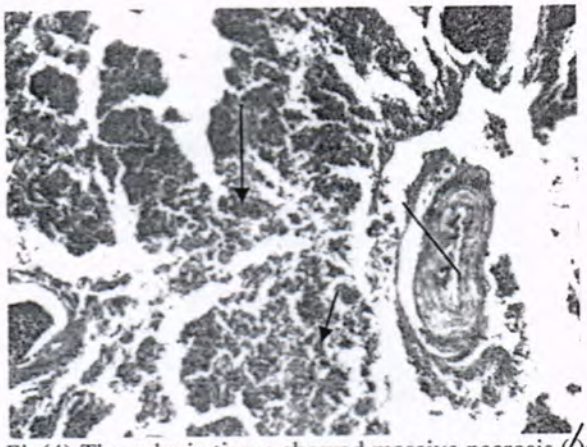

Fig(4):The splenic tissue showed massive necrosis ( )and congestion with hemorrhage associated with slight fibro muscular hyper atrophy of splenic artery( ),at37day,(H&Estain, X40)

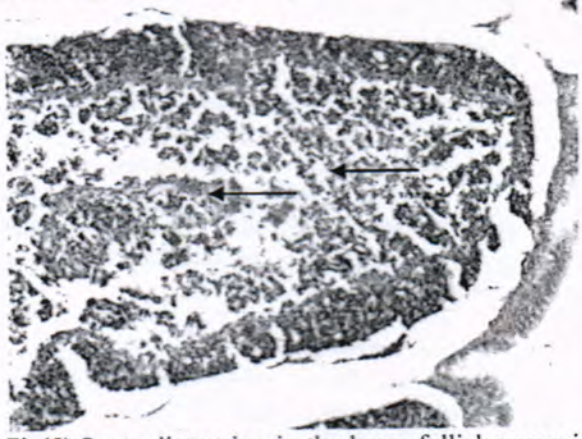

Fig(5):Sever distraction in the bursa follicles associated with sever necrotic changes in the medullary region ( ),at 37 day.(H&E stain, X20).

The histopathological examination of control group at 48 day, demonstrate sever epithelial ling distraction of sub mucosal glands associated with cellular infiltration in cecum and number of degenerated merozoite developed in some mucosal glands resulting in cystic distension of these glands with necrotic tissue debris.

Fig(6):Cecum section changes showed cystic distention of degenerated mucous gland, containing number of degenerated merozoites with cellular infiltration in the Lomina Propria(,) at 48 day (H&E staine.X40).

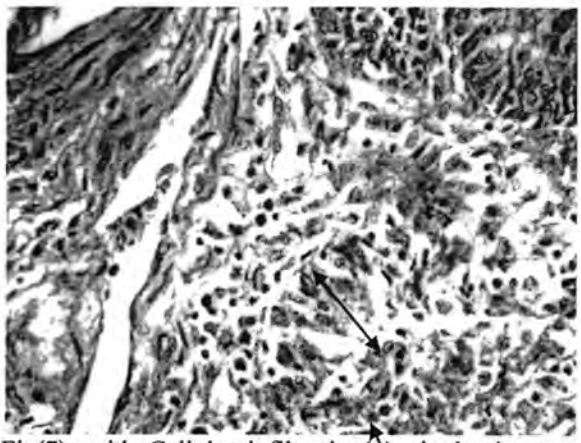

Fig(7): with Cellular infiltration( ) in lamina propria resulting in submucosal thickness of cecum tissue,at 48day (H&E stain,X40).

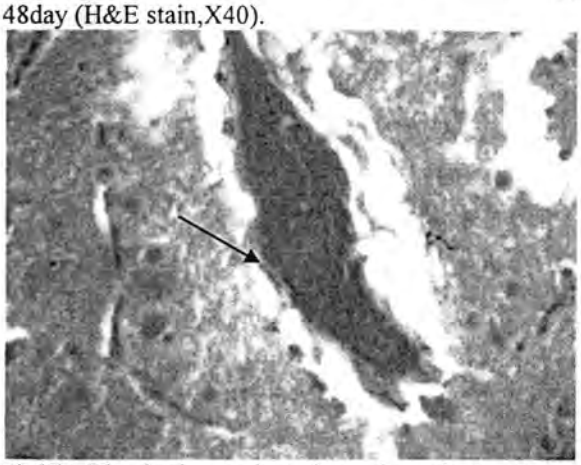

Fig(8): The brain section showed moderate to severe neoronal degenerative changes with blood vessels congestion( )(H&Estain, X40).

2-The microscopical appearance in group 2 (*Urtica Diocia*. treated in food 1% at 37 day old)There was massive diffused necrosis in the liver parenchyma associated with sever congestion of blood vessels and sinusoids.

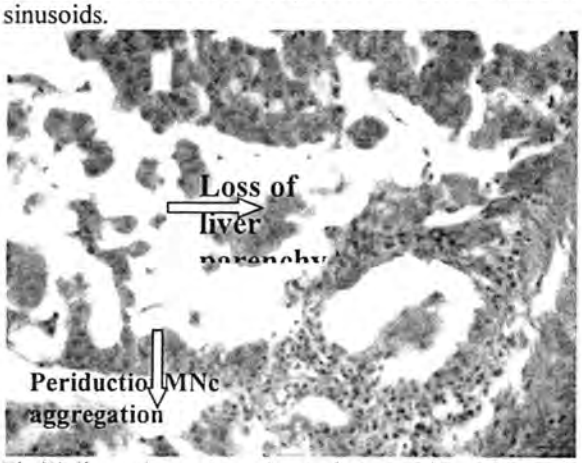

Fig(9):liver showed moderate heterophilic MNc cellular aggregate( ) mainly around bile duct together with various degree of sloughing of its epithelium, also there was loss of parenchyma( )with atrophy of surviving them, at 37day. (H&Estain,X 40) .

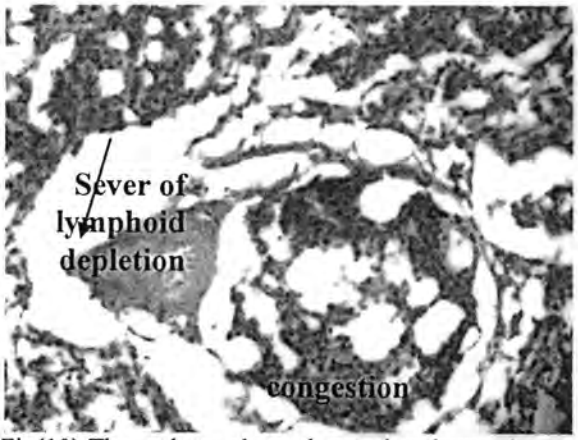

Fig(10):The spleen showed massive hemorrhage and congestion ( )in red pulp with massive lymphoid depletion ( )in white pulp,at37day (H&E,stain, X40)

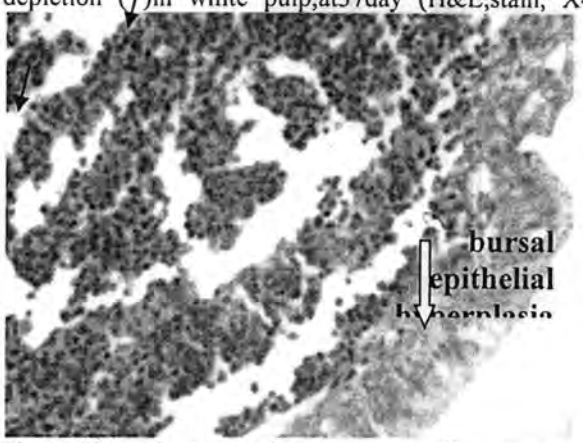

Fig.11:There is sever destruction in all structures of treated bursal tissue involving the lymphoid tissue that showed sever lymphocytosis specially in the cortex with sever dilation of Lumina propria,fig(11&12) and slight hyperplasia ( )with slight squamous metaplasia in the epithelial mucosa, at 37day.(H&E.stain,X40)

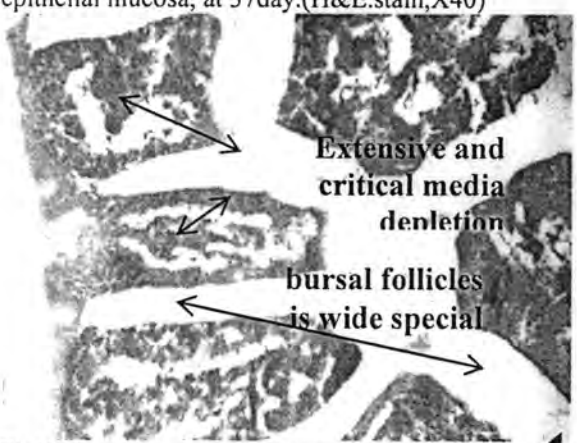

Fig(12): wide space between bursal follicles ( )with extensive cortical media lymphoid depletion ( ), at 37 day (H&E stain , X20).

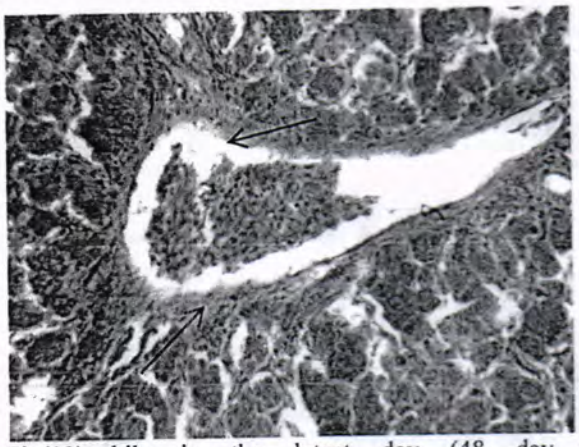

Fig(13):while in the latest day (48 day the histopathological lesion of the group 2 that treated with *Urtica dioica* in food there was sever congestion and dilation of central vein ( )together with slight per central fibrosis of the liver tissue. at 48 day.(H&Estain,X40).

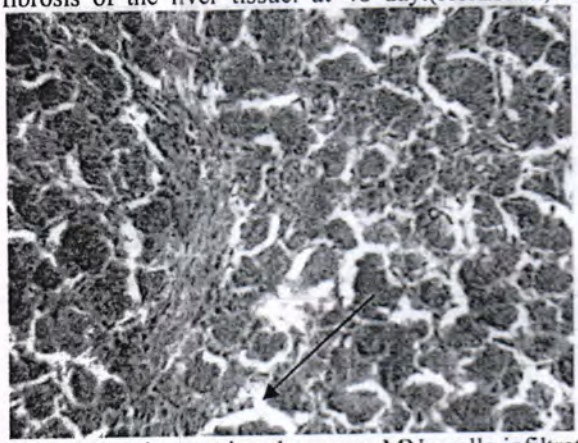

Fig(14):Another section there was MNc cells infiltration ( ) with slight fibrosis that seen mainly in portal area in liver.at 48 day (H&E.stain, X40).

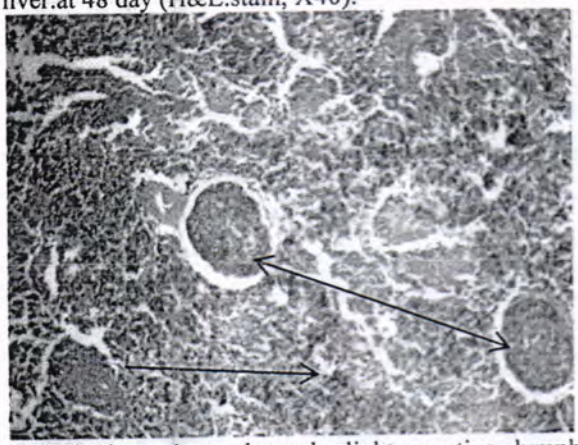

Fig(15):The spleen showed slight reactive lymphoid hyperplasia ( )of white pulp together with hemorrhage in red pulp( ),at 48 day. (H&E stain,X20).

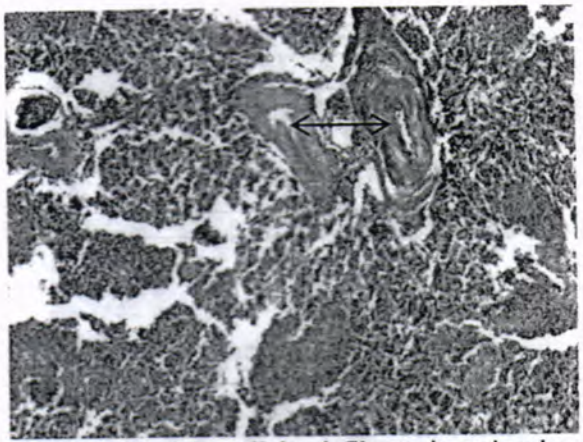

Fig(16):And slight cellular infiltrate in red pulp with muscular hypertrophy of spelnic blood vessels ( )at 48 day (H&E.stain,X20)

The bursal tissue show similarity to previous group except accompanied with slight cortical lymphoid by sever distension and dilation in Lamina propria with congestion and slight hyperplasia of cortical lymphoid follicle, at 48 day.(H&E stain, X20).

The cecum in this group at 48 day showed sever epithelial ling distraction of sub mucosal glands associated with cellular infiltration.

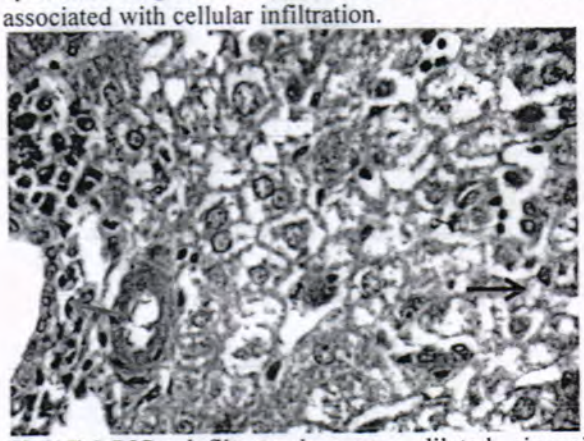

Fig(17):MNCs infiltrate in some dilated sinusoide( )and per duct of cellular infiltration( )as well as necrotic lesion may also absorved in the cecum at surface epithlium with subepithilum hetrophilic infiltration with blood vessels congesting ( )and goblet cell hyperplasia, also PMNCs, eosinphil and MNCs inflitration in the top of villi,at 48 day.fig (18).

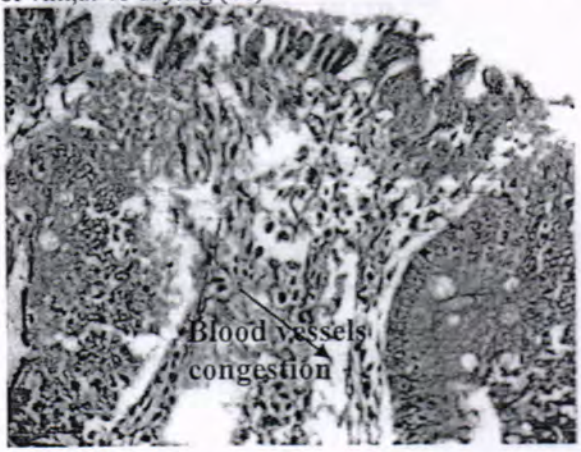

Fig.(18) blood vessels congesting ( )and goblet cell hyperplasia, also PMNCs, eosinphil and MNCs inflitration in the top of villi,at 48 day.

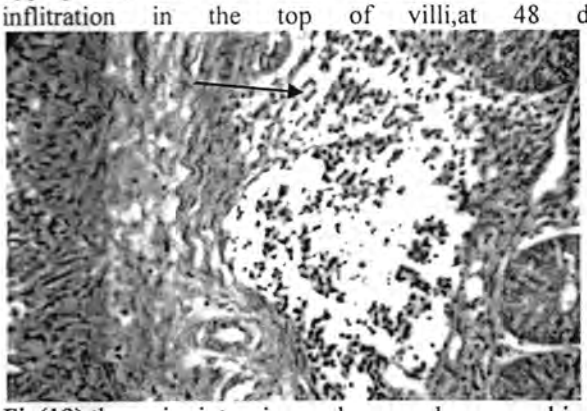

Fig(19):there is intensive submucosal accombind ( )depletion fibrosis, at 48 day. (H&E,stain).

The brain showed sever hemorrhage and blood vessels congestion and meninges cerebral together with neuronal degeneration as well as necrosis in other neurons, at 48 day (H&Estain,X40).

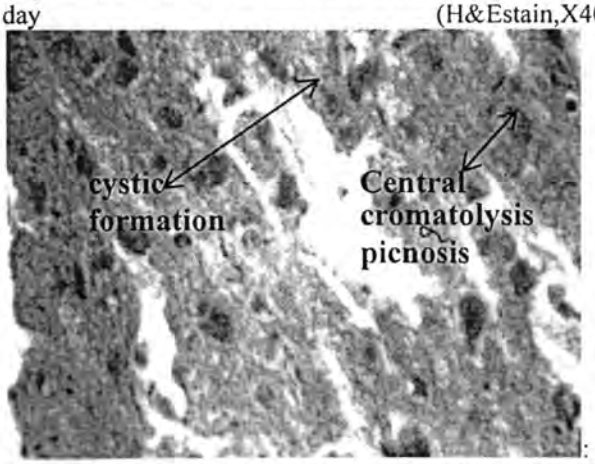

Fig(20):also associated with cystic formation that containing cellular depress and the neurons showed various degree of necrosis(central cromatolysis picnosis),at 48 day. (H&E,stain,X40).

The Microscopical section in the liver of group 3 (Urtica dioica L.) treated in water (37 day old) showed sever congestion in portal area associated with focal cellular aggregation with sinusoids congestion and dilatation of blood vessels with inflammatory cellular in filter together with slight portal fibrosis.

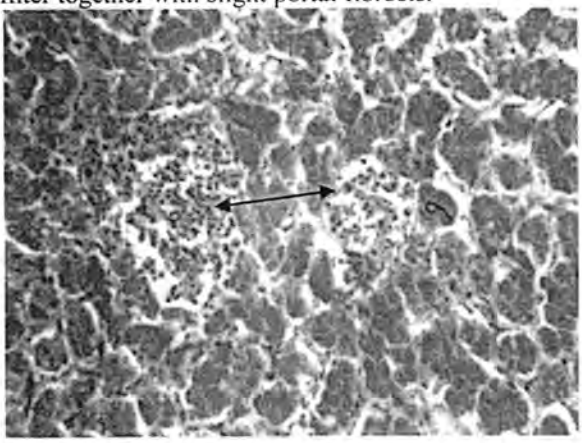

Fig(21):Multifocal cellular aggregation consist mainly of heterophils ( )and lymphocytes together with slight dilation of sinusoid,at 37day.(H&E stain, X20).

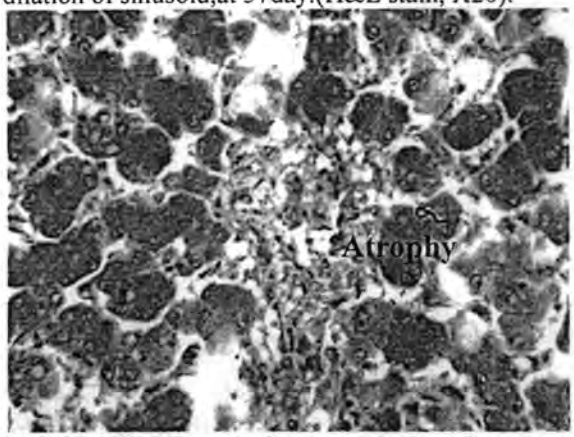

Fig(22):diffused and focal necrosis of parenchyma together with atrophy of surviving hepatocyte of liver. at 37day.(H&E stain, X40).

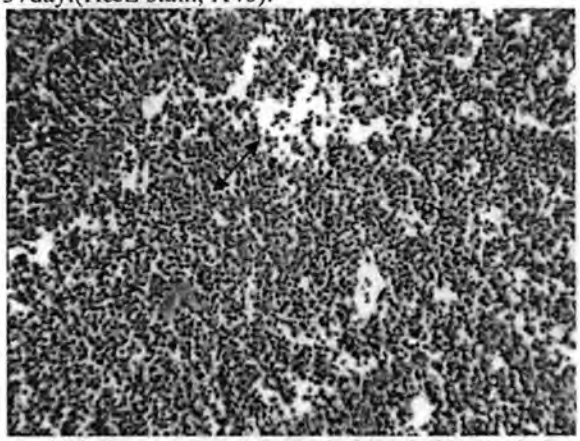

Fig.(23):the section showed lymphoid depletion of splenic white pulp with slight cellular infiltration( ), at 37 day, (H&E stain, X20)

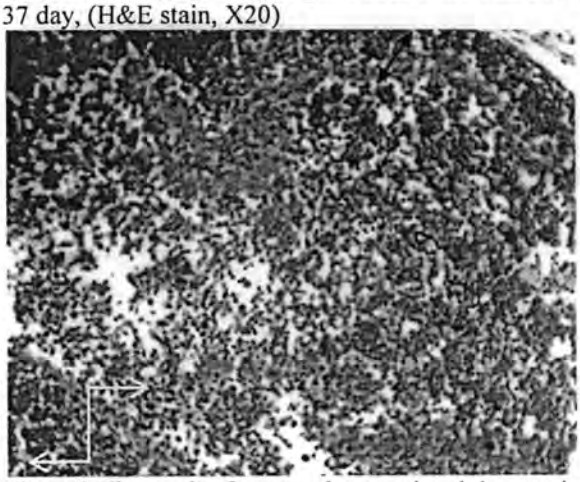

Fig.(24):The main feature characteri-zed by moderate lymphoid depletion mainly observed in the medullar area associated with degenerative changes(,)at 37day.(H&E stain, X40).

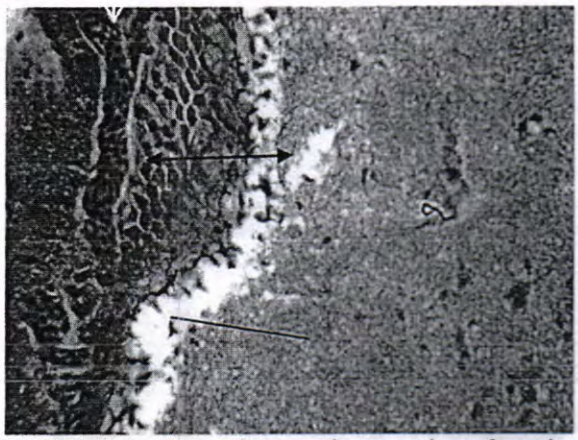

Fig.(25):Sever hemorrhage and congestion of meningeas and cerebral parenchyma ( )with slight vacuolar degeneration and clear view of cerebral edema( )with congestion of blood vesicles. at37day.(H& E stain, X40).

The group 3 that treated with Urtica dioica extract watery (48 day old) showed multifocal aggregation of mononuclear cells in hepatic tissue mainly around blood vessels in portal region.

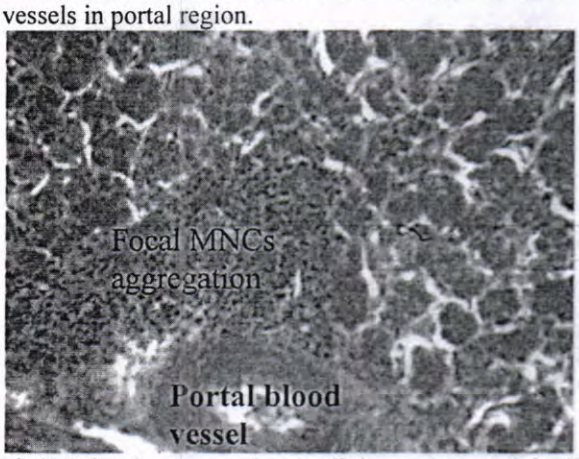

Fig(26):focal mononuclear cellular aggregated in liver parenchyma mainly around blood vesicle in portal area with proliferation of kupffer cells, at 48 day.(H&E stain, X40).

There was variable degree of reaction lymphoid hyperplasia were demons-trated in splenic tissue of this group,as in fig(19), at 38 day (H&E stain, X20).

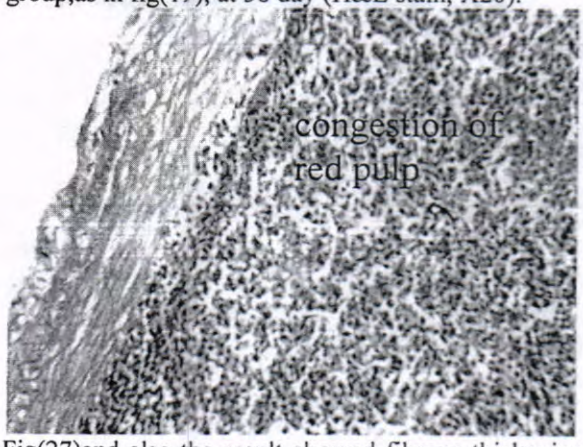

Fig(27)and also the result showed fibrous thickening of splenic capsule in addition to slight congestion of red pulp and medial thickening and proliferation of splenic arterioles, at 48day.(H&E stain, X40).

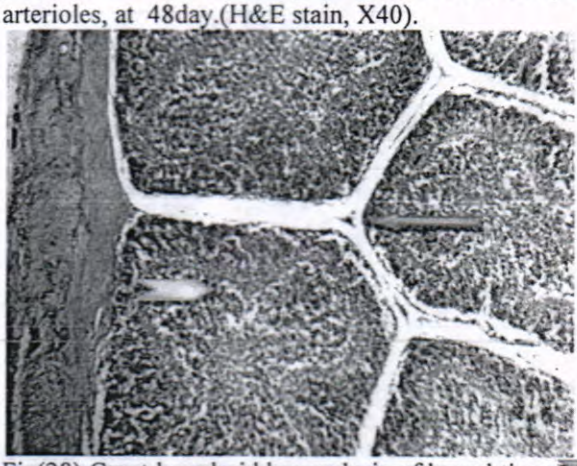

Fig(28):Great lymphoid hyperplasia of bursal tissue associated with fibrous thickening of intestinal connective tissue( ), at 48 day(H&E stain, X20).

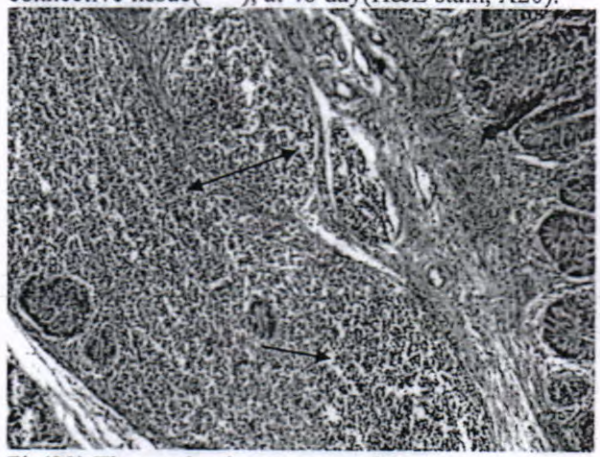

Fig(29):The predominant cecum feature was intense sub mucosal and lomina propria MNCs and PMNCs infiltration( )that result in great thickness of Lomina Propria, together with marked sub epithelial hetrophilic and MNCs that consist of macrophage, plasma cells infiltration ( )with on clear lesion in the epithelial vili. (fig.32), at 48 day.(H&E stain,X40).

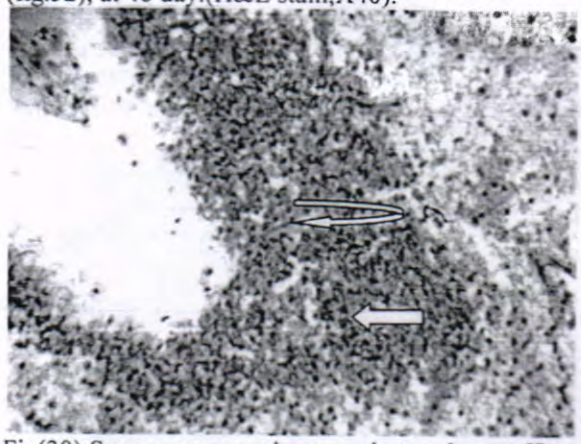

Fig(30):Sever mononuclear peri-vascular cuffing of cerebral blood vessels with slight congestion( ) and dilation of blood vessels with per vascular MNCs cuffing together with MNCs infiltration( )in cerebral parenchyma of brain at 48 day.(H&E, stain X 40).

Discussion:-

The microscopical observation of control revealed morphological alteration of the splenic arteriole wall, which were subject of clear in duration while the cytoplasm of monocyte showed increased acidophilic and contained vacuoles this data were in consistence with Patial *et al.*,(**12**).The general effects include changes in the cellular kinetics and morphology of the villi. The pathological changes are mainly due to the second generation schizonts (**13**). By the fifth or sixth day the caeca are dilated, the contents containing unclotted and partly clotted blood, schizonts. In primary infection, numbers of heterophils and mast cells were increased during the acute inflammation process which indicates mast cells play a role as primary inflammatory cells(**14**). Heterophils predominated when necrosis was extensive;otherwise,mononuclear cells were the main inflammatory cells(**5**)

The current data of control group showed sever morphological changes in the internal examined organs and the ceca are dilated, the numbers of heterophils and mast cells were increased during the acute inflammation process which indicates mast cells (**14**). Heterophils predominated when nicrosis was extensive,otherwise mononuclear cells were the main inflammatory cells(**15**)

Urtica dioica can stimulate lymphocytic proliferation as well as of neutrophils hepatoprotective changes(**16**) and these observation in consistence with our observations mainly in the examined organs of aqueous *Urtica dioica* extract in 48 days old groups particularly in liver and spleen as well as splenic lesions in second group that fed on *Urtica dioica* in feed. At 37days old showed similar pathological changes but lesser than the previous group, however, other researches Harput *et al.*, (**17**) demonstrate that aqueous *Urtica dioica* extract stimulate the proliferation of T- lymphocyte and suppressed the production of lipopolysaccharide (LPS) stimulated macrophages without affecting cell viability, while Richemann *et al.*,(**18**) showed that part of the anti-inflammatory affected of *Urtica dioica* extract might be a scribed to its inhibitory effected on NF-cappa-B-activation.

According to above observation concerning the effects of even when it's applied in small dose of an *Urtica dioica* on the lymphoid organsbroilers infected with *E.tenella* parasite, while the liver and bursal gland morphology attention was also paid to the structure and appearance of blood vessels. In chicken from experimental groups in 48 days the severity of lesions in arteries was significantly lower than in birds from groups in 37 days. Riehemann *et al.*, (19) were suggested the effective of feed additive; Alisma canaliculatum with probiotics (ACP) on the growth performance, meat composition, oxidative stability, and fatty acid composition of broiler meat. No similar studies on birds seem to be an available on bird for comparison of results. However, in the present study none of these organs (liver, spleen, bursa, cecum and brain) were effected significantly by level of *Urtica dioica* extract in drinking water compared to the studies on mice and rats absence of frank necrotic changes This may be due to anti-oxidant and anti-inflammatory protective properties of *Urtica dioica*(**20**), in addition there was evidence of clear perivascular MNCs aggregation in brain tissue mainly (that treated *Urtica dioica* extract 0.5% at age 37 day) and (that treated *Urtica dioica* extract 0.5% at age 48day), this observation may indicate has possibly anti apoptotic supplement promoting cell survival in brain which can be preventive against later injuries(**21**).

Liver in the (treated with *Urtica dioica* in food 1% at aged 37day) may explain morphological alteration characterized by sever vacuolar degeneration mainly in peripheral zone of portal area may indicate the possibility for hepatoprotective effects of *Urtica dioica* extract may be related to antioxidant activity to prevent liver damage depends on the antinflmmatory effect of it(**5**).

The Flavonide play an important role as antioxidant which acts as transition metal ion chelaters because the free radical generation is mainly catalyzed , however excessive intake of flavonoids which cause decrease in essential trace elements [Cu and Zn] and their related enzyme activities(**22**) which lead to long-terms of supra-physiological doses of flavonoids increased gastrointestinal absorption of essential elements (Zn-cu-Fe) and their tissue, availability in brain and liver. This effected seems to be different with vibrations of structural(**13**).

Phenolic compounds of nettle are very important plant constituent because of their scavenging ability which is due to their hydroxyl group and stabilizing lipid peroxidation in the cell membrane (**22**) together with elevated but partial inhibitory effects on cyclooxygenase and lipoxygenase derived reaction, additionally , isolated phenolic acid from *Urtica dioica* to inhibit leukotriene B4-synthesis in a concentration dependent manner in vetro(**23**).

In conclusion, our study has shown that experimental diet treatment at 0.5% level might have potential efficacy on immunity in *Urtica dioica* extract mixed diet is able to stimulate the immune parameters in *Urtica dioica* herb, These results suggested that *Urtica dioica* extract may provide a new therapeutic value in specific and nonspecific immunity in the broiler chicks infected experimentally with *E.tenella* and low doses certainly did not cause any pathogical lesion in liver. However, the effect of *Urtica dioica* mixed diet used as an immuneostimulant by oral delivery has to be further studies .

Reference:

1-Nobakht,A.; Mansoub,N.H. and Nezhady, M.A.M. (2011). The replacement effects of peppermint (*Lamiaceae menthe piperita*) by nettle (*Urtica dioica*) in mixture of different levels of medicinal plants on carcass traits in female and male broilers. Annals of Biol. Res.,2(5):642-646

2-Habibi,H.; Firouzi,S.; Nili,H.; Razavi,M.; Asadi, S.L. and Daneshi, S. (2014). Anticoccidial effects of

herbal extracts on *Eimeria tenella* infection in broiler chickens: in vitro and in vivo study. J. Parasite Dis. 517-4.

3-Grela, E.R. and Kowalczuk, E. (2007). Herbal in animal feeding. Institute of animal nutrition Agricul. Unvi. U.l. Akademicka 13, 20-934 lublin ,Poland. 360-366.

4-Wagner, H.; Willer, F. and Kreher, B. (1989). Biologically active compounds from the aqueous extract of *Urtica dioica*. Planta Med.,55:452-454.

5-Nassiri-Asl, M.; Tani, F.Z.; Abbsi, E.; Daneshi,M.M.and Zangivand,A. (2009). Effects of *Urtica dioica* extract on lipid profile in hyper cholesterolemic rats. J. Chines Intergative Med.,7(5):428-433.

6-Harbone,J.B. and Mabray,H. (1975). Physiological and function of flavonoid, Academic Press, N.Y. :970-1024.

7-Calnek,B.W.;Barnes,H.J.;Beard, C.W. ;Mc-Dougald,L.R. and Saif,Y.M.(1997). Disease of The Poultry. 10th ed. Mosby, Woife., 865-878.

8-Davis,S.F.M.; Joyner,L.P. and Kendall ,S.B.(1963). Coccidiosis of domestic poultry in: Coccidiosis. ed. by Oliver A. and Boyd, Ltd M., Edinburgh, London, 1st ed., Pp.86-117.

9-Vogl, C.R. and Hartl, A. (2003). Production and processing of organically grown ® ber nettle (*Urtica* **dioica** L.) and its potential use in the natural textile industry: A review. Amer. J. Altern. Agric., 18(3):119-128.

10-Jorgensen,W.K.;Stewart,N.P.; Jeston ,P.J.; Molloy,J.B.; Blight,G.U. and Dalgliesh,R. (1997). Isolation and pathogenicity of Australian strain of *Eimeria praecox* and *E.mitis*. Animal Res., 41:10-18.

11-Luna,L.G.(1968). Manual of histological staining methods of armed forces institute of pathology.3rd ed. Morgaa-Hillbook Com., NY. Toronto, Sydney. 12-31.

12-Patial,V.; Asrani,R.K. and Patil, R.D. (2013). Safety evaluation of seabuckthorn (*Hippophaerhamnoides*) leaves in Japanese quail, Vet. World, 6(9):596-600.

13-Gülçin,I.K.; Küfrevio,l.U.; Oktay, M. and Büyükokuro, M.E. (2004). Antioxidant, antimicrobial,antiulcer and analgesic activities of nettle (*Uritica dioica* L.).J. Ethnopharacol.,90:205-215.

14-kadhim,L.I.(2014). Histopathological changes of broilers immunized with sonicated oocysts against *Eimeria tenella*. I.J.A.B.R., 4(1):31-35.

15-Reid,W.M.(1978). Coccidiosis. In Diseases of Poultry, 7th ed., ed. Hofstad, M.S.; Calnek,B.W.; Helmboldt,C.F.; Reid, W.M. and Yoder, H.W. Jr. Ames, IA: Iowa State Univ. Press.P784-815.

16-Gutowska,I.; Jakubczyk, K.; Dec, K.; Baranowska-Bosiacka,I.; Drozd,A.; Janda,K.; Wolska,J.; Łukomska,A.; Dębia, K. and Chlubek, D.(2014). Effect of the extract from nettle (*Urtica dioica* L.) Fruit cluster on the synthesis of pro-inflammatory agents in hepatocytes treated with fluoride. Res. Report fluoride, 47(2):109-118.

17-Harput,U.S.; Saracoglu,I. and Ogihara,Y. (2005). Stimulation of lymphocyte proliferation and inhibition of nitric oxide production by aqueous *Urtica dioica* extract. Phytother Res,. 19(4):346-348.

18-Riehemann,K,; Behnke,B. and Schulze-Osthoff,K.(1999). Plant extracts from stinging nettle (*Urtica dioica*), an antirheumatic remedy, inhibit the proinflammatory transcription factor NF-kappa B. FEBS Lett., 442(1):89-94.

19-Hossain,M.D.;Kim,G.M.;Lee,S.K. and Yang, C.H.(2012). Growth performance, meat yield, Oxidative stability, and fatty acid composition of meat from broilers fed diets supplemented with a medicinal plant and probiotics. Asian-Australas J. Anim. Sci., 25(8):1159-1168.

20-Ghasemi, H.A.; Taherpour, K.; Hajkhodadadi, I. and Akhavan-Salamat, H. (2014). Comparative effects of nettle (urtica dioica) and commercial feed additives on productive performance and blood lipid profile of broiler chickens. J. Anim. Sci. Adv., 4(1):633-640.

21-Toldy,A.; Stadler,K.; Sasv,M.; Jakus, J.; Jung,K.J.; Chung,H.Y.; Berkes,I.; Nyakas, C. and Rad´ak, C.(2005). The effect of exercise and nettle supplementation on oxidative stress markers in the rat brain. Brain Res. Bulletin, 65:487-493.

22-Oktay,M.;Gülçin,˙I.and Küfrevio- ˘glu,Ö.I. (2003). Determination of in vitro antioxidant activity of fennel (Foeniculum vulgare) seed extracts. Lebensmittel-Wissenchaft und Techno-logie, 36:263-271.

23-Kanter,M.; Meral,I.; Dede,S.; Gunduz,H.; Cemek, M.; Ozbek, H. and Uygan,I.(2003). Effects of Nigella sativa L. and *Urtica dioica* L. on lipid peroxidation, antioxidant enzyme systems and some liver enzymes in CCl4-treated rats. J Vet Med A Physiol Pathol. Clin. Med, 50(5): 264-8.

Al-Mustansiriyah Journal of Science
Vol. 27, No 2, 2016

journal homepage:www.mjs-mu.com

The weight changes in bodies and some organs system of albino mice treated with silver nanoparticles

Genan Adnan Al-Bairuty , Mohammed Naji Taha
Collage of Education for Pure Science-Ibn Al-Haitham / Department of Biology

Articleinfo

Received
5/5/2015
Accepted
18/5/2015

Keywords: Silver nanoparticles, mice, body weight, organs weight.

ABSTRACT

This study was conducted to determine the weight changes in their bodies and some organs system of albino mice that orally administrated with silver nanoparticles (Ag-NPs). Use 20 mice were divided into two groups: the first group as a control (5 animals) and the second group administrated with 200 mg/kg BW of Ag-NPs for 5, 10, and 15 days. Each period involved 5 animals. The animals weighted before and after the end of the treatment period and dissected to collect the organs (liver, spleen, kidney, gastrointestinal tract (GIT), heart and seminal vesicle) for weighting. Results indicated to obtain significant decrease ($P<0.05$) in the average body weights of animals after the end of each treatment period compared to the period before treatment. The results also showed a significant decrease ($P<0.05$) in the average coefficient relative weight of the spleen after 5 days of treatment compared to the control group. Whereas, there was a significantly increase ($P<0.05$) in the average coefficient relative weight of the kidneys, GIT, lung and heart after 10 days of treatment compared with the control groups. So, it seems that Ag-NPs have a negative effect on the animals' body weights and the internal organs system. Therefore more studies are necessary to evaluate the effects of this material on the histology structure of these organs.

الخلاصة

يهدف البحث الى دراسة واجراء التحليل المورفومتري لمروحة الطيب الواقعة الى الجنوب الشرقي من العراق اعتمادا على التفسير البصري للبيانات الفضائية للقمر الصناعي لاندسات الفضائية المحسنة وتم ربط التفسير البصري بالتفسير الرقمي الناتج بواسطة برنامج نظم المعلومات الجغرافية (ArcGIS) بعد اجراء التصحيح الجغرافي لهم.
تم استخدام برنامج (ArcGIS) لرسم شبكة تصريف المروحة اعتمادا على أنموذج الأرتفاع او التضرس الرقمي (DEM 30m) المستخرج من البيانات الفضائية لتحديد شكل المروحة ومطابقتها بقنوات التصريف الخاصة بها.
استخدم برنامج (ArcGIS) لحساب القياسات المورفومترية لتوضيح الخواص المساحية والحدة والتضرس للمروحة .
اتضح ان لمروحة الطيب خمس مراتب لقنوات التصريف وهذا يدل على انها تتغذى من مياه الأمطار بشكل اكثر من المياه السطحية. تم تحديد منطقة التغذية للمروحة بواسطة تحليل انموذج التضرس الرقمي (DEM). دلت التحاليل على قلة الغطاء النباتي والنفاذية العالية للمنطقة والتي بالتالي تعمل على زيادة ترشيح مياه الأمطار تحت السطح. كذلك دلت النتائج على ان حوض المروحة يبتعد عن الشكل الدائري وتقريبا ممتد في شكله وبالتالي الحوض له شكل مثلث. تبين ايضا من خلال النتائج ان سطح الحوض ذو ميل كبير وله تضاريس قليلة الوعورة.

INTRODUCTION

Nanoparticles (NP) are defined as substances made within the nanoscale between 1–100 nm in diameter that show exclusive new properties of the structural integrity as well as chemical and physical properties [1]. Silver nanoparticles (Ag NPs) is considered as a one of the most commonly used metal based nanoparticles, which are widely used in consumer products and medical uses [2 and 3]. Ag NPs have also abilities for inhibitory and bactericidal effects as well as a slow down the growth of mold, harmful spores and germs [2]. Due to increased uses of Ag-NPs, human exposure to these materials has been increased. Limited information have been recounted for silver nanoparticles by oral routes of exposure. Oral exposure to Ag-NPs (56 nm) over a period of 90 days in male rats caused a significant decrease ($P < 0.05$) in the body weight of animals after 4 weeks of exposure [4]. Whereas [5] found that intragastric administration of 2.5,5, and 10 mg/kg TiO_2 NPs in mice caused decreased body weight, elevation kidney indices, unbalance of element distribution, creation of reactive oxygen species and peroxidation of lipid, protein and DNA in mouse kidney tissue after 90 days of exposure. The main objective of this study was to investigate the effect of Ag NPs on body weight and some organs in the mice body during different time of exposure.

Material and methods

Preparation and characterization of Ag NPs

The Ag-NPs used were purchased from Sigma Aldrich company and had (manufacturer's information) a spherical configuration with an average particle size >80 nm and 99.9 % purity. The powder had a dark gray color. The 200 mg/kg Ag NPs solutions or 50 mg /1 ml were prepared by diluted 750 mg of Ag NPs with 15 ml of distilled water and then put it overnight on magnetic stirrer to dissolve.

Animal treatments

All laboratory mice were purchased from the Health Center for Control and Pharmaceutical Research. Twenty male ICR mice (10–13 weeks old, 29–33 g body weight) were used in oral administration test. The experimental mice were housed in plastic cages in a ventilated animal room under 12:12 hr light dark cycle, and temperature of 25 °C. They were provided with pelleted commercial food and tap water *ad libitum* all over the experiment. Animals were randomly divided into 2 groups: one control group and one experimental group (200 mg/kg BW of Ag NPs). The experimental groups divided into 3 groups depend on the period of exposure (5, 10, and 15 days). Each group had 5 animals and each treated animal received 0.1 ml from stock Ag-NPs solution daily. The remaining 5 mice were used as the positive control group. The mice received Ag-NPs at the limited dose of 200 mg/kg orally using a suitable intubation cannula at each period of exposure. At 5, 10 and 15 days after gavage, five mice in each group were sacrificed. Whole body weight was recorded before and after one day of the end of the dose. Various organs such as gastrointestinal tract (GIT), liver, spleen, lung, kidney, seminal vesicles and heart were also collected from mice and then weight recorded (Figure 1). The organ weight/body weight (BW) coefficients of GIT, liver, spleen, lung, kidney, seminal vesicles and heart, were calculated as organ weight (wet weight, g)/BW (g) x 100%.

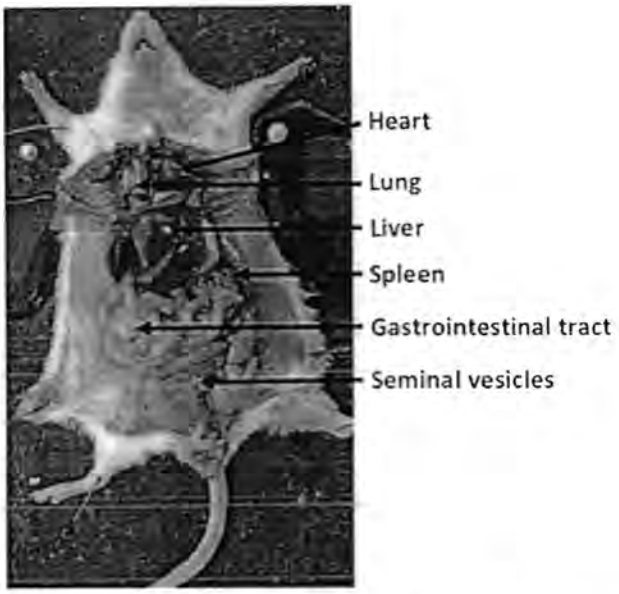

Figure 1 shows the organs position which are collected from mice.

Statistical analysis

The results of this experiment were expressed as means (Mean ± S.E.). Data were analyzed by using the SPSS statistical software (ver. 20, SPSS Inc., Chicago, IL). All data were analyzed by using one-way analysis of variance followed by t test. A value of ($P< 0.05$) was considered statistically significant.

Result and Discussion

Animal observation

The general behavior of animals belonging to the all experimental mice that orally administrated with 200 mg/kg of silver nanoparticles (Ag-NPs) were similar. During the experiment, several stress symptoms such as reduced appetite and elevated aggression were seen in all Ag-NPs treated groups. The current results is agreement with [6] that found the treatment of anemia progression by magnetite and folate nanoparticles in rats caused vomiting, loss of appetite, and severe lethargy demonstrate and the author suggest that magnetite and folate-coated magnetite nanoparticles have severe toxicological effects *in vivo*.

Body weight

The results showed significantly decrease ($P<0.05$) in the average weight of animals body after 5, 10 and 15 days of exposure to Ag-NPs compared to the same animals groups before treated. The body weight decrease was about 3–4 g. While the animals of control group exhibit a statistically significant increased ($P<0.05$) in the average of body weight after gavage with distill water compare to the same animal group before treated (Figure 2). The body weight increase was 4 g.

Decreases in the average body weight reported in the current study are consistent with literature showing that oral exposure to 30, 125, and 500 mg/kg of Ag-NPs for

13 weeks in male rats caused a significant decrease ($P< 0.05$) in the body weight after 4 weeks of exposure [4]. Another study found also that oral administration of 1100 µg/kg gold nanoparticles over 28 days caused a decrease in the body weight [7]. [7] suggest that oral exposure to NPs could produce some effects on the digestive system.

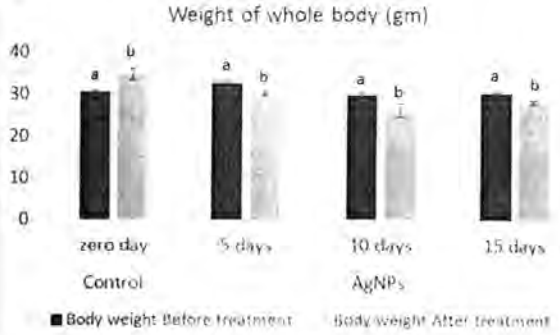

Figure 2 shows the whole body weight of albino mice before and after orally administration with 200 mg/kg body weight of Ag NPs for 5, 10, and 15 days. Data are means ±S.E.M. (n = 5). Different letters denote significant difference between treatment groups (P<0.05). Similar letters denote no significant difference between treatment groups (P>0.05).

Organs weight

The coefficient-relative of some organs weights in all treatments during different time of exposure, relative to the control are shown in Table 1. The present study exhibit a statistically significant decrease ($P<0.05$) in the coefficient of spleen weight after 5 days of exposure to 200 mg/kg Ag-NPs compared to control groups (Figure 3 and Table 1). Whereas other period time (10 and 15 days) of treated animals does not show any significant difference when compared to the control. This may indicate that the oral administration can disturb the gastrointestinal system and then can damage the immune system [7]. In addition, the spleen is one of the target organs for nanoparticles (TiO_2 NPs) accumulation [8]. The current results is agreement with [7] That found the oral administration of gold nanoparticles(550-2200 µg/kg) for14 days in mice caused significant decreases in body weight, spleen index, and red blood cells.

The coefficient-relative of kidney, GIT, lung and heart weight in the present study showed statistically significant increase after 10 days of orally administrated with 200 mg/kg Ag-NPs compared to group mice. While other period time (5 and 15 days) does not show any significant difference when compared to control animal.

Absorption of silver after oral administration has been revealed to be first-pass through the liver, resulting in elimination into the bile duct [9]. Un-cleared silver has been revealed to be deposited in the basement membrane of renal glomerular [10-12], mesangium [13], Kupffer cells and endothelium cells in the sinusoid of the liver [14].

In previous study, the target organs for Ag-NPs were revealed to be the liver after 28 days of oral administration [15] and the liver and lungs after 90 days of inhalation exposure [16]. The alteration that observed in the coefficient-relative of kidney, GIT, lung, heart weight could be due to the injuries that occurred in these organs. Study by [5] found that intragastric administration of 2.5, 5, and 10 mg/kg body weight of TiO_2 NPs for 90 days in mice induced body weight reduction, increased kidney indices, histopathological alteration, apoptosis, oxidative stress, and deterioration of element balance in kidney with elevation of TiO_2 NPs doses. The increased coefficients lung weight suggested that the inflammation may be made and kept in the pulmonary tissues for one week after rat exposure of TiO_2 NPs [17].Study by [16] showed that inhalation of Ag-NPs in rats for 90 days caused chronic alveolar inflammation, accumulation of alveolar macrophages, and a mixed cell perivascular in lungs.

In this study, oral administration of Ag-NPs had effect on coefficient weight of the heart. This may occurred due to the pathological effects. This was relatively in agreement with previous reports. [18] found that oral administration of ZnO NPs caused pathological effects (mild hyaline degeneration of the heart muscle tissue with severe anemia and high condensation of nuclei as well as bleeding) on the heart of rats.

The coefficient-relative of liver and seminal vesicle weight does not shown any statistically significant difference ($P>0.05$) as compared to control groups Table 1. This may indicate that the liver work to detoxify the blood to rid it of harmful substances (Ag-NPs). The current result is agreement with [4] that found the oral administration of Ag-NPs over 90 days in rats did not caused alteration in the weight of liver and seminal vesicles.

Figure 3 Show the spleen of control groups and treated animal with Ag-NPs.

Conclusion

An animal toxicity study using 200 mg/kg silver nanoparticles in mice was carried out. Animal observation, body weight, and coefficient organs weight were detected over 15 days. The results show that Ag-NPs at 200 mg/kg induce significant decrease in body weight. Obvious effects on coefficient organs weight have been revealed that spleen, kidney, GIT, lung and heart is considered as a target organs to Ag-NPs toxicity.

Table (1) shows a coefficient-relative organs weight in albino mice treated with 200 mg/kg of Ag NPs for 5, 10 and 15 days.

Treatment	Time/ Day	N	The coefficient weight of						
			Liver	Spleen	Kidney	GIT	Lung	Heart	Seminal vesicle
Control	zero	5	6.49 ± 0.35	0.66 ± 0.07 a	0.68 ± 0.04 a	12.69 ± 0.45 a	0.81 ± 0.02 a	0.49 ± 0.01 a	0.46 ± 0.03
200 mg/kg AgNPs	5	5	5.82 ± 0.25	0.44 ± 0.06 b	0.68 ± 0.05 a	14.52 ± 0.72 a	0.76 ± 0.05 a	0.52 ± 0.02 a	0.54 ± 0.13
	10	5	5.56 ± 0.42	0.66 ± 0.03 ac	0.86 ± 0.04 bc	15.88 ± 1.80 b	1.14 ± 0.04 bc	0.66 ± 0.03 bc	0.57 ± 0.08
	15	5	6.15 ± 0.22	0.60 ± 0.03 ac	0.76 ± 0.06 a	15.52 ± 0.48 a	0.83 ± 0.04 ac	0.55 ± 0.02 d	0.45 ± 0.13

Data are means ±S.E.M. Different letters denote significant difference between treatment groups (P<0.05). Similar letters denote no significant difference between treatment groups (P>0.05).

References

1- Thomas, K. and Sayre, P. (2005). Research strategies for safety evaluation of nanomaterials, Part I: Evaluating the human health implications of exposure to nanoscale materials. *Toxicol. Sci.*, 87: 316–321.

2- Chen, X. and Schluesener, H.J. (2008). Nanosilver: A nanoproduct in medical application. *Toxicol. Lett.*, 176: 1–12.

3- Edwards-Jones, V. (2009). The benefits of silver in hygiene, personal care and healthcare. Lett. Appl. Microbiol., 49 (2): 147–152.

4- Kim, Y.S.; Song, M.Y.; Park, J.D.; Song, K. S.; Ryu, H. R.; Chung, Y. H.; Chang, H. K.; Lee, J. H.; Oh, K. H.; Kelman, B. J.; Hwang, I. K. and Yu, I. J. (2010). Subchronic oral toxicity of silver nanoparticles. Part. Fibre Toxicol., 7 (20):1-11. doi:10.1186/1743-8977-7-20

5- Gui, S.; Sang, X.; Zheng, L.; Ze, Y.; Zhao, X.; Sheng, L.; Sun, Q.; Cheng, Z.;
Cheng, J.; Hu, R.; Wang, L.; Hong, F. and Tang, M. (2013) Intragastric exposure to titanium dioxide nanoparticles induced nephrotoxicity in mice, assessed by physiological and gene expression modifications. Part. Fibre Toxicol., 10 (4):1-16.

6- Elsayed, H. H.; Al-Sherbini, A.A.M.; Abd-Elhady, E. E. and Ahmed, K.A. (2014) Treatment of anemia progression via magnetite and folate nanoparticles *In Vivo*. Hindawi Publishing Corporation, ISRN Nanotechnology, Article ID 287575, 13 pages http://dx.doi.org/10.1155/2014/287575.

7- Zhang, X-D.; Wu, H-Y; Wu, D.; Wang, Y-Y; Chang, J-H; Zhai, Z-B; Meng, A-M; Liu, P-X; Zhang, L-A and Fan, F-Y (2010) Toxicologic effects of gold nanoparticles in vivo by different administration routes. Int. J. Nanomedicine, 5:771-781.

8- Tassinari R, Cubadda F, Moracci G, Aureli F, D'Amato M, Valeri M, De Berardis B, Raggi A, Mantovani A, Passeri D, Rossi M, Maranghi F (2014). Oral, short-term exposure to titanium dioxide nanoparticles in Sprague-Dawley rat: focus on reproductive and endocrine systems and spleen. Nanotoxicology, 8 (6): 654-662.

9- Furchner, J.E.; Richmond, C.R. and Drake, G.A. (1968). Comparative metabolism of radionuclides in mammals–IV. Retention of silver-110 m in the mouse, rat, monkey, and dog. Health Phys., 15:505-514.

10. Creasey, M. and Moffat, D.B (1973). The deposition of ingested silver in the rat kidney at different ages. Experientia, 29:326-327.

11. Moffat, D.B. and Creasey, M. (1972). The distribution of ingested silver in the kidney of the rat and of the rabbit. Acta Anat., 83:346-355.

12. Day, W.A. ; Hunt, J.S. and McGiven, A.P. (1976). Silver deposition in mouse glomeruli. Pathology, 8:201-204.

13-Ham, K.N. and Tange, J.D. (1972). Silver deposition in rat glomerular basement membrane. Aust. J. Exp. Biol. Med. Sci., 50:423-434.

14. Danscher, G. (1981). Light and electron microscopic localization of silver in biological tissue. Histochemistry, 71:177-186.

15- Kim, J.S.; Kuk, E.; Yu, K.N.; Kim, J.H.; Park, S.J.; Lee, H.J.; Kim, S.H.; Park, Y.K.; Park, Y.H.; Hwang, C.Y.; Kim, Y.K.; Lee, Y.S.; Jeong, D.H. and Cho, M.H. (2007). Antimicrobial effects of silver nanoparticles. Nanomedicine, 3:95-101.

16- Sung, J. H.; Ji, J. H.; Park, J. D.; Yoon, J. U.; Kim, D. S.; Jeon, K. S.; Song, M. Y.; Jeong, J.; Han, B. S.; Han, J. H.; Chung, Y. H.; Chang, H. K.; Lee, J. H.; Cho, M. H.; Kelman, B. J. and Yu, I. J. (2009). Subchronic Inhalation Toxicity of Silver Nanoparticles. Toxicol. Sci., 108 (2):452-461.

17- Liu, R.; Yin, L.; Pu, Y.; Liang, G.; Zhang, J.; Su, Y. ; Xiao, Z. and Ye, B. (2009). Plumonary toxicity induced by three forms of titanium dioxide nanoparticles via intra-tracheal instillation in rats. Prog. Nat. Sci., 19: 573–579.

18- Saman, S.; Moradhaseli, S.; Shokouhian, A. and Ghorbani, M (2013) Histopathological effects of ZnO nanoparticles on liver and heart tissues in wistar rats. Adv. Biores., 2: 83- 88

Al-Mustansiriyah Journal of Science
Vol. 27, No 2, 2016

journal homepage:www.mjs-mu.com

Isolation and identification of *Fusarium oxysporum* and *Aspergillus fumigates* from blood specimens in iraq and study efficiency of some plant essential oils

Mohsen H. Risan
College of biotechnology, Al-Nahrain University, Baghdad-Iraq

Articleinfo

Received
10/12/2015
Accepted
25/1/2016

Keywords:
Aspergillus, *Fusarium*, blood, essential oils.

ABSTRACT

Ten blood samples were collected from immunocompromised patients. *Fusarium oxysporum, Aspergillus fumigatus* were isolated and identified based on morphological characteristics which include hyphae, macroconidia, microconidia, conidiophores, conidial color, vesicle, matulae and phialides. Five isolates of *F. oxysporum* (F1-12, F2-13, F3-14, F4-15, F5-16) and four isolates of *A. fumigates* (AS1, AS2, AS3, AS4) were identified. Five types of plant essential oils, peppermint oil, clove oil, cardamom oil, chamomile oil and castor oil were used. Results shown that all plant essential oils at different concentrations inhibit growth of *F. oxysporum* F5-16. Peppermint oil, olive oil and castor oil at highest concentration (35mg/ml) caused highest reduction of mycelail growth (100%) and same at highest concentration (35mg/ml), peppermint, cardamom and chamomile was found most effective (83.4-100%) in reducing mycelia growth of *A. fumigates* AS1, compared with the control.

الخلاصة

تم جمع عشرة عينات دم من مرضى نقص المناعة ، عزل الفطرين *Fusarium oxysporum* و *Aspergillus fumigatus* وتم تشخيصها على أساس خصائص الشكل الخارجي التي تتضمن الخيوط الفطرية (hyphae) والجراثيم الصغيرة (macroconidia) ، والجراثيم الكبيرة والحوامل الكونيدية conidiophores ولون الجراثيم والحويصلة و matulae والذنيبات phialides . تم تشخيص خمس عزلات للفطر *oxysporum F.* (F1-12، F2-13، F3-14، F4-15، F5-16) وأربع عزلات للفطر *A. fumigates* (AS1، AS2، AS3، AS4). استخدمت خمسة أنواع من الزيوت النباتية الأساسية زيت النعناع، زيت القرنفل , زيت الهيل، زيت البابونج وزيت الخروع. اوضحت النتائج ان جميع الزيوت النباتية وبالتراكيز المختلفة ثبطت نمو الفطر *F. oxysporum* F5-16. زيت النعناع وزيت الزيتون وزيت الخروع في تركيز (35 ملغم / مل) سببت خفض مرتفع لنمو الغزل الفطري بلغ 100% وبنفس التركيز اظهرت زيوت النعناع والهيل والبابونج فعالية عالية للتثبيط النمو للفطر *A. fumigates* AS1 , اذ بلغ التثبيط (83.4-100%) مقارنة مع معاملة السيطرة .

INTRODUCTION

The genus *Fusarium* belongs to the Ascomycota phylum, Ascomycetes class, Hypocreales order, while the teleomorphs of *Fusarium* species are mostly classified in the genus *Gibberella*. *Fusarium* species produce three types of spores: macroconidia, microconidia and chlamydospores. Septated macroconidia can be produced on monophialides and polyphialides in the aerial mycelium. Microconidia can vary in shape and size, and are produced in the aerial mycelium in clumps or chains, both on monophialides and polyphialide. Finally, chlamydospores are resistance structures with thickened walls and high lipid content; in the case of their presence, they can form in the middle of the hyphae or at their termini [1, 2].

Some species are known to cause diseases of humans such as onychomycosis (nail infections), keratomycosis of the cornea, ulcers, necroses, skin infections and fatal infections of internal organs, especially in immunocompromised patients [3]. Mycotoxins produced by some species of *Fusarium* affect on human and animal health. The main toxins produced by these *Fusarium* species are fumonisins and trichothecences, zearalenone and vomitoxin. [4]. Zearalenone, an oestrogenic hormone from *F. graminearum*, causes vulvovaginitis and infertility in cattle and pigs, and trichothecenes such as T-2 toxin from several other *Fusarium* species cause toxic aleukia (reduction in white blood cell count) in farm animals and humans [5].

Fusarium colonies are usually fast growing, pale or brightly colored (depending on the species). Its color of the thallus varies from whitish to yellow, brownish, pink, reddish or lilac shades. [4, 5]. The aerial mycelium of *F. oxysporum* first appears white, then may change to a variety of colors, ranging from violet to dark purple, according to the strain (or special form) [6]. The most frequent cause of human infections is *F. solani, F. oxysporum, F. moniliforme, F. proliferatum, F. chlamydosporum, F. anthophilum, F. dimerum, F. sacchari, and F. erticillioides* [7-11]. *Aspergillus fumigatus* is considered to be an

opportunistic pathogen to immunocompromised individuals, it is an important pathogen of humans and animals. [12]. Because spread of antibiotic resistant pathogens is one of the most serious menaces to successful treatment of microbial diseases [13]. Therefore, present study was undertaken to isolate, identify *Fusarium oxysporum* and *Aspergillus fumigatus* from blood and study efficiency of plant essential oils in laboratory.

Materials and Methods

Collection of samples

Ten blood samples were collected from the National center of hematology - University of Al - Mustansiriya, Baghdad. Of immunocompromised patients and during the period between January 2014 to June 2014, in age ranging 15-55 years. All samples were kept at 4 °C before use.

Isolation of *Fusarium oxysporum* and *Aspergillus fumigates* from blood specimens

Fusarium oxysporum and *Aspergillus* spp were isolated from blood specimens by the method of [14]. Using Sabourauds Dextrose agar (SDA: 40 g dextrose, 10g peptone, 20 g agar, in 1 L distilled water) with added chloramphenicol 250 mg/1L [15]. Spread 1 ml blood was cultured on SDA plates and incubated at 28 °C for 7 days and purified *Fusarium oxysporum* and *Aspergillus* spp colonies were subsequently subcultured on SDA medium.

Morphological identification of fungi

Fusarium oxysporum isolates were grown on 9 cm plates on SDA, for 7 days at 28 °C. Colonies growth rates and microscopic feature were examined. Species was identified based on specific keys described by [1, 16, 17, 3, 18]. Identification of *Fusarium* species is depend on shape and size of conidia and colony colour) through, colony growth diameters, culture pigmentation and microscopic morphology including shape of the macroconidia; presence or absence of microconidia; shape and mode of formation of microconidia; nature of the conidiogenous cell bearing microconidia; and presence or absence of chlamydospores.

Aspergillus spp isolates were purified and diagnosed by taxonomic features mentioned in [14].

Plant essential oils

Five types of plant essential oils, peppermint oil, clove oil, cardamom oil, chamomile oil and castor oil were used, producer from ALEmad company - Iraq. The oils were 100% pure according to the manufacturers and were obtained from Pharmacies, use 100 ml of each oil. Oils were kept in dark bottle till used.

Determination of Essential oils activity

Essential oils of peppermint oil, clove oil, cardamom oil, chamomile oil and castor oil, were mixed alone with Tween 80 (0.05%). Dilute oils with ethanol 70% to give concentrations 15, 25 and 35 mg/ml. 1 ml of each concentration was spread on 20ml of Sabourauds Dextrose agar plates. Then dishes were inoculated by disc diameter 0.5 cm of fungi at a rate of one disc in the center of each dish and concentration. The plates were incubated at 28°C for one week. Calculated inhibition through taking the colony diameter in cm by taking the radial growth rate of two diagonals perpendicular to the colonies growth upon the arrival of each fungus growth to the edge of the dish in the control treatment and, A ruler used to measure the radial growth, calculated inhibition by the equation. The two readings were used to calculate percentage inhibition of radial growth using the formula developed [3].

$$\text{Inhibition } \% = R1 - R2 / R1 \times 100$$

Where R1: maximum radial growth of the pathogenic fungus colony of control treatment.
R2: maximum radial growth of the pathogenic fungus colony In dishes containing inoculate plant oils .

RESULTS AND DISCUSSION

Morphological identification

Five *Fusarium oxysporum* isolates (F1-12, F2-13, F3-14, F4-15, F5-16) were identified based on cultural and microscopic characteristics. Using identification keys by [1, 16, 17, 3, 18]. The identified isolates were deposited in Mycology laboratory, Dept. biotechnology, Al-Nahrain University (Table 1).

Fusarium oxysporum isolates showed rapid growth rates (5-7cm/5 days). *F. oxysporum* colonies were white and growing rapidly, conidiophores are short, single, lateral monophialides in the aerial mycelium. Macroconidia are fusiform, mostly three septate. Microconidia are abundant, never in chains, mostly non-septate, ellipsoidal to cylindrical, Chlamydospores are terminal or intercalary, hyaline, smooth or rough-walled. Results agrees with [1, 17].

Four *Aspergillus fumigates* isolates (AS1, AS2, AS3, AS4) were identified, using identification keys by [14]. (Table 1). *A. fumigates* colonies show typical blue-green surface pigmentation with a suede-like surface consisting of a dense felt of conidiophores. Conidial heads are typically columnar and uniseriate. Conidiophore stipes are short, smooth-walled and have conical-shaped terminal vesicles which support a single row of phialides on the upper two thirds of the vesicle [19].

Table 1. Isolated of *Fusarium oxysporum* and *Aspergillus fumigates* isolated from blood samples

Isolate number	Fungal isolates	Isolates
5	*F. oxysporum*	F1-12, F2-13, F3-14, F4-15, F5-16
4	*A. fumigatus*	AS1, AS2, AS3, AS4

Fusarium species most frequent cause of human infections as *F. solani* but *F. oxysporum, F. moniliforme, F. proliferatum, F. chlamydosporum, F. anthophilum, F. dimerum, F. sacchari, and F. verticillioides* have also been implicated. [7-11].

Fusarium species possess several virulence factors, including the ability to produce mycotoxins such as trichothecenes, which suppress humoral and cellular immunity and may also cause tissue breakdown.

Fusarium species have the ability to adhere to prosthetic material and to produce proteases and collagenases. [17]. The clinical form of fusariosis depends largely on the immune status of the host. *Fusarium* species cause a broad spectrum of infections in humans, as superficial infection and locally invasive. Risk factors for severe fusariosis include prolonged neutropenia and T-cell immunodeficiency, especially in hematopoietic stem cell transplant recipients with severe graft-versus-host disease. [20]. Isolate [21]. *Fusarium* species from blood and tissues. Pathogenicity of *A. fumigatus* associated with invasive aspergillosis has been attributed to the production of proteolytic enzymes by these strains. However, conclusive evidence to substantiating the involvement of specific *A. fumigatus* strains in different clinical conditions [22].

Determination of Essential oils activity

Selected isolation F5-16 of *F. oxysporum* and isolation AS1 of *A.fumigatus* because of its growth rapid therefore used in subsequent experiments. Results shown (Table 2) that all plant essential oils at different concentrations significantly inhibit growth of *F. oxysporum* F5-16.

However, the peppermint oil, olive oil and castor oil at highest concentration (35mg/ml) caused highest reduction of mycelail growth (100%) followed by cardamom oil (81.1%), and chamomile oil (31.1%) at the same concentration, compared with the control treatment.

Table 2. Percent inhibition of radial mycelial growth of *F. oxysporum* F5-16 colonies by plant essential oils after 7 dayes.

*Con.	% I. F.					
(mg/ml)	Peppermint	Olive	Cardamom	Chamomile	Castor	Control
15	51.1	71.1	57.7	12.2	61.1	
25	76.6	86.6	75.5	24.4	84.4	100
35	100	100	81.1	31.1	100	

*** Con. : Concentration of plant essential oil; I. F. : Inhibition of fungus**

It was also observed from the study table (3) that amongst the plant essential oils at highest concentration (35mg/ml), peppermint, cardamom and chamomile was found most effective (83.4-100%) in reducing mycelia growth of A. fumigates AS1 followed by olive (61.2%) and castor (47.7%), Compared with the control.

Table (3) Percent inhibition of radial mycelial growth of A. fumigates AS1 colonies by plant essential oils after 7 dayes.

*Con.	% I. F.					
(mg/ml)	Peppermint	Olive	Cardamom	Chamomile	Castor	Control
15	44.4	24.4	48.8	55.8	20.0	
25	77.7	51.1	66.6	83.9	33.3	100
35	100	61.2	83.4	100	47.7	

*** Con. : Concentration of plant essential oil; I. F. : Inhibition of fungus**

Similar finding were reported by [23]. In this study indicates that b-caryophyllene and caryophyllene oxide detected in Bidens pilosa essential oils may play an important role in antifungal activities F. oxysporum, F. solani. On the other hand, the fungitoxic activities of the flower essential oils were higher than those of the leaves. The mechanism of antifungal activity of these essential oils is still unknown [23]. Suprapta and Khalimi [24]. show that five plant species namely Albizia saman, Piper betle, Syzygium aromaticum, Sphaeranthus indicus and Alpinia galangal exhibited strong antifungal activities. The minimum inhibitory concentration (MIC) of the tested plants varied from 2 mg/ml to 13 mg/ml, however, the extract of Albizia saman showed the lowest MIC (2 mg/ml) against all tested isolates (LS05, LS14) of F. oxysporum f.sp. capsici. In study, 16 essential oils (Cinnamomum zeylanicum (Cinnamon), Syzygium aromaticum (Clove), Carum carvi (Caraway), Cymbopogon citrates (Lemongrass), Foeniculum vulgare (Fennel) and Myristica fragrans (Nutmeg). Moderately effective oils were of Gaultheria procumbens (Wintergreen), Pinus palustris (Turpentine), Sesamum indicum (Sesame), Trachyspermum ammi (Ajowain) and Origanum vulgare (Oregano). The oils of Lavandula augustifolia (Lavender), Elletaria cardamomum (Cardamon) and Cymbopogon nardus (Citronella) showed minimum activity. Azadirachta indica (Neem) and Linum usitatissimum (Linseed)) were used against Aspergillus niger and A. fumigatus of which about 14 oils proved to be effective. Essential oils been used as antifungal, anti-infectious and antimicrobial agents. Inhalation of vapours of the essential oils kill invaders attached to the inner respiratory lining and work synergistically with the body defences. [25]. Plants Ficus septica, F. syocomorus, F. benjamina, F. religiosa, F. racemosa, F. pumila, F. vasta, F. thonningii, F. capensis and F. bengalensis could inhibit the growth of Fusarium spp. with diameter of inhibition zone by 14 mm [26]. Different Concentration of methanolic extract (6.25, 12.5, 25, 37.5, 50, 62.5 µg/ml) of Semecarpus anacardium were tested against four

fungal strains namely F. oxysporum, Rhizctonia solani, Alternaria spp., and Sclerotium rolfsii. The excellent inhibitory activity was observed against R. solani (100%) followed by S. rolfsii (92.59 %), Alternaria spp. (72.34 %) and F. oxysporum (47.19 %) at 62.5 µg/ml [13].

Conclusions:

The present study concluded that Peppermint oil, olive oil and castor oil) inhibit growth of F. oxysporum F5-16., at highest concentration (35mg/ml) and same at highest concentration (35mg/ml), peppermint, cardamom and chamomile oils was found most effective in reducing mycelia growth of A. fumigates AS1.

References:

1. Booth, C. Fusarium: Laboratory Guide to the Identification of The Major Species. Commonwealth Mycological Institute, Kew, Surrey, England. 1977

2. Moretti, N. A. Taxonomy of Fusarium genus: A continuous fight between lumpers and splitters . Zbornik Matice srpske za prirodne nauke, ; (117): 7–13. 2009

3. de Hoog, G. S. ; Guarro, J. ; Gene, J. and Figueras, M. J. Atlas of Clinical Fungi (second edition). Centraalbureau voor Schimmelcultures, Utrecht, The Netherlands. 2000

4.Elliott, M. L. First report of Fusarium wilt caused by Fusarium oxysporum f. sp. palmarum on canary island data palm in florida. plant diseases 96: 356. 2012

5. Moss, M. O. Mycotoxin review-2. Fusarium. Mycologist, 16: 158-161. 2002.

6. Smith, I. M. ; Dunez, J. ; Phillips, D. H. ; Lelliott, R. A. and Archer, S. A. European Handbook of Plant Diseases. Blackwell Scientific Publications: Oxford. 583pp. 1988.

7. Boutati, E. I. and Anaissie, E. J. Fusarium, a significant emerging pathogen in patients with hematologic malignancy: ten years' experience at a cancer center and implications for management. Blood, 90: 999. 1997.

8. Krcmery, V. J. ; Jesenska, Z. and Spanik, S. Fungaemia due to Fusarium spp. in cancer patients. J. Hosp. Infect., 36: 223. 1997

9. Guarro J, Nucci M, Akiti T, Fungemia due to Fusarium sacchari in an immunosuppressed patient. J. Clin. Microbiol. 38:419. 2000a.

10. Guarro, J. ; Nucci, M. ; Akiti, T. and Gene, J. Mixed infection caused by two species of Fusarium in a human immunodeficiency virus-positive patient. J. Clin. Microbiol. 38: 3460. 2000b

11.Austin, B. ; McCarthy, H. ; Wilkins, B. ; Smith, A. and Duncombe, A. Fatal disseminated Fusarium infection in acute lymphoblastic leukaemia in complete remission. J. Clin. Pathol., 54: 488-490. 2005

12. Latgé, J. P. Aspergillus fumigatus and aspergillosis. Clin. Microbiol. Rev., 12 : 310–350. 1999

13. Jain, P. ; Singh, S. K. ; Sharma, H. P. and Basri, F. Phytochemical screening and antifungal activity of Semecarpus anacardium l. (ananti-cancer plant). I. J. P. S. R. 5(5): 1884-1891. 2014.

14. Pitt, J. I. and Hocking, A. D. Fungi and Food Spoilage. 3rd edition, Springer New York, USA, pp. 540. 2009

15. Guy, S. G. and Summerbell, R. C. Identifying fungi: a Clinical Laboratory Handbook, 2nd ed, English Belmont: Star Publishing Company. 2011

16. Domsch, K. H. ; Gams, W. and Anderson, T. H. Compendium of soil fungi. V1. Academic Press. 1980

17. Nelson, P. E. ; Dignani, M. C and Anaissie, E. J. Taxonomy, biology, and clinical aspects of Fusarium species. Clin. Microbiol. Rev. 7 : 479. 1994

18. Leslie, F. J. and summerell, A. B. The Fusarium Laboratory Manual. P: 212-218. 2006.

19. Ellis, D. ; Davis, S. ; Alexiou, H. ; Handke, R. and Bartley, R. Descriptions of medical fungi, second edition, p. 61-167. 2007

20. Nucci, M. and Anaissie, E. Fusarium infections in immunocompromised patients. Clin. Microbiol. Rev. 20(4): 695-704. 2007

21. Hue, F.X. ; Huerre, M. ; Rouffault, M. A. and de Bievre, C. Specific detection of Fusarium species in blood and tissues by a PCR technique. J. Clin. Microbiol., 37: 2434-8. 1999.

22. García, M. E. ; Blanco, J. L. and Kurup, V. P. Immunochemical reactivity of Aspergillus fumigates antigens from different sources Rev. Iberoam. Micol., 14: 55-59. 1997.

23. Deba, F. ; Xuan, T. D. ; Yasuda, M. and Tawata, S. Chemical composition and antioxidant, antibacterial and antifungal activities of the essential oils from Bidens pilosa Linn. var. radiata. Food Control, 19: 346-35. 2008.

24. Suprapta, D. N. and Khalimi, K. Anti-fungal activities of selected tropical plants from Bali Island. Phytopharmacology 2 (2), 265-270. 2012

25. Uniyal, V. ; Bhatt, R. P.; Saxena, S. and Talwar, A. Antifungal activity of essential oils and their volatile constituents against respiratory tract pathogens causing Aspergilloma and Aspergillosis by gaseous contact. J. Apppl. Nat. Sci. ence 4(1): 65-70. 2012

26. Hossain, S. and Shahadat, M. In vitro antimicrobial activity of ethyl acetate extract of Ficus bengalensis Lam. Inter. J. Pharm. Hytochemical Res. 6(1): 56-58. 2014

Al-Mustansiriyah Journal of Science
Vol. 27, No 2, 2016

journal homepage:www.mjs-mu.com

Efficiency of Lactic Acid Bacteria as biological control agents against some Fungi

Rana Hadi Al-Shammari , Huda Zuheir Majeed
Department of Biology, College of Science, University of Al-Mustansiriyah

Articleinfo

Received
1/9/2015
Accepted
21/12/2016

ABSTRACT

In this study, Lactic Acid Bacteria (*Lactobacillus fermentum* , *Lactobacillus reuteri* , *Lactobacillus* sp. no.1, *Lactobacillus* sp.no.2 and *Lactococcus* sp.) were screened *in vitro* for antifungal activity against (*Fusarium oxysporum* , *Phytophthora infestans* , *Pythium ultimum* and *Alternaria* sp.).The inhibition ratio was (100 %) on the MRS(Man, Rogosa, Sharpe) agar for all the LAB isolates against all fungi used at both 30 °C and 37 °C for 5 days . On the other side, all LAB had significantly high inhibition ($P< 0.05$) on PDA (Potato Dextrose Agar) medium at 37 °C than that at 30 °C for 5 days .

The results of the Overlay assay showed that the five LAB used inhibit the growth of all fungi used by more than > 8 % of plate area except by more than > 8 % of plate area except *L. fermentum* inhibit *Alternaria* sp. by (3-8) % of the plate area and *Lactococcus* showed no visible inhibition against *Fusarium oxysporum* at $30C^0$.

The statistical analysis of antifungal activity of LAB cell-free supernatant showed significant differences ($P<0.05$) after 24 h against all fungi used. The LAB have shown that there were high significant inhibition ($P<0.05$) on MRS agar than on PDA agar. This study led to suggest that food-derived LAB strains could be selected for biotechnological application to control phytopathogenic fungi.

الخلاصة

في هذه الدراسة تم فحص فعالية السلالات التالية من بكتريا حامض اللبنيك(*Lactobacillus fermentum* , *Lac.* *reuteri* , *Lactobacillus* sp. no.1, *Lactobacillus* sp.no.2 and *Lactococcus* sp. في المختبر ضد الفطريات التالية (*Fusarium oxysporum* and *Pythium ultimum* , *Phytophthora infestans* sp. *Alternaria*) . اعطت جميع عزلات البكتريا تثبيط كامل 100% في وسط (Man, Rogosa, Sharpe) MRS ضد جميع اجناس الفطريات المستخدمه عند درجتي الحرارة (30و37) م° لمدة خمسة ايام حضانة بالاضافة الى ذلك كان التثبيط اعلى معنويا" عند مستوى($P<0.05$) على وسط دكستروز البطاطا في درجة حرارة 37م° منه في درجة30م° لمدة خمسة ايام حضانة.

كما اظهرت نتائج فحص التشابك او التراكب Overlay assay ان جميع عزلات بكتريا حامض اللبنيك ثبطت نمو جميع الفطريات بواقع اكثر من 8 > % من مساحة الطبق عدا *Lactobacillus fermentum* التي ثبطت الفطر *Fusarium oxysporum* بـ(3-8)% من مساحه الطبق و *Lactococcus* التي لم تعطي اي تثبيط بدرجة 30 م° ضد *Fusarium oxysporum* .

اظهرت نتائج التحليل الاحصائي ان هناك فروق معنوية عند مستوى ($P<0.05$) في تثبيط جميع الفطريات المستخدمة عند استخدام راشح بكتيريا حامض اللبنيك بعد 24 ساعة من الزراعة اذ كان التثبيط اعلى معنويا" عند مستوى ($P<0.05$) على وسط (MRS) منه على وسط دكستروز البطاطا .

هذه الدراسة تقودنا لاقتراح استخدام بكتريا حامض اللبنيك المعزولة من الغذاء في تطبيقات السيطرة البايولوجية ضد الفطريات الممرضة للنبات.

INTRODUCTION

Some fungi are pathogenic for many economically important plants and most of them are soil borne fungi like *Fusarium oxysporum*, *Phytophthora infestans* ,*Pythium ultimum* , and *Alteraria* sp.[1-4]. Many physical and chemical methods have been developed inhibiting of fungi for many years.

The search for alternative bioproducts to replace chemicals and toxic pesticides, has found growing interest in recent years because the extensive use of synthetic chemicals and pesticides in food and agriculture pose a health risk for human and animals and affect the ecological equilibrium of the environment [5]. For this purpose, using bacteria or natural compounds which exhibit the same inhibitory effect on pathogenic and spoilage microbes was not only shown to be efficient in storage life extension and nutritive and safety

value retention, of food products but also the environment safeguarding [6].

Lactic Acid Bacteria (LAB) contribute technological and nutritional properties and influence the food. They also extend the microbiological shelf-life of final products. LAB produce antimicrobial compounds which can act as food preservatives. Biopreservation refers to extended shelf life and enhanced safety of foods gained by the natural or added microflora or their antimicrobial products [7]. LAB have traditionally been used as natural biopreservatives in food and animal feed. Using microorganisms in order to control the fungi growth appears as a good alternative [8].

LAB are a group of Gram-positive, non-spore forming, not motile and catalase negative bacteria, which excrete lactic acid as major end product [9]. They are also selected as probiotic, which are able to promote health and prevent infections against enteropathogenic bacteria [10]. LAB have been studied for their inhibitory action against different microbes but not well established yet. Antagonistic activity of LAB is connected with the inhibitory compounds they produce. Metabolites with inhibitory properties include lactic acid, hydrogen peroxide and bacteriocins [11]. LAB have been reported to show antagonistic properties against pathogenic microorganisms .Therefore it is possible to use LAB as biopreservative.

The objective of this study was to evaluate the antifungal activity of LAB in different degrees of temperature. Further, LAB and their products can be applied as biological control agents.

Materials and methods

Fungi and LAB isolates

The antagonistic activity in this study tested between the fungi (*Fusarium oxysporum* , *Phytophthora infestans* , *Pythium ultimum* and *Alternaria* sp.) which were isolated from soil and examined under microscope diagnosis based on morphological features of the spores and colonies depending on the taxonomic keys [12-14] and 22 Species of lactic acid bacteria isolated from local cheese, cereal, yoghurt and sourdough were tested to their ability to suppress fungi. LAB were identified depending on [15] .

Comparison of the antifungal activity of LAB on PDA medium and MRS Agar

Dual method used which is described by [16] with few modifications. LAB cells were streaked on PDA (Difco/ USA) medium and MRS agar (Hi-Media/ India) plates, in two streak parallels of 2 cm, and were incubated for 48 h at 30°C and 37°C , and then the center of the same plates containing LAB was inoculated with *Fusarium oxysporum* , *Phytophthora infestans* , *Pythium ultimum* and *Alternaria* sp. isolated from the colony edge after 7 days incubation on PDA media with a standard cork borer (5 mm of disc).

Plates were incubated at 30°C and 37°C for 5 days, after incubation inhibition percentage of fungal growth was calculated according to [17] by measuring the distance between the edges of fungal colonies and bacteria as the formula:

$$\text{Inhibition percentage \%} = \frac{C - T}{C} \times 100$$

C: radial growth of the fungus in control
T: radial growth in dual culture

Overlay assay

The method used is the one described by [18] with few modifications. LAB were inoculated in two 2 cm lines on 15 ml of MRS agar plates and allowed to grow at 30°C for 48 h in anaerobic jars. The plates were then overlaid with 10 ml of soft PDA prepared with (0.7) % agar, containing (10^3) spores per ml (Zoospores counted on the haemocytometer slide (Neubauer improved))of *Fusarium oxysporum* , *Phytophthora infestans* , *Pythium ultimum* and *Alternaria* sp. . After 72 h of aerobic incubation at 30°C and 37°C, the inhibition zones around the bacterial streaks were measured and scored as follows: - = no visible inhibition, += no fungal growth on (0-(1–3)) % of petri dish area, ++ =no fungal growth on (3–8) % of petri dish area, +++ = no fungal growth on >8 % of petri dish area.

Determination of the antifungal activity of LAB cell-free supernatant

The method used is the one described by [19] with few modifications. Cell free supernatants of the LAB isolates were obtained by centrifuging at 8000 g for 10 mins, MRS broth cultures of 24 h anaerobic incubation at 30°C, and then sterilized of the supernatant by passing through millipore filter (0.22 µm in diameter).

According to well diffusion method the antifungal activity of LAB cell free suspension was determined by adding 100 µl of cell free supernatant was spotted onto the well in the surface of PDA agar which had been inoculated with 0.1 ml of a mould spore suspension (10^3) spores/ml. After incubation of the plates for three days at 30°C, the zones of fungal inhibition were examined.

Statistical analyses

In all tests, the standard deviations (SD) of the means were calculated. All the statistical analyses were performed using SPSS Statistics 17.0 software [20]. The data were analyzed using a two-way analysis of variance (ANOVA), and the significant means compared using Duncan's test, ($P<0.05$) was considered statistically significant.

Results and Discussion

Only five species showed the antagonistic activity which are (*Lactobacillus fermentum* , *Lactobacillus reuteri* , two of *Lactobacillus* sp. and *Lactococcus* sp.) .A comparative analysis of the inhibition of LAB strains on PDA and MRS agar are shown in Figure 1,2 and 3 , where the radial growth of the tested fungi are

significantly lower than those of the control plates ($P<0.05$). The results of the direct confrontation assay of LAB against fungi on modified MRS agar and PDA media (Figures1,2 and 3) showed that there is a better inhibition by the LAB on modified MRS agar this result agreed with[19] .

According to the obtained results which shown in (Table 1,2,3 and 4) we see that the inhibition ratio is (100 %) on the modified MRS agar for all the LAB strains against *Fusarium oxysporum* , *Phytophthora infestans* , *Pythium ultimum* and *Alternaria* sp. at both 30 C° and 37 C° . On the other side, All Lactic Acid Bacteria had significantly high inhibition on PDA medium at 37 C° than that at 30 C° ($P<0.05$) ,in this study we used 30 C° as mean of 25 C° which optimum for fungi and 37C° which optimum for bacteria, this results agreed with[21,22] they conform the antifungal activity of LAB against *Fusarium* spp. at 30C°.

The antifungal activity of LAB is a complex phenomenon, where different many compounds act synergistically against organisms. Further studies will unravel the identity of the compounds responsible for the antifungal activity of *Lactobacillus brevis* which make it easier to estimate the potential of the strain to serve e.g. as a biopreservative against the growth of the fungus *Fusarium* during food processing or as a biological agent to control *Fusarium* [21],they found that the inhibition was 100 % on the MRS agar for all LAB strains against *Fusarium oxysporum* [22], this was explained due to the existence in this medium of compounds which would activate or act in synergy with the entities produced by LAB strains . These hypotheses were the same conclusions of certain authors [23], they found that certain compounds of MRS would influence the antifungal activity of LAB, such as the replacement of the glucose by the sorbitol, mannitol and trehalose [24].

Fermentation of some foods by LAB is one of the oldest forms of biopreservatrion especially by mankind. Bacterial antagonism has been recognized for over a century, but in recent years this phenomenon has gained more scientific attention, particularly the use of many strains of Lactic Acid Bacteria. LAB has a broad spectrum of antagonistic activity against microorganisms, mainly through production of metabolites such as lactic acid, hydrogen peroxide and bacteriocins [25].

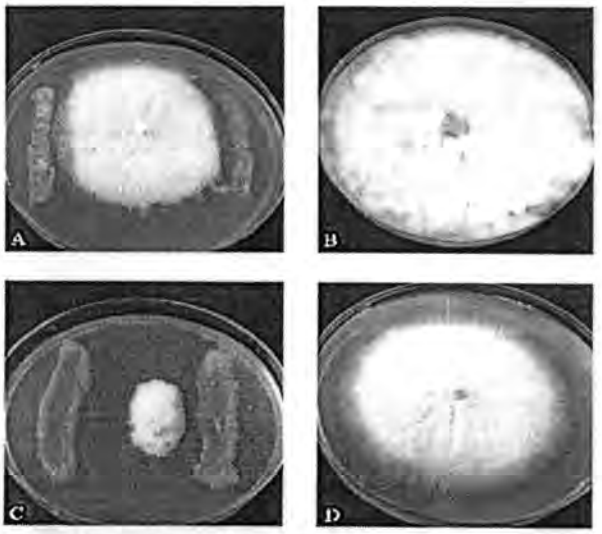

Figure 1: Antifungal activity of Lactobacillus against *Fusarium oxysporum*
(A) dual culture on PDA (B) PDA control (C) dual culture on MRS (D) MRS control after incubation at 30°C for 5 days

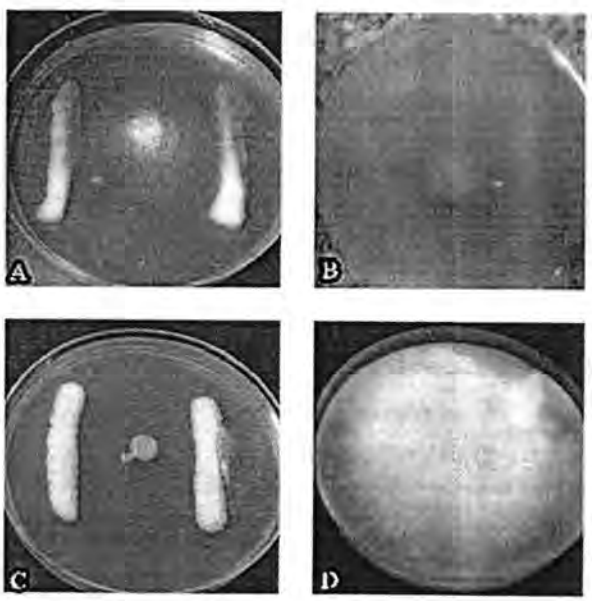

Figure 2: Antifungal activity of *Lactobacillus* against *Pythium ultimum*
(A) dual culture on PDA (B) control PDA (C) dual culture on MRS (D) control MRS after incubation at 30°C for 5 days

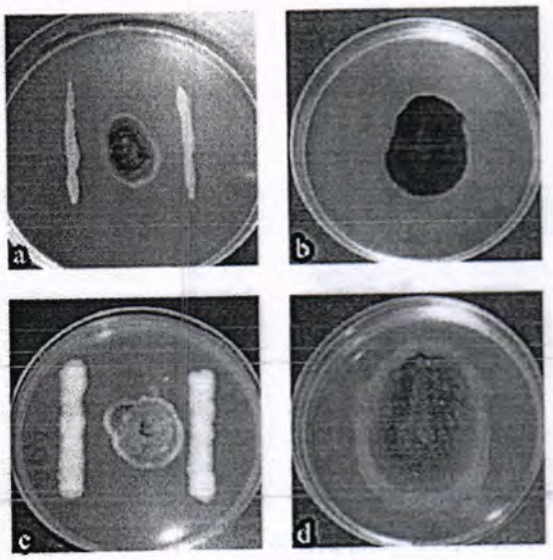

Figure 3: Antifungal activity of *Lactobacillus* against *Alternaria* sp.
(A) dual culture on PDA (B) control PDA(C)dual culture on MRS (D) control MRS after incubation at 30°C for 5 days

Table 1: Inhibition Percentages of *Fusarium oxysporum* by LAB.

Lactic Acid Bacteria	Inhibition%			
	MRS agar		PDA agar	
	30°C	37°C	30°C	37°C
Lactobacillus fermentum	100	100	29	55
Lactobacillus sp.1	100	100	11	15
Lactobacillus sp.2	100	100	13	33
Lactobacillus reuteri	100	100	38	51
Lactococcus sp.	100	100	21	55

Table 2: Inhibition Percentages of *Phytophthra infestans* by LAB.

Lactic Acid Bacteria	Inhibition%			
	MRS agar		PDA agar	
	30°C	37°C	30°C	37°C
Lactobacillus fermentum	100	100	33	57
Lactobacillus sp.1	100	100	21	67
Lactobacillus sp.2	100	100	42	77
Lactobacillus reuteri	100	100	29	82
Lactococcus sp.	100	100	37	38

Table 3: inhibition percentages of *Pythium ultimum* by LAB.

Lactic Acid Bacteria	Inhibition%			
	MRS Agar		PDA Agar	
	30°C	37°C	30°C	37°C
Lactobacillus fermentum	100	100	21	55
Lactobacillus sp.1	100	100	31	75
Lactobacillus sp.2	100	100	23	68
Lactobacillus reuteri	100	100	18	85
Lactococus sp.	100	100	28	95

Table 4: inhibition percentages of *Alternaria* sp. by LAB.

Lactic Acid Bacteria Isolates	Inhibition%			
	MRS Agar		PDA Agar	
	30°C	37°C	30°C	37°C
Lactobacillus fermentum	100	100	33	65
Lactobacillus sp.1	100	100	39	80
Lactobacillus sp.2	100	100	10	73
Lactobacillus reuteri	100	100	22	82
Lactococus sp.	100	100	38	93

The results of the Overlay assay illustrated in (Table 5), show that the five LAB used inhibit the growth of *Fusarium oxysporum* , *Phytophthora infestans* , *Pythium ultimum* and *Alternaria* sp. by more than > 8 % of plate area except *L. fermentum* inhibit *Alternaria* sp. by (3-8) % of the plate area and *Lactococcus* showed no visible inhibition against *Fusarium oxysporum* , this was compatible with [22]. LAB bacteria cells and their supernatant in liquid and solid medium showed strong antifungal activity against the fungi *Phytophthora infestans* and *Aspergillus oryzae* [26, 27]. A total of 22 lactic acid bacteria isolated from Tarhana and LAB were screened for antifungal activity using dual agar overlay method and well method against *Aspergillus fumigatus*, *A. oryzae*, *A. parasiticus*, *Alternaria alternata Penicillium griseofulvum, P. chrysogenum, P. notatu, P. citrinum, P. roquefort*. Supernatant of 10 isolates with strong antifungal activity was evaluated by well method and they inhibited the growth of the fungi at 30°C for 72 h. *Alternaria* sp. was the most sensitive strain in dual-culture agar overlay methods [28], this was compatible with the present study. *L. rhamnosus* reported to inhibit the growth of *Aspergillus, Penicillium* and *Fusarium* [29]. LAB isolated from fermented guava juice inhibited the spore germination and mycelia growth of *A.oryzae* [27].

Table 5: Antifungal activity of LAB by overlay assay.

Fungi Isolates / Lactic Acid Bacteria Isolates	*Fusarium oxysporum*		*Phytophthra infestans*		*Pythium ultimum*		*Alternaria sp.*	
	30°C	37°C	30°C	37°C	30°C	37°C	30°C	37°C
L. fermentum	+++	+++	+++	+++	+++	+++	+++	++
Lactobacillus sp.1	+++	+++	+++	+++	+++	+++	+++	+++
Lactobacillus sp.2	+++	+++	+++	+++	+++	+++	+++	+++
L. reuteri	+++	+++	+++	+++	+++	+++	+++	+++
Lactococcus sp.	-	+++	++	+++	+++	+++	++	+++

+++ = no fungal growth on > 8 % of petri dish area
- = no visible growth.

The antifungal activity of LAB cell-free supernatant as indicated in (Table 6), there is antifungal activity by cell-free supernatant after 24 h against *Fusarium oxysporum* , *Phytophthora infestans* , *Pythium ultimum* and *Alternaria* sp. except *Lactococcus* against *Fusarium oxysporum* at $30C^0$. The antifungal activity of cell-free supernatant of LAB strains was explained due to LAB production metabolites that inhibit the growth of *Fusarium oxysporum* [22].

When we used cell-free supernatant, there was appearance of inhibition zones after 24h of incubation (Figure 4) and the significant differences between inhibition zones shown in (Table 7) as seen *Alternaria* sp. the most sensitive to LAB cell-free supernatant among other fungus, the same observations were made by [30], whereas [31] reported an antifungal activity after 48 h.

The growth of conidia and mycelia of *Asp. oryzae* were inhibited by the supernatant of the LAB isolates by the well method, The isolates identified as *Pediococcus pentosaceus* , *L. fermentum*, and *L. pentosus* [27].

Figure 4: Inhibition of fungi growth with LAB cell-free supernatant after 24 h of incubation.

1: *Lactobacillus fermentum* , 2: *Lactobacillus* sp.1, 3: *Lactobacillus* sp.2. 4: *L. reuteri* 5: *Lactococcus* sp. (A) *Fusarium oxysporum*, (B) *Phytophthora infestans*, (C) *Pythium ultimum*,(D) *Alternaria* sp.

No antifungal activity was detected by [18]. What tends to suggest, the high power of the antifungal compounds of our LAB strains. The antifungal activity by cell-free supernatant was also observed on *Aspergillus niger*, *Aspergillus tubingensis* and *Penicillium crustosum* by [32], and on *Weissella* by [33], who also measured a strong inhibitory activity. Other studies revealed [34] suggested that some soluble compounds in culture supernatant may be responsible for inhibition of *Candida* albicans, Also [35] observed that cells and supernatant can be used together to inhibit *Colletotrichum gloeosporioides*. Author [22] observed that the four LAB cells and cell-free supernatant used showed a good antifungal activity against phytopathogen *Fusarium oxysporum*.

Table 6: Antifungal activity of cell free supernatant against fungi.

Lactic Acid Bacteria Isolates \ Fungal Isolates	*Fusarium oxysporum*		*Phytophthora infestans*		*Pythium ultimum*		*Alternaria* sp.	
	30°C	37°C	30°C	37°C	30°C	37°C	30°C	37°C
L. fermentum	-	+++	+++	+++	+++	+++	-	-
Lactobacillus sp.1	-	+++	+++	+++	+++	+++	++	+++
Lactobacillus sp.2	-	+++	+++	++	+++	+++	+	+++
L.reuteri	-	+++	+++	+++	+++	+++	-	+++
Lactococcus sp.	-	+++	+++	+++	+++	+++	++	+++

+++ = no fungal growth on > 8 % of petri dish area
++= no fungal growth on (3-8) % of petri dish area
+= no fungal growth on (0-(1-3)) % of petri dish area
- = no visible growth.

Table 7: Inhibition zone mm (Mean± SD) of LAB cell-free supernatant against fungi .

Lactic Acid Bacteria Isolates \ Fungal Isolates	*Fusarium oxysporum*	*Phytophthora infestans*	*Pythium ultimum*	*Alternaria* sp.
L. fermentum	11.3±0.08 ^{a,A}	12.7 ±0.09 ^{a,A}	18 ±0.12 ^{a,A}	26.3 ±0.12 ^{c,A}
Lactobacillus sp.1	12± 0.06 ^{a,A}	15.8 ±0.05 ^{a,B}	20.3 ±0.23 ^{a,B}	22.1 ±0.05 ^{c,B}
Lactobacillus sp.2	12.3 ± 0.03 ^{a,A}	13.5 ±0.08 ^{a,A}	27.8 ±0.05 ^{b,C}	25.5 ±0.03 ^{c,B}
L.reuteri	15.5 ±0.22 ^{a,B}	16.6 ±0.1 ^{a,B}	15.3 ±0.08 ^{a,A}	27.1 ±0.02 ^{b,A}
Lactococcus sp.	15.2 ±0.32 ^{a,B}	13.5 ±0.19 ^{b,A}	29.2 ±0.11 ^{c,C}	23.3 ±0.05 ^{c,B}

^{a,b,c} means within a row with different coordinating are different significantly ($P< 0.05$).
^{A,B,C} means within a column with different coordinating are different significantly ($P< 0.05$).

Conclusions and Recommendation

More characterization was needed for the products of LAB such as its molecular weight, effect of conditions on its activity, further studies *in vivo* should be carried out to determine the potential of their LAB as a biocontrol against fungi.

References

[1] Messian,C.D. Blancard, F. Rouxel, and Lafon, P. Disease of the market-Gardening Plants. INRA, Paris, France, pp 387.1991.

[2] Fry, W. *Phytophthora infestans*: the plant (and R gene) destroyer. Mol. Plant Pathol., 9: 385-402.2008.

[3] Martin,A. Frank, N. and Loper , E. Soil borne Plant Diseases Caused by *Pythium* spp.: Ecology, Epidemiology, and Prospects for Biological Control. Critical Reviews in Plant Sciences, 18:111-181.1999.

[4] Rotem, J. The genus *Alternaria* biology, epidemiology, and pathogenicity, 1st Ed. The American Phtyopathological Society, St. Paul, Minnesota. 48: 203. 1994.

[5] Huang, J.K. Qiao, F.B. Zhang, L.X. and Rozelle, S. Farm pesticide, rice production and human health. EEPSEA Working Paper, EEPSEA, Singapore. Pp: 67.2000.

[6] Pastor, N. Carlier, E. Andr´es, J. Rosas, S.B. and Rovera, M. Characterization of rhizosphere bacteria for control of phytopathogenic fungi of tomato. J. Env. Man., 95: S332-S337.2012.

[7] Schnürer, J. and Magnusson, J. Antifungal lactic acid bacteria as biopreservatives. Trends in Food Sci. Tech, 16: 70-78.2005.

[8] Dalie ,D.K. Deschamps, A.M. and Richard-Forget, F. Lactic acid bacteria potential for control of mould growth and mycotoxins: a review. Food Control ,21: 370-380.2010.

[9] Konings, W.N. Kok, J. Kuipers, O.P. and Poolman, B. Lactic acid bacteria: the bugs of the active new millennium. Curr. Opi. Microbiol., 3(3): 276-282.2000.

[10] Fern´andez, M.F. Boris, S. and Barb´es, C. Probiotic properties of human lactobacilli strains to be used in the gastrointestinal tract. J. App. Microbiol., 94(3): 449- 455.2003.

[11] Mishira, C. and Lambert, J. Production of anti-microbial substances by probiotics. Asia Pacific . J. Clin. Nut. , 5: 20-24.1996.
[12] Barnett, H.L. and Hunter, B. B. Illustrated genera of imperfect fungi. Burgess Pub. Co., Minneapolis, Minnesota, USA. Barnett H.L. Illustrated Genera of Imperfect Fungi. 2 nd. Ed. Burgess publishing company.1972.
[13] Booth, C. The genus Fusarium-Commonwealth mycological Institute, Kew, Surrey, England. pp. 237.1971.
[14] Watanabe,T. *Pictorial Atlas of* Soil and Seed Fungi. Morphologies of Cultured Fungi and Key to Species .Second Edition . CRC PRESS.pp:506.2002.
[15] Wood , B . J. B. and Holzapfel , W.H. (Eds.) . The Lactic acid bacteria , the genera of lactic acid bacteria ., Vol. 2, Blackie Academic and Professional , London.1995.
[16] Brunner, K. Zeilinger, S. Ciliento, R. Woo, S.L. Lorito, M. Kubicek, C.P. and Mach, R.L. Improvement of the fungal biocontrol systemic disease resistance both antagonism and induction of Plant Agent *Trichoderma atroviride* to Enhance. App. Env. Microbiol. , 71: 3959–3965.2005.
[17] Hammami, I., Trabelsi, H. D. and EL Gazzah, M. *In vitro* screening of soil bacteria for inhibiting phytopathogenic fungi. Afric. J. of Biotech.,11(81): 14660-14670.2012.
[18] Magnusson, J. Ström, K. Roos, S. Sjögren, J. and Schnürer, J. Broad and complex antifungal activity among environmental isolates of lactic acid bacteria. FEMS Microbiol. Lett. , 219: 129–135.2003.
[19] Laref ,N. and Guesses, B. Antifungal activity of newly isolates of lactic acid bacteria. Innovative Romanian Food Biotechnol., 13, 80-88.2013.
[20] SPSS . Statistical Package for the Social Sciences. Sigma Stat Statistical Software. SPSS Marketing Department, Chicago, IL.1997.
[21] Mauch , A., Dal Bello , F. Coffey , A. and Arendt, E.K. The use of *Lactobacillus brevis* PS1 to *in vitro* inhibit the outgrowth of *Fusarium culmorum* and other common *Fusarium* species found on barley . Int. J. Food Microbiol., 141 : 116–121.2010.
[22] Zebboudj , N. Yezli ,W. Hamini-Kadar, N. Kihal, M. and Henni ,J. Antifungal activity of lactic acid bacteria against *Fusarium oxysporum* f. sp. *albedinis* isolated from diseased date palm in South Algeria , Int. J. Biosci., 5 (9): 99-106.2014.
[23] Schillinger ,U. and Villarreal ,J.V. Inhibition of *Penicillium nordicum* in MRS medium by lactic acid bacteria isolated from foods. Food Control ,21: 107-111.2010.
[24] Laref ,N. ; Guessas, B. and Kihal ,M. Antifungal compounds production in different temperatures, pH and modified MRS Agar by *Lactobacillus* strains. J. Bio. Sci., 13: 94-99.2013.
[25] Vuyst, L. and Leroy, F. Bacteriocins from lactic acid bacteria. Production, purification and food application. J. Mol. Microbiol. Biotechnol. , 13(4): 194-199.2007.
[26] Guo, J. Brosnan ,B. Furey, A. Arendt, E. K. Axel, C. and Coffey, A. Anti-oomycete potential of *Lactobacillus amylovorus* JG2 against the potato blight pathogen *Phytophthora infestans* Int. J. Curr. Microbiol. App. Sci. , 3(1): 630-647.2014.
[27] Muhialdin, B. J. and Hassan, Z. Screening of Lactic Acid Bacteria for antifungal activity against *Aspergillus oryzae* . Am. J. Appl. Sci., 8 (5): 447-451.2011.
[28] Kıvanc, M. Kıvanc, S. A. and Pektas, S. Screening of Lactic Acid Bacteria for Antifungal Activity against Fungi . J. Food Process Technol. , 5:310-320.2014.
[29] Plockova ,M. Stilesm, J. Chumchalova, J. and Halfarova, R. Control of mold growth by *Lactobacillus rhamnosus* VT1 and *Lactobacillus reuteri* CCM 3625 on milk agar plates. Czech J. Food Sci., 19: 46-50.2001.
[30] Adebayo, C.O. and Aderiye ,B. I. Antifungal activity of bacteriocins of lactic acid bacteria from some Nigerian fermented foods. Res. J. Microbiol. , 5: 1070-1082.2010.
[31] Teniola ,O.D. and Odunfa ,S.A. Microbial assessment and quality evaluation of ogi during spoilage. World J. Microbiol. Biotech., 18: 731-737.2002.
[32] Ndagano ,D. Etude de l'activité antifongique des bactéries lactiques isolées de produits alimentaires fermentés et caractérisation de leurs métabolites inhibiteurs. Ph D thesis, University of Liege, Belgium.2012.
[33] Valerio, F. Favilla, M. ; De-Bellis, P. Sisto, A. , De-Candia ,S. Lavermicocca, P. Antifungal activity of strains of lactic acid bacteria isolated from asemolina ecosystem against *Penicillium roqueforti, Aspergillus niger* and *Endomyces fibuliger* contaminating bakery products. Sys. Appl. Microbiol., 32: 438-448.2009.
[34] Tang ,H. Ren, J. Yuan, J. Zeng, B. and Wei ,H. An *in vitro* assessment of inhibitory effect of 16 strains of probiotics on the germination of *Candida albicans*. Afr. J. Microbiol. Res., 4: 1252-1256.2010.
[35] El-Mabrok ,A.S. Hassan, Z. Mokhtar, A.M. and Aween ,M.M. Efficacy of *Lactibacillus plantarum* C5 cell and their supernatant against *Colletotricum gloeosporioides* on germination rate of chilli seeds. Res. J. Biolog. Sci., 7: 159-164.2012.

Al-Mustansiriyah Journal of Science
Vol. 27, No 2, 2016

journal homepage:www.mjs-mu.com

Detection of Epstein-Barr virus infection in patients with arthritis by immunological and molecular methods

Nuha. S. Jassim , Rana. S. Aboud. , Hula. Y. Fadil
Depatment of Biology, Collage of Science, Baghdad University, Baghdad. Iraq.

Articleinfo

Received
29/9/2015
Accepted
16/11/2016

Keywords: :
EBVNA-1 IgG, Rheumatoid arthritis, Reactive arthritis, Ankylosing spondylitis

ABSTRACT

To determine the role of EBV in pathogenesis of Rheumatoid arthritis, reactive arthritis and Ankylosing spondylitis .Sixty two patients (52 patients with AR, five patients with ReA, and five patients AS) have been investigated. The mean age 47.3, 47.7, 34.5) of RA, ReA and AS respectively and compared to 24 apparently healthy individuals with the mean age 28.3. All the study groups were carried out to measure EBV NA-1 antibodies IgG by ELISA technique, and detection of EBV DNA by convential PCR. There was a significant elevation ($P< 0.05$) in the concentration of EBVNA-1IgG antibodies compared to control groups. The result of present study revealed from fifty two of RA patients was 44 positive to EBV DNA in a percentage 84.62% while only 15.38% was negative to it, and all patients with ReA and AS was positive 100.0% where no negative result. Compare to control group and the statistical analysis show highly significant different ($P<0.01$) between studied groups. The results of current study indicate that infection with EBV play a role as a triggering factor in pathogenesis of RA, ReA and AS.

الخلاصة

لغرض تعيين دور فيروس ابشتايين بار فيروس في أمراضية التهاب المفاصل الرثوي ، التهاب المفاصل التفاعلي و تشمع العمود الفقري. تم التحري عن 62 مريضا (52 مريض مصابا بالتهاب المفاصل الرثوي، 5 مرضى مصابين بالتهاب المفاصل التفاعلي، و 5 مرضى مصابين بتشمع العمود الفقري) وكان متوسط العمر (47,3 , 47,7 , 34,5) لمرضى التهاب المفاصل الرثوي, التهاب المفاصل التفاعلي و تشمع العمود الفقري على التوالي وبالمقارنة مع 24 فردا من الاشخاص الاصحاء وكان متوسط اعمارهم 28,3 . خضعت جميع عينات الدراسة لقياس مستوى أضداد المستضد النووي EBVNA-1IgG لفيروس ابشتاين بار فيروس الصنف جي باستخدام تقنية الامتزاز المناعي المرتبط بالانظيم والتحري عن الحامض النووي منقوص الأوكسجين للفيروس باستخدام تفاعل سلسلة البلمرة التقليدي PCR . اظهرت النتائج ارتفاعا معنويا ($P< 0.05$) في تركيز أضداد المستضد النووي الصنف EBVNA-1IgG مقارنة بمجاميع السيطرة. كما أوضحت نتائج الدراسة من اصل 52 مريض بالتهاب المفاصل الرثوي كانت هنالك44 نتيجة ايجابية لـ EBVDNA وبنسبة 84,62% بينما 15,38 اظهرت نتيجة سلبية له.كما واظهر جميع مرضى التهاب المفاصل التفاعلي وتشمع العمود الفقري نتائج ايجابية بنسة 100% ولم تلاحظ هنالك نتائج سلبية مقارنة بمجاميع السيطرة وأوضحت نتائج التحليل الإحصائي وجود فروق معنوية عالية($P<0.01$) بين مجاميع الدراسة.
تشير نتائج الدراسة بان الخمج بفيروس الابشتلين بار فيروس يلعب دورا كعامل قدح في أمراضية التهاب المفاصل الرثوي , التهاب المفاصل التفاعلي و تشمع العمود الفقري.

INTRODUCTION

Epstein-Barr virus (EBV) is a gammaherpes virus discovered in 1964, it's widespread in all areas of the world, infecting over 95% of the adult population worldwide, being a life –long persistent infection virus, transmitted by salivary contact, its primary infection occurs during childhood with latent infection of B lymphocyte [1].EBV has been associated not only with a wide range of lymphoid malignancies but also with autoimmune disease such as lupus erythematosus, rheumatoid arthritis, and in particular, multiple sclerosis[2]. RA is the most common systemic autoimmune disease in the world [3]. Reactive arthritis (ReA) develops in response to an infection in other part of the body [4]. Ankylosing spondylitis (AS) is a chronic inflammatory joint disease that affects the sacroiliac joints and spine [5]. An association between EBV and rheumatoid arthritis (RA) was first proposed on the basis of high titers of EBV specific antibodies found in some patients with RA [6] .

Several research has focused on the role of molecular mimicry presented by EBV.Alspangh and Tan reported that EBV was implicated in RA pathogenesis who noticed that sera of RA were reactive against nuclear Ag in EBV-transformed lymphocyte. Antibodies against glycine/alanine rich repeat in EBNA-1 are cross-react with 62kDa protein found in synovium of RA patients. Also, antibodies against EBNA-1 Ag recognize and denaturated collagen and keratin, these support mechanism that molecular mimicry is involved in the pathogenesis of RA. [7]. EBV serology is the gold standard for diagnosis EBV-infection in

immunocompetent individuals, but is of only limited value in immunocompetent individuals therefore, quantitative PCR is a guide to the severity of infection and a guide to management [8].The aim of the current study was to determine the role of EBV as triggering factor in Rheumatoid arthritis, Reactive arthritis and Ankylosing spondylitis.

Patients and methods:

The current study consisted of sixty two patients ,52 with Rheumatoid antigen, 5 with Reactive arthritis, and 5 with Ankylosing spondylitis, who attended to AL-yarmouk teaching hospital/Rheumatology clinic .The samples were collected from the first of November 2014 until February 2015.The ages of the patients ranged from (28-70) years. Twenty-four samples of apparently healthy individuals; 15 female and 9 male were studied as a control groups of same ages and sex.

All samples were marked by the number of samples, name of patient and a day of sample collection.

Blood samples collection:

Blood samples (5ml) were collected by disposable syringe then separated into 2 tubes; the first EDTA tubes (2ml of whole blood) for extraction of DNA, the second plane tube (3 ml of whole blood) which stands at room temperature until the coagulant was form. Then the samples were centrifuged at 3000 rpm for 5 minutes. Serum samples were dispended separated on Eppendroff tubes. All samples stored at (-20) C until carried out to immunological examination.

Immunological examination

All the studied groups were carried out to measure EBV nuclear antigen (EBV-NA-1) antibodies IgG by ELISA technique (Demeditec Diagnostics/Germany) according to the leaflet of kit.

Molecular methods.

DNA Extraction.

DNA was extracted from blood samples using AccuPrep® Genomic DNA extraction kit provided by supplier (Bioneer). The DNA extracted was stored at -70C until use for conventional PCR technique.

PCR amplification

The extracted DNA, primers (forward primer sequence5'- CGAGTCATCTACGGGGACACGGA-3', reverse primer sequence3'-AGC ACC CCC ACA TAT CTC TTC TT -5'[9], and PCR premix, were thawed at 4 ^{0}C, vortex and centrifuged briefly to bring the content to the bottom of their tubes. PCR mixture was set up in a total volume 20 µl included: 1.2µl of each primer (forward and reverse) 5 µl of DNA template and 13 µl of nuclease free water.

The PCR reaction tubes were mixed briefly and placed into thermocycler PCR instrument where DNA was amplified according to the PCR program.

Statistical analysis

The statistical analysis system-SAS [10] was used to effect of different factors in study parameters .Chi-square test was used to significant comparison between percentage and least significant difference. LSD test was used to significant compression between means in this study.

Results and Discussion:

The result of this study revealed that there were a significant elevation ($P<0.05$) in concentration of EBVNA-IgG 1 Ab in sera of patients groups 31.88±4.71U/m compared with control group which was 48.08 ± 7.63 as shown in table 1.

Table 1 Mean level of EBVNA- IgG 1in a serum of studied groups.

Group	Means ± SD
Patients	31.88 ± 4.71
Control	48.08 ± 7.63
LSD value	9.337*
*(p<0.05)	

The results revealed that the AS group have higher mean of concentration which was 50.2U/ml, while the concentration of EBV NA 1 IgG Abs in ReA patients was 30.4U/ml and the mean concentration of EBV NA 1 IgG Abs was 29.01U/ml in RA patients Compared to control group which was 48.08 ± 5.83 as shown in fig 1.

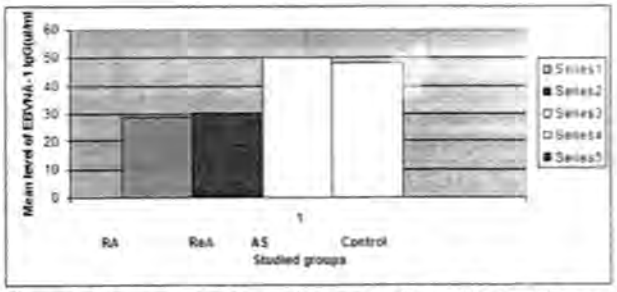

Figure (1): Comparison between RA, ReA ,AS and control group in EBV-NA1 IgG Ab.

The result of present study was disagreement with study of Margarel *et al.*, [11] who noticed that nuclear antigen was detected in 90 % of RA patients while 8-15% of healthy control .While study done by shimada *et al.*, [12] showed that the titer of anti-EBVNA was 80. The result of current study was higher than study done by Kannangai *et al.*, [13] who showed that (52%) of rheumatoid arthritis patients were positive for EBNA1 antibody.

One research revealed that patients with RA have higher level of EBV-encoded proteins such as, VCA, EA, EBNA-1 and EBNA-2 than control group. Also, patients with RA have EBV DNA load in peripheral blood

mononuclear cell and higher number of circulating EBV-infect B-cell compared to control group [14].

Another study showed that patients with RA have higher titers of IgG Abs specific for both latent and lytic EBV encoded Ags[15]. Higher frequencies of EBV-infected B cells and up to 10-fold increased viral copy number in circulating mononuclear cells have also been detected in RA patients [15].

Patients with RA are considered immunosuppressed, thus this may explain the high rate of EBV positivity seen in the case control study, it is known that RA patients face some impairment in immunity that can lead to the development of serious bacterial infections and granulomatous infections [16].

Mechanisms by which infectious agents may initiate RA and/or autoimmunity include molecular mimicry and epitope spreading ,molecular mimicry can be initiated when lingering autoreactive T cells become activated by peptides from infecting organisms that bear similar structure and/or amino acid sequence to that of same host peptide, i.e proteins/peptides that share a similar molecular structure to that of host tissue peptides, and which therefore can perpetuate inappropriate immune reactions to self [14].

The result of present study indicated from fifty two of RA patients 44 were positive to EBV DNA in a percentage 84.62% while only 15.38% were negative to it, while all patients with ReA and AS were positive 100.0% where no negative result. Comparison with control group where 23 from 24 was positive (95.83%) and only one was negative 4.17%, the statistical analysis showed highly significant different (P<0.01) as shown in table 2 and fig 2

Table 2 Distribution of RA, ReA, AS & Control (Positive and negative) of PCR.

	Total	Positive (%)	Negative (%)	Chi- sruare
RA	52	44 (84.62%)	8 (15.38%)	13.59 **
ReA	5	5 (100.0%)	0 (0.00%)	15.00 **
AS	5	5 (100.0%)	0 (0.00%)	15.00 **
Control	24	23 (95.83%)	1 (4.17%)	14.71 **
Chi- square	---	6.027 **	6.027 **	----
** (P<0.01).				

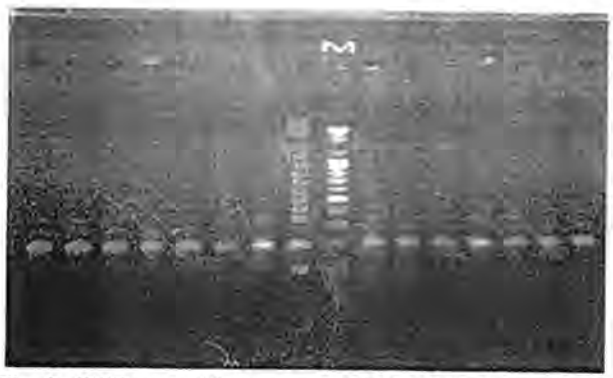

Fig 2: PCR amplification of EBV DNA from whole blood sample detected by 1.5% agarose gel electrophoresis. Lane M: 100pb molecular size marker ladder. Lanes: 1-10 positive samples.

The result of this study was higher than the result showed by A' lvarez-Lafuente, *et al*[17] who reported that DNA prevalence of EBV was 56% in RA patients. The present study coincides with Magnusson *et al.*, [18] who mentioned that 87 % of RA patients was positive.

The result of present study was similar to results obtained by Balandraud *et al.*, [19] :who observed that higher EBV load in patients with RA than in controls. Could detect EBV in 88% of patients with RA, 93% of patients with inflammatory rheumatic conditions other than RA (non-RA patients), and 89% of healthy controls.

A recent study using real-time polymerase chain reaction has demonstrated a 10-fold increase in the EBV DNA load in the peripheral blood mononuclear cells of patients with RA [20].

Patients suffering from RA have a 10-fold increase in EBV DNA load in peripheral blood mononuclear cells compared with that in controls; this elevation is stable and not influenced by the presence or absence of RF, age, duration of RA, disease activity, or RA treatment [21].

It is reported that patients with rheumatoid arthritis have very high EBV load in peripheral blood lymphocytes than healthy controls [13].

A few studies also attempted to detect infectious virus or EBV DNA in peripheral blood or synovial fluid cells of patients with RA. However, by molecular biologic analysis, the EBV DNA load of peripheral blood or synovial fluid cells from RA patients did not differ from that of the same cells from controls [22].

Conclusion:

The results of current study indicate that infection with EBV play a role as a triggering factor in pathogenesis of RA, ReA and AS and each patient with arthritis should be tested for EBV diagnostic tests even by detection of nuclear antigen or detection of virus DNA especially in case of patient with EBV NA-1 was negative.

References:

1-Korcum, A. F. ;Ozyar, E. and Ayhan,A.2006.Epstein-Barr virus genes andnasopharyngeal cancer.*TJ C 36:97-107.*

2- Casiraghi , C. and Horwitz, M. 2013. Epstein-Barr virus and autoimmunty.*Fut.Virol.8(2):173-182.*

3-Widdifield, J. ; Paterson, J.M. ; Bernatsky, S. ; Tu, K. ; Thorne, J.C. ; Ahluwalia, V.;Ivers, N. ; Butt, D.; Jaakkimainen, L. ; Tomlinson, G. And Bombardier, C. 2013.The rising burden of rheumatoid arthritis surpasses rheumatology supply in Ontario. *Can J Public Health. 104:450-455.*

4-Kwiatkowska, B. and Maślińska, B.2011. Ocular Symptoms (Conjunctivitis, Uveitis) in Reactive Arthritis, Conjunctivitis - A Complex and Multifaceted Disorder, Pelikan, Z.(Ed.).*InTechEurope.Croatia.*

5-Wolf, A. .2012. Clinical Features of Ankylosing Spondylitis, P:978-953.Armas, S. A.(ed) Clinical and Molecular Advances in Ankylosing. *InTech.Vienna.*

6- Toussirot, E. and Roudier, J. 2007. Pathophysiological links between rheumatoid arthritis and the EpsteineBarr virus: An update.*Join.Bon.Spin.74:418-426.*

7- Goldstein, B.L.; Chibnik, L.B.; Karlson, E.W. and Costenbader, K.H. 2012. Epstein-Barr Virus Serologic Abnormalities and risk of Rheumatoid Arthritis among WomenAutoimmun.*45(2():161-168.*

8- Westergaard, M.W.; Draborg, A.H.; Troelsen, L.; Jacobsen, S. and Houen, G. 2015. Isotypes of Epstein-Barr Virus Antibodies in Rheumatoid Arthritis: Association with Rheumatoid Factors and Citrulline-Dependent Antibodies.*Bio.Med.Res.Inter.2015(2015).Article ID472174:9.*

9- Acharya,S. ; Phusingha,p.;vatanasap,P.; promther,S.;Eklaksananan,T. And Pientong,C.2013.Prevalance of Eptein-Barr virus(EBV) in oral Exfoliated Cells:A pilot Prospective squamous Cell Carcinoma.*Srinagarind Med J 28:286-290*

10-SAS. 2012. Statistical Analysis System, User's Guide. Statistical.Version 9.1th ed. SAS.Inst. *Inc. Cary.N.C. USA.*

11-Margaret, A. A.; Henle, G.; Lennette, E. T.AndHenle, W.1981. Elevated Levels of Antibodies to Epstein-Barr Virus Antigens in Sera and Synovial Fluids of Patients with Rheumatoid Arthritis. *J. Clin. Invest. 67: 1134-1140.*

12-Shimada, H. ;Dobashi, H.; Morimoto, H. ; Kameda, T. ;Susaki, K. ; Izumikawa, M. ;Takeuchi, Y. ; Nakashima, S. ; Imataki, O. and Bandoh, S.2015. Primary central nervous system lymphoma in a rheumatoid arthritis patient treated with methotrexate: a case report. *BMC Research Notes .8:88.*

13-Kannangai, R. ; Sachithanandham, J.; Kandathil, A. J.; Ebenezer, D. L. ; Danda , D.; Vasuki, Z. ; Thomas, N.; Vasan, S. K.andSridharan, G.2010. Immune responses to Epstein-Barr virus in individuals with systemic and organ specific autoimmune disorders. . *Indian J Med Microbiol .28: 120-123.*

14-Deo, S. S. ;Shetty, R. R. ; Mistry, K.J. and Chogle, A. R.2010.Detection of Viral Citrullinated Peptide Antibodies Directed Against EBV or VCP: In Early Rheumatoid Arthritis Patients of Indian Origin. *J Lab Physicians.2:93-99.*

15-Lu¨nemann, J. D. ;Oliver Frey, O. ; Eidner, T. ; Baier, M. ;Susanne Roberts, S.;Sashihara, J.;Volkmer, R. ; Cohen, J. I.; Hein, G. ;Kamradt, T. and Mu¨nz, C.2008.Increased Frequency of EBV-Specific Effector Memory CD8 T Cells Correlates with Higher Viral Load in Rheumatoid Arthritis1.*J. immunol. 181:991-1000.*

16-McKeown, E.; Pope, J.E. and Leaf, S.2009.Epstein-Barr Virus (EBV) Prevalence and the Risk of Reactivation in Patients with Inflammatory Arthritis Using Anti-TNF Agents and in those who are Biologic Naïve. *Open Rheumatol J. 3: 30-34.*

17-Ivarez-Lafuente, R. A. ; Gutie´rrez, F. ; Miguel, S. D. ; Jover, J. A. ; Rollin, R. ; Loza, E. ; Clemente, D. and Lamas, J. R.2005. Potential relationship between herpes viruses and rheumatoid arthritis: analysis with quantitative real time polymerase chain reaction. *Ann RheumDis64:1357–1359.*

18-Magnusson, M. ;Brisslert, M.;Zendjanchi, K. ; Lindh, M. and Bokarewa, M. I.2010.Epstein Barr virus in bone marrow of rheumatoid arthritis patients predicts response to rituximab treatment.*Rheumatology.49:1911-9.*

19-Balandraud,N.; Meynard,J. B.; Auger,I.; Sovran,H.; Mugnier,B.; Reviron,D. ; Roudier,J. and Roudier, C.2003. Epstein-Barr Virus Load in the Peripheral Blood of Patients With Rheumatoid Arthritis. *Arthritis Rheum. 48:1223–1228.*

20-Pender, M.P. 2004.Epstein-Barr Virus and Autoimmunity. pp. 163-170in Shoenfeld, Y. and Rose , N.R.(ed.)*Infection and autoimmunity Elsevier, Amsterdam.*

21-Costenbader, K.H. and Karlson, E.W.2006. Epstein–Barr virus and rheumatoid arthritis: Is there a link? *Arthritis Res Ther:8: 204.*

22-Saal, J. G.;Krimmel, M. ;Steidle, M. ;Gerneth, F.;Wagner, S.Fritz, P. ;Koch, S. ;Zacher, J.;Sell, S.;Einsele, H. and Mu¨ller. C.A.1991. Synovial epstein-barr virus infection increases the risk of rheumatoid arthritis in individuals with the shared hla–dr4 epitope. *Arthritis Rheum.24: 1485–1496*

Al-Mustansiriyah Journal of Science
Vol. 27, No 2, 2016

journal homepage:www.mjs-mu.com

Plasmid Profile of Lactose Fermenters Enterobacteriaceas Isolated from Environmental and Clinical Samples

Israa AbdulJabbar Ibrahim , Tuqa Abdul Kareem Hameed
Department of Biology, College of Education for Pure Science, Ibn Al-Haitham, University of Baghdad, Iraq

Articleinfo

Received
27/10/2015
Accepted
21/12/2015

Keywords:
Enterobacteriaceas, clinical isolates, environmental isolates, plasmid.

ABSTRACT

A total of 183 isolates were collected from environmental and clinical sources during a period of 5 months from 1st September 2014 to the 1st February 2015. Our results showed that gram negative bacterial isolates were obtained from environmental samples are in the descending order as follows: 54.117 % *Escherichia coli,* 36.47% *Klebsiella pneumoniae,* 2.352% *Klebsiella oxytoca,* 1.176% *Raoultella planticola*, and 5.885% non-lactose fermenters enterobacteriaceae while bacterial isolates were obtained from clinical samples as follows: 75.51% *E. coli*, 15.306% *K. pneumoniae*, 5.102% *Enterobacter aerogenes*, 3.061% *Serratia marcescens* and 1.02% *Citrobacter freundii*. The plasmid DNA analysis showed that most isolates containing plasmid with molecular weight equal 10000 bp. All *K. pneumoniae* isolates (from both sources) and all *E.coli* environmental isolates have plasmid, but approximately
half of *E. coli* clinical isolates was free of plasmid. In conclusions, plasmid is important for bacterial isolates from environment, may be due the role of plasmid in enhancement the resistance of bacteria to many factors such as heavy metal and toxic substance to live in complex environmental conditions.

الخلاصة

جمعت 183 عزلة بيئية وسريرية خلال فترة خمسة اشهر من اول ايلول 2014 الى اول شباط 2015. اظهرت النتائج ان العزلات البكتيرية المستحصلة من العينات البيئية كما يلي: 54.117% *Escherichia coli*, 36.47% *Klebsiella pneumoniae* و 2.352% *Klebsiella oxytoca* و 1.176% *Raoultella planticola* و 5.885% غير مخمرة لسكر الاكتوز ضمن العائلة المعوية. بينما البكتريا المعزولة من العينات السريرية كما يلي: 75.51% *Escherichia coli*, 15.306% *Klebsiella pneumoniae* و 5.102% *Enterobacter aerogenes* و 3.061% *Serratia marcescens* و 1.02% *Citrobacter freundii*. لقد اظهر التحليل البلازميدي امتلاك اغلب العزلات بلازمد ذات وزن جزيئي مساوي الى 10000 زوج قاعدي. جميع عزلات الكلبسيلا الرئوية البيئية والسريرية وعزلات اشريكيا القولون البيئية احتوت على البلازمد. بينما كان نصف عزلات اشريكيا القولون السريرية خالية من البلازمد. نستنتج, ان اهمية وجود البلازمد في البكتريا المعزولة من البيئة يرجع الى دوره في تعزيز مقاومتها للعومل المختلفة المتواجدة في البيئة مثل المعادن الثقيلة والمواد السامة مما يساعدها على المعيشة في هذه البيئة المعقدة.

INTRODUCTION

"Enterobacteriaceae may account for 80% of clinically significant isolates of Gram-negative bacilli and 50% of clinically significant bacteria in clinical microbiology" [1]. The genera *Escherichia, Klebsiella, Enterobacter, Serratia, Citrobacter* and *Proteus* include overt and opportunistic pathogens responsible for a wide range of infections [2].

Plasmids form a vital part of the bacterial genome and can constitute up to 10% or more of the DNA in a bacterial cell [3]. Plasmids size range from 1 kbp to 2,000 kbp [4], which often carry and disseminate genes that confer to the bacteria certain characteristics such as resistance, virulence, the ability to metabolize rare substances, and persistence under extreme conditions [5, 6]. The example of antimicrobial resistance and virulence plasmid such as: Enterohaemorrhagic *E. coli* (EHEC) carry a large plasmid (91.2 kbp) that is associated with the presence of fimbriae [7] and genes such as bla_{SHV}, bla_{TEM}, bla_{CTX} and bla_{AMPC} presented in *E. coli, K. pneumoniae* and *Acinetobacter spp.* encode extended-spectrum β-lactamases (ESBLs) that are often located on plasmids [8]. "Plasmid profile analysis is useful in determining the epidemical strain in outbreaks caused by multiple species: *Escherichia, Klebsiella, Pseudomonas,Serratia, Streptococcus*, and so on" [9]. The promiscuity of transposons jumping from DNA to DNA, whether in a plasmid, chromosome, or phage, is a major factor in dissemination of antibiotic resistance [10]. The aim of this study is to determine the most plasmid size frequency in lactose fermenter Enterobacteriaceae isolates from clinical and environmental sources.

Materials and Methods

Specimens

In this study, 183 isolates were analyzed, 85 environmental specimens (36 chicken feces, 35 water Tigris river, and 14 agriculture soil) and 98 clinical specimens (75 urine, 7 sputum, 6 blood, and 10 wounds) were obtained from five hospitals in Baghdad city (Ibn Al Balady Hospital, Imam Ali Hospital, Al Kindy Teaching Hospital, Al-Shaheed Al-Sader Hospital, Educational Laboratory/ Medical City). Samples collection was carried out from 1st September 2014 to 1st February 2015.

Biochemical tests

Gram negative bacteria isolated on its respective selective and differential media (MacConkey agar and EMB) were identified on the basis of culture characteristics (colonies morphologies), Gram stain, and biochemical tests such as: IMViC (Indol test, methyl red test, voges- Proskauer test, and citrate test), Urea, Kligler Iron Agar [11] and also used automatically identification system Vitek 2 with GN card.

Plasmid DNA extraction procedure

Plasmid DNA was isolated from bacterial cells by alkaline method [12], by using AccuPrep® Plasmid Mini Extraction Kit (Bioneer- Korea) and separated on a 1% agarose, at 70 volt for 1.5 hours. The DNA bands were visualized and photographed under UV light after the gel had been stained with ethidium bromide.

Results and Discussion

The results showed that 54.117 %(46/85) *E.coli*, 36.47% (31/85) *K. pneumoniae*, 2.352% (2/85) *K.oxytoca*, 1.176% (1/85) *R. planticola* and 5.882% (5/85) non-lactose fermenters enterobacteriaceae of environmental samples. While clinical sample showed 75.51% (74/98) *E. coli*, 15.306% (15/98) *K. pneumoniae*, 5.102% (5/98) *E. aerogenes*, 3.061% (3/98) *S. marcescens* and 1.02% (1/98) *C. freundii*. The most common lactose fermenter enterobactericea are *E. coli* and *K. pneumoniae* of environmental and clinical sample (Figure 1, 2).

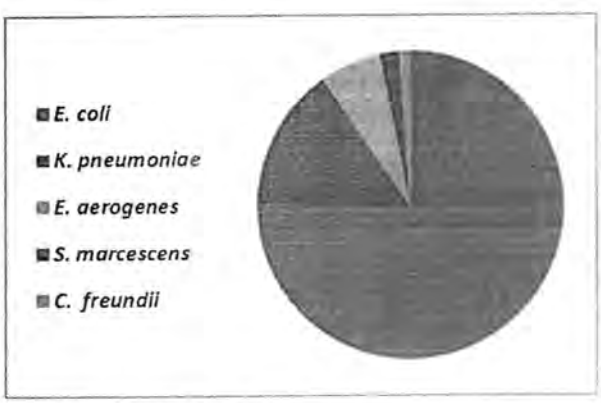

Figure 1: Clinical isolates

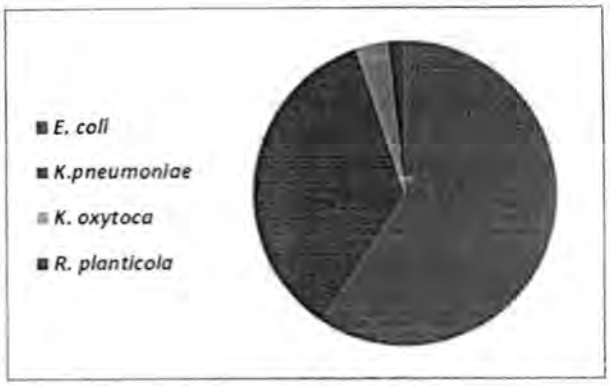

Figure 2: Environmental isolates

The results showed that the most isolates have plasmid size equal to 10,000 bp (10 Kbp). While all *K. pneumoniae* and *E. coli* isolated from environmental sources have frequency of plasmid from one to four times. In the other hand one isolate of *K. pneumoniae* from clinical sources showed free plasmid, but *E. coli* clinical sources revealed 7 isolates free plasmid from 12 isolates. Multiple plasmids were seen in environmental sources *R. planticola* and *K. oxytoca* (Figure 3, 4, 5, 6).

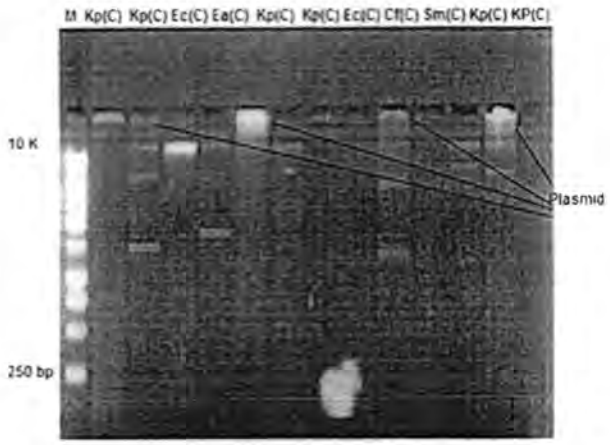

No.	isolates	No. of plasmid ≤ 10000 bp	No. of Mega plasmid > 10000 bp
1	Kp (C)	-	1
2	Kp (C)	3	-
3	Ec (C)	1	-
4	Ea (C)	2	-
5	Kp (C)	-	2
6	Kp (C)	1	-
7	Ec (C)	-	-
8	Cf (C)	-	-
9	Ec (C)	3	1
10	Sm (C)	-	-
11	Kp (E)	2	-
12	Kp (E)	-	2

Figure No.(3): Plasmid profile of clinical bacterial isolates (Lanes No. 1-10) and environmental isolates (No.11-12). Kp (*Klebsiella pneumoniae*), Ec (*Escherichia coli*), Ea (*Enterobacter aerogenes*), Cf (*Citrobacter freundii*), Sm (*Seratia marcescens*), C (clinical), E(Environmental). Lanes: (M) ladder (molecular weight ranged from 250- 10000 bp).

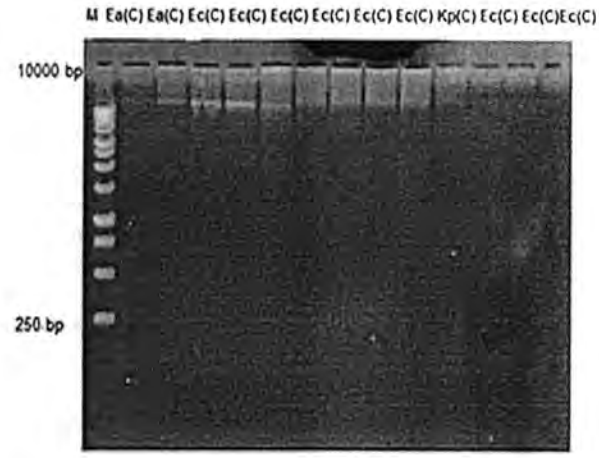

No.	isolates	No. of plasmid ≤ 10000 bp	No. of Mega plasmid > 10000 bp
1	Ea (C)	-	-
2	Ea (C)	1	-
3	Ec (C)	1	-
4	Ec (C)	1	-
5	Ec (C)	1	-
6	Ec (C)	-	-
7	Ec (C)	-	-
8	Ec (C)	-	-
9	Kp (C)	-	-
10	Ec (C)	-	-
11	Ec (C)	-	-
12	Ec (C)	-	-

Figure No.(4): Plasmid profile of clinical bacterial isolates (lanes No. 1-12) Kp (*Klebsiella pneumoniae*), Ec (*Escherichia coli*), Ea (*Enterobacter aerogenes*), C (clinical). Lanes: (M) ladder (molecular weight ranged from 250- 10000 bp)

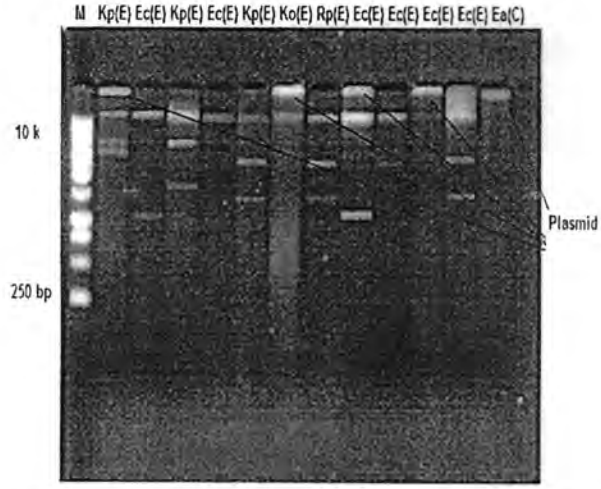

No.	isolates	No. of plasmid ≤ 10000 bp	No. of Mega plasmid > 10000 bp
1	Kp (E)	3	-
2	Ec (E)	2	-
3	Kp (E)	4	-
4	Ec (E)	2	-
5	Kp (E)	3	-
6	Ko (E)	-	2
7	Rp (E)	3	-
8	Ec (E)	1	2
9	Ec (E)	1	-
10	Ec (E)	-	1
11	Ec (E)	3	-
12	Ec (E)	-	1

Figure No.(5): Plasmid profile of environmental bacterial isolates (Lanes No. 1-12). Kp (*Klebsiella pneumoniae*), Ko (*Klebsiella oxytoca*), Rp (*Raoultella planticola*), Ec (*Escherichia coli*), Ea (*Enterobacter aerogenes*), E (Environmental). Lanes: (M) ladder (molecular weight ranged from 250- 10000 bp).

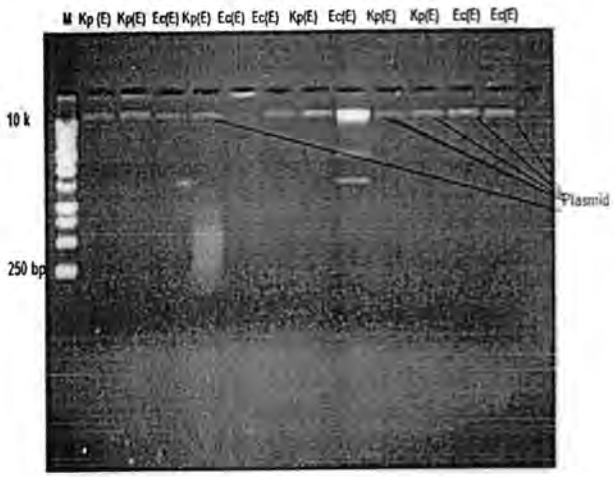

No.	isolates	No. of plasmid ≤ 10000 bp	No. of plasmid > 10000 bp
1	Kp (E)	1	-
2	Kp (E)	1	-
3	Ec (E)	1	-
4	Kp (E)	1	-
5	Ec (E)	-	1
6	Ec (E)	1	-
7	Kp (E)	1	-
8	Ec (E)	3	-
9	Kp (E)	1	-
10	Kp (E)	1	-
11	Ec (E)	1	-
12	Ec (E)	1	-

Figure No.(6): Plasmid profile of environmental bacterial isolates (Lanes No. 1-12). Kp (*Klebsiella pneumoniae*), Ec (*Escherichia coli*), E (Environmental). Lanes: (M) ladder (molecular weight ranged from 250- 10000 bp).

Coliform bacilli (*Escherichia, Klebsiella, Enterobacter, Serratia*, and *Citrobacter*) and Proteus which cause nosocomial infection, is responsible for 46% of urinary tract and 24% of surgical site infections, 17% of the bacteremia and 30% of the pneumonia [2]. *E. coli* and *K. pneumoniae* are the most common isolates from clinical and environmental samples, also many previous studies revealed that the prevalence of *E. coli* and *K.pneumonia* among enterobacteriaceae in clinical and environmental sources [13, 14].

The main observation of the present research was revealed 100% plasmids contain in environmental isolates and 45% plasmid contain in clinical isolates. Plasmid and chromosomal analysis is important to determine the site of virulence factor. One advantage of plasmid profiles over many other typing systems is that a single set of reagents and equipment is applicable to many species of bacteria [10]. Previous local study of children diarrhea showed that all *E. coli* isolates contained plasmids with molecular weight range between 4.507 kbp and 5.07 kbp [15]. Plasmids allow the movement of genetic material, including antimicrobial resistance genes, between bacterial species and genera [16]. Previous study in China revealed *K. pneumoniae* isolates harbored a 90-kb IncFII plasmid carrying blaCTX-M-15 [17]. Previous study by Adeyankinnu et al revealed that Plasmid profiles of tested isolates ranged from 9 kbp to 26 kbp for *E. coli* and *K. pneumoniae* from clinical samples [18]. Plasmid pRSB107 (120 megabase pair), which was isolated from bacteria present in sludge from a sewage treatment plant, encoded resistance to at least 9 different antimicrobials in *E.coli* transformants[19]. Other study by Hamada et al (2008) demonstrates that resistance gene from plasmid of *E. coli* isolates are increasing in healthy persons [20]. Science 1988 by Mayer confirm when doing plasmid profiles, it must be shown that control isolates from non-outbreak related patients and environmental isolates are different from the outbreak strain [10].

References

1-Murray, P. R.; Baron, E. J.; Jorgensen, J. H.; Pfaller, M. A. & Yolken, R. H (2003). Enterobacteriaceae, Introduction and identification. In: Farmer, JJ III (eds). Manual of Clinical Microbiology. Elsevier, Philadelphia, USA, pp. 647.

2-Baron, S. (1996). Medical Microbiology, 4th ed. Chapter 26 *Escherichia, Klebsiella, Enterobacter, Serratia, Citrobacter*, and *Proteus*. M. Neal Guentzel. University of Texas Medical Branch at Galveston, Galveston, Texas, Galveston.

3- Thorsted P. B., Macartney D. P., Akhtar P., Haines, A. S., Ali, N., and Davidson, P.(1998). Complete Sequence of the IncP Beta Plasmid R751: Implications for Evolution and Organization of the IncP Backbone. *J. Mol. Biol., 282*, 969-990.

4-Madigan, M.; Martinko, J. & Parker, J. (2003). Brock Biology of Microorganisms. 10th ed. Upper Saddle River, NJ, USA: Prentice Hall.

5-Actis, L. A.; Tolmasky, M. E. & Crosa, J. H. (1999). Bacterial plasmids: replication of extrachromosomal genetic elements encoding resistance to antimicrobial compounds. *Front. Biosci.*, 4:43– 62.

6-Johnson, T. J. & Nolan, L. K. (2009). Pathogenomics of the virulence plasmids of *Escherichia coli*. *Microbiol. Mol. Biol. Rev.*, 73:750 –774.

7-Karch, H.; Heesemann, J.; Laufs, R. O.;'Brien, A. D.; Tacket, C. O. & Levine, M. M. (1987). A plasmid of enterohemorrhagic *Escherichia coli* O157:H7 is required for expression of a new fimbrial antigen and for adhesion to epithelial cells. *Infect. Immun.*55:455–461.

8-Carattoli, A. (2009) Resistance plasmid families in Enterobacteriaceae. *Antimicrob. Agents Chemother.*, 53: 2227–2238.

9-Wachsmuth, K. (1986). Molecular epidemiology of bacterial infections: examples of methodology and of investigations of outbreaks. *Rev. Infect. Dis.*, 8:682–692.

10- Mayer L. W. (1988). Use of Plasmid Profiles in Epidemiologic Surveillance
of Disease Outbreaks and in Tracing the Transmission of Antibiotic Resistance
Clinical Microbiology Reviews, American Society for Microbiology. 1(2):228-243.
11-Forbes, B. A.; Sahm, D. F.; Weissfeld, A. S. & Bailey, W. R. (2007). Bailey
& Scott's diagnostic microbiology. 12th ed. St. Louis, Mo.: Elsevier Mosby .
12-Birnboim, H. C. & Doly, J. (1979). A rapid alkaline extraction procedure for screening recombinant plasmid DNA. *Nucleic Acids Res.* 7(6):1513-1523.
13-Riaz, S.; Faisal, M. & Hasnain S. (2012). Prevalence and comparison of Beta- lactamase producing *Escherichia coli* and *Klebsiella* spp from clinical and environmental sources in Lahore, Pakistan. *Afr. J. Microbiol. Res.* 6(2):465-470.
14-Guet-Revillet, H.; Le Monnier, A.; Breton, N.; *et al.* (2012). Environmental contamination with extended-spectrum beta-lactamases: is there any difference between *Escherichia coli* and *Klebsiella* spp? *Am. J. Infect. Control*, 40: 845-848.
15-Ibrahim I. AJ.; Al-Shwaikh, R. M. & Ismael M. I. (2014). Virulence and antimicrobial resistance of *Escherichia coli* isolated from Tigris River and children diarrhea. *Infect. Drug Resist.*, 7: 317–322.
16-Sherley, M.; Gordon, D. M. & Collignon P. J. (2004). Evolution of multi- resistance plasmids in Australian clinical isolates of *Escherichia coli. Microbiol.*, 150:1539–1546.
17-Zhuo, C.; Li, X-Q.; Zong, Z-Y. & Zhong, N-S. (2013) Epidemic Plasmid Carrying ^{bla}CTX-M-15 in *Klebsiella penumoniae* in China. *PLOS ONE*, 8 : Issue 1:1-8.
18-Adeyankinnu, F. A.; Motayo, B. O.; Akinduti, A.; Akinbo, J.; Joseph, I.; Ogiogwa, J. I.; Bukola, W.; Aboderin, B. W. & Agunlejika, R. A. (2014). A Multicenter Study of Beta-Lactamase Resistant Escherichia coli and *Klebsiella pneumoniae* Reveals High Level Chromosome Mediated Extended Spectrum β-Lactamase Resistance in Ogun State, Nigeria. *Interdisciplinary Perspectives Infect. Dis.*, Article ID 819896, 1-7.
19-Beceiro, A.; Tomas, M. & Bou, G. (2013). Antimicrobial Resistance and Virulence: a Successful or Deleterious Association in the Bacterial World? *Clin. Microbiol. Rev.*, 26 (2):185–230.
20-Hamada, T. A.; Mahmood, A. R. & Ahmed, I. A. (2008). Antibiotic resistance in pathogenic bacteria isolated from UTIs in Tikrit province. *Tikrit Med. J.*, 14(1):203-210.

Al-Mustansiriyah Journal of Science
Vol. 27, No 2, 2016

journal homepage:www.mjs-mu.com

Studying some structural and sensing properties of ZnO films as ammonia sensors prepared by two different methods

Reem saadi
Department of Physics, College of Education, Al-Mustansiriyah University

Articleinfo

Received 20/12/2015
Accepted 25/1/2016

Keywords: Titanium oxide; phase transformation; Photo catalytic activity, acid modifier, para-nitrophenol

ABSTRACT

Chemical spray pyrolysis method and electrophoretic deposition (EFD) method were used to deposit ZnO films as NH_3 gas sensors on glass and stainless steel substrates respectively. ZnO_{EPD} film has high crystallinity and large grain as X-ray diffraction (XRD) patterns and atomic force microscopy (AFM) confirm. The performance of these gas sensors were investigated at 75, 100 and 150 ^{0}C temperatures. Sensitivities of ZnO_{EPD} and ZnO_{Spray} to NH_3 gas were temperature dependence. The reaction between used gas and the adsorbed oxygen species play essential role in fabricated sensors work. Dissimilar structures of the two ammonia sensors and different surface topography of them produce different responses. The methods of deposition and substrates types have a direct effect on NH_3 sensors functioning.

الخلاصة

أستخدمت طريقة الرش الكيميائي وطريقة الترسيب بالهجرة الكهربائية لترسيب اغشية اوكسيد الزنك كمتحسسات لغاز الامونيا على قواعد زجاجية وستيل على التوالي.أغشية أوكسيد الزنك المرسبة بطريقة الهجرة الكهربائية امتلكت تبلور وحجم حبيبي كبير كما أكدت ذلك انماط حيود الاشعه السينية و مجهر القوة الذرية. أستُقصي أداء هذين المتحسسين عند درجات الحرارة 75, 100 و 150 درجة مؤية. تحسسية كل من هذين الغشائين لغاز الامونيا كانت معتمدة على درجة الحرارة. التفاعل بين الغاز المستخدم واصناف الاوكسجين المُمتز لُعب دور أساسي في عمل المُتحسسات المُصنعه. التركيب غير المتشابه لمتحسسي الامونيا والإختلاف في التضاريس السطحية يعطي استجابتين مختلفتين. كان لطريقة الترسيب واختلاف قواعد الترسيب دور مُباشر في أداء مُتحسسي الامونيا.

INTRODUCTION

The human being has different natural sensors. In our bodies; there are ability to sense light, temperature, taste, pressure, and so forth. But to widen our feeling and the limits of our sensing to things like magnetic field sensor devices are greatly helpful. Many commercial and industrial performances include monitoring of the environment and the controlling. Efforts must achieve to improve the controlling usually lies at the interface between surrounding to be monitored and the system, i.e. the sensor. It is not possible to get any advances in instrumentation and control without sensors [1].

ZnO has hexagonal wurtzite structure; it's belonging to semiconductor material (II–IV group). This material has unique characteristics which make it suitable for huge applications in different fields such as gas sensors, and conduction electrode transducers, etc[2].

NH_3 is a hazardous colorless and caustic gas with a characteristic pungent odor. In agricultural environments, because it is present in animal waste ammonia high concentrations can become high enough to kill them. To monitor and control these environments an ability to fabricate sensitive ammonia sensor is highly desirable[3].

Many methods were used to deposit ZnO films as NH_3 sensor on different substrates. New sensing properties can be obtained by different modifications like: changing the deposition conditions, doping ZnO films with various elements, annealing deposited films, using different substrates and other doings [4-6]. In this contribution there is an attempt to get better sensing properties to NH_3 gas by deposition ZnO films on different substrates using two deposition methods.

Experimental part

A- Deposition of ZnO by Spray on glass substrate

A homogeneous ZnO thin film on glass slide was deposited by spray pyrolysis using chemical solution prepared as following; dissolving 0.1 M ($ZnCl_2$) with 99.99% purity in distilled water. Prevention the creation of $(ZnOH)_2$ inside this solution was done by adding HCl

two drops. During deposition the substrate was put on hot plate maintained at 400°C. The nozzle to substrate distance was 28 cm. A carrier gas of chemical solution was air with 2ml/min spraying rate.

B-Deposition of ZnO by EFD on stainless steel substrate

Teflon container is used to deposit ZnO film by this method as illustrated by figure 1. One gram ZnO powder is put on 50 ml methanol, and then the solution is mixed by magnetic stirrer for 10 minute. Graphite disc represents the anode and circular stainless steel (substrate) with radius (1.5cm) is utilized as cathode. Power supply with 30 volt was connected to both electrodes. The distance between cathode and anode was 0.5 cm. The coated sample is immersed inside a solution consist from 1gm of Poly vinyl alcohol (PVA) dissolved in hot water. The last process was done to prevent cracks which may appear on coated layer. To remove PVA; the samples are heated to 500°C in air atmosphere. Samples characterizations have been measured by using XRD and SEM instruments. Standard PDF files (050664 and 330397) were utilized to specify XRD peaks for ZnO and stainless steel respectively.

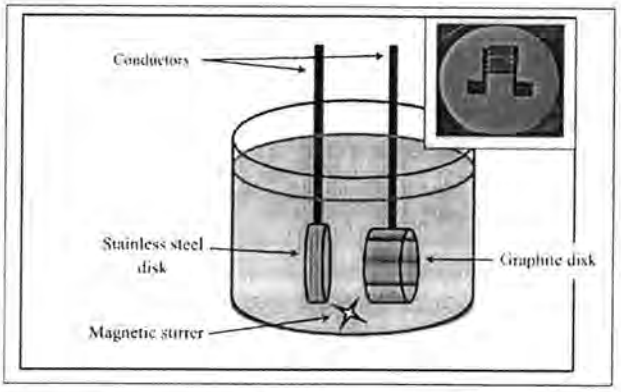

Figure1. Diagram of EFD cell with graphite disc as anode pole and stainless steel disc as cathode pole. The inset shows ZnO_{EPD} film covered by mask pattern

C- Gas sensor system

Figure 2 shows this system, it has the following parts: 6 liter sealed chamber made from stainless steel, controllable heater, vacuum system, ohmmeter and thermo couple. There are two methods to enter NH_3 gas inside the chamber depending on the amount of gas. For small amount, NH_3 solution is evaporated inside output unit and then transfers the gas to the chamber, see figure 2. For large amount, ammonia solution is injected inside chamber directly and then evaporates when it touch hot plate inside chamber. To evaporate small NH_3 amount micropipette type (DRAGONMED-made in china) volume 5-50μl was used. Ammonia solution type (Scharlau-Spain, 32% concentration) is used.

Figure 2. Gas sensor system

Results and discussion

A- XRD patterns and AFM images of ZnO_{EPD} and ZnO_{Spray} films

Beside the peaks of ZnO; ZnO_{EPD} XRD pattern in figure 3 contains the peaks that belong to stainless steel substrate. For this film; the intensity of (100) and (002) peaks are high so it has high crystallinity. All peaks of ZnO_{spray} XRD pattern {(100),(002) and (101)} belong to ZnO material and the rest of this pattern refer to glass substrate.

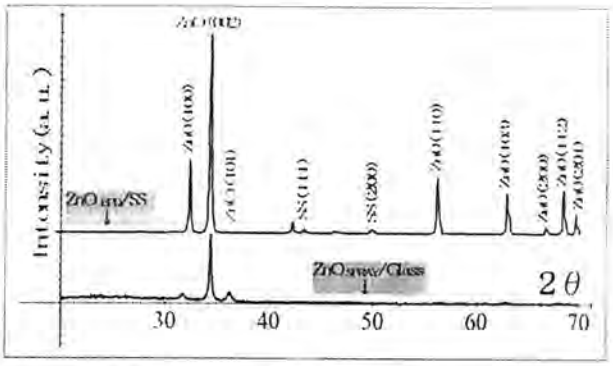

Figure 3. XRD patterns of ZnO_{EFD} and ZnO_{SPRAY} films deposited on stainless steel and glass substrates respectively

The methods of deposition give the films specific surface topography and may then different response. Figure 4 illustrates AFM images of ZnO_{EFD} and ZnO_{SPRAY} films.

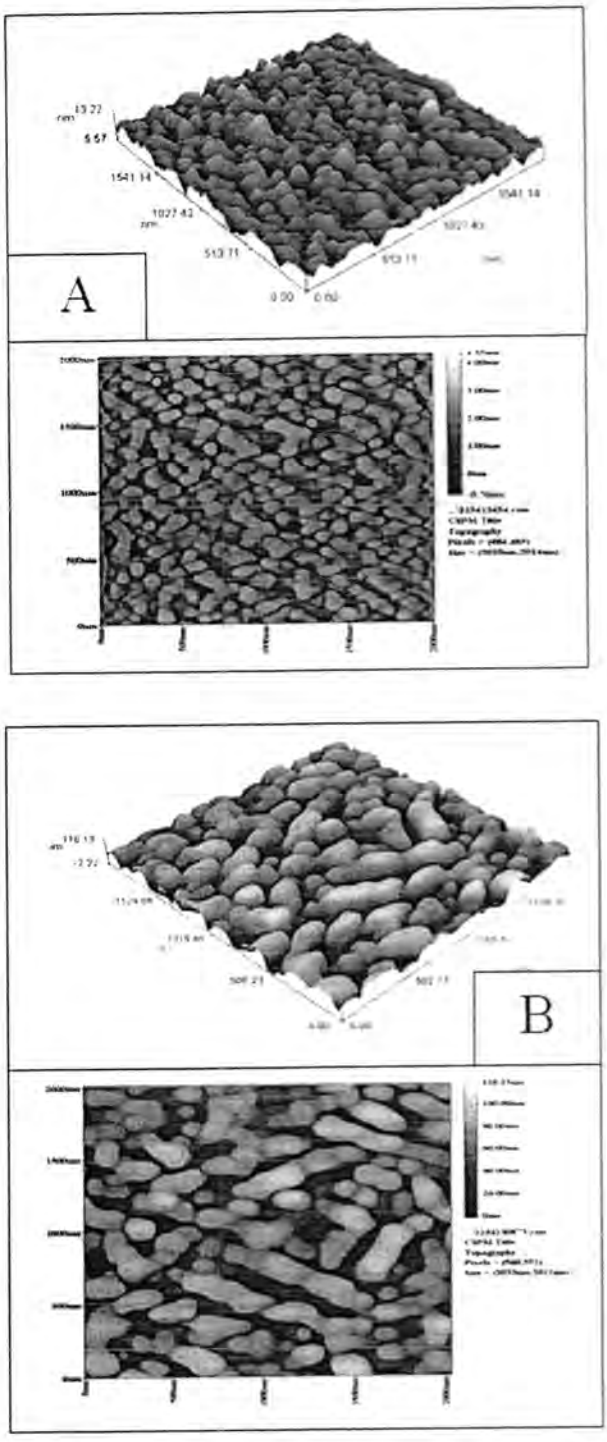

Figure 4. AFM images of A- ZnO_{SPRAY} and B- ZnO_{EPD} surfaces

Table 1 shows the surfaces properties of these two films.

AFM data of ZnO_{Spray} and ZnO_{EPD} that listed in table 1 is extracted from the images of figures 4. Investigation of table 1 confirms the topography differences between the two ZnO films. These differences will be the reasons behind their performances.

Table 1 Topography's data for ZnO films prepared by two methods

Deposition method	Roughness average (nm)	Grain Size(nm)	Root mean square(nm)	Peak-peak height (nm)
Spray	0.775	80.26	0.51	7.65
EPD	22	100.72	25.3	89.1

B- ZnO_{EPD} sensor

Figure 5 shows the relation between the resistance of ZnO_{EPD} and time for three sample's temperature: 75,100,150^{0}C. The behaviors of figure 5 curves can be explained as follows:

For n-type semiconductor such as SnO_2 and ZnO, the concentration of electrons available for conduction can be changed by either an oxidation or reduction process [7].

The resistance of the ZnO sensor must be increased by exposure to oxidizing gas. At the working temperature in air, the adsorption of atmospheric oxygen take place on the film surfaces and grain boundary surfaces and the oxygen accepts electrons to become O_2^-, O^-, or O^{2-}.

Consequently, this increases the resistance of the sensor, which is ascribed to the decrease of the carrier concentration and/or the decrease of the mobility [8]. Thus the increase of the resistance of the ZnO sensor for exposure to ammonia gas may be interpreted by either one or both of the following two processes: (1) Ammonia gas is directly adsorbed on the sensor surface and this accepts electrons available for conduction ; (2) the adsorption of atmospheric oxygen is enhanced by exposure to ammonia gas.

Hidehito et al. found that the increase of the resistance of the ZnO sensor is not observed for exposure to ammonia gas in pure argon ambient [9].

Their result supports the second process mentioned above. It can be expected that at higher ammonia concentration the resistance change of the sensor should be increased or saturated with increasing the concentration, if only the reaction with ammonia gas due to the second process as mentioned above is caused.

The sensing mechanism for ammonia gas can be explained also as the result of sensing hydrogen gas produced by the decomposition of ammonia gas. The rate of ammonia decomposition is temperature dependent [10]. . So it can be interpret the behavior of figure 5 curves as a result to dissociation ammonia molecules. The dissolved hydrogen atoms will diffuse back to the surface, where they are oxidized and removed.

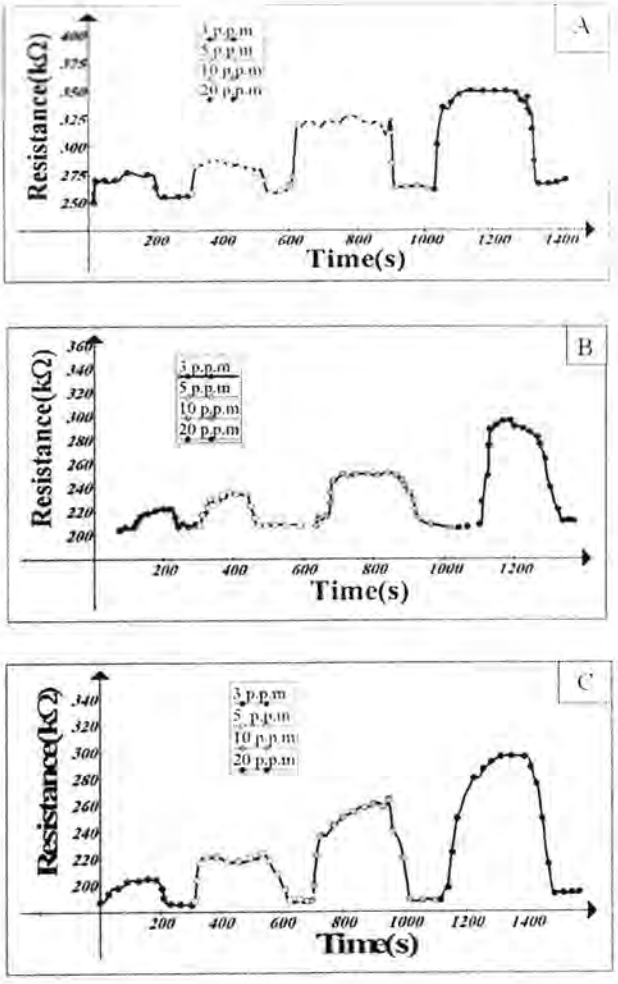

Figure 5. ZnO_{EPD} response to ammonia gas for different injected ammonia solution volumes. Sample's temperature: A- 75^{0}C, B- 100^{0}C and C- 150^0 C

Equation (1) is used to calculate the sensitivity

$$Sensitivity = \left|\frac{R_a - R_g}{R_a}\right| = \frac{\Delta R}{R_a} \quad \text{-------(1)}$$

Where Ra resistance of a sensor in air, Rg resistance of the sensor in a gas. Figure 6 illustrates sensitivity of ZnO_{EPD} to ammonia gas. It confirms that the sensitivity of ZnO_{EPD} to NH_3 is temperature dependence. The continuous increasing of sensitivity values with gas concentration agree with other worker [6]. After NH_3 adsorption by ZnO surface, this molecule can undergo variable processes. Through an oxygen species NH_3 dehydrogenation is probable process, these species capture the hydrogen atom and form OH group and NH_x species:

$$NH_3 + O_2 \rightarrow NH_x + 2OH \text{ - - - - - - - - - - - - - (2)}$$

After this process there are two main paths: first one is the interaction of one NH_x species with another one to form N_2 (molecular nitrogen). The second path is reaction of these species with an oxygen center (either lattice oxygen or chemisorbed) to form (NO) [4].

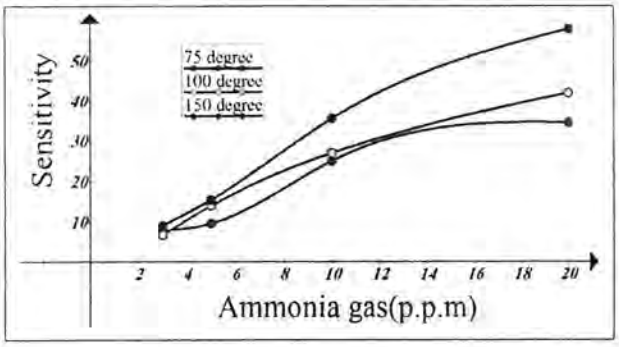

Figure 6. Sensitivity of ZnO_{EPD} to NH_3 gas

C- ZnO_{SPRAY} sensor

Figure 7 shows ZnO_{Spray} resistance changes with time for different injected ammonia gas volumes. Many ZnO ammonia sensors of other groups [11-12] observed resistance decreasing of their sensors after exposure to ammonia gas in similar manner to our observation in figure 7.The following is the explanation of ZnO_{SPRAY} ammonia sensor behavior: Exposure to atmosphere result in electrons trapping by adsorbed oxygen on ZnO surface. This produces reduction of surface conductivity. Once ammonia gas (which is reducing gas) is introduced inside chamber an interaction between this gas and adsorbed oxygen occur. This interaction release trapped electrons onto ZnO surface and then decreasing its resistance. The following equation illustrates this sensing mechanism [5]:

$$2NH_3 + 5O^-(ad) \rightarrow 2NO + 3H_2O + 5e^- \text{ - - - - - - - - - - (3)}$$

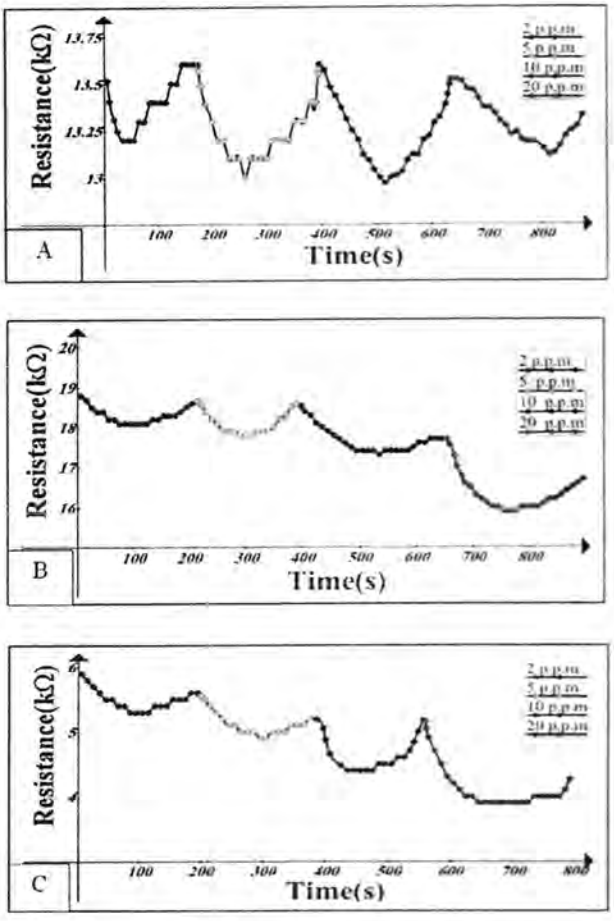

Figure 7. Resistance of ZnO_{Spray} as a function of time for different injected ammonia solution volumes. Sample's temperature: A-75^{0}C, B- 100^{0}C and C- 150^{0}C

Figure 8 illustrates the sensitivity of ZnO_{Spray} to ammonia gas. It shows the dependence of ZnO_{SPRAY} sensor sensitivity on the temperature of sample. These behaviors like that of ZnO_{EPD} sensor. This common behavior might attribute to the increasing of oxygen adsorption with sample's temperature and then increasing of ammonia reaction with ZnO material.

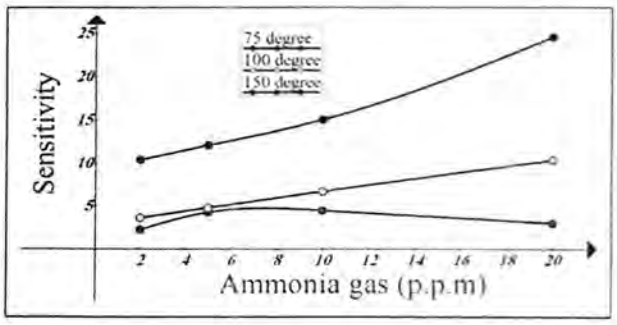

Figure 8. ZnO_{SPRAY} sensor sensitivity to ammonia gas.

Conclusions:

- The mechanism of ammonia sensing by ZnO_{EPD} differs from that by ZnO_{Spray} due to their dissimilar surface topographies.
- Varying substrates contribute beside deposition methods to produce two ammonia sensors with different response.
- The same material which used to fabricate different gas sensors is not requirement (or condition) to give these sensors same response if their substrates and deposition methods are different.

References:

1- Yongki M. Properties and sensor performance of zinc oxide thin films. Ph.D. Thesis, Massachusetts institute of technology(USA),2003.p.15. ,

2- Gao X. D., Li X.M. and Yu W.D. .Rapid preparation, characterization, and photoluminescence of ZnO films by a novel chemical method , Materials research bulletin. 40(7): 1104-1111;2005.

3- George F. F., Leon M. C., Ayo A. and Russell B.. Metal oxide semi-conductor gas sensors in Environmental monitoring. Sensors 10: 5469-5502; 2010

4- Oleg L., Sergiu Sh., Lee Ch. and Teodor Sh.. Nanostructured zinc oxide gas sensors by successive ionic layer adsorption and reaction method and rapid photothermal processing. Thin Solid Films. 516: 3338 – 3345;2008 .

5- Ganesh K. M. and John B. B.. A highly selective room temperature ammonia sensor using spray deposited zinc oxide thin film. Sensors and Actuators B. 183:459-466;2013.

6- Chandrakant D. . Characterization of nanosized zinc oxide based ammonia gas sensor. Applied Science Research. 5(6):96-102;2013.

7- Watson J.. The tin oxide gas sensor and its applications. Sensors and Actuators. 5:29-42;1984.

8- Minami T., Nato H., and Takata S..The stability of Zinc oxide transparence electrods fabricated by R. F. magnetron sputtering. Thin solid films. 111:167-174;1984.

9- Hidehito N., Tadatsugu M., and Shinzo T., Zinc-oxide thin film ammonia gas sensors with high sensitivity and excellent selectivity. J. Appl. Phys. 60(2):482-484;1986.

10- Winquist F., Spetz A., Armgarth M., Nylander C., and Lundstrom. Modified palladium metal-oxide semiconductor structures with increased ammonia gas sensing Appl. Phys.Lett. 43(9):839841;1983.

11- Mariappan R., Ponnuswamy V., Suresh P., Ashok N., Jayamurugan P.and Chandra B., Influence of film thickness on the properties of sprayed ZnO thin films for gas sensor applications, Superlattices and Microstructures. 71:238–249;2014.

12- Nichev H. , Angelov O. , Pivin J. , Nisumaa R. and Dimova-Malinovska D. Sensitivity of Co doped ZnO films to NH_3 at room temperature - influence of the deposition temperature, Journal of Physics: Conference Series .113: 012035;2008.

Al-Mustansiriyah Journal of Science
Vol. 27, No 2, 2016

journal homepage:www.mjs-mu.com

Creep Properties of Particles Materials Reinforced Epoxy Composites

Randa K. Hussain and Hussein K. Hashem
Al-Mustansyriya University, College of Science, Physics Dept.

Articleinfo

Received
17/9/2015
Accepted
21/12/2015

Key Word:
Creep, Epoxy, Composite, particles filler.

ABSTRACT

Composites were prepared from epoxy and particles fillers of copper, aluminum and calcium carbonate. Added effect has been studied to creep properties at room temperature and load 12.26 MPa. Properties that include creeping studied , primary creep, creep rate , the time of the fracture, exponential factor and activation energy, found that the addition of calcium carbonate particles to reduce the creep rate (0.0011) compared to epoxy, also more than doubled the time of the fracture , while primary aluminum particles than to creep in to a (0.1). Except imbricated epoxy / calcium carbonate , all materials tend to behave in a manner flexible exponential factor where it is located with in the range (0.26 – 0.38). Finally , all the filling had improved the activation energy results.

Particles of copper, aluminum and carbonated calcium filled epoxy for composites were prepared. The effect of addition on the creep properties of composites was assessed at room temperature and (12.26 MPa) loading. Creep properties that studied included: initial creep, creep rate, time to rapture, exponent factor, and activation energy. It is found that added carbonated calcium particles reduced the creep rate to (0.0011) comparing to epoxy and increased the rupture time to more twice times, while aluminum increased the initial creep strain to be (0.1). Except epoxy/$CaCO_3$ materials tend to behave in elastic manner where their exponent factor lies within range (0.26-0.38). Finally fillers enhanced the activation energy results.

الخلاصة

تم تحضير متراكبات من الايبوكسي وحشوات جسيمات كل من النحاس, الالمنيوم و كاربونات الكالسيوم. وقد دُرس تأثير الاضافة على خصائص الزحف عند درجة حرارة الغرفة وحمل (12.26 MPa). تتضمن خصائص الزحف التي دُرست: الزحف الابتدائي, معدل الزحف, زمن الكسر, العامل الأسي و طاقة التنشيط. وُجد ان اضافة جسيمات كاربونات الكالسيوم تقلل معدل الزحف الى (0.0011) مقارنة بالايبوكسي, كما تزيد زمن الكسر الى الضعف, بينما تزيد جسيمات الالمنيوم الزحف الابتدائي ليصبح (0.1). ماعدا متراكب الايبوكسي/ كاربونات الكالسيوم فأن كل المواد تميل لتتصرف بطريقة مرنة حيث يقع العامل الاسي لها ضمن المدى (0.38 - 0.26). أخيرا فان كل الحشوات قد حسنت من نتائج طاقة التنشيط.

INTRODUCTION

Over recent decades, a sustained effort has been spent to enrich knowledge of materials properties, however, limited information concerning the creep behavior of composites structural has been found. Many studies and researches specifically focus on the analysis of the creep behavior of materials and also the possibility to reinforce them with fibers, fillers as particles [1-3]. In fact, many studies deals with the development properties of materials structural to overcome creep behavior especially for metals, where they use polymers resins to reinforcement metals such as steel, but serious limitations appear like interfacial stresses and de-bonding [4]. The reinforcement as a composite exhibits a dramatically improved in mechanical properties, including reducing time dependent deformation of materials [5]. Because of a lack in fundamental knowledge on how creep affects and to understand creep mechanisms, this work aims to study creep and to enhancement mechanical properties to overcome or reducing creep deformation. When materials operate in their creep range, they undergo time-dependent deformation. For polymers creep takes place at or near their Transition glass temperature Tg [6]. Creep deformation usually occurs over a period of time when a material (or structure) is subjected to constant load (or stress) (i.e. time-dependent deformation). Strain (or deformation) increases with load, temperature, relative humidity and time. Polymeric materials, such as adhesives can undergo creep deformation at room temperature.

Theoretical Approaches

Materials are known a perfectly elastic if it stressed until compressed or stretched, then it return to its original shape when the stress is removed. In this situation the atoms of the stressed material are not moved from their positions during compressed or stretched, but the bond between atoms are compressed or stretched. In materials that are the atoms moved in their positions know as plastic materials. Material that has a permanent deformation, which is continues with the stress maintained. This slow gradual deformation is called creep. Creep rate ($\dot{\varepsilon}$) is calculated by change of dimensions ($\Delta\varepsilon$) over time (Δt) that is [7]:

$$\dot{\varepsilon} = \Delta\varepsilon/\Delta t \quad \ldots\ldots\ldots\ldots (1)$$

Due to their structure of chain – like molecules that forms polymers, creep is takes place in complex processes, the common equation described creep behavior in polymers is [8]:

$$\varepsilon = \varepsilon_0 + B\sigma^m t^k \ldots\ldots\ldots\ldots (2)$$

Where: (ε_0) is the initial strain, (m) is the polymer constant, and (k) is the constant of the exponent. The energy is needed to atoms of material to move past each other that causing creep is defined as activation energy (Q), it is written in term of gradient of creep rate and temperature by [8]:

$$Q = \frac{\Delta(ln\dot{\varepsilon})R}{\Delta(\frac{1}{T})} \ldots\ldots\ldots\ldots (3)$$

Where: R is general gas constant (8.31 J/mol.K). T is Absolut temperature

Materials and Methods

Epoxy material is increasingly found in structural applications for their light weight and durability, but it nature is not hard enough, exhibits a time-dependent behavior. Epoxy / particles composites were prepared by mixing epoxy with its hardener in (2:1) ratio. Particles of Cu, Al and $CaCO_3$were added (50wt%) to epoxy with continues mixing to ensure a good distribution of particles into polymer and leave to dry. Then material was cut into specimen that in figure (1) as illustrated dimensions.

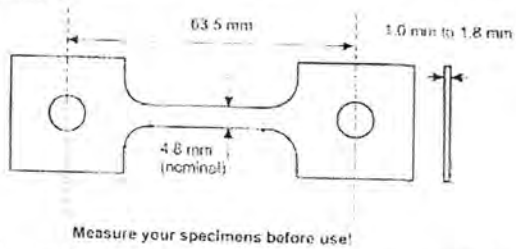

Fig.(1): Schematic of shape and dimensions of the samples[8].

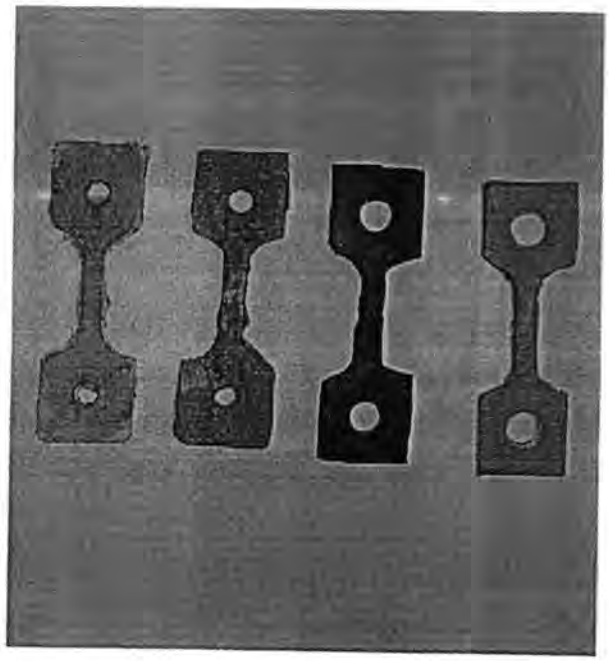

Fig(2): The samples of Epoxy- CaCO3 , Epoxy- Al , Epoxy – Cu and Epoxy

Results and Discussion

Creep properties of epoxy as a pristine material, as well as composites with particle fillers of copper, aluminum and carbonated calcium were investigated. Basically creep properties were studied in term of instantaneous creep, creep rate and creep fracture and activation energy for $50^0/_0$ filler to epoxy ratio and 12.26 MPa applied load at room temperature for each specimen, it is also examined the material behavior, creep mechanism, and creep activation energy. The test is done using creep machine model SM1006.

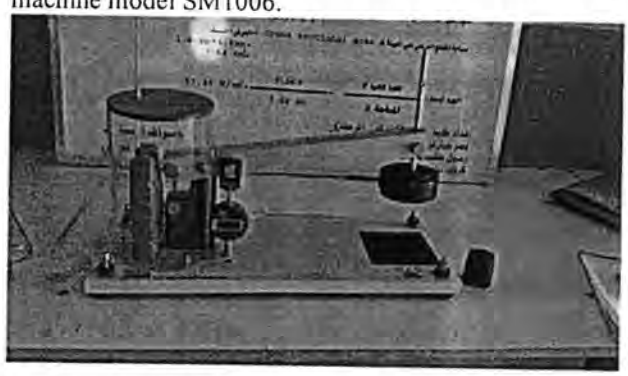

Fig(3): Creep Testing Machine.

Epoxy strain elongation maintained with time is not showed an expected typical creep behavior, this is the same for epoxy/Cu and epoxy/Al composites, and in both strains has constant increasing with time reaching to failed point. Adding Cu and Al to epoxy reduced the strains increments. This behavior may be attributed to epoxy structure nature of resins that give epoxy a soft form, this structure is enhanced creep deformation

resistance by adding particle filler of copper and Aluminum where the strain is clearly is lowered but this is not importance for time to failure which is still not high enough. Carbonated calcium particles were dramatically changed the strain behavior when added to epoxy; the curve is become near the well-known typical curve of creep besides that strain increment is lower than of epoxy longer life time, which is may due to that the epoxy structure is become stiffer but material did not lost its elasticity therefore material appears a small primary region of creep and longer secondary creep region as shown in figure (4).

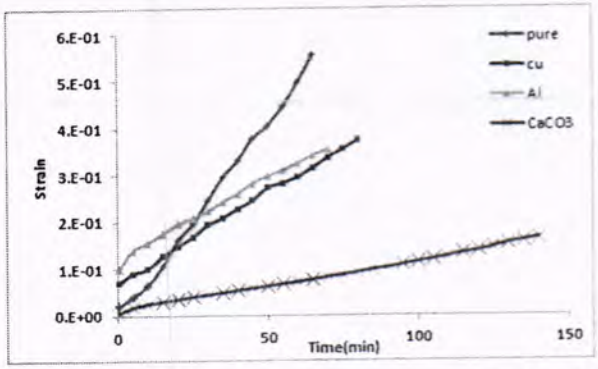

Fig (4): Typical strain – time creep curves of epoxy composites.

Creep rate is defined as steady –state creep that is calculated as strain gradient in secondary creep region. This region is importance stage that is because the material is must stay in duty within this stage and not cross to the third region (tertiary region). By using equation (2) creep rate is calculated for epoxy and epoxy composites of Cu, Al, and $CaCO_3$ particles fillers. Table (1) showed the creep properties of epoxy composites, steady – state creep is improved when using fillers of more than one order respecting to value of epoxy.
Correspondingly to decreasing of creep rate that make material needs longer to deform, the time to reach fracture is become longer, that is increased to 140 min for epoxy/$CaCO_3$ sample, it is more than twice of pure epoxy.

Table (1): Creep properties of epoxy composites.

Material	Epoxy	Epoxy/Cu	Epoxy/Al	Epoxy/$CaCO_3$
Creep rate (1/min)	0.0118	0.004	0.0031	0.0011
Initial strain	$2x10^{-2}$	$7x10^{-2}$	$1x10^{-1}$	$5x10^{-3}$
Fracture time (min)	65	80	70	140

It is range where the material is still in its elasticity, initial strain or as known as instantaneous creep that appear in table (1) are varied between increasing ($1x10^{-1}$) to decreasing ($5x10^{-3}$) according to initial strain in epoxy ($2x10^{-2}$), but is still small.
If the initial strain is very small, it may be neglected, thus, a linear relation of plot log of strain and log of time, the slope will give value of the exponent of k. The obtained value of k is a measure of the relative contribution elastic or plastic deformation to the creep process. Figure (3) is produces a relation between strain and time of epoxy and epoxy composites, where it is clear that are two distinctly linear regions; the first one is due to initial strain and the second is related to secondary creep. Table (2) gives values of exponent of k for epoxy and its composites. Each of epoxy, epoxy/Cu and epoxy/Al are behave in elasticity way, while $CaCO_3$ make the material tend to behave in plasticity manner, that is accordingly to relative high values of exponent constant k.

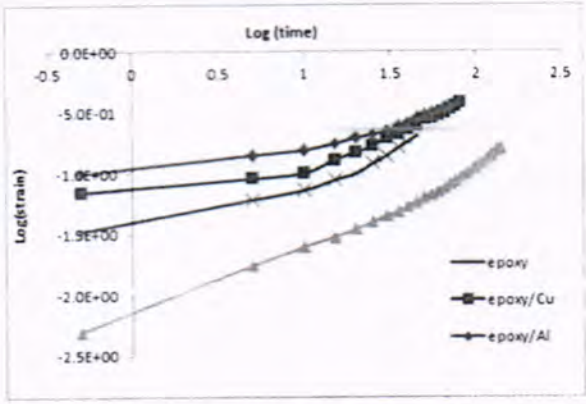

Fig (5): Relation between log strain and log time for k.

Table (2): Exponent values compression of epoxy and its composites.

Material	Epoxy	Epoxy/Cu	Epoxy/Al	Epoxy/$CaCO_3$
k values	0.389	0.370	0.269	0.633

The equation (3) is used to find the activation energy of creep process occurring, figure (4) shows a plot of two different stress levels at two different temperatures. From the vertical distance between the two lines and different between used absolute temperatures, the energy required to creep is found, its values given in table (3). It is observed that the activation energy is enhancement at adding filler, but $CaCO_3$ is provides the best result.

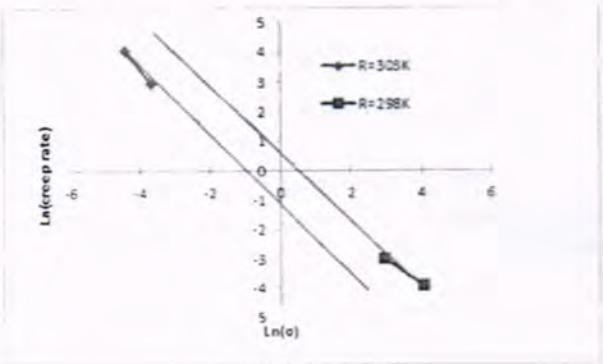

Fig.(6): Finding of activation energy of epoxy.

In same way the activation energy of epoxy- Cu, epoxy – Al and epoxy – CaCO3 was found which are given in table (3).

Table (3): Activation energy values compression of epoxy and its composites.

Material	Epoxy	Epoxy/Cu	Epoxy/Al	Epoxy/$CaCO_3$
Q (KJ/mol.K)	5.69	9.24	11.72	18.56

Conclusions

Generally the used particles fillers improved the creep resistance of epoxy, and well bonding is achieved. Each composite in this study showed a low in deformation according to their elastic behavior and them later the elasticity to plasticity transition.

References:

[1] Y. Moses, I. Simon, I. Maxwell, Mechanical Properties of Carbon Fiber and Metal Particles Filled Epoxy Composite, International Journal of Emerging Technology and Advanced Engineering, Volume 3, Issue 11, November 2013

[2] I. A. Mahmoud, W. A. Soud, O. S. Abdullah, Effects of Different Types of Fillers on Dry Wear Characteristics of Carbon-Epoxy Composite, Al-Khwarizmi Engineering Journal, Vol. 9, No. 2, P. 85 -93 , 2013

[3] G. Agarwal, A. Patnaik, R. K. Sharma, Mechanical and Thermo–Mechanical Properties of Bi- Directional and Short Carbon Fiber Reinforced Epoxy Composites, Journal of Engineering Science and Technology ,Vol. 9, No. 5 ,590 – 604 ,2014

[4] J. P. Agrawal, Composite Materials, Scientist Explosives Research & Development Laboratory Pune, 1990

[5] H-C. Wong, C.M. Sung and J. Hamilton, Mechanical Properties of Polymers, Journal of Material Science Letters, 1998

[6] D.A. William , K. Vipim, A Discrete Complex Compliance Spectra Model of the Nonlinear Viscoelastic Creep and Recovery of Microcellular Polymers , University of Washington, Department of Mechanical Engineering, 1999

[7] L.M. Ward, D.W. Hadley, An Introduction to the Mechanical Properties of Solid Polymers, John Wiley & Sons Ltd, West Sussex, England, 1993.

[8] Q. Tec (Tec Quipment), SM1006, Creep Machine , User Guide , 2009

[9] A.V. Tobol sky, Properties and Structure of Polymers, John Wiley & Sons Inc. New York, 1960.

Al-Mustansiriyah Journal of Science
Vol. 27, No 2, 2016

journal homepage:www.mjs-mu.com

Wake potential of individual ion in plasma gas

Baida M.Ahmed, Kalid A.Ahmed, Riayhd K.Ahmed
Al-Mustansyriya University, College of Science, Physics Dept.

Articleinfo

Received
29/9/2015
Accepted
16/11/2015

ABSTRACT

In present work the expression of the wake potential in classical plasma are studied by using Vlasove-Poisson models depending on dielectric dispersion function $(\in (k,\omega))$ for of plasma (tokamak, Z-pinch and incident proton in different parameters on three systems ICF).

The wake potential that excited by a test charge moving through dense plasma containing electrons, ions and neutral atoms calculate by using different densities and velocities of incident individual proton in classical plasma target. The value of wake potential increase with increased density for each system (ICF, Z-pinch and tokamak). So when compare between three systems note the wake potential for ICF system is the larger than other systems because the most density.

الخلاصة

تم دراسة ايقاظ الجهد في البلازما الكلاسيكية باستخدام نموذج (Vlasove-Poisson) بالاعتماد على دالة تشتت العزل $(\in (k,\omega))$ لعدة محددات للبرتون الساقط على ثلاث منظومات (tokamak, Z-pinch and ICF).

تم حساب الجهد المثار بواسطة شحنة اختبار تتحرك في وسط كثيف من البلازما يتكون من الالكترونات، الايونات والذرات المتعادلة باستخدام كثافات وسرع مختلفة للايون الساقط على المنظومات من خلال تسقيط ايون منفرد على هدف البلازما. نلاحظ ان الجهد يزداد مع الكثافة لكل منظومة (ICF, Z-pinch and tokamak)، لذلك عند المقارنة بين المنظومات الثلاثة نجد ان الجهد في منظومة ال ICF اكبر من المنظومات الاخرى بسبب كثافتها العالية.

INTRODUCTION

The interaction of charged particles with matter has been an issue of overall investigations throughout the whole century. Bohr considered the first one which start to treatment the energy loss of fast projectiles with the classical description theoretically. Bethe and repeated by Bloch Later a quantum mechanical treatment of the energy transfer to bound electrons was defined[1].

The partially ionized in plasma such as electron-electron collisions, electron-ion collisions, electron-neutral collisions, etc. collision processes are conveniently described by the concept of a cross section. Since some of the simple cross sections are modified by the plasma. For example, in the case of an electron or proton impinging on plasma, the cross section (known as the Rutherford cross section) is logarithmically divergent at large impact parameters, if the particles are free. This divergence is a result of the long-range nature of the coulomb force [2,3]. In a plasma the logarithmic divergence is avoided because the potential around a particular charge falls off as 1/r only within a Debye length, and then it decreases exponentially with radius [4].

Dielectric and dispersion functions in plasma gas

Dielectric formalism became one of the most used method to describe the stopping and electrostatic potential, is usually valid for high velocity projectiles and in a weak coupling limit of plasma [5]. Dielectric function by Fried-Conte expression used to calculate various aspects of energy loss of an ion moving in the plasma as shown in eq.(1) [6].

$$\in (k,\omega) = 1 + w\left[\frac{\omega}{k}\right]\frac{1}{k^2} \quad (1)$$

Where $\in (k,\omega)$is the dielectric function, k represent the wave vector and ω is the plasma frequency [7].

$$w(\zeta) \equiv X(\zeta) + iY(\zeta) \quad (2)$$

Where,

$$X(\zeta) = 1 - \zeta e^{-\zeta^2/2}\int_0^{\zeta} dx\, \exp(x^2/2) \quad (3)$$

$$Y(\zeta) = \left(\frac{\pi}{2}\right)^{1/2}\zeta ex\, p(-\zeta^2/2), \quad (4)$$

Where $X(\zeta)$ and $Y(\zeta)$ are real function.

To solve equations (3) and (4) must use spatial subroutine.[8], and dependence Dawson formal to solve this type of integral, Where (w) that was given in Eq.(2) represents the plasma dispersion function [9].

Debye length

Debye length is an important physical parameter in a plasma that provides the distance over which the influence of the electric field of an individual charged particle [10,11].

$$\lambda_D = 7.43 \times 10^2 \frac{[T(eV)]^{1/2}}{[n_e(cm^{-3})]^{1/2}} \quad (5)$$

Where λ_D is the Debye length in atomic unite., n_e density of electrons (or ions) and T is the electron temperature,

$$N_D = n_e\lambda_D^3 = \frac{3}{4\pi} \times 1.72 \times 10^9 \frac{[T(eV)]^{1/2}}{[n_e(cm^{-3})]^{1/2}} \quad (6)$$

N_D is the number of electrons with in a Debye sphere,

$$\omega_p = 5.69 \times 10^4 [n_e(cm^{-3})]^{1/2} \frac{rad}{sec} \quad (7)$$

ω_p is the electron plasma frequency,

$V_{th} = \sqrt{K_B T/m_e}$, is the thermal electron velocity,

Individual ions in plasma

The interaction of a fast ion beam impinging on a gas or plasma target is usually treated theoretically in the test particle approximation, i.e. under the assumption that each individual beam ion interacts without being aware of the presence of the other beam ions [12,13]. This assumption is reasonable in a great variety of experiments since in general the number density of the beam ions n_b is much smaller than the electron density n_e of the plasma target [14].

Plasma systems

- ***Tokamak system:***

A tokamak is a device using to confine a plasma by a magnetic field in the shape of a torus. To get a stable plasma equilibrium requires fined magnetic field lines that move around the torus in a helical shape. Such as helical field can be generated by a toroidal field and a poloidal field. In a tokamak, electromagnets one of the most effect to generated the toroidal field, is produced by that surround the torus, and the electric current responsible to create the poloidal field is the result of a toroidal that flows inside the target (plasma). This current is induced inside the plasma with a second set of electromagnets [15,16].

- **Z-pinch system**

Z-Pinch physics it's one of most important a device to create the plasma. Where use to determine the quantity of plasma and considered in the development of a simplified Z-Pinch fusion thermodynamic model. The important parameters used in Z-Pinch plasma system is rate of expansion, temperature and energy production to calculate parameters and characterize a propulsion system [17].

- **ICF-system**

ICF-system consider is one of the most systems used in inertial confinement fusion (ICF), dependent on some parameters a high density, low temperature plasma can be obtained during the compression phase, so minimizing the energy needed for compression. If the final temperature reached is low enough to degenerate the electrons of the plasma. In this case, bremsstrahlung emission is hardly suppressed and inflammation temperature becomes lower than in classical plasmas, which shows a new design [18].

Electrostatic potential in plasma

The understanding of potential distributions around a test charge in plasmas is of fundamental importance. It is well known that in a classical electron–ion collisionless plasma the short range potential. While the far-field potential of a moving test charge falls off as the inverse third power of the distance r between the test charge and the observer [19]. Due to collisional effects the far-field potential may fall off as the inverse square of the distance in classical plasmas with high temperatures and low densities [20]. The wake potential for individual proton can start from the following simple formula:

$$\emptyset_{ind} = -z_j e \int E.d\vec{r} \quad , \quad d\vec{r} = \vec{v}dt \quad (8)$$

$\emptyset_{ind}$ represent the wake potential of individual proton.

$z_j e$ is the charge of the target plasma, Since the distribution of charge density gives,

$$\rho(\vec{r},t) = \sum_i z_i e\, \delta(\vec{r} - \vec{r}_i - \vec{v}t) \quad (9)$$

Use the laplace transition at t=0, get

$$\rho(\vec{k},t) = \sum \frac{z_i e}{(2\pi)^{3/2}} e^{-ik.\vec{r}} \quad (10)$$

The electric field in dielectric function become,[21]

$$E(r,t) = \frac{-1}{2\pi^2}\sum_i ze \int d^3k \frac{2ik}{k^2} exp(ik.(r - r_i - vt)/\in (k.kv)) \quad (11)$$

After some derivative [18] get,

$$\varphi_{ind} = -z_j \left(\frac{-1}{2\pi^2}\right)\sum_i z_e \iint d^3k \frac{2ik.v}{k^2} \frac{exp\left(ik.(r_j - r_i - vt)\right)}{\epsilon(k,k.v)} dt \quad (12)$$

Eq (12) represent the wake of proton move in density of plasma at t=0, after integrations the equation obtain two parts real and imaginary in terms sin and cos equations,

$$\emptyset_{ind} = \sum_j \frac{-z_j e^2}{2\pi^2}\sum_i z_i \int \frac{2\pi\vec{k}.dk}{k^2\vec{v}} d\omega \times \left\{cos(\vec{k}.\vec{r}_{ji}) Re\left[\frac{1}{\epsilon(\vec{k},\vec{k}.\vec{v})}\right] - sin(\vec{k}.\vec{r}_{ji}) Im\left[\frac{1}{\epsilon(\vec{k},\vec{k}.\vec{v})}\right]\right\} \quad (13)$$

Therefore, the stopping force, $F = -\frac{\delta\emptyset}{\delta r}$ become,

$$F_j = \sum_j \frac{-z_j e^2}{\pi}\sum_i z_i \int \frac{\vec{k}.dk}{k.\vec{v}} d\omega \times \left\{sin(\vec{k}.\vec{r}_{ji}) Re\left[\frac{1}{\epsilon(\vec{k},\vec{k}.\vec{v})}\right] + cos(\vec{k}.\vec{r}_{ji}) Im\left[\frac{1}{\epsilon(\vec{k},\vec{k}.\vec{v})}\right]\right\} \quad (14)$$

From the condition of dielectric function,

$$\epsilon(-\vec{k},-\vec{k}.\vec{r}_{ji}) = \epsilon^*(\vec{k},\vec{k}.\vec{r}_{ji}) \quad (14)$$

from condition sin and cos expression,

$$sin(-\vec{k}.\vec{r}_{ji}) = -sin(\vec{k}.\vec{r}_{ji}) \quad \text{and} \quad \cos(-\vec{k}.\vec{r}_{ji}) = cos(\vec{k}.\vec{r}_{ji}) \quad (15)$$

Therefore Eqs. (12,13) become,

$$\emptyset_{ind} = \sum_j \frac{-z_j e^2}{\pi}\sum_i \int \frac{\vec{k}.dk}{k.\vec{v}} d\omega cos(\vec{k}.\vec{r}_{ji}) Re\left[\frac{1}{\epsilon(\vec{k},\vec{k}.\vec{v})}\right] \quad (16)$$

$$F_j = \sum_j \frac{-z_j e^2}{\pi} \sum_i z_i \int \frac{\vec{k}.dk}{k.\vec{v}} d\omega \cos(\vec{k}.\vec{r}_{ji}) Im\left[\frac{1}{\epsilon(\vec{k},\vec{k},\vec{v})}\right] \quad (17)$$

Therefore Eq. for self term of induced potential $\emptyset_s, \emptyset_{corr.}$ is given as follows

$$\emptyset_s = \frac{-2v_T^2 e^2}{\pi v^2} \int_0^\infty dk \int_0^{v/v_T} zdz \, |\rho_q|^2 \, Re\left[-\frac{1}{\epsilon(\vec{k},\vec{k},\vec{v})}\right] \sum_i z_i^2 \,] \quad (18)$$

$$F_s = \frac{2v_T^2 e^2}{\pi v^2} \int_0^\infty dk.k \int_0^{v/v_T} zdz \, |\rho \;\; |^2 \, Im\left[-\frac{1}{\epsilon(\vec{k},\vec{k},\vec{v})}\right] \sum_i z_i^2 \quad (19)$$

Where $z = \omega/kv_T$

Results and Discussion

Eqs. (18, 19) represent the wake potential and force in polar coordinates for individual proton.

The ions and electrons transition assumed by laplace transition according to eq.(10), and derived the most equation for wake potential.

Using equation (18) to calculated the wake potential of individual ion movement in classical plasma target for three systems (tokamak, Z-pinch and ICF). The potential distribution of single ion studied numerically through dielectric dispersion function has been programmed.

In figures (1,2 and 3) the study of wake potential as a function of distance in different densities of incident ions in dens plasma, show the wake potential increase with density for each system, ICF ($1x10^{22}$,$3x10^{22}$ and $7x10^{22}$)cm^{-3}

Z-pinch ($1x10^{18}$, $5x10^{18}$ and $7x10^{18}$) and tokamak system ($1x10^{13}$, $5x10^{13}$ and $9x10^{13}$) as well when compare between three system see the wake potential for ICF system is the larger than other systems because the most density.

As well the oscillator decreases with decrees the density and almost disappear in Tokamak system because it's less dense. At the highest density a deep wake potential exists close to the ion and the cone that formed end the ion to be the deepest how appear in the figures (1,2 and 3). When reducing density the number of electrons that deflected reduce by the ion.

Figures (4,5 and 6) shows the induced potential for self-interaction $\emptyset_s$ given in Eq. (18). The relation of electrostatic potential as a function to ζ=x-vt in 3D for three systems calculate for single ion in target plasma.

In ICF system see the waves increased with velocity, so in system Z-pinch shows the potential become large at $\zeta = 0$, and the area of potential increases with velocity in tokamak system.

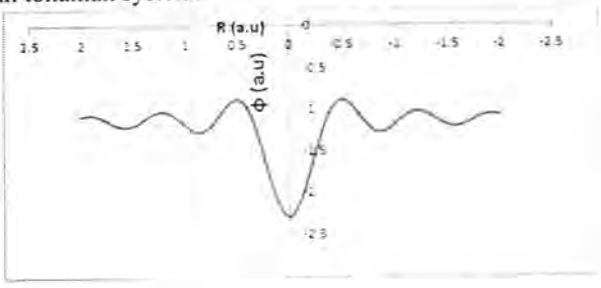

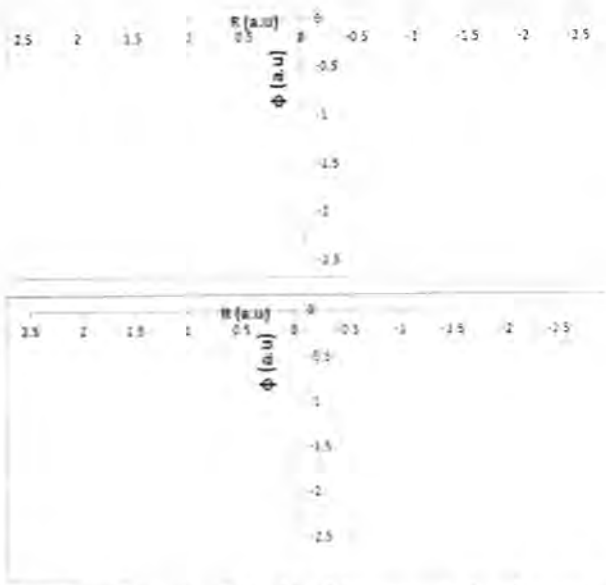

Fig. (1) wake potential of incident proton in plasma gas at T=300 eV and different densities (a) ($1x10^{22}$ (b) $3x10^{22}$ (c) $7x10^{22}$)cm^{-3} for ICF system.

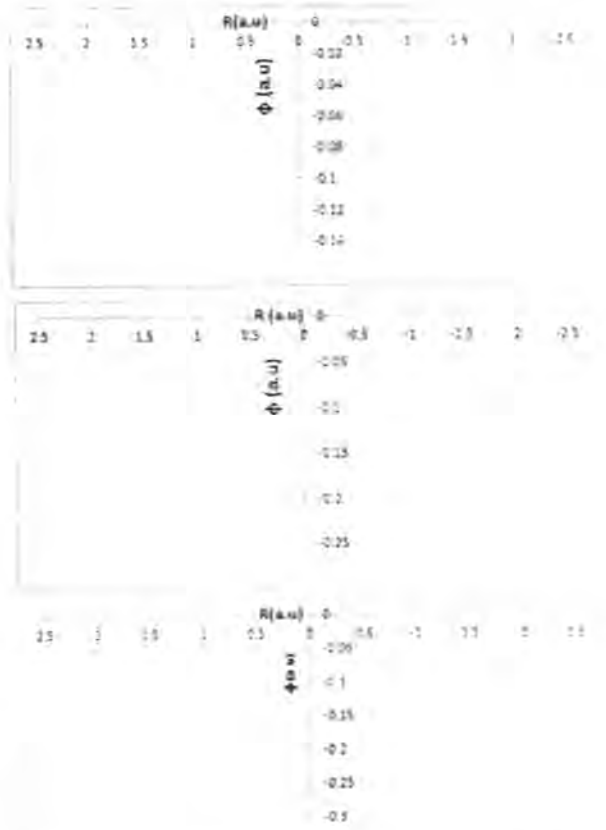

Fig. (2) wake potential of incident proton in plasma gas at T=20 eV and different densities (a)($1x10^{18}$ (b) $5x10^{18}$ (c) $7x10^{18}$)cm^{-3} for Z-pinch system.

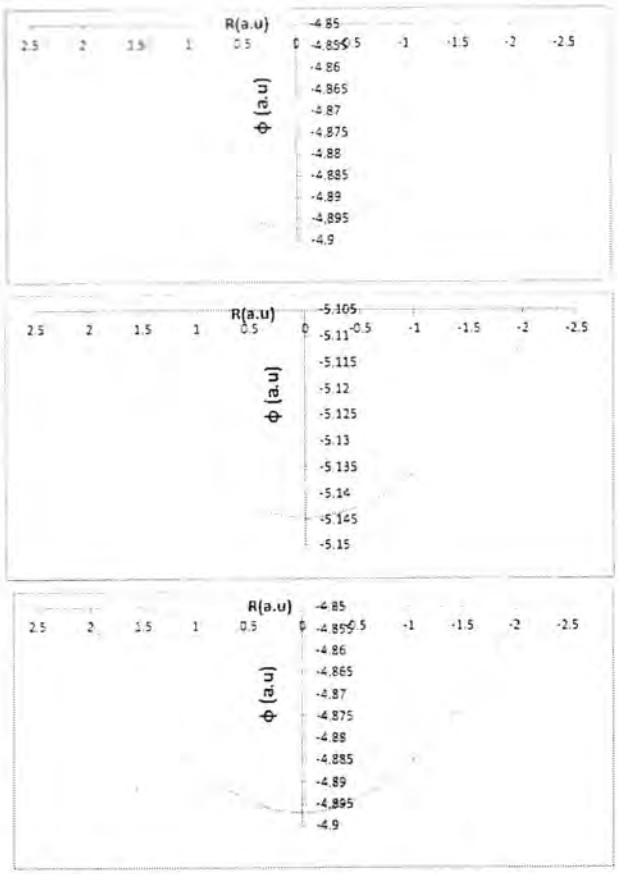

Fig. (3) wake potential of incident proton in plasma gas at T=1000 eV and different densities (a) $1x10^{13}$ (b) $5x10^{13}$ (c) $9x10^{13}$ for Tokmak system.

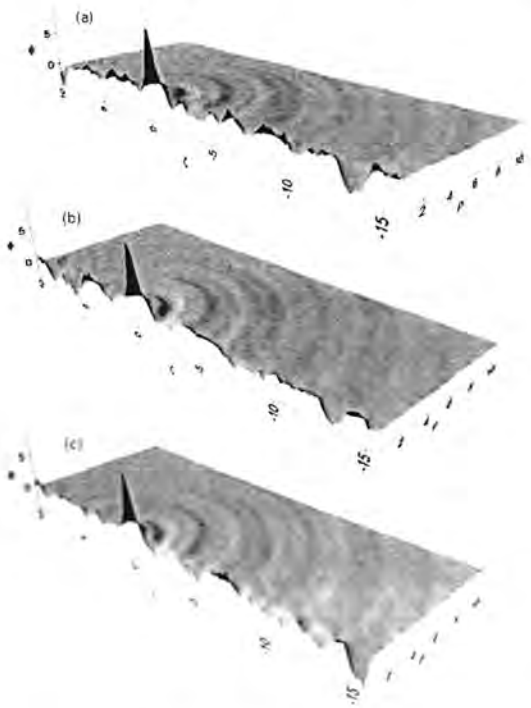

Fig. (4) The normalized ESP for single projectile (ϕ), the normalized axial position ζ=x-vt and the normalized radial position ρ, with Z=1 and λ=14.1. for system ICF, (a) v=0.025, (b) v=3.025 (c) v=5.025.

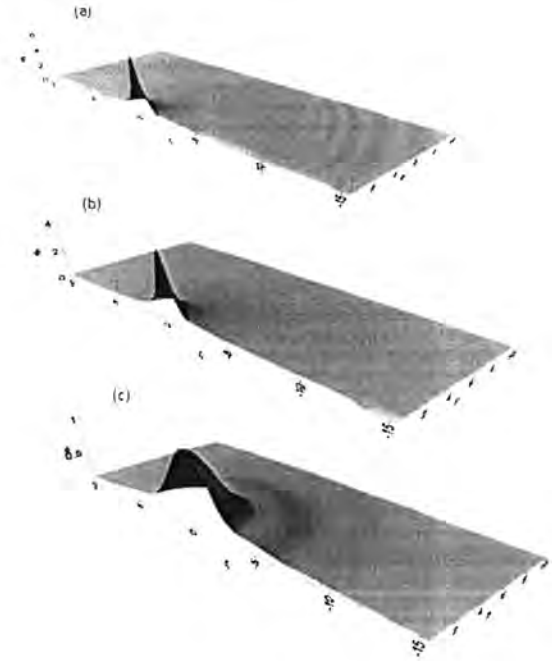

Fig. (5) The normalized ESP for single projectile (ϕ), the normalized axial position ζ=x-vt and the normalized radial position ρ, with Z=1 and λ=630. for system Z-pinch, (a) v=0.025, (b) v=1.025 (c) v=3.025.

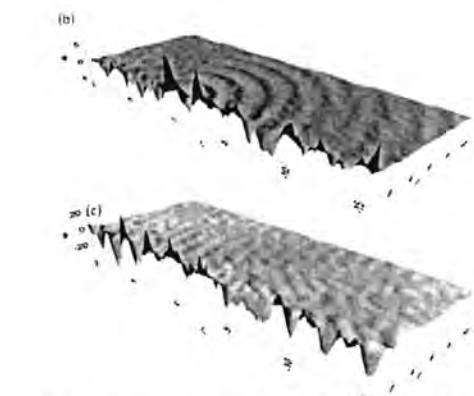

Fig. (5) The normalized ESP for single projectile (ϕ), the normalized axial position ζ=x-vt and the normalized radial position ρ, with Z=1 and λ=1.4x10^6. for system Tokamak, (a) v=50, (b) v=100 (c) v=150.

Conclusion

Dielectric dispersion function is very important in the presented work, the wake potential of proton has been studied theoretically and analytical for group of parameters in classical dielectric. Vlasove equation it's one of important method to calculate the wake potential in different cases in medium such as plasma because contain mathematical expression on dispersion function.

Wake potential increase with increase velocity that cause to the perturbation in plasma, and the wake potential increase with density for each system.

References:

[1] Zhang Y., Yuan-Hong S., "Study of stopping power for a proton moving in a plasma with arbitrary degeneracy" Physics of plasma 20, 102121, 2013.
[2] Hrachya B. N., Claude D., "A number-conserving linear response study of low-velocity ion stopping in a collisional magnetized classical plasma" arXiv: 1009.1700v1 [physics.plasm-ph] 9Sep 2013.
[3] Isidro V., Nestor R. A., "Stopping power and polarization induced in a plasma by a fast charged particle in circular motion" J. Phys. B,1455–1465, 2002.
[4] Hrachya B., "Energy loss of ions by electric–field fluctuations in a magnetized plasma" arXiv:1104.0878v2 [physics.plasm-ph], 2013.
[5] Brinca A. L., "Approximations to the Plasma Dispersion Function" NASA Grant NGL 05-020-176, SU-IPR Report No.500,1972.
[6] Della-Negra S., A.Brunelle, Nucl. Instrum. Methoeds B74,453,1993.
[7] Basbas G. and Ritchie R.H., Phy. Rev. A 25, 1982.
[8] Ahmed B.M.,"energy loss and wake potential of proton in plasma), thesis, (2015)
[9] Deustch C. and Fromy P., "Correlated ion stopping in a dense classical plasma" Phys. Rev.E, vol.51, No.1, 1994.
[10] Shafiq M., "Test Charge Response of a Dusty Plasma with Grain Size Distribution and Charging Dynamics" thesis, Stockholm 2006.
[11] Shukla P.K.,"Introduction to Dusty Plasma Physics" book,IOP Publishing Ltd 2002.
[12] Bringa E.M. and Arista N.R., "energy loss of correlated ions in plasmas: collective and individual contributions" Phys. Rev. E 54, 4101, 1996.
[13] Javier F., "Collective effects in the energy loss of large hydrogen clusters" Phys. Rev.A, Vol.54, No.5, 1996.
[14] Yoshi H., "Stopping Power of High Temperature Plasma" Progress of Theoretical Physics, Vol. 23, No.3, 1960.
[15] PINES D., "A Collective Description of Electron Interactions: II. Collective vs Individual Particle Aspects of the Interactions" Phys.Rev Vol.85, No.8, 1951.
[16] Schmidt J. A., Thomassen K.I. "The Design of the Tokamak Physics Experiment (TPX)" journal of Fusion Energy, Vol. 12, No. 3, 1993.
[17] J. Cassibry, R. Cortez, J. Santarius, "Z-Pinch Pulsed Plasma Propulsion Technology Development" Advanced Concepts Office (ED04) book ,2010.
[18] International Atomic Energy Agency "Plasma physics and controlled nuclear fusion research" Vol. 3, Printed by the IAEA in Austria, 1996.
[19] Shukla P.K, Eliasson B., "Screening and wake potentials of a test charge in quantum plasmas" Physics Letters A 372, 2897–2899, 2008.
[20] Nambu M., "Three-Dimensional Wake Potential due to Ion Cyclotron Waves in a Flowing Magnetized Plasma Physica Scripta. T98, 130^133, 2002.
[21] Murtaza, G. and H.Nasim M., "Anisotropic energy loss of a pair of charged projectiles in a dusty plasma", Physica Scipata, Vol.64, 346-350,2001.

Al-Mustansiriyah Journal of Science
Vol. 27, No 2, 2016

journal homepage:www.mjs-mu.com

Mathematical Models of Moving Bubbles in the water

[1]Fatima I.Abbas , [2] Ali Abid Dawood Al – Zuky , [2]Anwar H.Mahdy
[1]Department of Physics, College of Education, AL-Mustansiriyah University,
[2]Department of Physics, College of Science, AL-Mustansiriyah University, Baghdad, Iraq.

Articleinfo

Received
2/6/2014
Accepted
16/11/2015

ABSTRACT

Bubbles and foams are important features of liquid surface phenomena, this research Provides, the study of the movement of air bubble in the water and rising through the channel (water hose) tight, with different diameters (0.4, 0.5,0.7,1,and 1.2)cm, by using image processing technology build a computer algorithms to analysis the motion in image planes for the successive frames for extract images of video clip using FUJIFILM camera, considering the number of snapshot represents function of the time, and determine the rising bubble location, speed and Acceleration . By using suitable processing for a software package, such as programs (Ulead Studio 2011, Matlab 2012b and Table Curve(TC) version 5.01). After that using fitting processing to estimate the best fitting model for the motion parameters. Then comparing between the real motion parameter deter as a function of times and the estimated values from the estimated model. Where have been found high a agreement between them.

الخلاصة

الفقاعات والرغوة هي السمات الهامة لظواهر سطح السائل ، تم في هذا البحث دراسة حركة فقاعة هواء في الماء والمتصاعدة عن طريق قناة (انبوب ماء) ضيق ، بأقطار مختلفة (1.2,1,0.7,0.5,0.4) سم ، باستخدام تقنية معالجة الصور ، وذلك ببناء خوارزميات حاسوبية لتحليل حركة الفقاعة في مستوي الصورة من خلال التسلسل المتتالي للصور(اللقطات) المستقطعة من الفديو باستخدام كاميرا FUJIFILM ،على اعتبار عدد اللقطات تمثل كدالة للزمن وتحديد الموقع والسرعة والتعجيل للفقاعة المتصاعدة . وباستخدام المعالجة المناسبة لمجموعة برامج ، مثل برامج (يوليد ستديو 2011،ماتلاب ٢٠١٢ و Table CurveTC version 5.01) . تم تقدير افضل نموذج لمعاملات الحركة .ومن ثم مقارنة بين معاملات الحركة الحقيقية بدلالة الزمن والقيم المقدرة من النموذج . حيث وجد توافق عالي بينها .

INTRODUCTION

Bubbles Known, it is a gas, surrounded by a liquid membrane or solid, very thin. And playing surface tension, essential role in the formation of bubbles, surface tension, is a physical property, attract particles with each other, thus behaving liquid surface like a roped membrane, make surfaces has a smaller space, thus take bubble form spherical. Bubbles consists, as a result of arent pressure or shaking out, and immediately remove the pressure or shaking out or arent, pushed, gas bubbles rising to the outside to the top surface of the water[1].

Air bubbles are used in chemical, biochemical, environmental, and food process for improving the heat and mass transfer. Bubbles play an important role in many applications such as; the fermentation process, the cooking processes, determining the rates of heat and mass transfer and coalescence, the pipeline transport applications, polymer and sludge processes and others [2]. The bubbles find uses in many process industries such as in vacuum pan operation in sugar industries which is an important process for the production of raw sugar. A number of researches have been conducted to study the bubbles and its properties in different ways, in the following some of these studies as following:

Jeong-Mo Hong et. al.[3] in 2003, presented a new fluid animation technique in which liquid and gas interact with each other, using the example of bubbles rising in water. In addition to the flowing motion, the interactions between liquid and gas cause buoyancy, surface tension, deformation and movement of the bubbles. They combine the volume-of-fluid method and the front-tracking method developed in the field of computational fluid dynamics.

Hassan N.M.S.et. al.[4] in 2007, Presented the bubble rise phenomena in different low concentration polymer solutions for higher Reynolds number(R_e). The main characteristics, namely, the bubble velocity, the bubble trajectory and the drag relationship are investigated. The results show that the average bubble rise velocity increases with the increase in bubble volume for different low concentration polymer solutions and the

bubble velocity is not dependant on the size of the test rig. In trajectory analysis, they seen that the smaller bubbles show helical or zigzag motion and larger bubbles follow spiral motion.

Jeong-Mo Hong et. al.[5] in 2008, presented a hybrid of Eulerian grid-based simulation and Lagrangian smoothed particle hydrodynamics (SPH) for the realistic simulation of multiphase fluids, focusing on bubbles, they used there heuristic bubble model, they could generate natural looking computer generated bubbly water.

Also Ho-Young Lee et. al.[6] in 2009, seeded Lagrangian bubble particles in air bubbles and caused them to move like molecules in order to create turbulence and consequently simulate realistic fluid in a grid based fluid simulation. In conclusion, the contributions of their paper is that it enables animators to control various fluid motions by creating turbulence with bubble particles and correcting the volume of air bubbles.

Markus Ihmsen et. al.[7] in 2011, proposed a velocity based heuristic that generates air bubbles for inflows. Thereby, trapped air is animated efficiently, i.e. without explicitly simulating the air phase surrounding the liquid. Also employ a simple foam model in order to simulate floating air bubbles.

While N.M.S.Hassan et. al.[8] in 2012, propose a comprehensive comparison of experimental results of the bubble trajectory and shapes are made for water, polymeric solutions and a crystal suspension.They were seen from their study that the trajectories of bubbles were significantly influenced by the bubble deformations and the surrounding liquid flow.

Our research is study the rising air bubble in the water basin, using image processing technology to bubble tracker, to generate the trajectory of an bubble over the time by locating its position in every frame of video typically, tracking over time consists of matching moving bubbles in successive frames, using FUJIFILM camera. Then estimated mathematical models for rising bubble motion ,location, velocity and acceleration as function of the time.

Fluid Dynamic Definitions

In fluid dynamics, the Morton number (M_o) is a dimensionless number used together with the Eötvös number(E_o) or Bond number(B_o) to characterize the shape of bubbles or drops moving in a liquid or continuous phase, The Morton number(M_o) and Eötvös number(E_o) are defined as[9],

$$M_o = \frac{g\mu_l^4 \Delta\rho}{\rho_l^2 \sigma^3} \qquad (1)$$

$$E_o(B_o) = \frac{gL^2\Delta\rho}{\sigma} \qquad (2)$$

Where g is the acceleration of gravity measured in (m/s^2), $\mu_l$is the viscosity of the surrounding fluid measured in (Pascal.sec), ρ_l the density of the surrounding fluid measured in (kg/m^3), $\Delta\rho$ the difference in density of the phase measured in (kg/m^3), σ is the surface tension coefficient measured in (N/m), and L is characteristic length measured in (m). The Morton number(M_o) can also be expressed by using a combination of the Weber number(W_e), Froude number(F_r) and Reynolds number(R_e)[9],

$$M_o = \frac{W_e^3}{F_r R_e^4} \qquad (3)$$

The Froude number(F_r) in the above expression is defined as[9]:

$$F_r = \frac{v_b^2}{g d_{eq}} \qquad (4)$$

Where v_b is the bubble rise velocity measured in (m/sec) and d_{eq} is the equivalent diameter measured in (m) of the drop or bubble. A high value of the Eötvös(E_o) or Bond number(B_o) indicates that the system is relatively unaffected by surface tension effects; a low value (typically less than one) indicates that surface tension dominates. Intermediate numbers indicate a non-trivial balance between the two effects, where weber number(W_e), and Reynolds number(R_e) are defined as[9]:

$$W_e = \frac{\rho_l v_b^2 d_{eq}}{\sigma} \qquad (5)$$

$$R_e = \frac{\rho_l d_{eq} v_b}{\mu_l} \qquad (6)$$

Bubbles Motion and Types

The characteristics of bubble motion in liquids are still not well understood because many parameters influence the terminal rise velocity, trajectory and shape of bubbles[10]. As the bubble motion is a complex problem, the degree of the complexity increases with bubble size[11]. When bubble rises through liquid, the most resistance will be imposed directly on top and the bubble first moves along a straight vertical path and then develops a zigzag motion which consequently can change into a spiraling motion, at the same incidence as the preceding zigzag[12]. In most reported studies, very small bubbles (less than 1 mm) rise through water maintaining their spherical shape due to surface tension. The trajectory of these bubbles follows a straight line until it completes its journey[13]. On the other hand, considerable deformations are observed for bubbles with diameters larger than 1 mm [14]. This deformation occurs due to the increase in the variations of hydrostatic and dynamic pressure over the bubble's surface[15]. Therefore, large bubbles cannot remain spherical and deform into oblate spheroids first and then become ellipsoidal, and with further increase in size they switch into a spherical or ellipsoidal cap. Bubble motion such as velocity and trajectory also change with the increase in bubble size [16].

The bubble is not always rising in straight path. When the bubble size increases, a straight path turns into zigzag or spiral in fluids of small Morton number(M_o). Then the path becomes nearly straight again for a spherical cap bubble. Only a straight path is observed in liquids of large Morton number(M_o) [17]. Aybers, N. M.et.al. reported different types of trajectories such as zigzag, helical or spiral and rocking motions[18]. Haberman, W. L.et.al. also observed rectilinear (R_e

(Renold's number)< *300*), spiral and rocking motions[19]. They indicated that the spiral path could be either clockwise or counter-clockwise, depending on the conditions of bubble release. The major axis of the bubble is always directed perpendicular to the direction of motion. Saffman, P. G. observed only zigzag bubble rise motions as the bubble rises in water when the radius of the bubble was less than 1 mm, but bubbles of larger radius showed either zigzag or spiral motions[20]. Feng, Z. C. et.al. verified various possible trajectories for different shape regimes[21]. A single bubble can follow a zigzag path at Re ≈600, accompanied with vortex shedding behind the bubble. Under the same experimental conditions, Yoshida, S. et.at. reported that the bubbles can also follow a spiral trajectory without vortex shedding[22]. Tsuge, H. et.al. reported that the trajectories of rising spherical and ellipsoidal gas bubbles at higher Reynolds numbers are identical[23].
The trajectories of bubbles are strongly influenced by the bubble deformations and the surrounding fluid flow [24]. Bubble deformations and fluid flow could be explained with dimensionless groups such as the Reynolds Number (R_e), the Weber number (W_e), the Morton number (M_o) and bubble aspect ratio (E) [16],[25]. In fluid mechanics, R_e gives a measure of the ratio of inertial forces to viscous forces and consequently quantifies the relative importance of these two types of forces for given flow conditions. On the other hand, W_e is often useful in analyzing fluid flows where there is an interface between two different fluids, especially for multiphase flows such as bubble rise in liquids. It can be thought of as a measure of the relative importance of the fluid's inertia compared to its surface tension. The quantity is useful in analyzing the formation of droplets and bubbles. The dimensionless number such as M_o, is also used together with the Eötvös number (E_o) to characterize the shape of bubbles or drops moving in a surrounding fluid or continuous phase. Eötvös number(E_o) is considered as proportional to buoyancy force divided by surface tension force[8],

$$E = \frac{d_w}{d_h} \qquad (7)$$

Where d_w is represent semi major axis, and d_h represent semi minor axis. Usually, R_e controls the liquid flow regime around the bubble and W_e, M_o and E characterize the bubble deformations and bubble shapes. Therefore, the influences of R_e , W_e and M_o are seen as important for elucidation of the bubble trajectories[8].

Bubble Shapes

The shape of the bubbles greatly influences the bubble rise velocity and it has a significant role in determining the rates of heat and mass transfer and coalescence. Normally, a motionless bubble has a spherical shape because surface tension minimizes surface area for a given volume. When a bubble has motion, different forces exist such as drag caused by the liquid, viscosity of the liquid, pressure difference between the top and bottom of the bubble as well as the wall effects. Mainly, three types of shape such as spherical, ellipsoidal and spherical-cap or ellipsoidal cap in free motion under the influence of gravity are observed in Newtonian liquids[8].
The shapes of bubble are related to the R_e, at low R_e, the bubble retains its shape as a sphere because interfacial forces and viscous forces are much more important than inertia forces. Most bubbles of small size fall into this category. The spherical shape of the bubble is shown in the Figure(1A). The next category of bubbles is termed "ellipsoidal"; these are oblate with a convex interface around the surface when viewed from the inside. The liquid viscosity may affect the bubble shape, stretching the bubble out laterally, so that actual shapes may differ considerably from true ellipsoids. However, the general shape is comparable to an ellipsoid which is shown in Figure(1B and 1D)[8].

Figure 1. Different types of bubble shape in Newtonian fluid[8].

Large bubbles have a flat base or a spherical wedge, which may look very similar to segments cut from a sphere. They are heavily distorted from the equilibrium shape of a sphere. In this case, the Reynolds number is high and these bubbles are termed as spherical-cap or ellipsoidal-cap, as shown in figure(1C)[8].

Determine The Bubbles Motion Parameters Models

A digital FUJIFILM camera (Z20-3X optical zoom-10 mega pixel) outside the water has been used in this study. The work system show as in the block-diagram in figure(2), design to determine the location r(x,y), change in displacement (Δr), velocity(v) and acceleration(A) for rising bubble in the water, in which the work was divided into several steps, the practical work and detail of the uses, tools, devices, algorithms and software for each steps will be explain:

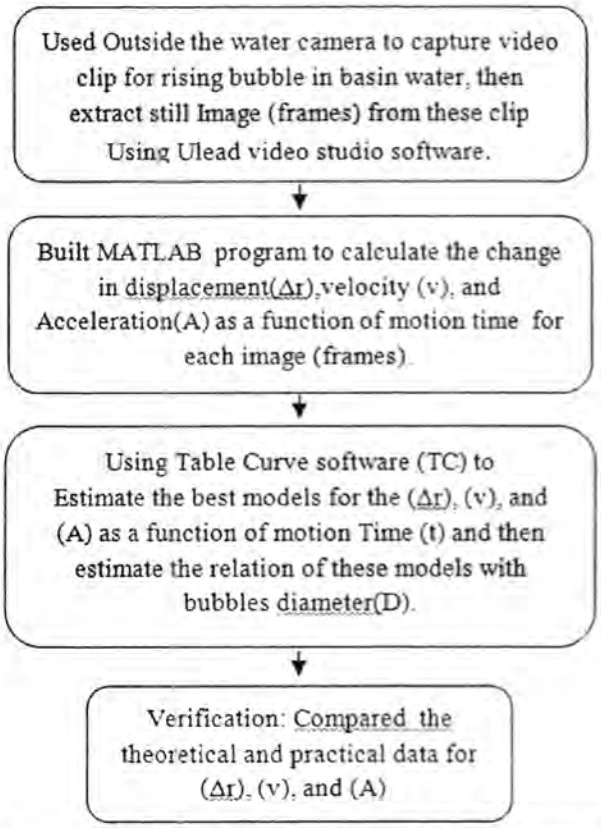

Figure (2) : The Block diagram explain the steps of estimate the motion statistic for rising bubble in the water.

The following steps, explain the processing steps study:
1. Extract Still Images (frames) From Video Clip: Rising bubbles produce by pumping a gas in hose then the gas will be reach the terminal end of the hose at the lowest depth of water in the basin . This gas after exit from the hose will be produce a bubble move up ward to the upper surface. Traditional digital camera outside the water imaging was performed. Basin dimensions is (80,37,50) cm^3 filled with water as show in figure(3a), have been used five different diameters(D) of hoses (0.4,0.5,0.7,1,and 1.2)cm. For constant space (k=50 cm, distance between the camera and rising bubble), have been taken video clip.
Using Ulead video studio 2011 plus software to convert video clip into still images (frames) this frames save in JPEG format, these video clip each second converted into 30 (fps). First frame $f(x_1,y_1)$ started from the bottom at initial time=0 sec, second frame $f(x_2,y_2)$ its time 1/30 sec, third frame $f(x_3,y_3)$ its time 2/30 sec...etc, these images extract as a frame of time $f(x_t,y_t)$. Thus determine the difference between two points from, $[f(x_{t+1},y_{t+1})-f(x_t,y_t)]$ as shown in the figure(3b), to reach the surface of the basin.

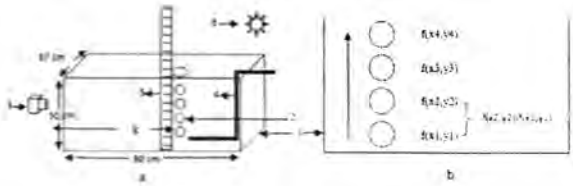

Figure (3) (a) the used basin : (1)basin water,(2)rise bubble,(3) traditional camera (FUJFILM), (4)hose,(5)ruler (6)source of light.(b) The sketch of the rising bubble in basin .

2. Analysis Algorithms: The first algorithm to compute the scale factor (Scf) for the more visible frame image, this is performed by measure the real value of bubble diameter(d_{cm}) by ruler putting in the basin through the itself image, and determining the bubble diameter(d_{pixel}) in image plane by selected two points on the boundary in the image by using computer mouse, see figure (4). Then used distance law as in the algorithm(1) to compute scale factor(Scf), this scale factor can used in another algorithm computation in this work.

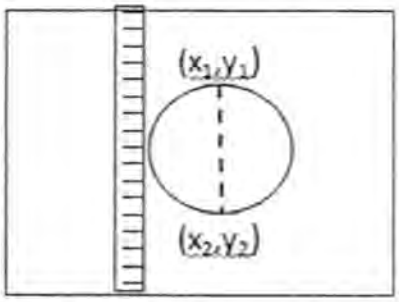

Figure (4) shows the Dotted line in image plane to determine the bubble diameter once manually by mouse in pixel unit and another by ruler in cm unit

Algorithm (1) Determine of Scale factor(Scf) for the frame image

Input:
1- The image of rising bubble in the basin (img).
2- Input known length (l_{cm}) on the ruler.
Out put:
Scale factor (Scf)
Start algorithm
1. load image(img) , to determine diameter of the bubble (x_1,y_1)
2. manually selected two fixed points length information on the ruler to determine the Diameter (corresponding points) of bubble's in the image plane to compute bubble diameter in pixel
this process can be explained in two step:
i. Used the property (mouse click) and determine the first point on the ruler(x_1, y_1) corresponding to point of the first end of known ruler length (1cm) in image plane
ii. Move and used the property again (mouse click) and determine the second point on the ruler (x_2, y_2) to second end of the known ruler length (1cm) in the image plane see figure (4)
3. Compute the length in pixels between points (x_1,y_1) and point(x_2, y_2) using:

$$l_{pixel} = \sqrt{(x_2 - x_1)^2 + (y_2 - y_1)^2}$$

4. Compute scaling factor for this image frame using:

$$Scf = \frac{l_{cm}}{l_{pixel}}$$

5. Print Scf.
6. End algorithm.

The second Algorithm describe the process in detail how can be calculate the rising bubble location r(x,y), change of displacement (Δr), the velocity(v) and the acceleration(A) for each frame image, by using following algorithm:

Algorithm (2) calculate the location r(x,y), change of displacement(Δr), the Velocity(v) and the Acceleration(A) of the moving bubble inside the water.

Input:

1- Scale factor (Scf).
2- The sequence n-frames $(img_{(1)}),(img_{(2)}),\ldots\ldots(img_{(n)})$.

Out put:

i. The distance between two balls images both in pixels and centimeters. (Δr)pixel, Δr(cm).
ii. The velocity(v) in centimeter.
iii. The Acceleration(A) in centimeter .

Step1.: manually selected two bottom points in input images $(img_{(1)})$ as a fallow:

i. Used the property of (mouse click) and determine the bottom point $(x_{(1)},y_{(1)})$ of ball image $(img_{(1)})$.
ii. Used the property again (mouse click) and determine the bottom point $(x_{(i+1)},y_{(i+1)})$ of ball image $(img_{(i+1)})$.

Step 2.: Compute the distance in pixels between the two points $(x_{(i)},y_{(i)})$, $(x_{(i+1)},y_{(i+1)})$ using:

$$\Delta r_{pixel} = \sqrt{(x_{i+1} - x_i)^2 + (y_{i+1} - y_i)^2}$$

Step 3.: Converted Δr from pixels to centimeters (cm) using.

$$\Delta r_{(cm)} = Scf * \Delta r_{(pixel)}$$

Step4.: Compute the velocity(v_i) in centimeter, depending on Δr_{cm} using the following equation :

$$v_i = \frac{\Delta r}{\Delta t} \quad \text{Where } t = \frac{1}{5} \text{ sec, and } \Delta t, \text{ represent the difference of two sequence frame.}$$

Step 5.: input image $(img_{(i+1)})$ and repeat steps (from step1 to step 4) for $(img_{(i+1)})$ and $(img_{(i+2)})$sequence frame by frame to compute (v_{i+1}).

Step 6.: Compute Δv_{cm} using

$$\Delta v_{cm} = v_{i+1} - v_i$$

Step 7.: Compute the Acceleration (A) in centimeter as following equation :

$$A = \frac{\Delta v}{\Delta t}$$

Step 8.: End algorithm.

3. Motion Parameters Modeling :

Used "Table Curve 2D Version 5.01" to fitting the practical Δr, v and A data for different Diameter of hose(D) to introduce appropriate mathematical function for captured Δr, v and A data for the frame images. This section contains the results of performing the suggested algorithms for the images frames Δr, v and A data fitting of a rising bubble in the water at constant distance space k=50 cm(distance between the camera and the rising bubbles), and various Diameter of hose D=0.4,0.7,1, and 1.2cm, see figures(5,6,and 7).

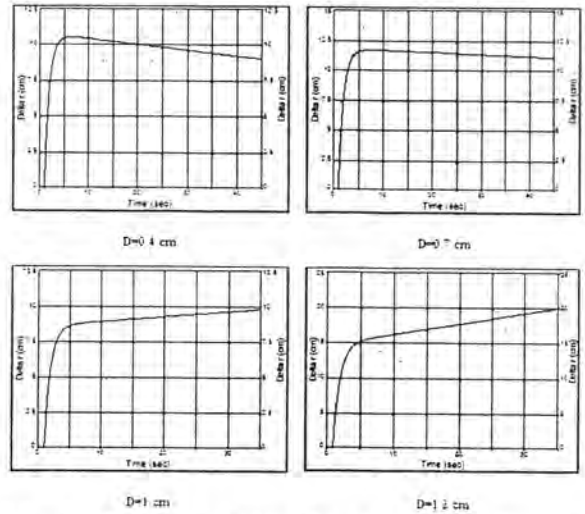

Figure (5) shows Delta r(cm) as a function of the time(sec) for various diameters D(cm)) of the hoses in water.

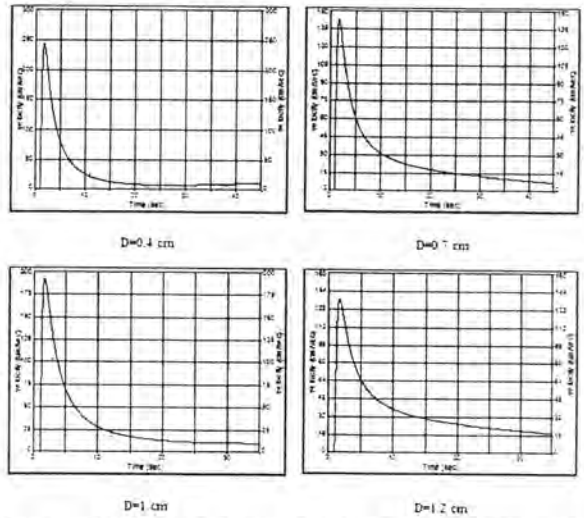

Figure (6) shows velocity(v) cm/sec as a function of the time(sec) for various diameters D(cm)) of the hoses in water

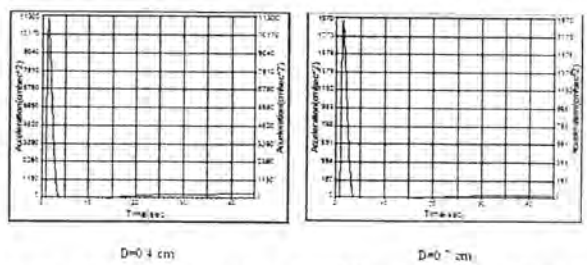

Figure (7) shows Acceleration(A) cm/sec^2 as a function of the time(sec) for various diameters D(cm)) of the hoses in water.

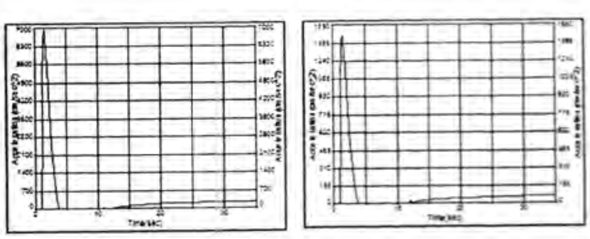

D=1 cm D=1.2 cm

Continue figure (7) shows Acceleration(A) cm/sec2 as a function of the time(sec) for various diameters D(cm)) of the hoses in water.

Table (1): The parameters of the fitting equations for three functions
Δr,v,A data and real various Diameter(D).

Diameter (D) cm	Change of displacement(Δr)				Velocity(v)				Acceleration (A)			
	a_i	b_i	c_i	r^2	a_j	b_j	c_j	r^2	a_k	b_k	c_k	r^2
0.4	10.86	0.04	-29.3	0.94	3.91	[illegible]	[illegible]	[illegible]	334.2	[illegible]	[illegible]	[illegible]
0.7	11.88	-0.02	-31.6	0.91	-2.15	[illegible]	4152.2	[illegible]	[illegible]	[illegible]	[illegible]	[illegible]
1	[illegible]	[illegible]	-35.9	[illegible]	[illegible]	[illegible]	[illegible]	[illegible]	[illegible]	[illegible]	[illegible]	[illegible]
1.2	14.72	0.152	[illegible]	[illegible]	[illegible]	[illegible]	[illegible]	[illegible]	[illegible]	[illegible]	[illegible]	[illegible]

The relation between (ai,bi and ci)-parameters as a function of the Diameter(D), using table curve TC software obtain the following equations:

$$a_i = 10.4 + 3.07D^2 \quad (11)$$
$$b_i = -0.07 + 0.16D^2 \quad (12)$$
$$c_i = -28.15 - 7.34D^2 \quad (13)$$

Eqs.(11,12 and 13) representing the relation between (ai,bi and ci)-parameters and Diameters (D) of hoses. By substituting these equations into eq. (8) get mathematical models that relates change displacement (Δr), Time (t) and Diameters (D):

$$\Delta r = (10.4 + 3.07D^2) + (-0.07 + 0.16D^2)t + (-28.15 - 7.34D^2)e^{-t} \quad (14)$$

Eq.(14) represented the mathematical motion model for Δr parameter of rising bubble in water.

While the mathematical model for velocity (v) parameter can be estimated in same way of estimated Δr, the estimated parameter is as follow:

$$a_j = -11.46 + 21.53D^3 \quad (15)$$
$$b_j = 0.52 - 0.49D^3 \quad (16)$$
$$c_j = 1463.67 - 484.53D^3 \quad (17)$$

Eqs.(15,16 and 17) representing the relation between (a_j,b_j and c_j)-parameters and Diameters (D). By substituting these equations into eq.(9) get mathematical model that relates velocity(v), time (t) and diameters (D)

$$v = (-11.46 + 21.53D^3) + (0.52 - 0.49D^3)t + (1463.67 - 484.53D^3)\frac{ln(t)}{t^2} \quad (18)$$

Equation(18) represent the mathematical model for v parameter of motion for the rising bubble in water at the constant space k=50 cm (distance between camera and rising bubbles).

Also can be found mathematical model for Acceleration (A)- parameters with the same way estimated in of Δr and v, the estimated parameter is:

$$a_k = 242.38 - 564.22D^2 ln(D) \quad (19)$$
$$b_k = -40218.83 + 11008.02D^2 ln(D) \quad (20)$$
$$c_k = 108669.93 - 312174.15D^2 ln(D) \quad (21)$$

Where the eqs.(19,20 and 21) representing the relation between (ak,bk and ck)-parameters and Diameters (D) for an acceleration of the rising bubbles. By substituting these equations into (10) get mathematical model that relates Acceleration (A), Time (t) and Diameters (D):

$$A = (242.38 - 564.22D^2 ln(D)) + \frac{(-40218.83 + 11008.02D^2 ln(D))}{t^2} + (108669.93 - 312174.15D^2 ln(D))e^{-t} \quad (22)$$

Eq.(22) represent the mathematical model for the acceleration(A) of rising bubble motion in water.

4. Models Verification: The verification have been preformed by canceled the practical results for diameter (D=0.5 cm) from fitting operation in previous modeling process. In order to determine their values theoretically from the estimated mathematical model and make a comparison between the experimental and theoretical data. now will be reviewing the graphically details for the practical and theoretical for each functions (Δr,v and A) of rising bubble, see figure(8).

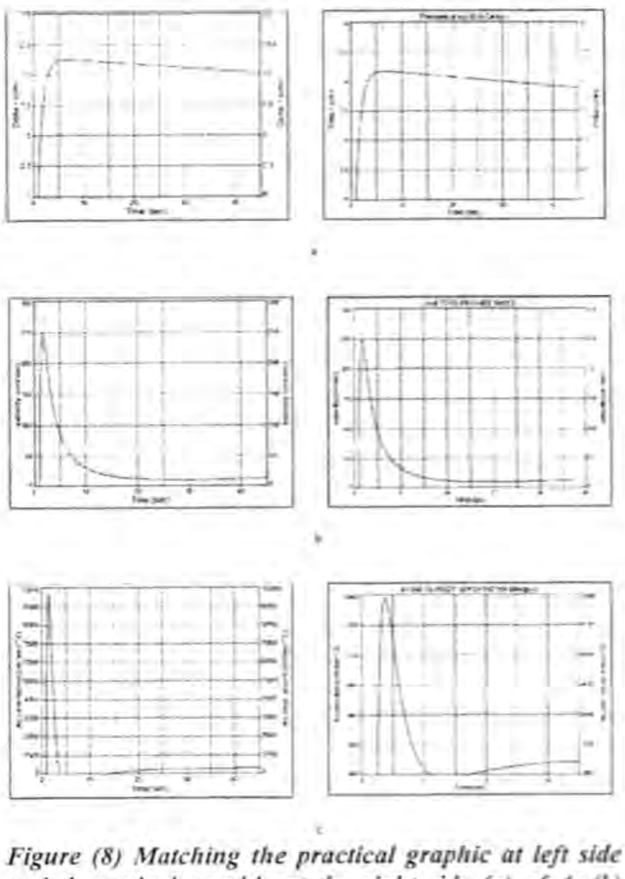

Figure (8) Matching the practical graphic at left side and theoretical graphic at the right side (a) of Δr,(b) Velocity(v),and(c)Acceleration(A) for the rising bubble in water.

As in figure (8) notes that the excellent match between the practical and theoretical curves, An error percentage

resulting between the practical and theoretical for Diamrter (D=0.5cm) tabulated in the table(2).

Table (2) Shows the error percentage resulting between the practical and theoretical data, D=0.5 cm

Functions	FUJIFILM camera		
	Theoretical	Practical	Error percentage %
Delta r (cm)	10.676	10.995	0.11%
Velocity (cm/sec)	250.56	250.08	0.19%
Acceleration(cm/sec²)	9860.6	9673.9	1.89%

Conclusions :

From the previous results of the present work, a three new mathematical models of obtained for the motion parameters in captured images;

- First model: The change in displacement (Δr) as in Eq.(14) its accuracy 0.11%.
- Second model: The velocity (v) as in Eq.(18) its accuracy 0.19%.
- Third model: The Acceleration (A) as in Eqs.(22) its accuracy 1.89%.

It is clear that from practical work small bubbles followed a helical motion while larger bubbles followed a spiral motion. As the bubble size increases, initially, the bubble follows straight path, attains its terminal velocity and shape, then it switches to spiral path. Addition to from the data notes bubble rise velocity increases with the increase in bubble volume. This confirming the validity interpretations of previous research.

References:

[1] Ho-Young Lee, Jeong - Mo Hong ,Chang – Hun Kim, "Simulation of swirling bubbly water using bubble particles", The Visual Computer , Volume 25 , Number 5-7, 707-712 , 2009.

[2] Shosho, C. and Ryan, Micheal, E.,"An experimental study of the motion of long bubbles in inclined tubes", Chemical engineering science, 56, 2191-2204, 2001.

[3] Jeong-Mo Hong and Chang-Hun Kim ,"Animation of Bubbles in Liquid", Department of Computer Science, Korea University,2003

[4] Hassan, N. M. S., KHAN, M. M. K. and Rasul, M. G.,"Characteristics of Air Bubble Rising in Low Concentration Polymer Solutions", AUSTRALIA,2007.

[5] Jeong-Mo Hong, Ho-Young Lee, Jong-Chul Yoon, Chang-Hun Kim_, "Bubbles Alive",Korea University,2008.

[6] Ho-Young Lee _ Jeong-Mo Hong _Chang-Hun Kim ,"Simulation of Swirling Bubbly Water using Bubble Particles", 2009.

[7] Markus Ihmsen, Julian Bader, Gizem Akinci, Matthias Teschner ,"Animation of air bubbles with SPH", University of Freiburg,2011

[8] N.M.S. Hassan, M.M.K. Khan and M.G. Rasul ,"Bubble Rise Phenomena in Non-Newtonian Crystal Suspensions", University AUSTRALIA, 2012 .

[9] Clift, R.; Grace, J. R.; Weber, M. E. ," Bubbles Drops and Particles ", New York: Academic Press. ISBN 0-12-176950-X, 1978.

[10] Frank, X., Li, H. Z., Funfschilling, D., Burdin, F. and Ma, Y.,"Bubble motion in non- Newtonian fluids and suspensions", Can J Chem Eng., 81:483–490, 2003.

[11] Kulkarni, A. A. and Joshi, J. B.,"Bubble formation and bubble rise velocity in gas-liquid systems ", 44, 5873-5931, Ind. Eng. Chem. Res., 2005.

[12] Zenit R and Magnaudet J ,"Measurements of the stream wise vorticity in the wake of an oscillating bubble", *Int. J. Multiph. Flow* 35 195–203, 2009.

[13] Duineveld, P. C., "The rise velocity and shape of bubbles in pure water at high Reynolds number", Journal of Fluid Mechanics, 292, 325-332, 1995.

[14] Ellingsen K and Risso F "On the rise of an ellipsoidal bubble in water: oscillatory paths and liquid induced velocity ", *J. Fluid Mech.* 440 235–68, 2001.

[15] Magnaudet J and Eames I, "The motion of high-reynolds-number bubbles in inhomogeneous flows", *Annu. Rev.Fluid Mech.* 32 659–708, 2000.

[16] Hassan, N. M. S., Khan, M. M. K and Rasul, M. G.,"Modelling and experimental study of bubble trajectory in non-Newtonian crystal suspension", Fluid Dynamics Research, IOP Publishing, 42, 065502, 2010a.

[17] Yang B," Numerical studies of single gas and vapor bubble flows ", *PhD Thesis* The John Hopkins University, Baltimore, MD, 2006.

[18] Aybers, N. M., and Tapucu, A.," The motion of gas bubble rising through stagnant liquid ", Warme und Stoffubertraguang 2, 118-128, 1969.

[19] Haberman, W. L. and Morton, R. K.," An experimental study of bubbles moving in liquids ", Trans ASCE 2799, 227-252, 1954.

[20] Saffman, P. G.," On the rise of small air bubbles in water ", Journal of Fluid Mechanics, Digital Archive, 1: 249-275, 1956.

[21] Feng, Z. C. and Leal, L. G.," Nonlinear bubble dynamics ", Ann. Rev. Fluid Mech. 29, 201-243, 1997.

[22] Yoshida, S. and Manasseh, R.,"Trajectories of rising bubbles", 16th Japanese Multiphase Flow Symposium , Touha, Hokkaido, 1997.

[23] Tsuge, H. and Hibino, S. I.," The onset conditions of oscillatory motion of single gas bubbles rising in various liquids" , Journal of Chemical Engineering of Japan 10, 66-68, 1997.

[24] Ellingsen K and Risso F," On the rise of an ellipsoidal bubble in water: oscillatory paths and liquid induced velocity ", *J. Fluid Mech.* 440 235–68, 2001.

[25] Hassan, N. M. S., Khan, M. M. K. and Rasul, M. G.," An investigation of bubble trajectory and drag co-efficient in water and non-Newtonian fluids", WSEAS Transactions on Fluid Mechanics, ISSN: 1790-5087, 3(3), 261 -270, 2008a.

Al-Mustansiriyah Journal of Science
Vol. 27, No 2, 2016

journal homepage:www.mjs-mu.com

Biological Solution Broadband Cavity Enhanced Absorption Spectroscopy Measurements

Noora Sh. Oraha Qas Nouna[1], Meez Islam[2], Liam O'Hare[2]
[1]Department of Physics, College of Science. Al-Mustamsiriyah University
[2]School of science and engineering, Teesside University.

Articleinfo
Received:18/5/2015
Accepted: 7/9/2015
KEYWORDS:
Broadband cavity enhanced absorption spectroscopy, (BBCEAS), Liquids, Absorption detection, Light emitted diode(LED).

ABSTRACT

In earlier studies, it was demonstrated that the sensitivity of conventional absorption spectroscopy can be improved significantly by using Cavity Enhanced Absorption Spectroscopy (CEAS). Sensitive liquid-phase measurements were made on the biological solution such as Lyophilied Bovine haemoglobin in a 1 cm cuvette. The Cavity Enhanced Factor (CEF) or the number of passes was calculated: 55 passes for the high reflectivity mirrors were obtained. The sensitivity of the experimental setup could be determined by calculating the minimum detectable change in the absorption coefficient α_{min} and it was 7.6×10^{-5} cm^{-1}. The limit of detection (LOD) for haemoglobin was 3nM.

الخلاصة

بينت الدراسات السابقة ان حساسية طيف الامتصاص التقليدي ممكن ان تحسن بشكل كبير باستخدام منظومة لتقنية محلل الامتصاص الطيفي المحسن (CEAS). اجريت قياسات لنماذج سائلة بايلوجية مثل الهيموكلوبين البقري المجفف بالتجميد الموضوعة في وعاء مختبري بعمق 1 سم. عامل التحسن لهذه التقنية (CEF) او عدد الانعكاسات للضوء في المنظومة حسبت والتي تساوي 55 انعكاس. الحساسية للمنظومة المختبرية قيمت بواسطة حساب اقل تغير في معامل الامتصاص α_{min} وكانت تساوي $7.6x10^{-5}$ cm^{-1}. حدود الكشف للمنظومة (LOD) للهيموكلوبين البقري تساوي 3 nM.

INTRODUCTION

The measurement of the lowest optical absorbance values is a continuous preoccupation of the trace analyst. The improvement of the limits of the absorbance detection for analytes by a conventional absorption spectroscopy is a main challenge in the analytical chemistry method development. In recent decades, several absorption techniques have been explored for making ultrasensitive absorption measurements at high resolution such as Cavity ring down spectroscopy (CRDS) [1] and more recently Cavity enhanced absorption spectroscopy (CEAS) [2] (also referred to as integrated cavity output spectroscopy (ICOS) [3].

These methods have the same principle in which the light passes back and forth as many times as possible between two high reflectivity mirrors of a stable optical cavity. The mirror reflectivity will create a high number of round trips within the cavity, resulting in an increase in the path length which was inserted inside the cavity to ten thousand times or more. In CRDS, the total losses from cavity alignment, mirror reflectivity, and sample absorption can be concluded by measuring the rate of the decay of light intensity inside the cavity, known as the ring-down time. CEAS does not measure a ring down event, but the intensity of the light exiting the cavity.

The application of CRDS and CEAS for quantitative optical absorption studies on gas phase species has been very successful [4] as the scattering and absorption losses are significantly lower than the measurements for liquid-phase and solid-phase species and thus a greater number of passes through the sample can be achieved.

CRDS was applied to measure the absorption for liquid-phase sample. A liquid sample requires a container such as a cuvette to insert into the cavity. Introducing this container into the cavity results in additional losses due to the reflection and dispersion from the surface of the cuvette. These effects were minimized by inserting the cuvette at a Brewster's angle to detect overtone CH stretch in benzene in the pure liquid and hexane solution at ~607 nm [5]. To date, many studies have been reported to explore the possibility of using CRDS as a detection technique for liquid phase [6-8]. Recently,

number of passes (CEF), the sensitivity of the setup and the limit of detection of many analytes [10] or by direct contact between high reflectivity mirrors and the liquid sample by using the cell [11,12].
This study aims to improve on the sensitivity of previous liquid-phase BBCEAS measurements. The experiments will be performed in a 1 cm cuvette using an uncooled compact charge-couple device (CCD) spectrograph.

Experimental Setup:

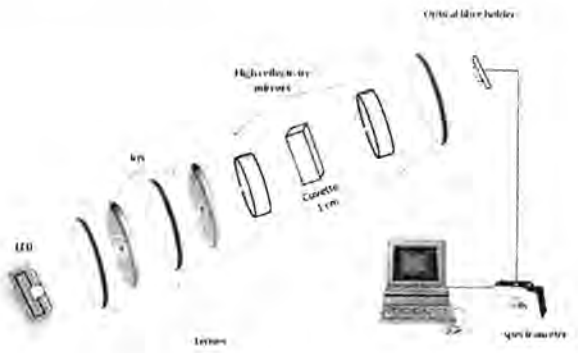

Figure 1: A schematic of the experimental setup for the liquid-phase BBCEAS measurements with an uncooled Ocean optics spectrometer.

A schematic of the experimental setup is shown in figure 1. Although the light from the white LED was partially collimated by the integrated optic this was not sufficient for effective coupling into the optical cavity. Therefore, the light was further collimated using a series of lenses and irises. The most suitable iris apertures and spacing between the lens and irises were empirically determined by preliminary experiments to obtain the greatest cavity enhancement with also the highest light intensity reaching the detector. As described previously the optical cavity consisted of two concave mirrors. The mirrors were each mounted into a custom mirror holder unit, with three micrometer screws. These allowed fine adjustment during cavity alignment. The light exiting the cavity was focused by a short focal length lens (f = 50 mm) directly onto the input of a 600 μm diameter, 1 m length, 0.22 numerical aperture quartz fibre optic cable (Thorlabs, UK). This was connected to the entrance slit of the spectrometer by an SMA905 fibre connection. The alignment of the empty cavity was achieved by the iterative adjustments of the front and back mirrors through the micrometer screws to obtain the maximum intensity of the light reaching the detector. The empty cuvette was inserted into the cavity at 0 degrees and the cuvette mount micrometers adjusted to minimize the absorption and scattering losses, followed by the front and back cavity mirrors to maximize the output intensity reaching the detector. This was then repeated with the cuvette filled with solvent. An appropriate integration time was chosen such that the intensity reaching the detector produced a counts value approximately two thirds of the maximum value. This maximised the counts signal without the risk of saturating the detector.

Experimental Methodology
As noted before, unlike CRDS the absorption coefficient in a CEAS experiment cannot be measured directly without knowledge of the reflectivity of the mirrors. The absorption coefficient (α) cannot be calculated directly. Therefore (α) can be calibrated by measuring the absorption of a known absorption sample and can be given by [13]:

$$\left(\frac{I_0}{I}\right)_{cavity} = 1 + \frac{2.303\,\varepsilon\,C\,l}{(1-R)} \qquad (1)$$

I_0 and I are the measured transmitted intensities with and without the absorber in the cavity, l is the optical path length through the sample in the cavity in cm, R is the average calibrated high mirror reflectivity, ε is the wavelength-dependent molar extinction coefficient in M^{-1} cm^{-1}, and C is the concentration of the sample in M.
A conventional single-pass experiment for low concentrations can be expressed as:

$$\left(\frac{I_0}{I}\right)_{singlepass} = 1 + 2.303\varepsilon\,C\,l \qquad (2)$$

The term $\frac{1}{(1-R)}$ equates to the cavity enhancement factor (CEF) relative to a single-pass experiment. For the liquid-phase measurements CEFs are affected by the absorption and scattering losses from the mirrors as well as additional losses due to scattering and absorption by the solvent and the cuvette window. CEFs can be calculated depended on eqn. 1 and 2 by using the following equation:

$$CEF = \frac{\left(\frac{I_0}{I}-1\right)_{cavity}}{2.303\,\varepsilon Cl} \qquad (3)$$

CEFs are calculated as a function of wavelength by the gradient of the plot of $\left(\frac{I_0}{I}-1\right)_{cavity}$ versus C. The ε values are determined by using single pass experiment. l is the path length of the cuvette which in our study is 1 cm. As a result of increase CEF factor the effective path length will be increased and can be calculated (l_{eff} = l × CEF). The sensitivity of setup α_{min} is calculated by the equation:

$$\Delta\alpha_{min} = \frac{2.303\,\Delta ABS_{min}}{l_{eff}} \qquad (4)$$

ΔABS_{min} is the minimum detectable absorbance change and it is calculated by the standard deviation in the absorbance value as a function of wavelength of the solvent.
The limit of detection *(LOD)* of analyte is usually defined as a minimum concentration of substance that can be measured and reported with 99% confidence that the analyte concentration is greater than zero. The value of the *(LOD)* of an analyte will depend on both ε and the path length of the measurement. In general, longer path lengths and larger values of ε will produce lower LODs. *(LOD)* is the usually calculated from

$$LOD = \frac{3\times\alpha_{min}}{2.303\times\varepsilon} \qquad (5)$$

Results:

Liquid-phase BBCEAS measurements have been achieved in a 1 cm cuvette for a Lyophilized Bovine haemoglobin (sigma Aldrich, U.K) dye dissolved in distilled water. All measurements were taken at the peak absorption wavelength for haemoglobin with a white LED and high reflectivity mirror set. Table I summarizes the measurements made in terms of the analyte studied, the reflectivity of the mirror set used, the wavelength of measurement, the CEF or number of passes obtained, the calculated α_{min} values for each measurement, the LOD for the dye, and the molar extinction coefficient ε of the analyte at the wavelength of measurement.

Table I: A review of the results obtained in terms of analyte, the spectrometer used the reflectivity of mirrors *R*, the wavelength of measurement λ, the CEF value, the sensitivity of setup α_{min}, and the LOD of the analyte.

Analyte	$R \geq$	λ/nm	CEF	α_{min}/cm^{-1}	LOD/M	$\varepsilon/M^{-1}cm^{-1}$
Haemoglobin	0.99	519	55	7.6×10^{-5}	3.1×10^{-9}	2.4×10^{4}

The absorption spectra of haemoglobin solution for a series of concentrations (~ 15 nM to ~ 150 nM) were recorded by BBCEAS using a white LED as the light source, the $R \geq 0.99$ mirror set, and an Ocean optics spectrometer are shown in figure 2.

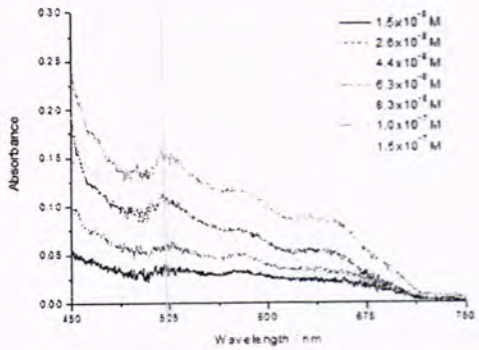

Figure 2: BBCEAS spectra of haemoglobin in distilled water in the range 450-750 nm.

Figure 3 shows a plot of the linearity between the intensity ratio $(\frac{I_o}{I-1})$ and concentration for haemoglobin at λ_{max}= 519 nm and a range of concentrations from ~15 nM to ~ 150 nM (recorded by BBCEAS using a white LED as the light source, the $R \geq 0.99$ mirror set). The inset figure shows an absorbance versus concentration plot of haemoglobin. Three replicate measurements were made at each concentration and the error bars for each concentration represent the standard deviation of the measurements. An error-weighted regression through the linear plot of intensity ratio versus concentration yields a straight line (equation of the line is given in fig. 3) with a correlation coefficient $R^2 = 0.995$.

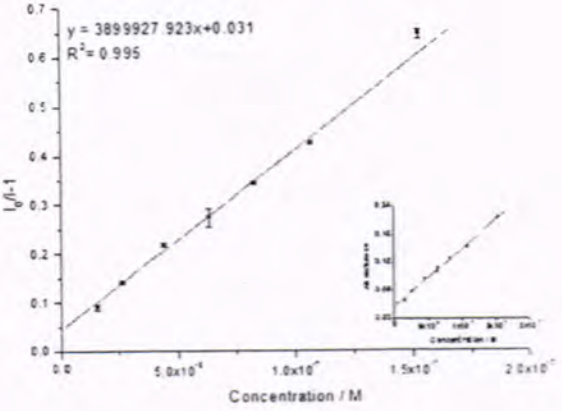

Figure 3: An intensity ratio (I_0-I/I) versus concentrations plot of haemoglobin.

Discussion

A simple, low cost experimental setup based on BBCEAS in a 1 cm cuvette has been demonstrated on the biological compound haemoglobin dissolved in distilled water. The experimental methodology was simple and similar to conventional UV-visible absorption spectroscopy. Measurements were made with a white LED and the $R \geq 0.99$ mirror set. The CEF values are limited by scattering and absorption losses from the cuvette and solvent of $\sim 6 \times 10^{-3}$ per pass. The value of sensitivity α_{min} of setup with Ocean optics spectrometer is relatively improved compared to the conventional absorption spectroscopy because the α_{min} values are inversely proportional to the total path length. Therefore, the improvement sensitivity of BBCEAS is affected by both the base path length of the cuvette and the number of passes. The *(LOD)* value for haemoglobin has been measured by using equation 5 and this value depends on the sensitivity of measurement and also the molar extinction coefficient of the analyte. A minimum value of $\sim 3.1 \times 10^{-9}$ M was calculated.

The sensitivity of the experimental setup could be improved in a number of ways. The simplest improvement would be to increase the path length of the cuvette. The CEF value could be increased by using a higher reflectivity of cavity mirrors, which is leads to an increase the effective path length, but there is not a corresponding improvement in the sensitivity due to increased noise from the uncooled CCD detector at longer integration times. This could be treated by using either a cooled detector which would allow the use of longer integration times without the associated increase in dark noise. Alternative methods for improving the sensitivity of the measurements could be by using a more powerful white LED which is provided additional photon flux inside the cavity; this lead to use shorter integration time or by using more efficient collimation of the light source.

REFERENCES

1- O'Keefe, A. and Deacon, D. A. G. (1988). "Cavity ring-down optical spectrometer for absorption measurements using pulsed laser sources", Review of Scientific Instruments, V 59, No. 12, 2544-2551.

2- Engeln, R., Berden, G., Peeters, R. and Mejier, G. (1998). "Cavity enhanced absorption and cavity enhanced magnetic rotation spectroscopy", Review of Scientific Instruments, V 69, No. 11, 3763-3769.

3- O'Keefe, A. (1998). "Integrated cavity output analysis of ultra-weak absorption", Chemical Physics Letters, V 293, No. 5-6, 331-336.

4- Nakamura, S., Matsugi, A., Susa, A. and Koshi, M. (2008). "UV-visible absorption spectra of silicon CVD intermediates", Thin Solid Films, V 516, No. 5, 517-520.

5- Xu, S., Sha, G. and Xie, J. (2002). "Cavity ring-down spectroscopy in the liquid phase", Review of Scientific Instruments, V 73, No. 21, 255-258.

6- Snyder, K. L. and Zare, R. N. (2003). "Cavity ring-down spectroscopy as a detector for liquid chromatography", Analytical Chemistry, V 75, No. 13, 3086-3091.

7- Alexander, A. J. (2004). "Reaction kinetics of nitrate radicals with terpenes in solution studied by cavity ring-down spectroscopy", Chemical Physics Letters,V 393, No. 1-3, 138-142.

8- Hallock, A., Berman, E. S. F. and Zare, R. N. (2002). "Direct monitoring of absorption in solution by cavity ring-down spectroscopy", Analytical Chemistry,V 74, No. 7, 1741-1743.

9- Fidler, S. E., Hese, A. and Ruth, A. A. (2005). "Incoherent broad-band cavity-enhanced absorption spectroscopy of liquids", Review of Scientific Instruments, V 76, No. 2, 023107-1-023107-7.

10- Islam, M. Seetohul, L. N. and Ali, Z. (2007). "Liquid-phase broadband cavity-enhanced absorption spectroscopy measurements in a 2 mm cuvette", Applied Spectroscopy, V 61, No. 6, 649-658.

11- McGarvey, T., Conjusteau, A. and Mabuchi, H. (2006). "Finesse and sensitivity gain in cavity-enhanced absorption spectroscopy of biomolecules in solution", Optics Express, V 14, No. 22, 10441-10451.

12- Seetohul, L. N., Ali, Z. and Islam, M. (2009). "Liquid-phase broadband cavity enhanced absorption spectroscopy (BBCEAS) studies in a 20 cm cell", Analyst, V 134, No. 9, 1887-1895.

13- van der Sneppen, L., Hancock, G., Kaminski, C., Laurila, T., Mackenzie, S. R., Neil, S. R. T., Peverall, R., Ritchie, G. A. D., Schnippering, M., Unwin, P. R. (2010). "Following interfacial kinetics in real time using broadband evanescent wave cavity-enhanced absorption spectroscopy: A comparison of light-emitting diodes and supercontinuum sources", Analyst, V135, No. 1, 133-139.

Al-Mustansiriyah Journal of Science
Vol. 27, No 2, 2016

journal homepage:www.mjs-mu.com

On Blow-up Solutions and Times Of a Fourth Order Nonlinear Partial Differential Equation

Maan A. Rasheed
Dept. of Maths. College of Basic Education, Al-Mustansirya University, Iraq.

Articleinfo

Received
6/10/2015
Accepted
3/1/2016

ABSTRACT

In this paper, we study blow-up solutions and blow-up times of a fourth order nonlinear partial differential equation. We show that the classical solutions of this equation blow up in C^2, i.e. the second order derivatives blow-up in L_∞ . The two steps finite difference scheme is used to compute the approximate values to the blow-up solution and times for a numerical experiment.

الخلاصة

في هذا البحث, نقوم بدراسة الحلول العددية والأزمان المتضخمة لمعادلة تفاضلية جزئية غير خطية من الرتبة الرابعة. نبين أن الحلول الكلاسيكية لهذه المعادلة , تتضخم في فضاء الدوال القابلة للاشتقاق مرتين ,اي ان المشتقات من الرتبة الثانية تتضخم في الفضاء المنتظم. الأسلوب ذات الخطوتين الذي يعتمد على الفروقات المنتهية يستخدم لإيجاد القيم التقريبية للحل المتضخم والزمن المتضخم لتجربة عددية.

1. INTRODUCTION

In this paper, we study a fourth order nonlinear partial differential equation which takes the form:

$$\frac{\partial^4 u}{\partial x^4} - \frac{\partial^3 u}{\partial t \partial x^2} + \left(\frac{\partial^2 u}{\partial x^2}\right)^2 = 0, \quad x \in [0,1] \dots\dots\dots (1)$$

with the initial and boundary conditions:

$$u(0,t) = u(1,t) = u_{xx}(0,1) = u_{xx}(1,t) = 0$$

$$u(x,0) = u_0(x),$$

where u_0 is a smooth function, and $u_0''(x)$is positive function in (0,1).

Blow-up phenomena for partial differential equations has been studied by many authors, see for instance [1-10]. It is well known that the classical solution of this problem can be continued in time, only if all the derivatives these appear in the equation are continuous, which means, in order to show that the solution of the problem blows up in finite time T in C^2 , it is sufficient to show that the second order derivative blows-up in L_∞,

i.e. $\sup_{x\in[0,1]} |u_{xx}(x,t)| \to \infty$ as $t \to T$

Since it is not easy to deal with problem (1) directly, we can deal with the second order reducing problem, which can be got form rewriting equation (1) as follows:

$$\frac{\partial w}{\partial t} = \frac{\partial^2 w}{\partial x^2} + w^2, \quad x \in [0,1] \dots\dots\dots (2)$$

where

$$w = \frac{\partial^2 u}{\partial x^2} \dots\dots\dots (3) \ ,$$

$$w(0,t) = w(1,t) = 0$$

$$w(x,0) = w_0(x) = u_0''(x)$$

2. Blow-up Results

The local existence of equation (2), can be guaranteed (see [5,9]), moreover, unless w is unbounded, the differential equation (3) has a unique solution, see[9]. This leads to: equation (1) has a unique local classical solution. While, it is well known that, for large initial function, the solution of problem (2) blows up in finite time at only a single point, see [5,10,11,12], which means there exist T_(b)>0, such that

$$\sup_{x\in[0,1]} |w(x,t)| \xrightarrow{t \to T_b} \infty$$

It follows that the solution of the general problem (1), has to blow-up in C^2 –space atT_b (the problem has no global classical solution). In fact, since the second derivative becomes unbounded in finite time, this will handle the continuity of solution, and eventually, the solution becomes unbounded in equal or larger finite time.

From above, we see that, in order to find the solution of problem (1), we can first solve problem (2) and then we

substitute w in equation (3), and finally from solving equation(3), we get the solution of problem (1). Moreover, in order to compute approximately, the blow-up time T_b of problem (1), we need only to estimate the blow-up time of problem (2).

3. The discrete problem

In fact, little attention has been devoted to the numerical study for problem (2), however, the numerical blow-up times of problem (2) has been studied by some authors, see for instance, [1, 11].

In order to compute the approximate values of blow-up solutions and blow-up times of problem (1), we can use finite difference operators to get the discrete problem of problem (1) as follows:

For J a positive integer, we set $J = 1/h$ and we defined the grids

$$x_j = jh, \qquad 0 \le j \le J$$

and$t_0 = 0,\ t_{n+1} = t_n + k_n,\ n = 0,1,\ldots$ where $k_n > 0$, is the time steps, and we denote to the approximate value of u and w at the point (x_j, t_n) by U_j^n, W_j^n respectively.

We approximate the time derivative w_t by the forward finite difference operator, while the second order derivatives by the standard second order centre finite difference operators. Thus, problem (2) can be written in discrete forms follows:

$$\frac{W_j^{n+1} - W_j^n}{k_n} = \frac{W_{j+1}^n - 2W_j^n + W_{j-1}^n}{h^2} + (W_j^n)^2 \quad \ldots\ldots\ldots (4)$$

$$W_0^n = W_j^n = 0, \quad \forall\, n$$

$$W_j^0 = u_{0xx}(x_j)$$

and equation (3) becomes

$$W_j^n = \frac{U_{j+1}^n - 2U_j^n + U_{j-1}^n}{h^2} \quad \ldots\ldots\ldots (5)$$

$$U_0^n = U_j^n = 0, \quad \forall\, n$$

$$U_j^0 = u_0(x_j)$$

4. Blow-up in the discrete problem

The solution $W^n = (W_0^n, W_1^n, W_2^n, \ldots., W_j^n) \in R^{J+1}$, of the difference equation (4) does not exist for all $n \in N$, because there exists $m \in N$ such that W^n become unbounded for $n \ge m$, see [1].

Remark 4.1

It is clear that the solution of problem (5), $U^n = (U_0^n, U_1^n, U_2^n, \ldots., U_J^n) \in R^{J+1}$,

Can be computed only if W^n is bounded.

Definition 4.2

let $\{W^n\}_{n\ge 0}$ be a nonnegative solution of (4), with the time steps $\{k_n\}_{n\ge 0}$. We say that $\{W^n\}_{n\ge 0}$ achieves blow-up in finite time, if there exist $m \in N$, such that

i- $\lim_{n\to m} ||W^n||_\infty = \infty$,

ii- $T_m^h = \sum_{n=0}^m (k_n) < \infty$,

where the time T_m^h is called the numerical blow-up time, and $||W^n||_\infty = \max_{0\le j\le J} |W_j^n|$.

In fact, the numerical blow-up time depends on the spatial grid h and also on the choice of time steps.

In [1], under certain assumptions, it has been proved that numerical solution of problem (4) convergent to the classical solution of problem (2), moreover, it has been studied the convergence of the numerical blow-up time of the discrete problem to the theoretical blow-up time of problem (2), which means

$\lim_{h\to 0} T_m^h = T_b$, and $\lim_{h\to 0} W_j^n = w(x_j, t_n)$

5. Numerical Scheme

The finite difference equation (4), can be rewritten in the explicit Euler formula as follows:

$$W_j^{n+1} = r_n W_{j+1}^n + (1 - 2r)W_j^n + r_n W_{j-1}^n + (W_j^n)^2 \quad \ldots\ldots\ldots (6)$$

where $r_n = k_n/h^2$

$$W_0^n = W_j^n = 0, \quad \forall\, n$$

$$W_j^0 = u_{0xx}(x_j)$$

It is well known that, $r_n \le 1/2$, is the stability condition of the explicit Euler method for the heat equation. In [2], it has pointed out that time stepping based on a fixed step can lead to a different behavior from theoretical blow-up properties. To overcome this problem, we will consider the time step procedure considered first in [1] as follows:

$$k_r = \min\left(\frac{h^2}{2}, \frac{h^\alpha}{||W^n||_\infty}\right) \quad \ldots\ldots\ldots (7)$$

where α is a fixed positive constant.

It is well known that, for each fixed time interval $[0, T]$, where the solution u of (2) is defined and sufficiently smooth, the numerical schemes (explicit Euler method) considered approximate u with a rate of convergence of $O(T + h^2)$, where $T = \max\ k_n$. Because of the choice of k_n, we have a rate of convergence $O(h^\alpha)$, as $h \to 0$.

The same order of convergence might be expected for the numerical blow-up times.

For any $n \in N$, in order to compute the numerical blow – up solution of problem (1), and the numerical blow-up time, we can use the following algorithm steps:

1- Use explicit Euler formula (6), to compute $\{W^n\}_{n>0}$ and the numerical blow-up time for w, $T_m^h = \sum_{n=0}^m (k_n)$, which can be taken at the first,

where$||W^n||_\infty \ge 10^{15}$.

2- Unless W^n is unbounded, substitute it in (5), we get a linear system and from solving this system we get

$U^n = (U_0^n, U_1^n, U_2^n, \ldots., U_J^n), \qquad n > 0$

3- The numerical blow-up time for u,$T_k^h = \sum_{n=0}^k (k_n)$,can be taken at the first time, where $||U^n||_\infty \ge 10^{15}$.

6. Numerical experiment

In this section, we present some numerical approximation to the blow-up solution and blow-up time of problem(1), with the initial function $u_0(x) =$

$\frac{-20}{\pi^2}\sin\pi x$, which implies $w_0(x) = u_0''(x) = 20\sin\pi x$.
So from the maximum principles we can show that, the solution of problem (1), u, and the solution of problem (2), w, are negative and positive functions in (0,1) respectively,
see [8,9].
Moreover, It is clear that u_0 takes its minimum value at the point $x = 1/2$,
while u_0'' takes its maximum at this point. Therefore, according to the known blow-up results for the semilinear heat equation (see [8]), the blow-up in problem (2), occurs only at a single point, which is $= 1/2$.
This problem will be solved numerically by using the algorithm, which was suggested in section 5, with using Matlab programming. We will consider different choices for the positive parameter α in the time stepping procedure(7), in order to examine experimentally, if there exists any rate of convergence for the numerical blow-up times with respect to the mesh size h.
In tables (1),(2) and (3), with respect to the corresponding to meshes 10, 20 and 40 subintervals respectively, every four rows of the table correspond to the use of indicated values for α in the time stepping procedure (7). In the first column, we show numerical blow-up times of problem (2),which arise from using explicit Euler method (6), and in column 2, we refer to the last iteration before numerical blow-up occurs by m. In the third column, we show numerical blow-up times of problem (1),which arise from solving the linear systems (5), and in the last column, we refer to the last iteration before numerical blow-up occurs by k.
In table (4), The errors in the numerical bow-up times, of problem (1), are computed by using
$E_J = |T_{2J}^k - T_J^k|$,.....(8)
where T_J^k refer to the numerical blow-up time, with respect to $J = \frac{1}{h}$, while T_{2J}^k refer to the numerical blow-up time, with respect to *2J*.
We will consider two values for h, $h = 10$, and $h = 20$.

Table 1,
Computed blow-up times for w and u, J=10

α	T_m	m	T_k	K
2	0.081862456799616	3823	0.081862456799617	4132
3/2	0.082485016226606	1221	0.082485016226607	1320
1	0.084446057128159	399	0.084446057128160	431
1/2	0.090006222238912	139	0.090006222238913	151

Table 2,
Computed blow-up times for w and u, J=20

α	T_m	m	T_k	k
2	0.082275767831658	17556	0.082275767831658	18930
3/2	0.082452564311300	3940	0.082452564311301	4249
1	0.083242065649699	896	0.083242065649700	966
1/2	0.085347269273309	238	0.085347269273310	255

Table 3,
Computed blow-up times for w and u, J=40

α	T_m	m	T_k	k
2	0.082393246952934	84208	0.082393246952934	90257
3/2	0.082441168069771	13331	0.082441168069771	14289
1	0.082744087031189	2124	0.082744087031190	2277
1/2	0.083415984832608	510	0.083415984832609	536

Table4,

Errors in the numerical bow-up times of u

$$E_J = |T_{2J}^k - T_J^k|$$

α	J=10	J=20
2	0.000413311032041	0.000117479121276
3/2	0.000032451915306	0.000011396241530
1	0.001203991478460	0.000497978618510
1/2	0.004658952965603	0.001931284440701

The next figures show the evolutions of the numerical bow-up solutions u &w,of problems (1) &(2) respectively, which arise from using Euler explicit method, for different values to J and α.

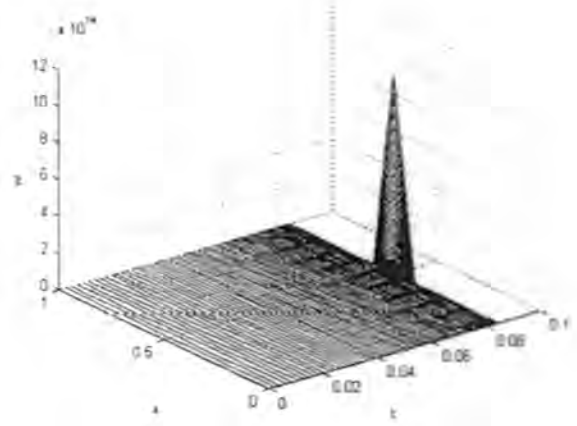

Figure 1,
$J = 10$, $\alpha = 1$, $t \in [0, T_m]$

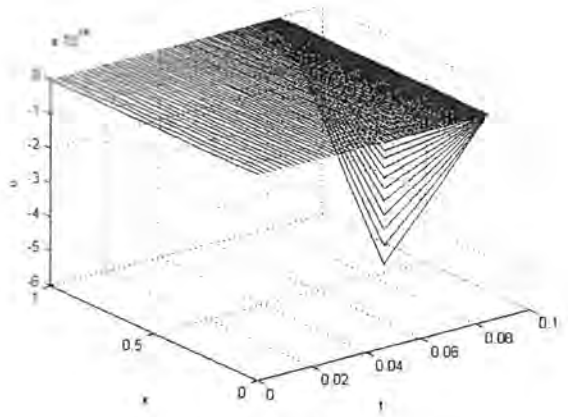

Figure 2,
$J = 10,\ \alpha = 1,\ t \in [0, T_k]$

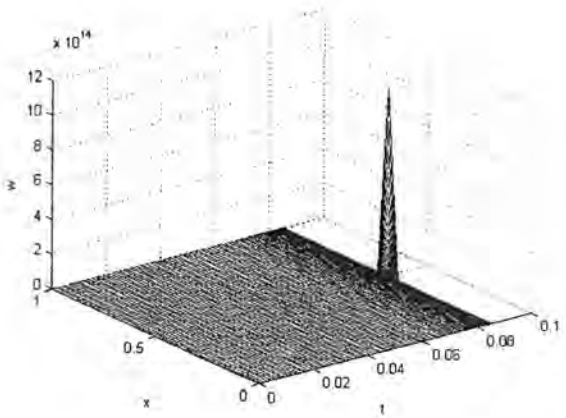

Figure 3,

$J = 20,\ \alpha = 1/2,\ t \in [0, T_m]$

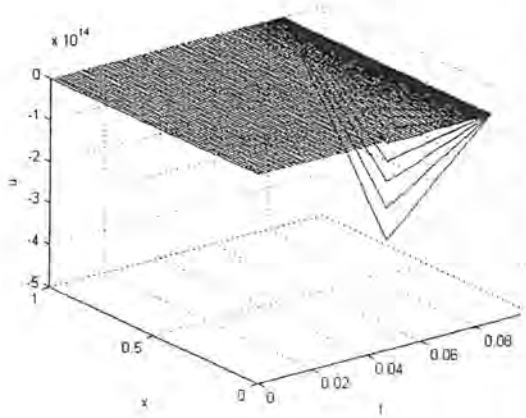

Figure 4,

$J = 20,\ \alpha = 1/2,\ t \in [0, T_k]$

Conclusions

From the numerical results, we can point out the following conclusions

1- The numerical blow-up time of problem (1), is mostly larger than the corresponding numerical blow-up times of problem (2), and $k > m$.
2- Decreasing the values of α,leads almost to decreasing the number of iterations, (k and m) until the numerical blow up occurs, and increasing the numerical blow-up times.
3- The table of error (4), in the computed blow-up times, that was computed using (8), shows that: for a fixed value of J, the latest error can be get where $\alpha = \frac{3}{2}$. On the other hand, for a fixed values for α and J, we have$E_{2J} < E_J$.
4- The figures (1-4) show that, the blow-up in problem (2) occurs only at a single point and that confirm the theoretical results see [4], also, we can see experimentally, that, problem (1) exhibits fixed point blow-up.

References

[1] Abia L.M., Lrpez-Marcos J.C. and Martinez J.; "Blow-up for semidiscretizations of reaction-diffusion equations", Appl. Numer. Math., Vol. 20, pp. 145-156, 1996.

[2] Abia L.M., Lrpez-Marcos J.C. and Martinez, "The Euler method numerical integration reaction-diffusion problems with blow-up", Appl. Numer. Math Vol. 38, pp. 287-313, 2001.

[3] Budd C.J., Huang W. and Russell R.D., "Moving mesh methods for problems with blow-up", SIAM J. Sci. Comput.,. Vol. 17, No. 2 : pp. 305-327, 1996.

[4] Chen Y. G. ; "Asymptotic behaviors of blowing-up solutions for finite difference analogue of $u_t = u_{xx} + u^p + a$,", J. Fac. Sci. Univ. Tokyo Sect. IA Math. Vol. 33, pp. 541-574, 1986.

[5] Friedman A. and McLeod B., "Blow-up of positive solutions of semilinear heat equations", Indiana Univ. Math. J. Vol. 34, pp. 425-447,1985.

[6] Lacey A. A., Diffusion models with blow-up, J. Comput. Appl. Math. Vol. 97, pp. 39-49, 1998.

[7] Liu W.;, The blow-up rate of solutions of quasilinear heat equation, J. Di_er.Equ, Vol. 77, pp. 104-122,1989.

[8] Nakagawa T.; "Blowing up on a finite difference solution to $u_t = u_{xx} + u^2$, " Appl. Math. Optim. Vol. 2 , pp. 337-350, 1976.

[9] Quittner P. and Souplet Ph., "Superlinear Parabolic Problems. Blow-up, Global Existence and Steady States", Birkhuser Advanced Texts, Birkhuser, Basel. 2007.

[10] Rasheed, M. A.; "On blow-up solutions of parabolic problems", Ph.D.
thesis, University of Sussex, 2012.
[11] Rasheed, M. A and A. G. Farhan , "Using Crank-Niclson Method to
Compute the Numerical Blow-up Time of a Semilinear Parabolic Problem",
IJMA Vol. 5, No. 9, pp. 95-99, 2014.
[12] Weissler F. B., "Single point blow-up for a semilinear initial value
Problem", J Differ. Equ. Vol.55, pp. 204-224.1984.

Al-Mustansiriyah Journal of Science
Vol. 27, No 2, 2016

journal homepage:www.mjs-mu.com

Best Approximation of Unbounded Functions by $L_{p,\alpha}$ - Trigonometric Polynomials

Alaa Hameed Alwan Abdullah* and Raad Falih Hassan**
*Ministry of Education, Baghdad Education Directorate, Al-Karkh the Second, Department of Specialized Supervision
**Department of Mathematics, College of Science, Al-Mustansiriyah University

Articleinfo

Received
5/4/2015
Accepted
7/9/2015

ABSTRACT

The aim of this paper is to study the best approximation of unbounded functions with respect to trigonometric polynomials with weighted normed spaces and find the degree of best approximation of these functions in terms of weighted modulus of continuity,thus have been presented indetails.

الخلاصة

الهدف من هذا البحث هو دراسة تقريب الدوال غير المقيدة بواسطة متعددات الحدود المثلثية في فضاءات ذات نظيم موزون وايجاد درجة أفضل تقريب لتلك الدوال بإستخدام نموذج الاستمرارية الموزونة.

Introduction:

There are many important applications of approximation theory, some of which are solving algebraic equations and the interpolating to minimize the error in the Lagrange interpolation formula. Theory of approximation of functions has been studied throughout trigonometric polynomials, spline functions and algebraic polynomials by number of researchers, such as:

S. K. Jassim and E. S. Bhaya [9] (2002), obtained standard method for the direct (Jackson) theorems for the order of best multi-approximation by algebraic polynomials from those for trigonometric polynomials in the spaces $L_p(1< p < \infty)$ and they provided inverse (Bernstein) theorems.

E. S. Bhaya [4] (2003), studied the constrained and unconstrained approximation in the space L_p $(1\leq p \leq \infty)$ and in her thesis she dealed with the extension of constrained and unconstrained algebraic polynomials approximation for the case $(0 < p < 1)$.

N. M. Kassim [5] (2004) , obtained some results about monotone approximation in the space L_p $(0< p < 1)$ in terms of modulus of smoothness.

B. M. Hussein [2] (2010), obtained some results concerning approximation of unbounded function in $L_{p,\alpha}$-spaces.

A. A. Hammod [1] (2012), introduced the estimation of any function (bounded and unbounded) by the k-functional and he found estimation for positive linear operator by new weighted modulus of continuity in $L_{1,\alpha}$-spaces.

R.F.Haassan and Sahib K.Jasim[7] (2014),study the approximation of unbounded functions by Bleimann-Butzer-Hahn positive linear operators in weighted space.

Now, we will list some definitions and theorems, which we need to prove our results.

Definition (1), [8]:

An integrable function w(x) is called a weight function on [a,b] if $w(x) \geq 0$, $\forall\ x \in [a,b]$, but $w(x) \neq 0$ on any subinterval of [a,b].

Definition (2), [10]:

The spectrum of bounded linear operator G is the set of all $\lambda \in$ K(scalar field) for which the operator $\lambda I - G$ dose not have an inverse. The spectrum of a given operator G is often defined by:

$S(G) = \{\lambda : \lambda I - G$ is not invertible$\}$

Definition (3):

An unbounded function f on R and periodic on T^*, where $T^* = [-2\pi, 2\pi]$, $L_{p,\alpha}(T^*) = \{f \mid f : T^* \longrightarrow R\}$, such that:

$$\|f\|_{p,\alpha} = \left(\int_{T^*} |f(x)e^{-\alpha x}|^p dx \right)^{1/p} < \infty; \quad 0 < p < \infty$$

$w(x) = e^{-\alpha x}$, $\alpha > 0$ and denoted T_n^* be the space of all trigonometric polynomials on T^* of degree $\le n$.

Definition (4):

Let $L(T_n^{*\perp})$ be the class of all functions of the form $L_{p,\alpha}(T^*)$, which have no spectrum in $[-n,n]$

$$L(T_n^{*\perp}) = \{f \in L_{p,\alpha}(T^*) : f \text{ has no spectrum in } [-n,n]\}$$

$$\|f\|_{p,\infty} = \sup_{x \in T^*} |f(x)e^{-\alpha x}|$$

$$\|f\|_{1,\infty} = \int_{T^*} |f(u)e^{-\alpha u}|^p du$$

and the degree of the best approximation of $f \in L_{p,\alpha}(T^*)$ is defined by:

$$E_n(f)_\alpha = \inf\{\|f - p\|_{p,\alpha} : p \in T_n^*\}$$

Definition (5)[3]:

The difference of f at a point x with step h is defined by:

$$\Delta_h^m f(x) = \sum_{i=0}^{m} (-1)^{m-i} \binom{m}{i} f\left(x - \frac{m}{2}h + ih\right)$$

Definition (6):

The weighted modulus of smoothness of a function $f \in L_{p,\alpha}(T^*)$ of order m is defined by:

$$\omega_m(f;\delta)_\alpha = \sup\{|\Delta_h^m f(x)e^{-\alpha x}| : |h| \le \delta, x \in T^*\}$$

Definition (7):

An unbounded function, $f \in L_{p,\alpha}(T^*)$ and I_x be the identity operator at $x \in T^*$, then defined

$$If(x)e^{-\alpha x} = I_x * (f(x)e^{-\alpha x}) = (f(x)e^{-\alpha x}) * I_x = f(x)e^{-\alpha x} \quad \ldots(1)$$

The averaging operator on $[x - h, x + h]$, $0 < h < 2\pi$ is bounded by:

$$I_x f(x)e^{-\alpha x} = \frac{1}{2h} \int_{x-h}^{x+h} f(u)e^{-\alpha u} du$$

$$= \frac{1}{2h}[f(x+h) - f(x-h)]$$

$$= \frac{f(x+h) - f(x-h)}{(x+h) - (x-h)}$$

$$= \frac{f(x+h) - f(x-h)}{2h}$$

On other words:

$$I_{x,h} f(x)e^{-\alpha x} = \int_{T^*} f(u)e^{-\alpha u} du B_h^1(x-u)du \quad \ldots(2)$$

$$I_{x,h} f(x)e^{-\alpha x} = (fe^{-\alpha x} * B_h^1)(x) \ldots(3)$$

$$B_h^1(x) = \begin{cases} \frac{1}{2h} & \text{if } x \in [-h,h] = [-h \le x \le h] \\ 0 & \text{if } x \notin [-h,h], \text{i.e., } x \in [-h,h]^c \end{cases}$$

Put $I_{x,h}^0 = I_x$, $I_{x,h}^1 = I_{x,h}$, then using (3), we get:

$$I_{x,h}^s f(x)e^{-\alpha x} = (I_{x,h})^s f(x)e^{-\alpha x} = (fe^{-\alpha x} * B_h^s)(x), \; s \ge 2$$

Remark: The following integral

$$\frac{h}{2\pi s} \int_{T^*} B_h^s(u)du = 1$$

Proof:

$$\frac{h}{2\pi s} \int_{T^*} B_h^s(u)du = \frac{h}{2\pi s} \int_{-2\pi}^{2\pi} \frac{s}{2h} du$$

$$= \left(\frac{sh}{2\pi s}\right)\frac{u}{2h}\Big|_{-2\pi}^{2\pi} = \left(\frac{sh}{2\pi s}\right)\left[\frac{2\pi}{2h} + \frac{2\pi}{2h}\right]$$

$$= \frac{sh}{2\pi s}\left(\frac{4\pi}{2h}\right) = 1$$

Also, the differentiation D on $I_{x,h} f(x)e^{-\alpha x}$ is defined by:

$$D'(I_{x,h}^s f(x)e^{-\alpha x}) = \frac{I_{x+h,h}^{s-1} f(x)e^{-\alpha x} - I_{x-h,h}^{s-1} f(x)e^{-\alpha x}}{2h}$$

$$D^{(m)}(I_{x,h}^s f(x)e^{-\alpha x}) = \frac{\sum_{i=0}^{m} (-1)^{m-i} \binom{m}{i} I_{x-mh,2ih}^s f(x)e^{-\alpha x}}{(2h)^m}$$

$$= (2h)^{-m} \sum_{i=0}^{m} (-1)^{m-i} \binom{m}{i} I_{x-mh,2ih}^s f(x)e^{-\alpha x}$$

$$= (2h)^{-m} \Delta_{2h}^m I_{x-mh,2ih}^s f(x)e^{-\alpha x}$$

Definition (8), [10]:

$f \in C(T)$ be a continuous function on T. The operators $W_{x,h,2k}^s f(x)$ are defined by:

$$W_{x,h,2k}^s f(x) = \sum_{i=0}^{2k} (-1)^{k-i} \frac{\binom{2k}{i}}{\binom{2k}{k}} I_{x,(i-k)h}^s f(x)$$

or:

$$W^{s}_{x,h,2k} f(x) = I_x - 2 \frac{\sum_{i=0}^{s} (-1)^{i+1} \binom{2k}{k+i} I^{s}_{x,ih} f(x)}{\binom{2k}{k}}$$

$$I^{s}_{x,-ih} = I^{s}_{x,ih}$$

Definition (9):

If $f \in L_{p,\alpha}(T^*)$, we define:

$$W^{s}_{x,h,2k} f(x)e^{-\alpha x} = \frac{\sum_{i=0}^{2k} (-1)^{k-i} \binom{2k}{i} I^{s}_{x,(i-k)h} f(x)e^{-\alpha x}}{\binom{2k}{k}}$$

Lemma (1):

$$\| W^{s}_{.,h,2k} f \|_{\alpha,\infty} \le \binom{2k}{k}^{-1} \frac{2\pi s}{h} \omega_{2k}(f,sh)_{\alpha}, \quad 0 < shk < 2\pi$$

if $f \in L_{p,\alpha}(T^*)$,

Proof:

Since:

$$W^{s}_{x,h,2k} f(x)e^{-\alpha x} = \frac{\sum_{i=0}^{2k} (-1)^{k-i} \binom{2k}{i} I^{s}_{x,(i-k)h} f(x)e^{-\alpha x}}{\binom{2k}{k}}$$

$$= \frac{(-1)^k}{\binom{2k}{k}} \sum_{i=0}^{2k} (-1)^{-i} \binom{2k}{i} I^{s}_{x,(i-k)h} f(x)e^{-\alpha x}$$

$$= (-1)^k \binom{2k}{k}^{-1} \sum_{i=0}^{2k} (-1)^{-i} \binom{2k}{i} \left\{ (fe^{-\alpha x} * B^{s}_{h})(x) \right\}$$

$$W^{s}_{x,h,2k} f(x)e^{-\alpha x} = (-1)^k \binom{2k}{k}^{-1} \Delta^{2k}_{h} \int_{T^*} f(x)e^{-\alpha x} B^{s}_{h}(u)\, du$$

If we take the norm of the two sided, we get:

$$\| W^{s}_{.,h,2k} f \|_{\alpha,\infty} = \left\| (-1)^k \binom{2k}{k}^{-1} \Delta^{2k}_{h} \int_{T^*} f(x) B^{s}_{h}(u)\, du \right\|_{\alpha,\infty}$$

$$= \binom{2k}{k}^{-1} \left\| \int_{T^*} \Delta^{2k}_{h} f(x) B^{s}_{h}(u)\, du \right\|_{\alpha,\infty}$$

$$= \binom{2k}{k}^{-1} \sup_{x \in T^*} \left| \int_{T^*} \Delta^{2k}_{h} f(x)e^{-\alpha x} B^{s}_{h}(u)\, du \right|$$

$$\le \binom{2k}{k}^{-1} \int_{T^*} B^{s}_{h}(u)\, du \sup_{x \in T^*} \left| \Delta^{2k}_{h} f(x)e^{-\alpha x} \right|$$

Using remark and Definition (6), we get:

$$\| W^{s}_{.,h,2k} f \|_{\alpha,\infty} \le \binom{2k}{k}^{-1} \frac{2\pi s}{h} \omega_{2k}(f,sh)_{\alpha}, \quad 0 < shk < 2\pi$$

Definition (10), [10]:

Valleé Poussin means is defined by:

$$V_{k,m} = \frac{1}{m} \sum_{i=km}^{(k+1)m-1} s_i = (k+1)\sigma_{(k+1)(m-1)} - k\sigma_{km-1}$$

where s_i is the operator of i-th partial Fourier sum and also Fejer's means is defined by:

$$\sigma_j = \frac{1}{j+1} \sum_{i=0}^{j} s_i$$

Theorem (A), [10]:

If f, $f^{(m)} \in C(T^{\perp}_{n})$, then:

$\|f\| \le F_m(n+1)^{-m} \|f^{(m)}\|$

where:

$$F_m = \frac{4}{\pi} \sum_{i=0}^{\infty} (-1)^{i(m+1)} (2i+1)^{-m-1}$$

$C(T) = \{ f \mid f: T^* \longrightarrow R \}$ such that f is continuous function on T, with:

$$\|f\|_{\infty} = \max_{x \in T} |f(x)|$$

$$\|f\|_{1} = \int_{T} |f(u)|\, du$$

Theorem (B), [6]:

$E_{n-1}(B^{r}_{1})_1 = k_r n^{-r}$

where:

$B^{r}_{p} = \{ f : [a,b] \longrightarrow R$, such that $\|f^{(r)}\|_p \le 1 \}$

$1 \le p \le \infty$, $r = 1, 2, \ldots$, k_r is a constant.

Theorem (1):

If f is an unbounded function, $f \in L_{p,\alpha}(T^*)$. If $f(x)e^{-\alpha x}$ and $(f(x)e^{-\alpha x})^{(m)} \in L_{p,\alpha}(T^*)$, then:

$\|f\|_{\alpha,\infty} \le F_m(n+1)^{-m} \|f^{(m)}\|_{\alpha,\infty}$

where:

$$F_m = \frac{4}{\pi} \sum_{i=0}^{\infty} (-1)^{i(m+1)} (2i+1)^{-m-1}$$

Proof:

From Theorem (A), we have if $f(x) \ge 0$, then $f(x) \le F_m(n+1)^{-m} |f^{(m)}(x)|$

Since $|f(x)e^{-\alpha x}| > 0$

$$|f(x)e^{-\alpha x}| \le F_m(n+1)^{-m} |(f(x)e^{-\alpha x})^{(m)}|$$

$$\sup_{x \in T^*} |f(x)e^{-\alpha x}| \le \sup_{x \in T^*} |F_m(n+1)^{-m} (f(x)e^{-\alpha x})^{(m)}|$$

$$\|f\|_{\alpha,\infty} \le F_m(n+1)^{-m} \sup_{x \in T^*} |(f(x)e^{-\alpha x})^{(m)}|$$

$$\le F_m(n+1)^{-m} \|f^{(m)}\|_{\alpha,\infty}.$$

Theorem (2):

Let $f \in L_{p,\alpha}$ and $f : [a,b] \longrightarrow R$, $\|(fe^{-\alpha x})^{(r)}\|_p \le 1$, then:

$E_{n-1}(B^{r})_{1,\alpha} = k_r n^{-r}$

Proof:

Since f is an unbounded function, thus $f.e^{-\alpha}(x)$ is a bounded one

By using Theorem (B), we get:
$E_{n-1}(B_i^r)_{1,\alpha} = k_r n^{-r}$.

Main Results:
In this section, the main results of this article is adpted on unbounded function of $L_{p,\alpha}$ and has been presented as[7].

Theorem (3):
Let f be an unbounded function, $f \in L_{p,\alpha}(T^*)$, we have:

$$\|f\|_{\alpha,\infty} \le \frac{2\pi s(k+1)}{h}\binom{2k}{k}^{-1}\omega_{2k}(f,3\beta\pi(2n)^{-1})_\alpha \quad , n \ge k$$

Proof:
Since f be an unbounded function, $f \in L_{p,\alpha}(T^*)$, $f(x)e^{-\alpha x}$ is bounded
From Definition (8), we have:

$$W_{s,h,2k}^s f(x)e^{-\alpha x} = I_s f(x)e^{-\alpha x} - 2\sum_{i=0}^{k}(-1)^{i+1}\frac{\binom{2k}{k+i}}{\binom{2k}{k}} I_{s,ih}^s f(x)e^{-\alpha x}$$

Since

$$I_{s,ih}^s f(x)e^{-\alpha x} = (B_{ih}^s * fe^{-\alpha})(x), \text{ for } f \in L_{p,\alpha}(T_n^* -)$$
$$= ((B_{ih}^s - p) * fe^{-\alpha})(x)$$
$$\|I_{s,ih}^s f(.)\|_{\alpha,\infty} = \|(B_{ih}^s - p) * f\|_{\alpha,\infty}$$
$$= \sup_{x\in T^*}|((B_{ih}^s - p) * fe^{-\alpha})(x)|$$
$$= \sup_{x\in T^*}\left|\int_{T^*}((B_{ih}^s - p)e^{-\alpha u} * fe^{-\alpha u})du\right|$$
$$\le \sup_{x\in T^*}\int_{T^*}\left|(B_{ih}^s - p)e^{-\alpha u}\right|du\left|f(x)e^{-\alpha x}\right|$$
$$\le \int_{T^*}(B_{ih}^s - p)e^{-\alpha u}du \sup_{x\in T^*}\left|f(x)e^{-\alpha x}\right|$$
$$\le \|B_{ih}^s - p\|_{1,\alpha}\|f\|_{\alpha,\infty}$$

Hence:

$$I_{s,ih}^s f(.)\|_{\alpha,\infty} \le \|B_{ih}^s - p\|_{1,\alpha}\|f\|_{\alpha,\infty}$$

Using Theorems (1) and (2), we get:

$$\inf_{p\in T_n^*}\|B_{ih}^s - p\|_{1,\alpha} \le F_{s-1}(n)^{-s+1}\|D^{s-1}B_{ih}^s\|_{1,\alpha} \quad ...(4)$$

and since:

$$D^{(m)}B_h^s(x) = (2h)^{-m}\Delta_{2h}^s B_h^{s-m}(x), \ s \ge m$$

then:

$$D^{(s-1)}B_{ih}^s(x) = (2ih)^{-(s-1)}\Delta_{2ih}^s B_{ih}^{s-(s-1)}(x)$$
$$= (2ih)^{-s+1}\Delta_{2ih}^s B_{ih}^1(x)$$

If we take the norm of the two sided, then:

$$\|D^{(s-1)}B_{ih}^s(x)\|_{1,\alpha} = \|(2ih)^{-s+1}\Delta_{2ih}^s B_{ih}^1(x)\|_{1,\alpha}$$
$$= (2ih)^{-s+1}\|\Delta_{2ih}^s B_{ih}^1(x)\|_1 \quad ...(5)$$

From (4) and (5)

$$\inf_{p\in T_n^*}\|B_{ih}^s - p\|_{1,\alpha} \le F_{s-1}(n)^{-s+1}(2ih)^{-s+1}\|\Delta_{2ih}^s B_{ih}^1(x)\|_{1,\alpha}$$
$$\le F_{s-1}(n)^{-s+1}(2hni)^{-s+1}\|\Delta_{2ih}^{s-1}B_{ih}^1(x)\|_{1,\alpha}$$

Take $s = 3$, $\beta = \frac{\pi}{\sqrt{6}}$, $h = \beta\pi(2\pi)^{-2}$, since:

$$\|I_{s,ih}^s f(.)\|_{\alpha,\infty} \le M\|f\|_{\alpha,\infty}, \ M = B(h,s,i)$$
$$\le B(h,s,i)\|f\|_{\alpha,\infty}$$

We get:

$$B(h,3,i) \le \inf_{p\in T_n^*}\|B_{ih}^s - p\|_{1,\alpha}$$
$$\le 4F_2(\beta\pi i)^{-2}$$
$$= \frac{1}{2\beta^2 i^2}$$

Hence, $B(h,3,i) \le \frac{1}{2\beta^2 i^2}$

$$2\sum_{i=1}^{k}\frac{\binom{2k}{k+i}}{\binom{2k}{k}}B(h,3,i) \le 2\sum_{i=1}^{k}\frac{\binom{2k}{k+i}}{\binom{2k}{k}}\frac{1}{2\beta^2 i^2}$$

Since:

$$\sum_{i=1}^{k}\binom{2k}{k+i} \le \binom{2k}{k+i}\sum_{i=1}^{k}\left(\frac{1}{i}\right)^2$$
$$\le \frac{6}{\pi^2}\frac{\binom{2k}{k+i}}{\binom{2k}{k}}\sum_{i=1}^{k}\left(\frac{1}{i}\right)^2$$

Since:

$$\frac{\binom{2k}{k+i}}{\binom{2k}{k}} = \frac{(2k)!/(k-1)!(2k-k-1)!}{(2k)!/k!(2k-k)!}$$
$$= \frac{(2k)!/(k+1)!(k-1)!}{(2k)!/k!k!}$$
$$= \frac{(2k)!}{(k-1)!(k-1)!}\frac{k!k!}{(2k)!}$$
$$= \frac{k!k(k-1)!}{(k-1)k!(k-1)!}$$
$$= \frac{k}{k+1}$$

$$\sum_{i=1}^{k}\binom{2k}{k+i} \le \frac{6}{\pi^2}\cdot\frac{k}{k-i}\sum_{i=1}^{k}\left(\frac{1}{i}\right)^2 < 1$$

$$2\sum_{i=1}^{k}\frac{\binom{2k}{k+i}}{\binom{2k}{k}}B(h,3,i) \le d(k) < 1, \ d(k) \text{ is a constant}$$

Since, $I_x f(x)e^{-\alpha x} = W_{s,h,2k}^s f(x)e^{-\alpha x}$
$$+ 2\sum_{i=0}^{k}(-1)^{i+1}\frac{\binom{2k}{k+i}}{\binom{2k}{k}}I_{s,ih}^s f(x)e^{-\alpha x}$$

By Definition (7) and taking the absolute value of both sides, yields to:

$$|L_n f(x)e^{-\alpha x}| = \left| W^s_{x,h,2k} f(x)e^{-\alpha x} - 2\sum_{i=0}^{k}(-1)^{i+1}\frac{\binom{2k}{k+i}}{\binom{2k}{k}} I^s_{x,ih} f(x)e^{-\alpha x} \right|$$

$$\sup_{x\in I_n^*} |L_n f(x)e^{-\alpha x}| = \sup_{x\in I_n^*} \left| W^s_{x,h,2k} f(x)e^{-\alpha x} - 2\sum_{i=0}^{k}(-1)^{i+1}\frac{\binom{2k}{k+i}}{\binom{2k}{k}} I^s_{x,ih} f(x)e^{-\alpha x} \right|$$

$$\|f\|_{\alpha,\infty} = \left\| W^s_{.,h,2k} f - 2\sum_{i=0}^{k}(-1)^{i+1}\frac{\binom{2k}{k+i}}{\binom{2k}{k}} I^s_{x,ih} f \right\|_{\alpha,\infty}$$

$$\le \| W^s_{.,h,2k} f \|_{\alpha,\infty} + 2\sum_{i=0}^{k}(-1)^{i+1}\frac{\binom{2k}{k+i}}{\binom{2k}{k}} \| f \|_{\alpha,\infty}$$

Hence:

$$\|f\|_{\alpha,\infty} - 2\sum_{i=0}^{k}(-1)^{i+1}\frac{\binom{2k}{k+i}}{\binom{2k}{k}} \| f \|_{\alpha,\infty} \le \| W^s_{.,h,2k} f \|_{\alpha,\infty}$$

$$\|f\|_{\alpha,\infty}\left(1 - 2\frac{\binom{2k}{k+1}}{\binom{2k}{k}}\right) \le \| W^3_{.,h,2k} f \|_{\alpha,\infty}$$

$$\|f\|_{\alpha,\infty}\left(1 - \frac{\binom{2k}{k+1}}{\binom{2k}{k}}\right) \le \| W^3_{.,h,2k} f \|_{\alpha,\infty}$$

From Definition (9), we get:

$$\| W^3_{.,h,2k} f \|_{\alpha,\infty} \le \frac{2\pi s}{\binom{2k}{k} h} \omega_{2k}(f,3h)_\alpha$$

Then:

$$\|f\|_{\alpha,\infty}\left(1 - \frac{\binom{2k}{k+1}}{\binom{2k}{k}}\right) \le \frac{2\pi s}{\binom{2k}{k} h} \omega_{2k}(f,3h)_\alpha$$

$$\|f\|_{\alpha,\infty}\left(\frac{\binom{2k}{k} - \binom{2k}{k+1}}{\binom{2k}{k}}\right) \le \frac{2\pi s}{\binom{2k}{k} h} \omega_{2k}(f,3h)_\alpha$$

$$\|f\|_{\alpha,\infty} \le \frac{2\pi s/h}{\binom{2k}{k} - \binom{2k}{k+1}} \omega_{2k}(f,3h)_\alpha$$

Since:

$$\binom{2k}{k} - \binom{2k}{k+1} = \frac{(2k)!}{k!k!} - \frac{(2k)!}{(k+1)!(k-1)!}$$

$$= (2k)!\left(\frac{1}{k!k!} - \frac{1}{(k+1)!(k-1)!}\right)$$

$$= (2k)!\left(\frac{1}{k!k!(k-1)!} - \frac{1}{(k+1)k!(k-1)!}\right)$$

$$= \frac{(2k)!}{k!(k-1)!}\left(\frac{1}{k} - \frac{1}{k+1}\right)$$

$$= \frac{(2k)!}{k!(k-1)!}\left(\frac{k+1}{k(k+1)} - \frac{k}{k(k+1)}\right)$$

$$= \frac{(2k)!}{kk!(k-1)!}\left(\frac{1}{k+1}\right)$$

$$= \frac{(2k)!}{k!k!}\left(\frac{1}{k+1}\right) = \binom{2k}{k}\frac{1}{k+1}$$

Hence:

$$\|f\|_{\alpha,\infty} \le \frac{2\pi s(k+1)}{\binom{2k}{k} h} \omega_{2k}(f,3\beta\pi(2n)^{-1})_\alpha .$$

Lemma (2), [3]:

Let the function f be defined and bounded in the interval [a,b] and let k be a natural number, then:

$\omega_k(f,\delta') \le \omega_k(f,\delta'')$, for $0 \le \delta' \le \delta''$

Lemma (3):

Let $f \in L_{p,\alpha}(T^*)$, then:

$\omega_k(f,\delta')_\alpha \le \omega_k(f,\delta'')$, for $0 \le \delta' \le \delta''$

Proof:

Since f is an unbounded function, thus $f(x)e^{-\alpha x}$ is bounded

Using Lemma (2), we get:

$\omega_k(f,\delta')_\alpha \le \omega_k(f,\delta'')$, for $0 \le \delta' \le \delta''$.

Theorem (4):

Let $f \in L_{p,\alpha}(T^*)$, then:

$$\|f - V_{k,m} f\|_{\alpha,\infty} \le \frac{2\pi s(k+1)^2}{\binom{2k}{k} h} \omega_{2k}\left(f, \frac{3\beta\pi}{km}\right)_\alpha , \quad m \ge 2$$

Proof:

Since f is an unbounded function, thus $f(x)e^{-\alpha x}$ is bounded By Definition (10):

$$\underline{V}_{k,m}(f(x)e^{-\alpha x}) = (k+1)\sigma_{(k-1)(m-1)}(f(x)e^{-\alpha x}) - k\sigma_{km-1}f(x)e^{-\alpha x}$$
$$= (k+1)f(x)e^{-2x} - \underline{k}f(x)e^{-\alpha x}$$
$$= f(x)e^{-\alpha x}$$

$\underline{V}_{k,m}(f(x)e^{-\alpha x}) \xrightarrow{u.c.} f(x)e^{-\alpha x}$ as $m \longrightarrow \infty$, uniform convergence

$$\lim_{m\to\infty} \underline{V}_{k,m}(f(x)e^{-\alpha x}) = f(x)e^{-\alpha x}$$

Then $\omega_{2k}(f,h)_\alpha \cong \omega_2 k(\underline{V}_{k,m}f,h)_\alpha$

Since $h < 2kh$, then using Lemma (3), we get:

$$\omega_{2k}(f,h)_\alpha \le \omega_{2k}(f,2kh)_\alpha$$
$$\le (2k+1)\omega_{2k}(f,h)_\alpha, \text{ from Theorem (3)}$$

Therefore:

$$\|f - \underline{V}_{k,m}f\|_{\alpha,\infty} \le \frac{2\pi s(k-1)}{\binom{2k}{k}h}\omega_{2k}(f - V_{k,m}f, 3\beta(n)^{-1})_\alpha$$
$$\le \frac{2\pi s(k+1)^2}{\binom{2k}{k}h}\omega_{2k}\left(f, \frac{3\beta\pi}{n}\right)_\alpha . \quad \blacksquare$$

Theorem (5):

$f \in \underline{L}_{p,\alpha}(T^*)$ and $0 < A < 1$, then:

$$\underline{E}_n(f)_\alpha \le \frac{2\pi s(k+1)^2}{\binom{2k}{k}h}\omega_{2k}\left(f, \frac{3\pi}{n}A\left(1+\frac{1}{k}\right)\right)_\alpha, \quad n \ge 2k$$

Proof:

Since f is an unbounded function, thus $f(x)e^{-\alpha x}$ is bounded, for the best approximation by trigonometric polynomials of degree $n = km + i$, $i \in [0, m-1]$

Since:

$$\underline{n} = km + i,\ 0 \le i \le m - i$$
$$= \underline{km} + m - 1 \le km - m - 1$$
$$\frac{n}{km} \le \frac{km}{km} + \frac{m}{km} - \frac{1}{km}$$
$$\le 1 + \frac{1}{k} - \frac{1}{km}$$
$$\le 1 + \frac{1}{k}$$

Hence, by dividing on n, we get:

$$\frac{1}{km} \le \frac{1}{n} + \frac{1}{nk}$$
$$\le \frac{1}{n}\left(1 + \frac{1}{k}\right) \qquad \ldots (6)$$

Since $n \le km$, then:

$$\underline{E}_n(f)_\alpha \le \underline{E}_{km}(f)_\alpha$$

Using Theorem (4),

$$\underline{E}_n(f)_\alpha \le \underline{E}_{km}(f)_\alpha \le \|f - \underline{V}_{k,m}f\|_{\alpha,\infty}$$
$$\le \frac{2\pi s(k+1)^2}{\binom{2k}{k}h}\omega_{2k}\left(f, \frac{3\beta\pi}{n}\right)_\alpha, \quad m \ge 2$$
$$\le \frac{2\pi s(k+1)^2}{\binom{2k}{k}h}\omega_{2k}\left(f, \frac{3\pi}{km}A\right)_\alpha, \quad A = \frac{3\beta}{4}$$

From (6), we get:

$$E_n(f)_\alpha \le \frac{2\pi s(k+1)^2}{\binom{2k}{k}h}\omega_{2k}\left(f, \frac{2\pi}{n}A\left(1+\frac{1}{k}\right)\right)_\alpha .$$

References:

[1] A. A. Hammed, **"Degree of best approximation in L_P -weighted space"** MSc .thesis,Al-Mustansiriya Uninversity. (2012).

[2] B. M. Hussein , **"Approximation of unbounded function"**, M.Sc. Thesis, Al-Mustansiriya Uninversity ,Department of Mathematics, College of Education (2010).

[3] B. Sendov and A. Popov, "The Averaged Moduli of Smoothness", Applications in Numerical Methods and Approximation, John Wiley and Sons, University of such that Andrews, (1988).

[4] E. S. Bhaya,**"On constrained and unconstrained approximation"**, P.h.D. thesis, Baghdad University, Department of Mathematics , College of Education (Ibn Al- Haitham).(2003).

[5] N.M. Kassim ,**"On the monotone and comonotone approximation"**, M.Sc .thesis , Kufa University , Mathematical Department of Mathematics, College of Education for girls ,(2004).

[6] R. A. Devore and G. G. Lorntz, "Constructive Approximation", Springer-Verlag, Berlin, (1993).

[7] R.F.Haassan and Sahib K.Jasim **"The degree of best approximation of unbounded functions by Bleimann-Butzer-Hahn positive linear operators in weighted space"**.international Journal of Mathematical Archives-5(4),74-81,India,(2014).

[8] R. L. Burden, "Numerical Analysis", Third Edition, Youngstown State University, (1985).

[9] S.K. Jassim, and E.S. Bhaya **"Direct and inverse theorems for best multi-approxmation in $L_{p,a}(1 < p < \infty)$"** Mathematics and physics Journal, 17(3)1-8, (2002).

[10]Y. Kryakin, "Bohr-Favard Inequality for Differences and Constants in Jackson-Stechkin Theorem", Math. CA Institute of Mathematics, University of Wroclaw, Poland, 2 Dec. (2005).

Al-Mustansiriyah Journal of Science
Vol. 27, No 2, 2016

journal homepage:www.mjs-mu.com

Fractional Operational Matrices for Solving Multi-Fractional Nonlinear Differential Equations with Mixed Boundary Conditions

Sameer Qasim Hasan and Dalia Raad Abed
Department of Mathematics, College of Education, Al-Mustansirya University

Articleinfo
Received
21/4/2015
Accepted
18/5/2015

ABSTRACT

The aim of this paper is to find the numerical solution of multi-fractional order nonlinear differential equation by using fractional operational matrices of order different than the order of the equation, with order of matrix is equal to the order of their types of fractional Chebyshev polynomial.

الخلاصة

الهدف من البحث هو إيجاد الحلول الحدودية للمعادلات غير الخطية ذات الرتب الكسرية المتعددة بأستخدام مصفوفات عملية كسرية لرتب كسرية مختلفة عن رتبة المعادلة التي تمثل رتبة المصفوفة الكسرية جبيجيف

INTRODUCTION

The multi-fractional order nonlinear differential equation (MFNDE) arise in modeling processes in applied sciences, as in physics, engineering, chemistry[1] and other sciences can be described very successfully by models using mathematical tools from fractional calculus, and concepts of fractional polynomials and fractional operational matrices [2,4,8,6].

The fractional operational matrices are usually difficult to formulate it analytically, so, it is required to obtain an efficient approximate solution of multi-fractional order nonlinear differential equation (MFNDE).

One of the attractive concepts in the initial and boundary value problems is differentiation and integration of fractional order (K.Diethelm 2010) , (Fox 1968),(K.B.Oldham 1974). Many researchers extend classical methods in studies of differential and integral equations of integer order to fractional type of these problems (X.Li 2012),(A.Saaadatmandi and etc. 2012). One of the wide classes of researches focuses to constructing the operational matrix of derivative in some spectral methods. Recently, a lot of attention has been devoted to construct operational matrix of fractional derivative [1,5,6,7].

This paper has presented the solution of multi-order fractional nonlinear differential equations with mixed boundary conditions using fractional operational matrices with different type of order of the equation and given the examples to illustrative the methods. Also different fractional operational matrices, one as originally and second as axillary orders explain in some examples.

Some Kinds of Fractional Order Chebyshev Polynomials

We introduce the fractional order Chebyshev polynomials of first, third and fourth kind

$T^*_{n+1}(x) = 2(2x-1)\ T^*_n(x) - T_{n-1}(x) \quad n=1,2,..$ (1)

And,

$V^*_{n+1}(x) = 2(2x-1)V^*_n(x) - V^*_{n-1}(x), \quad n = 1,2,..$(2)

with,

$W^*_{n+1}(x) = 2(2x-1)W^*_n(x) - W^*_{n-1}(x), \ n = 1,2..$(3)

by, changing the variable $x = x^\alpha$ which $\alpha > 0$ in(1),(2)and(3) we get,

1. $T^*_n(x^\alpha)$ as $\bar{T}^\alpha_n(x)$.
2. $V^*_n(x^\alpha)$ as $\bar{V}^\alpha_n(x)$.
3. $W^*_n(x^\alpha)$ as $\bar{W}^\alpha_n(x)$.

From the recurrence relation of the shifted Chebyshev polynomials of all above kinds, can be obtained the following recurrence formulas :

i. $\bar{T}_{n+1}^{\alpha}(x) = 2\,x^{\alpha}\,\bar{T}_{n}^{\alpha}(x) - \bar{T}_{n-1}^{\alpha}(x)\,, \quad n = 1\,,2\,,\cdots$ ..... (4)

where $\bar{T}_{0}^{\alpha}(x) = 1\,,\ \bar{T}_{1}^{\alpha}(x) = 2x^{\alpha} - 1$

ii. $\bar{V}_{n+1}^{\alpha}(x) = 2(2\,x^{\alpha} - 1)\bar{V}_{n}^{\alpha}(x) - \bar{V}_{n-1}^{\alpha}(x)\,, \quad n = 1\,,2\,,\cdots$ ..... (5)

where $\bar{V}_{0}^{\alpha}(x) = 1\,,\ \bar{V}_{1}^{\alpha}(x) = 4x^{\alpha} - 3$

iii. $\bar{W}_{n+1}^{\alpha}(x) = 2(2\,x^{\alpha} - 1)\bar{W}_{n}^{\alpha}(x) - \bar{W}_{n-1}^{\alpha}(x)\,, \quad n = 1\,,2\,,\cdots$ ....(6)

where $\bar{W}_{0}^{\alpha}(x) = 1\,,\ \bar{W}_{1}^{\alpha}(x) = 2x^{\alpha} + 1$

Lemma(1):

1. $\bar{T}_{n}^{\alpha}(x)$ are orthogonal functions with respect to the weight function

$\omega_{1,\alpha}^{*}(x) = \frac{1}{x^{\alpha}\sqrt{x^{-2\alpha}-1}}$,and we have

$$\int_0^1 \bar{T}_{n}^{\alpha}(x)\cdot\bar{T}_{m}^{\alpha}(x)\cdot\omega_{1,\alpha}^{*}(x)\,dx = \begin{cases} 0 & n \neq m \\ \frac{\pi c_i}{4\cdot\alpha} & n = m \end{cases} \quad \text{.....(7)}$$

where, $c_i = \begin{cases} 2 & if \quad i = 0 \\ 1 & if \quad i \geq 1 \end{cases}$.

2. $\bar{V}_{n}^{\alpha}(x)$ are orthogonal with respect to the weight function

$\omega_{3,\alpha}^{*}(x) = x^{\alpha-1}\sqrt{(x^{-\alpha}-1)^{-1}}$,and we have

$$\int_0^1 \bar{V}_{n}^{\alpha}(x)\cdot V_{m}^{\alpha}(x)\cdot\omega_{3,\alpha}^{*}(x)dx = \begin{cases} \frac{\pi}{2\cdot\alpha} & if \quad n = m \\ 0 & if \quad n \neq m \end{cases}$$

.....(8)

3. $\bar{W}_{n}^{\alpha}(x)$ are orthogonal with respect to the weight function

$\omega_{4,\alpha}^{*}(x) = x^{\alpha-1}\sqrt{x^{-\alpha}-1}$, and we have

$$\int_0^1 \bar{W}_{n}^{\alpha}(x)\cdot\bar{W}_{m}^{\alpha}(x)\cdot\omega_{4,\alpha}^{*}(x)\,dx = \begin{cases} 0 & if \quad n \neq m \\ \frac{\pi}{2\cdot\alpha} & if \quad n = m \end{cases}$$

.....(9)

Proof:

1. by taking $t = x^{\alpha}$ and $dt = \alpha x^{\alpha-1}dx$, substituting these valued in

$$\int_0^1 T_{n}^{*}(t)\cdot T_{m}^{*}(t)\cdot\omega_{1}^{*}(t)dt = \begin{cases} 0 & if \quad n \neq m \\ \frac{\pi c_i}{4} & if \quad n = m \end{cases}$$

we get,

$$\int_0^1 T_{n}^{*}(x^{\alpha})\cdot T_{m}^{*}(x^{\alpha})\cdot\omega_{1,\alpha}^{*}(x)\cdot\alpha x^{\alpha-1}dx = \begin{cases} 0 & if \quad n \neq m \\ \frac{\pi c_i}{4} & if \quad n = m \end{cases} \quad \text{... (10)}$$

$$\alpha\int_0^1 \bar{T}_{n}^{\alpha}(x)\cdot\bar{T}_{m}^{\alpha}(x)\cdot\frac{x^{\alpha-1}}{x^{\alpha}\sqrt{x^{-2\alpha}-1}}\,dx = \begin{cases} 0 & if \quad n \neq m \\ \frac{\pi c_i}{4} & if \quad n = m \end{cases}$$

$$\int_0^1 \bar{T}_{n}^{\alpha}(x)\cdot\bar{T}_{m}^{\alpha}(x)\cdot\omega_{1,\alpha}^{*}(x)\,dx = \begin{cases} 0 & if \quad n \neq m \\ \frac{\pi c_i}{4\cdot\alpha} & if \quad n = m \end{cases}$$

..... (11)

2. for taking $t = x^{\alpha}$ and $dt = \alpha x^{\alpha-1}dx$, substituting these valued in

$$\int_0^1 V_{n}^{*}(t)\cdot V_{m}^{*}(t)\cdot\omega_{3}^{*}(t)dt = \begin{cases} 0 & n \neq m \\ \frac{\pi}{2\cdot\alpha} & n = m \end{cases}$$

we obtain,

$$\int_0^1 V_{n}^{*}(x^{\alpha})\cdot V_{m}^{*}(x^{\alpha})\cdot\omega_{3,\alpha}^{*}(x)\cdot\alpha x^{\alpha-1}dx = \begin{cases} 0 & if \quad n \neq m \\ \frac{\pi}{2} & if \quad n = m \end{cases} \quad \text{.... (12)}$$

$$\alpha\int_0^1 \bar{V}_{n}^{\alpha}(x)\cdot\bar{V}_{m}^{\alpha}(x)\cdot\sqrt{\frac{x^{\alpha}}{1-x^{\alpha}}}\cdot x^{\alpha-1}\,dx = \begin{cases} 0 & if \quad n \neq m \\ \frac{\pi}{2} & if \quad n = m \end{cases}$$

$$\alpha\int_0^1 \bar{V}_{n}^{\alpha}(x)\cdot\bar{V}_{m}^{\alpha}(x)\cdot\frac{x^{\frac{1}{2}\alpha}}{x^{\frac{1}{2}\alpha}}\sqrt{\frac{1}{x^{-\alpha}-1}}\cdot x^{\alpha-1}\,dx = \begin{cases} 0 & if \quad n \neq m \\ \frac{\pi}{2} & if \quad n = m \end{cases}$$

$$\alpha\int_0^1 \bar{V}_{n}^{\alpha}(x)\cdot\bar{V}_{m}^{\alpha}(x)\cdot x^{\alpha-1}\cdot\sqrt{(x^{-\alpha}-1)^{-1}}\,dx = \begin{cases} 0 & if \quad n \neq m \\ \frac{\pi}{2} & if \quad n = m \end{cases}$$

Then

$$\int_0^1 \bar{V}_{n}^{\alpha}(x)\cdot V_{m}^{\alpha}(x)\cdot\omega_{3,\alpha}^{*}(x)\,dx = \begin{cases} 0 & if \quad n \neq m \\ \frac{\pi}{2\cdot\alpha} & if \quad n = m \end{cases}$$

3. Now for taking $t = x^{\alpha}$ and $dt = \alpha x^{\alpha-1}dx$, substituting these valued in

$$\int_0^1 W_{n}^{*}(t)\cdot W_{m}^{*}(t)\cdot\omega_{4}^{*}(t)dt = \begin{cases} 0 & if \quad n \neq m \\ \frac{\pi}{2} & if \quad n = m \end{cases}$$

we get,

$$\int_0^1 W_{n}^{*}(x^{\alpha})\cdot W_{m}^{*}(x^{\alpha})\cdot\omega_{4,\alpha}^{*}(x)\cdot\alpha x^{\alpha-1}dx = \begin{cases} 0 & if \quad n \neq m \\ \frac{\pi}{2} & if \quad n = m \end{cases} \quad \text{....(13)}$$

$$\int_0^1 \bar{W}_{n}^{\alpha}(x)\cdot\bar{W}_{m}^{\alpha}(x)\cdot\frac{x^{\frac{1}{2}\alpha}}{x^{\frac{1}{2}\alpha}}\sqrt{x^{-\alpha}-1}\cdot\alpha x^{\alpha-1}\,dx = \begin{cases} 0 & if \quad n \neq m \\ \frac{\pi}{2} & if \quad n = m \end{cases}$$

$$\alpha\int_0^1 \bar{W}_{n}^{\alpha}(x)\cdot\bar{W}_{m}^{\alpha}(x)\cdot x^{\alpha-1}\cdot\sqrt{x^{-\alpha}-1}\,dx = \begin{cases} 0 & if \quad n \neq m \\ \frac{\pi}{2} & if \quad n = m \end{cases}$$

$$\int_0^1 \bar{W}_{n}^{\alpha}(x)\cdot\bar{W}_{m}^{\alpha}(x)\cdot\omega_{4,\alpha}^{*}(x)\,dx = \begin{cases} 0 & if \quad n \neq m \\ \frac{\pi}{2\cdot\alpha} & if \quad n = m \end{cases}$$

Lemma(2):

1)The fractional-order first kind Chebyshev function $\bar{T}_{n}^{\alpha}(x)$, has precisely n zeros in the form:

$$t_m = \left(\frac{1+\cos\frac{\left(m-\frac{1}{2}\right)\pi}{n}}{2}\right)^{\frac{1}{\alpha}} \qquad m = 1\,,2\,,\cdots,n$$

..... (14)

2)The fractional-order third kind Chebyshev function $\bar{V}_n^{\alpha}(x)$, has precisely n zeros in the form:

$$t_m = \left(\frac{1+\cos\frac{(m-\frac{1}{2})\pi}{n+\frac{1}{2}}}{2} \right)^{\frac{1}{\alpha}} \qquad m = 1, 2, \cdots, n.$$

.....(15)

3)The fractional-order forth kind Chebyshev function $\bar{W}_n^{\alpha}(x)$,has precisely n zeros in the form:

$$t_m = \left(\frac{1+\cos\left[\frac{m\pi}{n+\frac{1}{2}}\right]}{2} \right)^{\frac{1}{\alpha}} \qquad m = 1, 2, .., n$$

..... (16)

***Proof*:**

1)The shifted Chebyshev polynomial of first kind $T_n^*(x)$ has n zeros

$$x_m = \left(\frac{1+\cos\left[\frac{(m-\frac{1}{2})\pi}{n}\right]}{2} \right) \qquad m = 1, 2, \cdots, n.$$

so, $T_n^*(x)$ can be written as

$T_n^*(x) = (x - x_1)(x - x_2) \cdots (x - x_n)$

..... (17a)

changing of variable $x = t^{\alpha}$ in(17a),yields

$\bar{T}_n^{\alpha}(t) = (t^{\alpha} - x_1)(t^{\alpha} - x_2) \cdots (t^{\alpha} - x_n)$

..... (17b)

so, the zeros of $\bar{T}_n^{\alpha}(t)$ are,

$t_m = (x_m)^{\frac{1}{\alpha}} \qquad m = 1, 2, \cdots, n$

..... (17c)

2)The shifted third kind Chebyshev polynomial $V_n^*(x)$ has n zeros

$$x_m = \left(\frac{1+\cos\frac{(m-\frac{1}{2})\pi}{n+\frac{1}{2}}}{2} \right) \qquad m = 1, 2, \cdots, n.$$

so, $V_n^*(x)$ can be written as

$V_n^*(x) = (x - x_1)(x - x_2) \cdots (x - x_n)$

..... (18a)

changing of variable $x = t^{\alpha}$ in(18a),yields

$\bar{V}_n^{\alpha}(t) = (t^{\alpha} - x_1)(t^{\alpha} - x_2) \cdots (t^{\alpha} - x_n)$

..... (18b)

so, the zeros of $\bar{V}_n^{\alpha}(t)$ are

$t_m = (x_m)^{\frac{1}{\alpha}} \qquad m = 1, 2, \cdots, n$

..... (18c)

3)The shifted fourth kind Chebyshev polynomial $W_n^*(x)$ has n zeros:

Then $W_n^*(x)$ can be written as

$W_n^*(x) = (x - x_1)(x - x_2) \cdots (x - x_n)$

..... (19a)

changing of variable $x = t^{\alpha}$ in (19a),yields

$\bar{W}_n^{\alpha}(t) = (t^{\alpha} - x_1)(t^{\alpha} - x_2) \cdots (t^{\alpha} - x_n)$

..... (19b)

so, the zeros of $\bar{W}_n^{\alpha}(t)$ are , $t_m = (x_m)^{\frac{1}{\alpha}}$ $m = 1, 2, \cdots, n$ ..... (19c)

Remark(1):

a- For any function $f \in L^2_{w\alpha_1}$ we write

$$f = \sum_{k=0}^{\infty} f_k \bar{T}_k^{\alpha}(x), \quad with \quad f_k = \frac{(f, \bar{T}_k^{\alpha})_{w\alpha_1}}{\|\bar{T}_k^{\alpha}\|^2_{w\alpha_1}}$$

..... (20)

where, f_k is the expansion coefficients associated with the family $\{\bar{T}_k^{\alpha}\}$.

b- For any function $f \in L^2_{w\alpha_3}$ we write

$$f = \sum_{k=0}^{\infty} f_k \bar{W}_k^{\alpha}(x), \quad with \quad f_k = \frac{(f, \bar{W}_k^{\alpha})_{w\alpha_3}}{\|\bar{W}_k^{\alpha}\|^2_{w\alpha_3}}$$

..... (21)

where, f_k is the expansion coefficients associated with the family $\{\bar{V}_k^{\alpha}\}$.

c- For any function $f \in L^2_{w\alpha_4}$ we write

$$f = \sum_{k=0}^{\infty} f_k \bar{W}_k^{\alpha}(x), \quad with \quad f_k = \frac{(f, \bar{W}_k^{\alpha})_{w\alpha_4}}{\|\bar{W}_k^{\alpha}\|^2_{w\alpha_4}}$$

..... (22)

where, f_k are the expansion coefficients associated with the family $\{\bar{W}_k^{\alpha}\}$.

The Operational Matrix of Fractional Derivative:

Let,

i- $\overline{T_{\alpha}}(x) = \{\bar{T}_0^{\alpha}(x), \bar{T}_1^{\alpha}(x), \cdots, \bar{T}_N^{\alpha}(x)\}^T$.

ii- $\overline{V_{\alpha}}(x) = \{\bar{V}_0^{\alpha}(x), \bar{V}_1^{\alpha}(x), \cdots, \bar{V}_N^{\alpha}(x)\}^T$

iii- $\overline{W_{\alpha}}(x) = \{\bar{W}_0^{\alpha}(x), \bar{W}_1^{\alpha}(x), \cdots, \bar{W}_N^{\alpha}(x)\}^T$.

and $X_{\alpha}(x) = \{1, x^{\alpha}, x^{2\alpha}, \cdots, x^{N\alpha}, \}^T$

we obtain,

a- $\overline{T_{\alpha}}(x) = F^{(1)} X_{\alpha}$.

..... (23)

or $\bar{T}_i^{\alpha}(x) = \sum_{j=0}^{N} f_{ij}^{(1)} x^{i\alpha} \qquad i = 0, 1, \cdots, N.$

b- $\overline{V_{\alpha}}(x) = F^{(3)} X_{\alpha}$.

..... (24)

or $\bar{V}_i^{\alpha}(x) = \sum_{j=0}^{N} f_{ij}^{(3)} x^{i\alpha} \qquad i = 0, 1, \cdots, N.$

c- $\overline{W_{\alpha}}(x) = F^{(4)} X_{\alpha}$.

..... (25)

or $\bar{W}_i^{\alpha}(x) = \sum_{j=0}^{N} f_{ij}^{(4)} x^{i\alpha} \qquad i = 0, 1, \cdots, N.$

The fractional derivative of order λ of the vector $T_{\alpha}(x)$, $V_{\alpha}(x)$ and $W_{\alpha}(x)$ can be expressed by,

1. $D^{\lambda}\overline{T_{\alpha}}(x) \cong \Delta^{\lambda}\overline{T_{\alpha}}(x)$

..... (26)

2. $D^{\lambda}\overline{V_{\alpha}}(x) \cong \Delta^{\lambda}\overline{V_{\alpha}}(x)$

..... (27)

3. $D^{\lambda}\overline{W_{\alpha}}(x) \cong \Delta^{\lambda}\overline{W_{\alpha}}(x)$

..... (28)

where Δ^{λ} is the $(n+1)(n+1)$ operational matrix of fractional derivative.

Lemma (3),[6]:
Let,$k = [(the\ largest\ integer\ such\ that\ k\alpha < [\lambda] \& for\ \alpha \in N\_0 @ \& for\ \alpha \notin N\ and\ \alpha < [\lambda])$ ..... (29a)

Then, we have $D^{\lambda}X_{\alpha}(x) \cong \bar{\Delta}^{\lambda}.X_{\alpha}^{\lambda}(x)$
where $\bar{\Delta}^{\lambda}$ is the following $(n+1)(n+1)$ diagonal matrix

$$\bar{\Delta}^{\lambda}=\begin{bmatrix} 0 & \cdots & 0 & \cdots & 0 \\ \vdots & \ddots & \vdots & \iddots & \vdots \\ 0 & \cdots & \frac{\Gamma((k+1)\alpha+1)}{\Gamma((k+1)\alpha+1-\lambda)} & \cdots & 0 \\ \vdots & \iddots & \vdots & \ddots & \vdots \\ 0 & \cdots & 0 & \cdots & \frac{\Gamma(N\alpha+1)}{\Gamma(N\alpha+1-\lambda)} \end{bmatrix}$$

..... (29b)
$X_{\alpha}^{\lambda}(x) = \left[0, \cdots, 0, x^{(k+1)\alpha-\lambda}, x^{(k+2)\alpha-\lambda}, \cdots, x^{N\alpha-\lambda}\right]^{T}$

Lemma (4),[6]:
we have, $X_{\alpha}^{\lambda}(x) \cong B\bar{U}_{i}^{\alpha}(x)$
where $B = (b_{ij})$ is the following $(n+1)(n+1)$ matrix,
$b_{ij} =$

$$\begin{cases} 0 & \begin{cases} i = 0,1,\cdots,k \\ j = 0,1,\cdots,N \end{cases} \\ \frac{\sqrt{\pi}}{\tau}\cdot\sum_{\ell=0}^{j-1} f_{j\ell}\frac{\Gamma\left(i-\frac{\lambda}{\alpha}+l+\frac{5}{2}\right)}{\Gamma\left(i-\frac{\lambda}{\alpha}+l+3\right)} - \frac{\Gamma\left(i-\frac{\lambda}{\alpha}+l+\frac{7}{2}\right)}{\Gamma\left(i-\frac{\lambda}{\alpha}+l+4\right)} & \begin{cases} i = k+1, k+2, \cdots, N \\ j = 0,1,\cdots,N \end{cases} \end{cases}$$

Theorem (5):

a- We have, $X_{\alpha}^{\lambda}(x) \cong D\bar{T}_{i}^{\alpha}(x)$
where, $G = (g_{ij})$ is the following $(n+1)(n+1)$ matrix .
$g_{ij} =$

$$\begin{cases} 0 & \begin{cases} i = 0,1,\cdots,k \\ j = 0,1,\cdots,N \end{cases} \\ \frac{2}{\pi\cdot c_i}\cdot\sum_{\ell=0}^{j} f_{j\ell}\frac{\Gamma\left(\frac{1}{2}(i+\ell)-\frac{\lambda}{2\alpha}+\frac{1}{2}\right)\Gamma\left(\frac{1}{2}\right)}{\Gamma\left(\frac{1}{2}(i+\ell)-\frac{\lambda}{2\alpha}+1\right)} & \begin{cases} i = k+1, k+2, \cdots, N \\ j = 0,1,\cdots,N \end{cases} \end{cases}$$

.....(30)

b- We have, $X_{\alpha}^{\lambda}(x) \cong H\cdot\bar{V}_{i}^{\alpha}(x)$
where, $H = (h_{ij})$ is the following $(n+1)(n+1)$ matrix .
$h_{ij} =$

$$\begin{cases} 0 & \begin{cases} i = 0,1,\cdots,k \\ j = 0,1,\cdots,N \end{cases} \\ \frac{-4}{\sqrt{\pi}}\sum_{\ell=0}^{j} f_{i\ell}\cdot\frac{\Gamma\left(i+l-\frac{\lambda}{\alpha}-\frac{1}{\alpha}+\frac{7}{2}\right)}{\Gamma\left(i+l-\frac{\lambda}{\alpha}-\frac{1}{\alpha}+3\right)} & \begin{cases} i = k+1, k+2, \cdots, N \\ j = 0,1,\cdots,N \end{cases} \end{cases}$$

..... (31)

c- We have, $X_{\alpha}^{\lambda}(x) \cong R\cdot\bar{W}_{i}^{\alpha}(x)$
where, $R = (r_{ij})$ is the following $(n+1)(n+1)$ matrix .
$r_{ij} =$

$$\begin{cases} 0 & \begin{cases} i = 0,1,\cdots,k \\ j = 0,1,\cdots,N \end{cases} \\ \frac{-1}{\sqrt{\pi}}\cdot\sum_{\ell=0}^{j} f_{i\ell}\cdot\frac{\Gamma\left(i+l-\frac{\lambda}{\alpha}+\frac{1}{2}\right)}{\Gamma\left(i+l-\frac{\lambda}{\alpha}+2\right)} & \begin{cases} i = k+1, k+2, \cdots, N \\ j = 0,1,\cdots,N \end{cases} \end{cases}$$

.....(32)

Proof:

a- Obviously, for $i = 0,1,2,\cdots,k$, we have $b_{ij} = 0$, now for $i > k$ approximate $x^{i\alpha-\lambda}$ by terms of fractional-order Chebyshev series, we get

$$x^{i\alpha-\lambda} \cong \sum_{j=0}^{N} g_{ij}\cdot\bar{T}_{i}^{\alpha}(x) \qquad (33)$$

By (23), we get

$$g_{ij} = \frac{4\cdot\alpha}{\pi\cdot c_i}\int_0^1 x^{i\alpha-\lambda}\cdot\bar{T}_{i}^{\alpha}(x)\cdot\frac{1}{x\cdot\sqrt{x^{-2\alpha}-1}}\,dx$$
$$= \frac{4\cdot\alpha}{\pi\cdot c_i}\int_0^1 x^{i\alpha-\lambda}\cdot\sum_{\ell=0}^{j} f_{j\ell}\cdot\frac{1}{x\cdot\sqrt{x^{-2\alpha}-1}}\,dx$$

where,

$$c_i = \begin{cases} 2 & i = 0 \\ 1 & i \geq 1 \end{cases}$$
$$= \frac{4\cdot\alpha}{\pi\cdot c_i}\cdot\sum_{\ell=0}^{j} f_{j\ell}\int_0^1 x^{i\alpha-\lambda}\cdot x^{\ell\alpha}\cdot\frac{1}{x\cdot\sqrt{x^{-2\alpha}-1}}\,dx$$
$$= \frac{4\cdot\alpha}{\pi\cdot c_i}\cdot\sum_{\ell=0}^{j} f_{j\ell}\int_0^1 x^{\alpha(i+\ell)-\lambda-1}\cdot\frac{1}{\sqrt{x^{-2\alpha}-1}}\,dx$$
$$= \frac{4\cdot\alpha}{\pi\cdot c_i}\sum_{\ell=0}^{j} f_{j\ell}\int_0^{\infty}\left(\frac{u^2}{1+u^2}\right)^{\frac{1}{2\alpha}[\alpha(i+l)-\lambda-1]}\cdot u\frac{u^{\frac{1}{\alpha}-1}}{\alpha(1+u^2)^{1+\frac{1}{2\alpha}}}\,du$$
$$= \frac{4}{\pi\cdot c_i}\cdot\sum_{\ell=0}^{j} f_{j\ell}\cdot\int_0^{\infty}\frac{(u)^{(i+\ell)-\frac{\lambda}{\alpha}}}{(1+u^2)^{\frac{1}{2}(i+\ell)-\lambda+1}}\,du$$
$$= \frac{2}{\pi\cdot c_i}\cdot\sum_{\ell=0}^{j} f_{j\ell}\int_0^{\infty}\frac{(t)^{\frac{1}{2}(i+\ell)-\frac{\lambda}{2\alpha}-\frac{1}{2}}}{(1+t)^{\frac{1}{2}(i+\ell)-\frac{\lambda}{2\alpha}+1}}\,dt$$
$$= \frac{2}{\pi\cdot c_i}\cdot\sum_{\ell=0}^{j} f_{j\ell}\cdot B\left(\frac{1}{2}(i+\ell)-\frac{\lambda}{2\alpha}+\frac{1}{2}\ ,\frac{1}{2}\right)$$

..... (34)

$$= \frac{2}{\pi\cdot c_i}\cdot\sum_{\ell=0}^{j} f_{j\ell}\frac{\Gamma\left(\frac{1}{2}(i+\ell)-\frac{\lambda}{2\alpha}+\frac{1}{2}\right)\Gamma\left(\frac{1}{2}\right)}{\Gamma\left(\frac{1}{2}(i+\ell)-\frac{\lambda}{2\alpha}+1\right)}$$

b- Obviously, for $i = 0,1,2,\cdots,k$, we have $h_{ij} = 0$, now for $i > k$ approximate $x^{i\alpha-\lambda}$ by $(N+1)$ terms of fractional-order Chebyshev series, we get

$$x^{i\alpha-\lambda} \cong \sum_{j=0}^{N} h_{ij}\cdot\bar{V}_{i}^{\alpha}(x)$$

..... (35)

by (24), we get

$$h_{ij} = \frac{2\cdot\alpha}{\pi}\int_0^1 x^{i\alpha-\lambda}\cdot V_{i}^{\alpha}(x)\cdot x^{\alpha-1}\sqrt{(x^{-\alpha}-1)^{-1}}\,dx$$
$$= \frac{2\cdot\alpha}{\pi}\int_0^1 x^{i\alpha-\lambda}\cdot\sum_{\ell=0}^{j} f_{i\ell}\cdot x^{\alpha-1}\sqrt{(x^{-\alpha}-1)^{-1}}\,dx$$
$$= \frac{2\cdot\alpha}{\pi}\cdot\sum_{\ell=0}^{j} f_{i\ell}\int_0^1 x^{i\alpha-\lambda}\cdot x^{l\alpha}\cdot x^{\alpha-1}\sqrt{(x^{-\alpha}-1)^{-1}}\,dx$$
$$= \frac{2\cdot\alpha}{\pi}\cdot\sum_{\ell=0}^{j} f_{i\ell}\int_0^1 x^{\alpha(i+l+1)-\lambda-1}\cdot\sqrt{(x^{-\alpha}-1)^{-1}}\,dx$$
$$= \frac{2\cdot\alpha}{\pi}\cdot\sum_{\ell=0}^{j} f_{i\ell}\int_0^1 G(x,i,\ell,\alpha,\lambda)$$

..... (36)

$$= \frac{2\cdot\alpha}{\pi}\ \frac{1}{\alpha}\sum_{\ell=0}^{j} f_{i\ell}\int_0^{\infty}\left[\left(\frac{u^2}{1+u^2}\right)^{\frac{1}{\alpha}}\right]^{\alpha(i+l+1)-\lambda-1}\cdot\frac{2u^2(1+u^2)-2u^4}{(1+u^2)^2}\cdot du$$
$$= \frac{4}{\pi}\cdot\sum_{\ell=0}^{j} f_{i\ell}\int_0^{\infty}\frac{(u^2)^{(i+l+1)-\frac{\lambda}{\alpha}-\frac{1}{\alpha}+2}}{(1+u^2)^{(i+l+1)-\frac{\lambda}{\alpha}-\frac{1}{\alpha}+2}}\cdot du$$

..... (37)

$$= \frac{2}{\pi} \cdot \sum_{\ell=0}^{j} f_{i\ell} \int_0^{\infty} \frac{(t)^{(i+l)-\frac{\lambda}{\alpha}-\frac{1}{\alpha}+\frac{5}{2}}}{(1+t)^{(i+l)-\frac{\lambda}{\alpha}-\frac{1}{\alpha}+3}} \cdot dt$$

$$= \frac{2}{\pi} \cdot \sum_{\ell=0}^{j} f_{i\ell} \cdot B\left((i+l)-\frac{\lambda}{\alpha}-\frac{1}{\alpha}+\frac{7}{2}\ ,-\frac{1}{2}\right)$$

$$= \frac{-4}{\sqrt{\pi}} \sum_{\ell=0}^{j} f_{i\ell} \cdot \frac{\Gamma\left((i+l)-\frac{\lambda}{\alpha}-\frac{1}{\alpha}+\frac{7}{2}\right)}{\Gamma\left((i+1)-\frac{\lambda}{\alpha}-\frac{1}{\alpha}+3\right)}$$

c- Obviously, for $i = 0,1,2,\cdots,k$, we have $r_{ij} = 0$, now for some $i > k$ approximate $x^{i\alpha-\lambda}$ by $(N+1)$ terms of fractional-order Chebyshev series, we get:

$$x^{i\alpha-\lambda} \cong \sum_{j=0}^{N} r_{ij} \cdot \overline{W}_i^{\alpha}(x)$$

..... (38)

by (25),we have

$$r_{ij} = \frac{2\cdot\alpha}{\pi} \int_0^1 x^{i\alpha-\lambda} \cdot \overline{W}_i^{\alpha}(x) \cdot x^{\alpha-1}\sqrt{x^{-\alpha}-1}\ dx$$

$$= \frac{2\cdot\alpha}{\pi} \int_0^1 x^{i\alpha-\lambda} \cdot \sum_{\ell=0}^{j} f_{i\ell} \cdot x^{\alpha-1}\sqrt{x^{-\alpha}-1}\ dx$$

$$= \frac{2\cdot\alpha}{\pi} \cdot \sum_{\ell=0}^{j} f_{i\ell} \int_0^1 x^{i\alpha-\lambda} \cdot x^{l\alpha} \cdot x^{\alpha-1}\sqrt{x^{-\alpha}-1}\ dx$$

$$= \frac{2\cdot\alpha}{\pi} \cdot \sum_{\ell=0}^{j} f_{i\ell} \int_0^1 x^{\alpha(i+l+1)-\lambda-1} \cdot \sqrt{x^{-\alpha}-1}\ dx$$

$$= \frac{2\cdot\alpha}{\pi} \cdot \sum_{\ell=0}^{j} \int_0^1 G(x,i,\ell,\alpha,\lambda)\ dx$$

..... (39)

$$= \frac{2\cdot\alpha}{\pi} \cdot \sum_{\ell=0}^{j} f_{i\ell} \int_{\infty}^{0} \left[\left(\frac{1}{1+u^2}\right)^{\frac{1}{\alpha}}\right]^{\alpha(i+l+1)-\lambda-1} \cdot u \cdot \frac{1}{\alpha}\left(\frac{1}{1+u^2}\right)^{\frac{1}{\alpha}-1} \cdot \frac{-2u}{(1+u^2)^2} du$$

$$= \frac{-4}{\pi} \cdot \sum_{\ell=0}^{j} f_{i\ell} \int_0^{\infty} \left(\frac{1}{1+u^2}\right)^{(i+l+1)-\frac{\lambda}{\alpha}-\frac{1}{\alpha}+\frac{1}{\alpha}-1} \cdot \frac{u^2}{(1+u^2)^2} \cdot du$$

$$= \frac{-4}{\pi} \cdot \sum_{\ell=0}^{j} f_{i\ell} \int_0^{\infty} \frac{u^2}{(1+u^2)^{i+l-\frac{\lambda}{\alpha}+2}} \cdot du$$

..... (40)

$$= \frac{-4}{\pi} \cdot \sum_{\ell=0}^{j} f_{i\ell} \int_0^{\infty} \frac{t}{(1+t)^{i+l-\frac{\lambda}{\alpha}+2}} \cdot \frac{1}{2}\, t^{-\frac{1}{2}}\, dt$$

$$= \frac{-2}{\pi} \cdot \sum_{\ell=0}^{j} f_{i\ell} \int_0^{\infty} \frac{t^{\frac{1}{2}}}{(1+t)^{i+l-\frac{\lambda}{\alpha}+2}} \cdot dt$$

..... (41)

$$= \frac{-2}{\pi} \cdot \sum_{\ell=0}^{j} f_{i\ell} \cdot B\left(\frac{3}{2}\ , i+l-\frac{\lambda}{\alpha}+\frac{1}{2}\right)$$

$$= \frac{-1}{\sqrt{\pi}} \cdot \sum_{\ell=0}^{j} f_{i\ell} \cdot \frac{\Gamma\left(i+l-\frac{\lambda}{\alpha}+\frac{1}{2}\right)}{\Gamma\left(i+l-\frac{\lambda}{\alpha}+2\right)}\ .$$

Theorem (6):

Let $\overline{T}_{\alpha}(x)$, $\overline{V}_{\alpha}(x)$ and $\overline{W}_{\alpha}(x)$ be fractional shifted Chebyshev vectors respectively, D^{λ} is the $(n+1)(n+1)$operational matrix of fractional derivative of order $\lambda > 0$ in caputo sense and $\alpha \in N_0$ or $\alpha > [\lambda]$ when $\alpha \notin N$ then:

a- $D^{\lambda} = F^{(1)}\bar{\Delta}^{\lambda} G\ \overline{T}_{\alpha}(x)$ for fractional order shifted Chebyshev polynomial of first kind

..... (42)

b- $D^{\lambda} = F^{(3)}\bar{\Delta}^{\lambda} H\ \overline{V}_{\alpha}(x)$ for fractional order shifted Chebyshev polynomial of third kind

..... (43)

c- $D^{\lambda} = F^{(4)}\bar{\Delta}^{\lambda} R\ \overline{W}_{\alpha}(x)$ for fractional order shifted Chebyshev polynomial of fourth kind

..... (44)

where,

$G = (g_{ij})$, $H = (h_{ij})$ *and* $R = (r_{ij})$, are given in theorem(5), and $\bar{\Delta}^{\lambda}$ is given in (29b)

Proof:

a- we can write λth order fractional derivative of $\overline{T}_{\alpha}(x)$ as

$$D^{\lambda}\overline{T}_{\alpha}(x) = F^{(1)}D^{\lambda}X_{\alpha}(x) = F^{(1)}\bar{\Delta}^{\lambda}X_{\alpha}^{\lambda}(x)$$
$$\cong F^{(1)}\bar{D}_{\lambda} \cdot G.\overline{T}_{\alpha}(x) = D^{(\lambda)} \cdot \overline{T}_{\alpha}(x)$$

b- we can write λth order fractional derivative of $\overline{V}_{\alpha}(x)$ as

$$D^{\lambda}\overline{V}_{\alpha}(x) = F^{(3)}D^{\lambda}X_{\alpha}(x) = F^{(3)}\bar{\Delta}^{\lambda}X_{\alpha}^{\lambda}(x)$$
$$\cong F^{(3)}\bar{D}_{\lambda} \cdot H.\overline{V}_{\alpha}(x) = D^{(\lambda)} \cdot \overline{V}_{\alpha}(x)$$

(c) have the same prove in (a)and(b).

Example (1):

Consider the following multi-fractional order nonlinear differential equation,

$$D^3\, u(x) + D^{\frac{5}{2}}\, u(x) + u^2(x) = x^4$$

..... (45)

with mixed boundary conditions,

$$u(0) = 0\ ,\ u^{(1)}(1) = 2\ ,\ u^{(2)}(1) = 2$$

..... (46)

To find the approximate solution with $m = 3$, $\alpha = 2$ the order of $\overline{T_{\alpha}}(x)$ polynomial, such that exact solution is $y(x) = x^2$.

By using (30) and lemma(3)with (42),we get

$$D^{\frac{5}{2}} \cong F^{(1)}.\bar{\Delta}^{\frac{5}{2}} \cdot G.\overline{T_2}(x)$$

..... (47)

also, from (23), we have

$$\overline{T_{\alpha}}(x) = F^{(1)}X_2$$

$$\begin{bmatrix} 1 \\ 2x^{\alpha}-1 \\ 8x^{2\alpha}-8x^{\alpha}+1 \\ 32x^{3\alpha}-48x^{2\alpha}+18x^{\alpha}-1 \end{bmatrix} = \begin{bmatrix} 1 & 0 & 0 & 0 \\ -1 & 2 & 0 & 0 \\ 1 & -8 & 8 & 0 \\ -1 & 18 & -48 & 32 \end{bmatrix} \begin{bmatrix} 1 \\ x^2 \\ x^4 \\ x^6 \end{bmatrix}$$

$$F^{(1)} = \begin{bmatrix} 1 & 0 & 0 & 0 \\ -1 & 2 & 0 & 0 \\ 1 & -8 & 8 & 0 \\ -1 & 18 & -48 & 32 \end{bmatrix}$$

..... (48a)

From (30), we have

$$G = \begin{bmatrix} 0 & 0 & 0 & 0 \\ 0 & 0 & 0 & 0 \\ 1.383 & 0.721 & 0.0088 & -0.01 \\ 1.052 & 0.708 & 0.182 & -0.0017 \end{bmatrix}$$

..... (48b)

From (29b), N=3, k=1 , $\alpha = 2$ and $= \frac{5}{2}$, we have

$$\bar{\Delta}^{\frac{5}{2}}=\begin{bmatrix}0&0&0&0\\0&0&0&0\\0&0&\frac{\Gamma((k+1)\alpha+1)}{\Gamma((k+1)\alpha+1-\lambda)}&0\\0&0&0&\frac{\Gamma(N\alpha+1)}{\Gamma(N\alpha+1-\lambda)}\end{bmatrix}=$$

$$\begin{bmatrix}0&0&0&0\\0&0&0&0\\0&0&18.054&0\\0&0&0&61.9\end{bmatrix} \quad \dots\dots(48c)$$

by substituting (48)(a),(b)and(c) in (47), we get

$$D^{\frac{5}{2}}=F^{(1)}.\bar{\Delta}^{\frac{5}{2}}\cdot G.\bar{T}_2(x)=$$

$$\begin{bmatrix}0&0&0&0\\0&0&0&0\\199.7501&351.6932&478.7938&590.2957\\8652888&1716.7250&2483.2904&3190.9273\end{bmatrix}$$

$$\cdot\begin{bmatrix}1\\2x^2-1\\8x^4-8x^2+1\\32x^6-48x^4+18x^2-1\end{bmatrix} \quad \dots\dots(49)$$

by using the first root of $x^{\alpha}=\frac{1}{2}$ of the polynomial $T^{\alpha}_{m+1-\lambda}(x)$, substituting this root in (45), we get

$-143.2792\,C_2-1862.4595\,C_3+(C_0-C_2)^2=0.25$

..... (50)

From (46), we obtain

$u(0)=C_0-C_1+C_2-C_3=0$

..... (51a)

$u^{(1)}(1)=4\,C_1+16\,C_2+36C_3=2$

..... (51b)

$u^{(2)}(1)=4C_1-80\,C_2-444C_3=2$

..... (51c)

From (50), (51)(a),(b)and(c), we obtain

$C_0=0.5000\ ,C_1=0.5000\ ,C_2=\ C_3=0$.

Then, the approximate solution is

$y(x)=0.5000+0.5000(2x^2-1)+0=0.5000+x^2-0.5000=x^2$

Example(2):

Consider the following multi-fractional order nonlinear differential equation,

$D^4u(x)+D^{\frac{7}{2}}u(x)+u^{(3)}(x)=x^9$

..... (52)

with mixed boundary conditions,

$u(0)=0\ ,\ u^{(1)}(1)=3\ ,\ u^{(2)}(1)=6\ ,\ \ u^{(3)}(1)=6$

..... (53)

To find the approximate solution with $m=4\ ,\alpha=3$ the order of fractional shifted Chebyshev polynomial of third kind such that the exact solution is $y(x)=x^3$.

By using equation (31) and lemma(3)with (43), we have

$D^{\frac{7}{2}}\cong F^{(3)}.\bar{\Delta}^{\frac{7}{2}}\cdot H.\bar{V}_3(x)$

..... (54)

also, from (24), we get

$\bar{V}_{\alpha}(x)=F^{(3)}X_3$

$$\begin{bmatrix}1\\4x^{\alpha}-3\\16x^{2\alpha}-20x^{\alpha}+5\\64\,x^{3\alpha}-112\,x^{2\alpha}+56x^{\alpha}-7\\256\,x^{4\alpha}-576\,x^{3\alpha}+432\,x^{2\alpha}-120x^{\alpha}+9\end{bmatrix}$$

$$=\begin{bmatrix}1&0&0&0&0\\-3&4&0&0&0\\5&-20&16&0&0\\-7&56&-112&64&0\\9&-120&432&-576&256\end{bmatrix}\begin{bmatrix}1\\x^3\\x^6\\x^9\\x^{12}\end{bmatrix}$$

$$F=\begin{bmatrix}1&0&0&0&0\\-3&4&0&0&0\\5&-20&16&0&0\\-7&56&-112&64&0\\9&-120&432&-576&256\end{bmatrix}$$

..... (55a)

by (31), we obtain

$R=$

$$\begin{bmatrix}0&0&0&0&0\\0&0&0&0&0\\-4.074&-6.403&-10.024&-13.999&-18\\-4.656&-6.726&-10.112&-14.005&-18\\-5.174&-7.055&-10.239&-14.031&-18.001\end{bmatrix}$$

..... (55b)

from (29b), N=4, k=1 , $\alpha=3$, and $\lambda=\frac{7}{2}$, we get

$\bar{\Delta}^{\frac{7}{2}}=$

$$\begin{bmatrix}0&0&0&0&0\\0&0&0&0&0\\0&0&\frac{\Gamma((k+1)\alpha+1)}{\Gamma((k+1)\alpha+1-\lambda)}&0&0\\0&0&0&\frac{\Gamma((k+2)\alpha+1)}{\Gamma((k+2)\alpha+1-\lambda)}&0\\0&0&0&0&\frac{\Gamma(N\alpha+1)}{\Gamma(N\alpha+1-\lambda)}\end{bmatrix}=$$

$$\begin{bmatrix}0&0&0&0&0\\0&0&0&0&0\\0&0&770.5041&0&0\\0&0&0&1261&0\\0&0&0&0&4015\end{bmatrix}$$

.....(55c)

by substituting (55)(a),(b)and(c)in (54), we get

$D^{\frac{7}{2}}\cong F^{(3)}.\bar{\Delta}^{\frac{7}{2}}\cdot H.\bar{V}_3(x)=$

$$\begin{bmatrix}0&0&0&0&0\\0&0&0&0&0\\-50224.5391&-107636.3407&-171421.7521&-241001.3544&-315991.5371\\-241560.492&-59863.9347&-68861.4308&-52405.8310&-51097.9640\\-5.2922\times10^{5}&-6.8854\times10^{4}&-1.0755\times10^{7}&-1.4883\times10^{7}&-1.9253\times10^{7}\end{bmatrix}$$

$$\cdot\begin{bmatrix}1\\4x^{\alpha}-3\\16x^{2\alpha}-20x^{\alpha}+5\\64\,x^{3\alpha}-112\,x^{2\alpha}+56x^{\alpha}-7\\256\,x^{4\alpha}-576\,x^{3\alpha}+432\,x^{2\alpha}-120x^{\alpha}+9\end{bmatrix} \quad \dots\dots(56)$$

from using the first root of $x^{\alpha}=\frac{3}{4}$ of the polynomial $V^{\alpha}_{m+1-\lambda}(x)$, substituting this root in (52), we get

$125956.5914c_2+163874.1185c_3+23052154.51c_4+(c_0-c_2-c_3)^3=0.4218$ ....(57)

From (53), we obtain

$c_0 - 3\,c_1 + 5\,c_2 - 7\,c_3 + 9\,c_4 = 0$

..... (58a)

$12\,c_1 + 36\,c_2 + 72\,c_3 - 510\,c_4 = 3$

..... (58b)

$24\,c_1 + 360\,c_2 + 1584\,c_3 + 4560\,c_4 = 6$

..... (58c)

$24\,c_1 + 1800\,c_2 + 19152\,c_3 + 98736\,c_4 = 6$

..... (58d)

By (57), (58)(a),(b),(c)and(d), we get

$c_0 = 0.7500\,, c_1 = 0.2500\,, c_2 = c_3 = c_4 = 0\,.$

Then, the approximate solution is

$y(x) = 0.7500 + 0.2500(4\,x^3 - 3) + 0$

$= 0.7500 + x^3 - 0.7500 = x^3\,.$

Table (1)

x	Approximate solution with $\alpha = 1.5$	Approximate solution with $\alpha = 2.5$	Approximate solution with $\alpha = 3$	Exact solution
0.1	-0.0002452	0.013	0.001	0.001
0.2	0.002415	0.032	0.008	0.008
0.3	0.014	0.073	0.027	0.027
0.4	0.04	0.138	0.064	0.064
0.5	0.086	0.232	0.125	0.125
0.6	0.159	0.354	0.216	0.216
0.7	0.266	0.507	0.343	0.343
0.8	0.414	0.692	0.512	0.512
0.9	0.609	0.913	0.729	0.729

Example(3):

Consider the following multi-fractional order nonlinear differential equation,

$D^5 u(x) + D^{\frac{9}{2}} u(x) + u^4(x) = x^{16}$

..... (59)

with mixed boundary condition,

$u(0) = 0\,,\ u^{(1)}(1) = 4\,,\ u^{(2)}(1) = 12\,,\ u^{(3)}(1) = 24,\ u^{(4)}(0) = 24$ ... (60)

To find the approximate solution with $m = 5\,,\ \alpha = 4$ the order of fractional shifted Chebyshev of fourth kind such that the exact solution is $(x) = x^4$.

By using (32)and lemma(3)with (44), we obtain

$D^{\frac{9}{2}} \cong F^{(4)}.\bar{\Delta}^{\frac{9}{2}} \cdot R.\overline{W_4}(x)$

..... (61)

by (25), we obtain

$\overline{W_\alpha}(x) = F^{(4)} X_4$

$$\begin{bmatrix} 1 \\ 2x^{\alpha}+1 \\ 8x^{2\alpha}-3 \\ 32x^{3\alpha}-16x^{2\alpha}-14x^{\alpha}+5 \\ 128x^{4\alpha}-128x^{3\alpha}-32x^{2\alpha}+48x^{\alpha}-7 \\ 512x^{5\alpha}-768x^{4\alpha}+96x^{3\alpha}+272x^{2\alpha}-110x^{\alpha}+9 \end{bmatrix} =$$

$$\begin{bmatrix} 1 & 0 & 0 & 0 & 0 & 0 \\ 1 & 2 & 0 & 0 & 0 & 0 \\ -3 & 0 & 8 & 0 & 0 & 0 \\ 5 & -14 & -16 & 32 & 0 & 0 \\ -7 & 48 & -32 & -128 & 128 & 0 \\ 9 & -110 & 272 & 96 & -768 & 512 \end{bmatrix} \begin{bmatrix} 1 \\ x^4 \\ x^8 \\ x^{12} \\ x^{16} \\ x^{20} \end{bmatrix}$$

$F^{(4)} =$

$$\begin{bmatrix} 1 & 0 & 0 & 0 & 0 & 0 \\ 1 & 2 & 0 & 0 & 0 & 0 \\ -3 & 0 & 8 & 0 & 0 & 0 \\ 5 & -14 & -16 & 32 & 0 & 0 \\ -7 & 48 & -32 & -128 & 128 & 0 \\ 9 & -110 & 272 & 96 & -768 & 512 \end{bmatrix}$$

.....(62a)

From (32), we have

$$H = \begin{bmatrix} 0 & 0 & 0 & 0 & 0 & 0 \\ 0 & 0 & 0 & 0 & 0 & 0 \\ -0.281 & -0.549 & 0.184 & -0.03 & 0.016 & -0.0098 \\ -0.134 & -0.299 & -0.053 & 0.035 & -0.0022 & 0.00070 \\ -0.082 & -0.196 & -0.092 & 0.0035 & 0.0077 & -0.0002 \\ -0.057 & -0.142 & -0.094 & -0.019 & 0.0046 & 0.0018 \end{bmatrix}$$

.....(62b)

From (29b), N=5 , k=1 , $\alpha = 4$, and $\lambda = \frac{9}{2}$, we get

$$\bar{\Delta}^{\frac{9}{2}} = \begin{bmatrix} 0 & 0 & 0 & 0 & 0 & 0 \\ 0 & 0 & 0 & 0 & 0 & 0 \\ 0 & 0 & \frac{\Gamma(1k+1)\alpha+1)}{\Gamma(1k+1)\alpha+1-\lambda)} & 0 & 0 & 0 \\ 0 & 0 & 0 & \frac{\Gamma((k+2)\alpha+1)}{\Gamma((k+2)\alpha+1-\lambda)} & 0 & 0 \\ 0 & 0 & 0 & 0 & \frac{\Gamma((k+3)\alpha+1)}{\Gamma((k+3)\alpha+1-\lambda)} & 0 \\ 0 & 0 & 0 & 0 & 0 & \frac{\Gamma(N\alpha+1)}{\Gamma(N\alpha+1-\lambda)} \end{bmatrix}$$

$$= \begin{bmatrix} 0 & 0 & 0 & 0 & 0 & 0 \\ 0 & 0 & 0 & 0 & 0 & 0 \\ 0 & 0 & 3.44\times10^{3} & 0 & 0 & 0 \\ 0 & 0 & 0 & 3.413\times10^{4} & 0 & 0 \\ 0 & 0 & 0 & 0 & 1.529\times10^{5} & 0 \\ 0 & 0 & 0 & 0 & 0 & 4688\times10^{5} \end{bmatrix}$$

.....(62c)

by substituting (62)(a),(b)and(c)in (61), we obtain

$$D^{\frac{9}{2}} \cong F^{(4)}.\bar{\Delta}^{\frac{9}{2}} \cdot R.\overline{W_4}(x) =$$

$$\begin{bmatrix} 0 & 0 & 0 & 0 & 0 & 0 \\ 0 & 0 & 0 & 0 & 0 & 0 \\ -7.792\times10^{4} & -1.822\times10^{5} & 5.102\times10^{5} & -851.84 & 448.048 & -271.734 \\ -1.308\times10^{5} & -2.961\times10^{5} & -6.509\times10^{4} & 3.989\times10^{5} & -5.29\times10^{4} & 1.308\times10^{5} \\ -9.855\times10^{4} & -2.469\times10^{5} & -1.589\times10^{6} & -8.108\times10^{5} & 1.585\times10^{5} & -5.865\times10^{4} \\ -4.756\times10^{4} & -1.257\times10^{5} & -1.176\times10^{6} & -4.885\times10^{5} & 2.078\times10^{5} & 4.486\times10^{4} \end{bmatrix}$$

$$\begin{bmatrix} 1 \\ 2x^{4}+1 \\ 8x^{8}-3 \\ 32x^{12}-16x^{8}-14x^{4}+5 \\ 128x^{16}-128x^{12}-32x^{8}+48x^{4}-7 \\ 512x^{20}-768x^{16}+96x^{12}+272x^{8}-110x^{4}+9 \end{bmatrix}$$

.....(63)

from using the first root of $x^{\alpha} = \frac{1}{4}$ of the polynomial $W^{\alpha}_{m+1-\lambda}(x)$, substituting this root in (59), we obtain

$-9793.1183\,c_2 + 105638.4983\,c_3 + 2210690\,c_4 + 7550000\,c_5 + (c_0 + 2c_1 - c_2 - 2c_3 + c_4 + 2c_5)^4 = 0.0625$ .....(64)

By (60), we get

$c_0 + c_1 - 3\,c_2 + 5\,c_3 - 7\,c_4 + 9\,c_5 = 0$

..... (65a)

$8\,c_1 + 64\,c_2 + 200\,c_3 + 448\,c_4 + 840\,c_5 = 4$

..... (65b)

$24\,c_1 + 448\,c_2 + 3160\,c_3 + 12608\,c_4 + 36824\,c_5 = 12$ ..... (65c)

$48c_1 + 2688c_2 + 36528c_3 + 251520c_4 + 1137072c_5 = 24$ ..... (65d)

$48\,c_1 + 13440\,c_2 - 336\,c_3 + 1152\,c_4 - 2640\,c_5 = 24$

..... (65e)

From (64), (65)(a),(b),(c),(d)and(e), we have

$c_0 = -0.5000\,,\ c_1 = 0.5000\,,\ c_2 = c_3 = c_4 = c_5 = 0$

Then, the approximate solution is

$y(x) = -0.5000 + 0.5000(2\,x^4 + 1) + 0$

$= -0.5000 + x^4 + 0.5000 = x^4$

CONCLUSIONS

The fractional operational matrices of fractional derivative of some types of fractional chebyshev polynomial depending on value of the orders have been given to supported the mixed boundary values multi-fractional nonlinear order to obtain the best numerical or exact solution some time.

REFERENCES

1. Bhrawy A.H. and Alofi A.S.,"The Operational Matrix of Fractional Integration for Shifted chebyshev Polynomials",Applied mathematics letters, Vol.26, No.1, PP. 25-131 ,(2013) .
2. Kazem S., Abbasbandy S. and Kumar S., "Fractional-Order Legendre Functions for Solving Fractional Order Differential Equations", Applied mathematical modeling, in press, http://dx.doi.org/10.1016/j.apm.2012.10.026.
3. Kazemi Nasab A., Kilicman A., Pashazadeh Atabakan Z. and Abbasbandy S., "Chebyshev Wavelet Finite Difference Method : a New Approach for Solving Initial and Boundary Value Problems of Fractional Order", hindawi publishing corporation, abstract and applied analysis, Vol.2013, Articale id 916456, 15 Pages, 2013
4. Khader M.M., "Numerical Solution of Nonlinear Multi-Order Fractional Differential Equations by Implementation of the Operational Matrix of Fractional Derivative", studies in nonlinear sciences, PP.05-12, ISSN: 2221-3910, 2011.
5. Lakestani X., Dehghan M., Irandoust-packchia, " The Construction of Operational Matrix Fractional Derivatives Using B-Spline Functions", commun nonlinear sei numer simelat, 17(2012) 1149-1162.
6. Mohammadreza Ahmadi Darani and Mitra Nasiri, "A fractional Type of Chebyshev Polynomials for Approximation of Solution of Linear Fractional Differential Equations Computational Methods for Differential Equations", Vol.1, No.2, PP:96-107, 2013.
7. Saadatmandi A., Dehghan M., "A new Operational Matrix for Solving Fractional-Order Differential Equations", comput. Math. Appl., 59(2010), 1326-1336.
8. Yang S., Xiao A. and Su H., "Conergence of the Variational Iterational Method for Solving Multi-Order Fractional Differential Equations", computer and mathematics with applications ,Vol.60, No.10, 2010, PP.2817-2879.

Al-Mustansiriyah Journal of Science
Vol. 27, No 2, 2016

journal homepage:www.mjs-mu.com

PROPERTIES OF SOME FAMILIES OF MEROMORPHIC MULTIVALENT FUNCTIONS WITH POSITIVE COEFFICIENTS INVOLVING CERTAIN LINEAR OPERATOR

Abdul Rahman S. Juma[1] and Husamaldin I. Dhayea[2]
DEPARTMENT OF MATHEMATICS, ALANBAR UNIVERSITY, RAMADI – IRAQ [1]
DEPARTMENT OF MATHEMATICS, TIKRIT UNIVERSITY, TIKRIT – IRAQ

Articleinfo

Received
20/5/2015
Accepted
16/11/2016

KEYWORDS:
Linear operator, Meromorphic, Positive coefficients, Hadamard product.

ABSTRACT

Making use of a linear operator, which is defined here by means of the Hadamard product (or convolution), we introduce two novel subclasses $M_{a,c,\lambda}[p,A,B,\lambda]$ and $\sum^{*}_{p,a,c,\lambda}[\lambda,\beta]$ of meromorphically multivalent functions. In this paper, we obtain coefficient estimates, distortion theorems, radii of starlikeness and convexity and partial sums for the class $M_{a,c,\lambda}[p,A,B,\lambda]$. We also derive many interesting results for the Hadamard products of functions belonging to the class $M_{a,c,\lambda}[p,A,B,\lambda]$.

INTRODUCTION

Let Σ_p denote the class of functions of the form:

$$f(z)=\frac{1}{z^p}+\sum_{n=0}^{\infty}a_{p+n}\,z^{p+n},\quad (a_{p+n}\geq 0, p\in\mathbb{N}), \tag{1}$$

which are meromorphic p-valent in the punctured unit disk $\Delta^{*}=\{z\in\mathbb{C}:0<|z|<1\}=\Delta\backslash\{0\}$; where $\Delta=\{z\in\mathbb{C}:|z|<1\}$.

Let $f,g\in\Sigma_p$, where f is given by (1) and g is defined by

$$g(z)=\frac{1}{z^p}+\sum_{n=0}^{\infty}b_{p+n}\,z^{p+n},\ (b_{p+n}\geq 0, p\in\mathbb{N}).$$

Then the Hadamard product (or convolution) $f*g$ is defined by

$$(f*g)(z)=\frac{1}{z^p}+\sum_{n=p}^{\infty}a_n b_n z^n=(g*f)(z).$$

Liu [12] and Liu and Srivastava [14] have introduced a linear operator $\hbar_p(a,c)$ is defined as follows

$$\hbar_p(a,c)f(z)=\mathcal{A}(a,c;z)*f(z),\quad f\in\Sigma_p \tag{2}$$

where $\mathcal{A}(a,c;z)$ is defined by

$$\mathcal{A}(a,c;z)=\frac{1}{z^p}+\sum_{n=0}^{\infty}\frac{(a)_{n+1}}{(c)_{n+1}}z^{p+n}, \tag{3}$$

$(z\in\Delta^{*};a\in\mathbb{R};c\in\mathbb{R}-\mathbb{Z}_0^{-};\mathbb{Z}_0^{-}=\{0,-1,-2,\ldots\})$ and $(\theta)_n$ is the Pochhammer symbol defined by

$$(\theta)_n=\frac{\Gamma(\theta+n)}{\Gamma(\theta)}=\begin{cases}1 & (n=0),\\ \theta(\theta+1)(\theta+2)\ldots(\theta+n-1), & (n\in\mathbb{N};\theta\in\mathbb{C}).\end{cases}$$

It is easily verified from the definitions (2) and (3) that

$$z\big(\hbar_p(a,c)f(z)\big)'=a\hbar_p(a+1,c)f(z)-(a+p)\hbar_p(a,c)f(z).$$ (cf. [8], [9])

We also note, for any integer $m>-p$ and for $f(z)\in\Sigma_p$, that

$$\hbar_p(n+p,1)f(z)=D^{m+p-1}f(z)=\frac{1}{z^p(1-z)^{m+p}}*f(z),$$

where $D^{m+p-1}f(z)$ is the differential operator studied by (among others) Uralegaddi and Somanatha [23] and Aouf [6].

Further M. K. Aouf et. al. [7] considered the generalized operators as follows:

Let

$$F_{p,a,c,\lambda}(z) = (1-\lambda)\hbar_p(a,c)f(z) + \frac{\lambda}{p}z\left(\hbar_p(a,c)f(z)\right)', \quad \left(f \in \Sigma_p; p \in \mathbb{N}; 0 \le \lambda < \tfrac{1}{2}\right)$$

$$= \frac{1}{z^p} + \sum_{n=0}^{\infty}\frac{(a)_{n+1}}{(c)_{n+1}}a_{p+n}z^{p+n} - \frac{\lambda}{z^p} - \sum_{n=0}^{\infty}\lambda\frac{(a)_{n+1}}{(c)_{n+1}}a_{p+n}z^{p+n} + \frac{-p\lambda}{pz^p} + \sum_{n=0}^{\infty}\frac{(p+n)\lambda}{p}\frac{(a)_{n+1}}{(c)_{n+1}}a_{p+n}z^{p+n}$$

$$= \frac{1-2\lambda}{z^p} + \sum_{n=0}^{\infty}\left[1-\lambda+\frac{\lambda p}{p} + \frac{\lambda n}{p}\right]\frac{(a)_{n+1}}{(c)_{n+1}}a_{p+n}z^{p+n}$$

$$F_{p,a,c,\lambda}(z) = \frac{1-2\lambda}{z^p} + \sum_{n=0}^{\infty}\left[1 + \lambda\left(\frac{n}{p}\right)\right]\frac{(a)_{n+1}}{(c)_{n+1}}a_{p+n}z^{p+n} \quad \left(p \in \mathbb{N}; 0 \le \lambda < \tfrac{1}{2}\right), \qquad (4)$$

since $f(z) \in \Sigma_p$ is given by (1). See A. R. S. Juma and Hazha Zirar [12]. From (4), it is easily verified that

$$zF'_{p,a,c,\lambda}(z) = \frac{-p}{z^p} + \sum_{n=0}^{\infty}(p+n)\left[1 + \lambda\left(\frac{n}{p}\right)\right]\frac{(a)_{n+1}}{(c)_{n+1}}a_{p+n}z^{p+n}$$

$$= \frac{-p}{z^p} + \sum_{n=0}^{\infty}p\left[1+\lambda\left(\frac{n}{p}\right)\right]\frac{(a)_{n+1}}{(c)_{n+1}}a_{p+n}z^{p+n} + n\left[1+\lambda\left(\frac{n}{p}\right)\right]\frac{(a)_{n+1}}{(c)_{n+1}}a_{p+n}z^{p+n}$$

$$= \frac{-p}{z^p} + p\sum_{n=0}^{\infty}\left[1+\lambda\left(\frac{n}{p}\right)\right]\frac{(a)_{n+1}}{(c)_{n+1}}a_{p+n}z^{p+n} + \sum_{n=0}^{\infty}n\left[1+\lambda\left(\frac{n}{p}\right)\right]\frac{(a)_{n+1}}{(c)_{n+1}}a_{p+n}z^{p+n}$$

$$= \frac{a}{z^p} + \sum_{n=0}^{\infty}\left[1+\lambda\left(\frac{n}{p}\right)\right]\frac{(a)_{n+1}}{(c)_{n+1}}a_{p+n}z^{p+n} - \frac{a}{z^p} - \sum_{n=0}^{\infty}a\left[1+\lambda\left(\frac{n}{p}\right)\right]\frac{(a)_{n+1}}{(c)_{n+1}}a_{p+n}z^{p+n} - \frac{p}{z^p} - p\sum_{n=0}^{\infty}\left[1+\lambda\left(\frac{n}{p}\right)\right]\frac{(a)_{n+1}}{(c)_{n+1}}a_{p+n}z^{p+n}$$

$$= \frac{a}{z^p} + \sum_{n=0}^{\infty}a\left[1+\lambda\left(\frac{n}{p}\right)\right]\frac{(a+1)_{n+1}}{(c)_{n+1}}a_{p+n}z^{p+n} - (a+p)\left(\frac{1}{z^p} + \sum_{n=0}^{\infty}\left[1+\lambda\left(\frac{n}{p}\right)\right]\frac{(a+1)_{n+1}}{(c)_{n+1}}a_{p+n}z^{p+n}\right)$$

$$= aF_{p,a+1,c,\lambda}(z) - (a+p)F_{p,a,c,\lambda}(z).$$

We say that a function $f(z) \in \Sigma_p$ is in the class $M_{a,c,\lambda}[p,A,B,\lambda]$ if it satisfies the following inequality:

$$\left|\frac{z^{p+1}F'_{p,a,c,\lambda}(z) + p(1-2\lambda)}{Bz^{p+1}F'_{p,a,c,\lambda}(z) + Ap(1-2\lambda)}\right| < 1 \quad (z \in \Delta^*), \qquad (5)$$

where the parameters A, B, p and λ are constrained as follows:
$-1 \le B < A \le 1, A + B \ge 0, p \in \mathbb{N}$ and $0 \le \lambda < \frac{1}{2}$.

We observe also that:

(1) $M_{a,c,\lambda}[p,-\beta,\beta,\lambda] = \Sigma^*_{p,a,c,\lambda}[\lambda,\beta] = \left\{f(z) \in \Sigma^*_p : \left|\frac{z^{p+1}F'_{p,a,c,\lambda}(z)+p(1-2\lambda)}{z^{p+1}F'_{p,a,c,\lambda}(z)-p(1-2\lambda)}\right| < \beta, p \in \mathbb{N}, 0 \le \lambda < \frac{1}{2}, 0 < \beta \le 1, z \in \Delta^*\right\}$.

(2) $M_{a,c,0}[p,-\beta,\beta,0] = \Sigma^*_{p,a,c}[\beta] = \left\{f(z) \in \Sigma^*_p : \left|\frac{z^{p+1}\left(\hbar_p(a,c)f(z)\right)'+p}{z^{p+1}\left(\hbar_p(a,c)f(z)\right)'-p}\right| < \beta, p \in \mathbb{N}, 0 < \beta \le 1, z \in \Delta^*\right\}$.

(3) $M_{a,a,0}[p,-\beta,\beta,0] = \Sigma^*_p[\beta] = \left\{f(z) \in \Sigma^*_p : \left|\frac{z^{p+1}f'(z)+p}{z^{p+1}f'(z)-p}\right| < \beta, p \in \mathbb{N}, 0 < \beta \le 1, z \in \Delta^*\right\}$.

Meromorphically multivalent functions have been extensively studied in a variety by Mogra [15, 16], Uralegaddi and Ganigi [22], Aouf [4, 5], Srivastava et al. [21], Owa et al. [17], Joshi and Srivastava [11], Liu [13], Liu and Srivastava [14], Aouf et al. [8], Raina and Srivastava [18] and Yang [24].

In this paper, we investigate various important properties and characteristics of the class $M_{a,c,\lambda}[A,B,\lambda]$, we obtain coefficient estimates, distortion theorems, radii of starlikeness and convexity and M. K. Aouf et al. [9] extend the concept of neighborhoods of analytic functions belonging to the class $M_{a,c,\lambda}[p,A,B,\lambda]$, are also derived.

2. Coefficient Inequality

We first mention a sufficient condition for a function to belong to the class $M_{a,c,\lambda}[p,A,B,\lambda]$.

Theorem 1. *Let $f \in \Sigma_p$ given by (1). Then $f \in M_{a,c,\lambda}[p,A,B,\lambda]$, if and only if*

$$\sum_{n=0}^{\infty}(p+n)\left[1+\lambda\left(\frac{n}{p}\right)\right](1-B)\frac{(a)_{n+1}}{(c)_{n+1}}a_{p+n} \leq (A-B)p(1-2\lambda), \quad (6)$$

Where
$-1 \leq B < A \leq 1, A+B \geq 0, p \in \mathbb{N}$ *and* $0 \leq \lambda < \frac{1}{2}$.

Proof.
Let $f(z) \in M_{a,c,\lambda}[p,A,B,\lambda]$. Then by (5), we have

$$\left|\frac{z^{p+1}F'_{p,a,c,\lambda}(z)+p(1-2\lambda)}{Bz^{p+1}F'_{p,a,c,\lambda}(z)+Ap(1-2\lambda)}\right| = \left|\frac{\sum_{n=0}^{\infty}(p+n)\left[1+\lambda\left(\frac{n}{p}\right)\right]\frac{(a)_{n+1}}{(c)_{n+1}}a_{p+n}z^{p+n}}{(A-B)p(1-2\lambda)+\sum_{n=0}^{\infty}B(p+n)\left[1+\lambda\left(\frac{n}{p}\right)\right]\frac{(a)_{n+1}}{(c)_{n+1}}a_{p+n}z^{p+n}}\right| < 1 \quad (z \in \Delta^*).$$

Since $\Re(z) \leq |z|$ $(z \in \mathbb{C})$, we have

$$\Re\left\{\frac{\sum_{n=0}^{\infty}(p+n)\left[1+\lambda\left(\frac{n}{p}\right)\right]\frac{(a)_{n+1}}{(c)_{n+1}}a_{p+n}z^{p+n}}{(A-B)p(1-2\lambda)+\sum_{n=0}^{\infty}B(p+n)\left[1+\lambda\left(\frac{n}{p}\right)\right]\frac{(a)_{n+1}}{(c)_{n+1}}a_{p+n}z^{p+n}}\right\} < 1. \quad (7)$$

Choose values of z on the real axis so that $z^{p+1}F'_{p,a,c,\lambda}(z)$ is real. Upon clearing the denominator in (7) and letting $z \to 1^-$ through real values, we obtain (6).

Conversely, we assume that the inequality (6) holds true. Then, if we let $z \in \partial\Delta$ $(z \in \partial\Delta = \{z \in \mathbb{C} \text{ and } |z| = 1\})$, we find from (1) and (6) that

$$\left|\frac{z^{p+1}F'_{p,a,c,\lambda}(z)+p(1-2\lambda)}{Bz^{p+1}F'_{p,a,c,\lambda}(z)+Ap(1-2\lambda)}\right| \leq \frac{\sum_{n=0}^{\infty}(p+n)\left[1+\lambda\left(\frac{n}{p}\right)\right]\frac{(a)_{n+1}}{(c)_{n+1}}a_{p+n}z^{p+n}}{(A-B)p(1-2\lambda)+\sum_{n=0}^{\infty}B(p+n)\left[1+\lambda\left(\frac{n}{p}\right)\right]\frac{(a)_{n+1}}{(c)_{n+1}}a_{p+n}z^{p+n}} < 1 \quad (z \in \partial\Delta = \{z \in C \text{ and } |z| = 1\}).$$

Hence, by the maximum modulus theorem, we have $f(z) \in M_{a,c,\lambda}[p,A,B,\lambda]$.
The proof is complete. ■

Corollary 1. *Let the function $f(z)$ defined by (1) be in the class $M_{a,c,\lambda}[p,A,B,\lambda]$. Then*

$$a_{p+n} \leq \frac{(A-B)p(1-2\lambda)}{(p+n)\left[1+\lambda\left(\frac{n}{p}\right)\right](1-B)} \cdot \frac{(c)_{n+1}}{(a)_{n+1}} \quad (n \geq 0),$$

The result is sharp for the function:

$$f(z) = z^{-p} + \frac{(A-B)p(1-2\lambda)}{(p+n)\left[1+\lambda\left(\frac{n}{p}\right)\right](1-B)} \cdot \frac{(c)_{n+1}}{(a)_{n+1}} \cdot z^{p+n} \quad (n \geq 0). \quad (8)$$

Putting $A = \left(1-2\gamma\frac{\alpha}{p}\right)\beta$ and $B = (1-2\gamma)\beta$ $\left(0 \leq \alpha < p, 0 < \beta \leq 1, \frac{1}{2} \leq \gamma \leq 1 \text{ and } p \in \mathbb{N}\right)$ in Theorem 1, we obtain

Corollary 2. *A function $f(z)$ defined by (1) be in the class $M_{a,c,\lambda}[\alpha,\beta,\gamma,\lambda]$ if and only if*

$$\sum_{n=0}^{\infty}(p+n)\left[1+\lambda\left(\frac{n}{p}\right)\right](1+2\beta\gamma-\beta)\frac{(a)_{n+1}}{(c)_{n+1}}a_{p+n} \leq 2\beta\gamma(p-\alpha)(1-2\lambda).$$

Putting $\lambda = 0$ and $a = c$ in Corollary 2, see [12], we obtain:

Corollary 3. *A function $f(z)$ defined by (1) be in the class $\sum_p^*[\beta]$ if and only if*

$$\sum_{n=0}^{\infty}(p+n)(1+2\beta\gamma-\beta)a_{p+n} \leq 2\beta\gamma(p-a).$$

3. Growth and Distortion Theorems

Next we prove the following growth and distortion properties for the class $M_{a,c,\lambda}[p,A,B,\lambda]$.

Theorem 2. *If the function $f(z)$ defined by (1) is in the class $M_{a,c,\lambda}[p,A,B,\lambda]$. and the sequence $\{C_n\} = \left\{(p+n)\left[1+\lambda\left(\frac{n}{p}\right)\right]\frac{(a)_{n+1}}{(c)_{n+1}}a_{p+n}\right\}$ $(n \geq 0; p \in \mathbb{N}; 0 \leq \lambda < \frac{1}{2})$ is nondecreasing, then*

$$\left\{\frac{(p+m-1)!}{(p-1)!} - \frac{(A-B)(1-2\lambda)}{(1-B)C_n} \cdot \frac{p!}{(p-m)!}r^{2p}\right\}r^{-(p+m)} \leq |f^{(m)}(z)| \leq \left\{\frac{(p+m-1)!}{(p-1)!} - \frac{(A-B)(1-2\lambda)}{(1-B)C_n} \cdot \frac{p!}{(p-m)!}r^{2p}\right\}r^{-(p+m)} \quad (9)$$

$(0 < |z| = r < 1; 0 \leq \lambda < p; p \in \mathbb{N}; m \in \mathbb{N}_0 = \mathbb{N} \cup \{0\}; p > m)$

The result is sharp for the function $f(z)$ given by

$$f(z) = z^{-p} + \frac{(A-B)(1-2\lambda)}{(1-B)} \cdot \frac{(c)_{n+1}}{(a)_{n+1}} z^{p} \quad (p \in \mathbb{N}). \tag{10}$$

Proof. In view of Theorem 1, we have

$$\frac{(a)_{n+1}}{(c)_{n+1}} \cdot \frac{p}{p!} \sum_{n=0}^{\infty} (p+n)!\, a_{p+n} \leq \sum_{n=0}^{\infty} (p+n)\left[1+\lambda\left(\frac{n}{p}\right)\right] \frac{(a)_{n+1}}{(c)_{n+1}} a_{p+n} \leq \frac{(A-B)p(1-2\lambda)}{(1-B)},$$

Which yields

$$\sum_{n=0}^{\infty} (p+n)!\, a_{p+n} \leq \frac{(A-B)(1-2\lambda)p!}{(1-B)} \cdot \frac{(c)_{n+1}}{(a)_{n+1}} \quad (p \in \mathbb{N}). \tag{11}$$

Now, by differentiate both sides of (1) m times with respect to z, we have

$$f^{(m)}(z) = (-1)^m \frac{(p+m-1)!}{(p-1)!} z^{-(p+m)} + \sum_{n=0}^{\infty} \frac{(p+n)!}{(p+m-n)!} a_{p+n} z^{p+m-n}, \tag{12}$$

$(m \in \mathbb{N}_0, p \in \mathbb{N}; p > m)$.

So, Theorem 2 follows from (11) and (12).

The proof is complete. ■

4. Radii of Meromorphic Starlikeness and Meromorphic Convexity

Next we determine the radii of meromorphically p-valent starlikeness of order $\delta(0 \leq \delta < p)$ and meromorphically p-valent convexity of order $\delta(0 \leq \delta < p)$ for functions in the class $M_{a,c,\lambda}[p, A, B, \lambda]$.

Theorem 3. *Let the function $f(z)$ defined by (1) be in the class $M_{a,c,\lambda}[p, A, B, \lambda]$. Then we have:*

(i) $f(z)$ is meromorphically p-valent starlike of order $\delta(0 \leq \delta < p)$ in the disc $|z| < r_1$, that is,

$$\Re\left[-\frac{zf'(z)}{f(z)}\right] > \delta \quad (|z| < r_1; 0 \leq \delta < p, p \in \mathbb{N}),$$

Where

$$r_1 = inf_{n\geq 0}\left[\frac{(p+n)\left[1+\lambda\left(\frac{n}{p}\right)\right](1-B)(p-\delta)}{(A-B)p(1-2\lambda)(p+n-\delta)} \cdot \frac{(a)_{n+1}}{(c)_{n+1}}\right]^{\frac{1}{2p+n}}. \tag{13}$$

(ii) $f(z)$ is meromorphically p-valent convex of order $\delta(0 \leq \delta < p)$ in the disc $|z| < r_2$, that is,

$$\Re\left[-\left(1+\frac{zf''(z)}{f'(z)}\right)\right] > \delta(|z| < r_2; 0 \leq \delta < p, p \in \mathbb{N}),$$

Where

$$r_2 = \inf_{n\geq 0}\left[\frac{\left[1+\lambda\left(\frac{n}{p}\right)\right](1-B)(p-\delta)}{(A-B)(1-2\lambda)(p+n-\delta)} \cdot \frac{(a)_{n+1}}{(c)_{n+1}}\right]^{\frac{1}{2p+n}}. \tag{14}$$

Each of these results is sharp for the function $f(z)$ given by (8).

Proof. (i) From Theorem 1, we have:

$$\sum_{n=0}^{\infty} (p+n)\left[1+\lambda\left(\frac{n}{p}\right)\right](1-B)\frac{(a)_{n+1}}{(c)_{n+1}} a_{p+n} \leq (A-B)p(1-2\lambda),$$

Let;

$$\left|\frac{zf'(z)+pf(z)}{f(z)}\right| = \left|\frac{\sum_{n=0}^{\infty}(2p+n)a_{p+n}z^{p+n}}{z^{-p}+\sum_{n=0}^{\infty}a_{p+n}\,z^{p+n}}\right| \leq \frac{\sum_{n=0}^{\infty}(p+n)a_{p+n}|z|^{2p+n}}{1+\sum_{n=0}^{\infty}a_{p+n}\,|z|^{2p+n}},$$

As known;

$$\left|\frac{zf'(z)+pf(z)}{f(z)}\right| \leq p-\delta \quad (0 \leq \delta < p),$$

such that

$$\sum_{n=0}^{\infty} \frac{(p+n-\delta)}{(p-\delta)} a_{p+n}|z|^{2p+n} \leq (p-\delta). \tag{15}$$

Then by Corollary 1 the inequality (15) will be true if

$$|z|^{2p+n} \leq \frac{(p+n)\left[1+\lambda\left(\frac{n}{p}\right)\right](1-B)(p-\delta)}{(A-B)p(1-2\lambda)(p+n-\delta)} \cdot \frac{(a)_{n+1}}{(c)_{n+1}},$$

That is

$$|z| \leq \left[\frac{(p+n)\left[1+\lambda\left(\frac{n}{p}\right)\right](1-B)(p-\delta)}{(A-B)p(1-2\lambda)(p+n-\delta)} \cdot \frac{(a)_{n+1}}{(c)_{n+1}}\right]^{\frac{1}{2p+n}},$$

The infimum of the above quantity is the radii of starlikeness of the function $f(z)$ in the class $M_{a,c,\lambda}[p, A, B, \lambda]$ The sharpness follows by choosing the same extremal function (10).

Which completes the proof of part (i).

(iii) It is enough to show that

(iv)

$$\Re\left[-\left(1+\frac{zf''(z)}{f'(z)}\right)\right] > \delta(|z| < r_2; 0 \le \delta < p, p \in \mathbb{N}),$$

or, let

$$\left|\frac{(zf'(z))' + pf'(z)}{f'(z)}\right| = \left|\frac{\sum_{n=0}^{\infty}(p+n)(2p+n)a_{p+n}z^{p+n-1}}{-pz^{-p-1} + \sum_{n=0}^{\infty}(p+n)a_{p+n}z^{p+n-1}}\right| \le \frac{\sum_{n=0}^{\infty}(p+n)(2p+n)a_{p+n}|z|^{2p+n}}{p - \sum_{n=0}^{\infty}(p+n)a_{p+n}|z|^{2p+n}}$$

so, as known that

$$\left|\frac{(zf'(z))' + pf'(z)}{f'(z)}\right| \le p - \delta \quad (0 \le \delta < p),$$

such that

$$\sum_{n=0}^{\infty}\frac{(p+n)(3p+n-\delta)}{p(p-\delta)}a_{p+n}|z|^{2p+n} \le 1.$$

From Theorem 1,we obtain

$$|z|^{2p+n} \le \frac{(p-\delta)\left[1+\lambda\left(\frac{n}{p}\right)\right](1-B)}{(A-B)(1-2\lambda)(3p+n-\delta)}.$$

Thus

$$|z| \le \left[\frac{(p-\delta)\left[1+\lambda\left(\frac{n}{p}\right)\right](1-B)}{(A-B)(1-2\lambda)(3p+n-\delta)}\right]^{\frac{1}{2p+n}} \quad (n \ge 0, p \in \mathbb{N}).$$

By choosing r_2 to be the infimum of the above quantity we get the result. The sharpness follows by choosing the same extremal function (8).

The proof is complete.■

5. Neighborhoods

Following the earlier works on neighborhoods of analytic functions by Goodman [10] and Ruscheweyh [19], and (more recently) by Altintas et al. ([1], [2] and [3]), Liu [13], and Liu and Srivastava [14], we begin

by introducing here the δ-neighborhood of a function $f(z) \in \Sigma_p$ of the form (1) by means of the definition given below:

$$N_\delta = \left\{g \in \Sigma_p : g(z) = z^{-p} + \sum_{n=0}^{\infty} b_{p+n}\, z^{p+n} \text{ and } \sum_{n=0}^{\infty}\frac{(p+n)\left[1+\lambda\left(\frac{n}{p}\right)\right](1+|B|)}{(A-B)p(1-2\lambda)}\cdot\frac{(a)_{n+1}}{(c)_{n+1}}|b_{p+n} - a_{p+n}| \le \delta\right\} \quad (16)$$

$(-1 \le B < A \le 1; p \in \mathbb{N}; 0 \le \lambda < \frac{1}{2}; \delta > 0)$. Making use of definition (16), we now prove Theorem 4 below.

Theorem 4. *Let the function $f(z)$ defined by (1) be in the class $M_{a,c,\lambda}[p, A, B, \lambda]$.*
If $f(z)$ satisfies the following condition:

$$\frac{f(z)+\tau z^{-p}}{1+\tau} \in M_{a,c,\lambda}[p, A, B, \lambda] \quad (\tau \in \mathbb{C}; |\tau| < \delta; \delta > 0), \quad (17)$$

then

$$N_\delta(f) \subset M_{a,c,\lambda}[p, A, B, \lambda].$$

Proof. It is clearly that from (5) the function $g(z) \in M_{a,c,\lambda}[p, A, B, \lambda]$ if and only if for any complex number ω with $|\omega| = 1$,

$$\left|\frac{z^{p+1}F'_{p,a,c,\lambda}(z) + p(1-2\lambda)}{Bz^{p+1}F'_{p,a,c,\lambda}(z) + Ap(1-2\lambda)}\right| \ne \omega \quad (z \in \Delta), \quad (19)$$

or

$$\frac{(g*h)(z)}{z^{-p}} \ne 0 \quad (z \in \Delta). \quad (20)$$

For convenience,

$$h(z) = z^{-p} + \sum_{n=0}^{\infty} c_{p+n}\, z^{p+n}$$

$$= z^{-p} + \sum_{n=0}^{\infty} \frac{(n-p)\left[1+\lambda\left(\frac{n}{p}\right)\right](1-\omega B)}{(A-B)p(1-2\lambda)\omega} \cdot \frac{(a)_{n+1}}{(c)_{n+1}} z^{p+n} \quad (21)$$

Then

$$|c_{p+n}| = \left|\frac{(n-p)\left[1+\lambda\left(\frac{n}{p}\right)\right](1-\omega B)}{(A-B)p(1-2\lambda)\omega} \cdot \frac{(a)_{n+1}}{(c)_{n+1}}\right|$$

$$\leq \frac{(p+n)\left[1+\lambda\left(\frac{n}{p}\right)\right](1+|B|)}{(A-B)p(1-2\lambda)} \cdot \frac{(a)_{n+1}}{(c)_{n+1}}$$

$\left(n, p \in \mathbb{N}; 0 \leq \lambda < \frac{1}{2}\right)$. Now, if $f(z) = z^{-p} + \sum_{n=0}^{\infty} a_{p+n} z^{p+n} \in \Sigma_p$ satisfies the condition (17), then (20) yields

$$\left|\frac{(f * h)(z)}{z^{-p}}\right| \geq \delta \quad (z \in \Delta; \delta > 0).$$

No letting $g(z) = z^{-p} + \sum_{n=0}^{\infty} b_{p+n} z^{p+n} \in N_\delta(f)$, we obtain that

$$\left|\frac{[g(z) - f(z)] * h(z)}{z^{-p}}\right| = \left|\sum_{n=0}^{\infty} (b_{p+n} - a_{p+n}) c_{p+n} z^{p+n}\right|$$

$$\leq |z| \sum_{n=0}^{\infty} \frac{(p+n)\left[1+\lambda\left(\frac{n}{p}\right)\right](1+|B|)}{(A-B)p(1-2\lambda)} \cdot \frac{(a)_{n+1}}{(c)_{n+1}} |b_n - a_n| \leq \delta$$

$(z \in \Delta; \delta > 0)$. Then we have (20), and hence also (19) for any $\in \mathbb{C}$, $|\omega| = 1$, which implies that $g(z) \in M_{a,c,\lambda}[p, A, B, \lambda]$.
This evidently proves the assertion (18) of Theorem 8.■

Now, we define the δ-neighborhood of a function $f(z) \in \Sigma_p^*$ of the form (1) as follows

$$N_\delta^+ = \left\{ g \in \Sigma_p : g(z) = z^{-p} + \sum_{n=0}^{\infty} |b_{p+n}| z^{p+n} \text{ and } \sum_{n=0}^{\infty} \frac{(p+n)\left[1+\lambda\left(\frac{n}{p}\right)\right](1+|B|)}{(A-B)p(1-2\lambda)} \cdot \frac{(a)_{n+1}}{(c)_{n+1}} \left||b_{p+n}| - |a_{p+n}|\right| \leq \delta \right\},$$

$\left(-1 \leq B < A \leq 1; p \in \mathbb{N}; 0 \leq \lambda < \frac{1}{2}; \delta > 0\right)$.

Theorem 5. *Let the function $f(z)$ defined by (1) be in the class $M_{a,c,\lambda}[p, A, B, \lambda]$, $\left(-1 \leq B < A \leq 1, -1 \leq B \leq 0, p \in \mathbb{N}$ and $0 \leq \lambda < \frac{1}{2}\right)$. Then $N_\delta^+(f) \subset M_{a,c,\lambda}[p, A, B, \lambda]$ $\left(\delta = \frac{2p}{\alpha+2p}\right)$, where α is complex parametr. The result is sharp in the sense that δ cannot be increased.*

Proof. Making use the same method as in the proof of Theorem 4, we can show that [cf. (21)]

$$h(z) = z^{-p} + \sum_{n=0}^{\infty} c_{p+n} z^{p+n}$$

$$= z^{-p} + \sum_{n=0}^{\infty} \frac{(p+n)\left[1+\lambda\left(\frac{n}{p}\right)\right](1-\omega B)}{(A-B)p(1-2\lambda)\omega} \cdot \frac{(a)_{n+1}}{(c)_{n+1}} z^{p+n}.$$

Thus, by the hypothesis $-1 \leq B < A \leq 1, -1 \leq B \leq 0, p \in \mathbb{N}$ *and* $0 \leq \lambda < \frac{1}{2}$, if $f(z) \in M_{a,c,\lambda}[p, A, B, \lambda]$ is given by (1), we obtain

$$\left|\frac{(f * h)(z)}{z^{-p}}\right| = |1 + \sum_{n=0}^{\infty} c_{p+n} |a_{p+n}| z^{p+n}|$$

$$\geq 1 - \frac{\alpha}{\alpha+2p} \sum_{n=0}^{\infty} \frac{(p+n)\left[1+\lambda\left(\frac{n}{p}\right)\right](1-\omega B)}{(A-B)p(1-2\lambda)\omega} \cdot \frac{(a)_{n+1}}{(c)_{n+1}} |a_{p+n}|.$$

As a result, by Theorem 1, we have

$$\left|\frac{(f * h)(z)}{z^{-p}}\right| \geq 1 - \frac{\alpha}{\alpha+2p} = \frac{2p}{\alpha+2p} = \delta.$$

The remaining part of the proof of Theorem 5 is similar to that of Theorem 4, and we skip the details involved.
To show the sharpness, we consider the functions $f(z)$ and $g(z)$ given by

$$f(z) = z^{-p} + \frac{(A-B)(1-2\lambda)}{(1-B)} \cdot \frac{(c)_{n+1}}{(a)_{n+1}} z^p \in M_{a,c,\lambda}[p, A, B, \lambda]$$

And

$$g(z) = z^{-p} + \left[\frac{(A-B)(1-2\lambda)}{(1-B)} \cdot \frac{(c)_{n+1}}{(a)_{n+1}} + \frac{(A-B)(1-2\lambda)\delta'}{(1-B)} \cdot \frac{(c)_{n+1}}{(a)_{n+1}}\right] z^p.$$

Where
$\delta' > \delta = \frac{2p}{\alpha+2p}$. Clearly, the function $g(z)$ belongs to $N_{\delta'}^{+}(f)$. On the other hand, we find from Theorem 1 that $g(z)$ is not in the class $M_{a,c,\lambda}[p,A,B,\lambda]$.
The proof is complete.■

6. Partial Sums

Theorem 6. *Let $f(z) \in \Sigma_p$ be given by (1) and define the partial sums $f_1(z)$ and $f_k(z)$ as*
$f_1(z) = z^{-p}$ *and* $f_k(z) = \frac{1}{z^p} + \sum_{n=0}^{k} a_{p+n} z^{p+n}$ $(k \in \mathbb{N}\backslash\{0\})$.

We suppose that

$$\sum_{n=0}^{\infty} d_n |a_{p+n}| \leq 1 \left(d_n = \frac{(p+n)\left[1+\lambda\left(\frac{n}{p}\right)\right](1+|B|)}{(A-B)p(1-2\lambda)} \cdot \frac{(a)_{n+1}}{(c)_{n+1}} \right). \quad (22)$$

Then:

(i) $f(z) \in M_{a,c,\lambda}[p,A,B,\lambda]$

(ii) *If* $\{\Psi_n\}$ $(n \in \mathbb{N})$ *is nondecreasing and*

$$\Psi_1 > \frac{(A-B)p(1-2\lambda)}{(p+n)\left[1+\lambda\left(\frac{n}{p}\right)\right](1+|B|)},$$

then

$$\Re\left\{\frac{f(z)}{f_k(z)}\right\} > 1 - \frac{1}{d_k} \quad (z \in \Delta; k \in \mathbb{N}), \quad (23)$$

and

$$\Re\left\{\frac{f_k(z)}{f(z)}\right\} > \frac{d_k}{1+d_k} \quad (z \in \Delta; k \in \mathbb{N}). \quad (24)$$

Each of the bounds in (23) and (24) is the best possible for each $k \in \mathbb{N}$.

Proof. (i) It is not difficult to see that $z^{-p} \in M_{a,c,\lambda}[p,A,B,\lambda]$. Thus, from Theorem 4 and the hypothesis (22), we have $N_1(z^{-p}) \in M_{a,c,\lambda}[p,A,B,\lambda]$ as asserted by Theorem 4.

(ii) Under the hypothesis in Part (ii) of Theorem 6, we can see from (22) that $d_{n+1} > d_n > 1$ $(n \in \mathbb{N})$. Therefore, we have

$$\sum_{n=0}^{k-1} a_n + d_k \sum_{n=k}^{\infty} a_n \leq \sum_{n=0}^{\infty} d_n a_n \leq 1, \quad (25)$$

use hypothesis (22) again and setting,

$$g_1(z) = d_k\left[\frac{f(z)}{f_k(z)} - \left(1 - \frac{1}{d_k}\right)\right] = 1 + \frac{d_k \sum_{n=k}^{\infty} a_n z^n}{1 + \sum_{n=0}^{k-1} a_n z^n},$$

with applying (25), we find that

$$\left|\frac{g_1(z)-1}{g_1(z)+1}\right| \leq \frac{d_k \sum_{n=k}^{\infty} a_n}{2 - 2\sum_{n=0}^{k-1} a_n - d_k \sum_{n=k}^{\infty} a_n} \leq 1 \quad (z \in \Delta),$$

which readily yields the assertion (23). If we take

$$f(z) = z^{-p} - \frac{z^{k-p}}{d_k}, \quad (26)$$

then

$$\frac{f(z)}{f_k(z)} = 1 - \frac{z^k}{d_k} \to 1 - \frac{1}{d_k} \quad (z \to 1^-)$$

which shows that the bound in (23) is the best possible for each $k \in \mathbb{N}$.

Similarly, if we put

$$g_2(z) = (1+d_k)\left[\frac{f_k(z)}{f(z)} - \left(\frac{d_k}{1+d_k}\right)\right] = 1 - \frac{(1+d_k)\sum_{n=k}^{\infty} a_n z^n}{1 + \sum_{n=0}^{k-1} a_n z^n}$$

and making use of (25), we can deduce that

$$\left|\frac{g_2(z)-1}{g_2(z)+1}\right| \leq \frac{(1+d_k)\sum_{n=k}^{\infty} a_n}{2 - 2\sum_{n=0}^{k-1} a_n - (1+d_k)\sum_{n=k}^{\infty} a_n} \leq 1 \quad (z \in \Delta),$$

which leads us immediately to the assertion (26). The bound in (24) is sharp for each $k \in \mathbb{N}$, with the extremal function $f(z)$ given by (26).
The proof is complete.■

7. Convolution Properties for the class $\mathbf{M_{a,c,\lambda}[\alpha,\beta,\gamma,\lambda]}$

For functions $f_j(z)$ defined by

$$f_j(z) = z^{-p} + \sum_{n=0}^{\infty} a_{p+n,j} z^{p+n}, \quad (j = 1,2), \tag{27}$$

belonging to the class Σ_p^*, we denote by $(f_1 * f_2)(z)$ the convolution (or Hadamard product) of the functions $f_1(z)$ and $f_2(z)$; that

$$(f_1 * f_2)(z) = z^{-p} + \sum_{n=0}^{\infty} a_{p+n,1} a_{p+n,2} z^{p+n}.$$

In this section, we assume further that the sequence

$$\left\{(p+n)\left[1+\lambda\left(\frac{n}{p}\right)\cdot\frac{(a)_{n+1}}{(c)_{n+1}}\right]\right\}\left(n \geq 0; p \in \mathbb{N}; 0 \leq \lambda < \frac{1}{2}\right) \text{ is nondecreasing.}$$

Theorem 7. *Let the functions $f_j(z)$ $(j = 1,2)$ defined by (27) be in the class $M_{a,c,\lambda}[\alpha,\beta,\gamma,\lambda]$. Then $(f_1 * f_2)(z) \in M_{a,c,\lambda}[\mu,\beta,\gamma,\lambda]$, where*

$$\mu = p - \frac{2\beta\gamma(p-\alpha)^2(1-2\lambda)}{p(1+2\beta\gamma-\beta)}\cdot\frac{(c)_{n+1}}{(a)_{n+1}}.$$

The result is sharp for the functions $f_j(z)$ $(j = 1,2)$ given by

$$f_j(z) = z^{-p} + \frac{2\beta\gamma(p-\alpha)(1-2\lambda)}{(1+2\beta\gamma-\beta)}\cdot\frac{(c)_{n+1}}{(a)_{n+1}} z^{p+n}, \quad (j = 1,2; p \in \mathbb{N}). \tag{28}$$

Proof. Employing the technique used earlier by Schild and Silverman [20], we need to find the largest μ such that

$$\sum_{n=0}^{\infty} \frac{(p+n)\left[1+\lambda\left(\frac{n}{p}\right)\right](1+2\beta\gamma-\beta)}{2\beta\gamma(p-\alpha)(1-2\lambda)}\cdot\frac{(a)_{n+1}}{(c)_{n+1}} a_{p+n,1}a_{p+n,2} \leq 1$$

for $f_j(z) \in M_{a,c,\lambda}[\alpha,\beta,\gamma,\lambda]$ $(j = 1,2)$. We readily see that

$$\sum_{n=0}^{\infty} \frac{(p+n)\left[1+\lambda\left(\frac{n}{p}\right)\right](1+2\beta\gamma-\beta)}{2\beta\gamma(p-\alpha)(1-2\lambda)}\cdot\frac{(a)_{n+1}}{(c)_{n+1}} a_{p+n,j} \leq 1 \quad (j = 1,2).$$

Therefore, by the Cauchy-Schwarz inequality, we obtain

$$\sum_{n=0}^{\infty} \frac{(p+n)\left[1+\lambda\left(\frac{n}{p}\right)\right](1+2\beta\gamma-\beta)}{2\beta\gamma(p-\alpha)(1-2\lambda)}\cdot\frac{(a)_{n+1}}{(c)_{n+1}} \sqrt{a_{p+n,1}a_{p+n,2}} \leq 1. \tag{29}$$

This implies that we only need to show that

$$\frac{1}{(p-\mu)} a_{p+n,1}a_{p+n,2} \leq \frac{1}{(p-\alpha)}\sqrt{a_{p+n,1}a_{p+n,2}} \quad (n \geq 0)$$

or, $\sqrt{a_{p+n,1}a_{p+n,2}} \leq \frac{p-\mu}{p-\alpha}$ $(n \geq 0)$. Hence, by (29), it is sufficient to prove that

$$\frac{2\beta\gamma(p-\alpha)(1-2\lambda)}{(p+n)\left[1+\lambda\left(\frac{n}{p}\right)\right](1+2\beta\gamma-\beta)}\cdot\frac{(c)_{n+1}}{(a)_{n+1}} \leq \frac{p-\mu}{p-\alpha} \quad (n \geq 0). \tag{30}$$

Then from (30) we get

$$\mu \leq p - \frac{2\beta\gamma(p-\alpha)^2(1-2\lambda)}{(p+n)\left[1+\lambda\left(\frac{n}{p}\right)\right](1+2\beta\gamma-\beta)}\cdot\frac{(c)_{n+1}}{(a)_{n+1}} \quad (n \geq 0).$$

Now, defining the function $\Psi(n)$ by

$$\Psi(n) = p - \frac{2\beta\gamma(p-\alpha)^2(1-2\lambda)}{(p+n)\left[1+\lambda\left(\frac{n}{p}\right)\right](1+2\beta\gamma-\beta)}\cdot\frac{(c)_{n+1}}{(a)_{n+1}} \quad (n \geq 0),$$

We have

$$\Psi(n+1) - \Psi(n) = \frac{2\beta\gamma(p-\alpha)^2(1-2\lambda)}{(1+2\beta\gamma-\beta)}\cdot\frac{(a)_{n+1}}{(c)_{n+1}} \times \left\{\frac{(p+n+1)(a+n+2p)\left|1+\lambda\left(\frac{n}{p}\right)\right| - (p+n)(c+n+2p)\left|1+\lambda\left(\frac{n}{p}\right)\right|}{(p+n)(a+n+2p)\left|1+\lambda\left(\frac{n}{p}\right)\right|\left|1+\lambda\left(\frac{n+1}{p}\right)\right|}\right\} > 0,$$

that is, that, $\Psi(n)$ is an increasing function of $n(n \geq 0)$. Therefore, we conclude that

$$\mu \leq \Psi(p) = p - \frac{2\beta\gamma(p-\alpha)^2(1-2\lambda)}{p(1+2\beta\gamma-\beta)}\cdot\frac{(c)_{n+1}}{(a)_{n+1}},$$

The proof is complete. ■

Using arguments similar to these in the proof of Theorem 7, we obtain the following result.

Theorem 8. *Let the function $f_1(z)$ defined by (27) be in the class $M_{a,c,\lambda}[\alpha,\beta,\gamma,\lambda]$. Suppose also that the function $f_2(z)$ defined by (27) be in the class $M_{a,c,\lambda}[\varphi,\beta,\gamma,\lambda]$. Then $(f_1 * f_2)(z) \in M_{a,c,\lambda}[\theta,\beta,\gamma,\lambda]$ where*

$$\theta = p - \frac{2\beta\gamma(p-\alpha)(p-\varphi)(1-2\lambda)}{p(1+2\beta\gamma-\beta)}\cdot\frac{(c)_{n+1}}{(a)_{n+1}}.$$

The result is sharp for the functions $f_j(z)$ $(j = 1,2)$ given by

$$f_1(z) = z^{-p} + \frac{2\beta\gamma(p-\alpha)(1-2\lambda)}{p(1+2\beta\gamma-\beta)} \cdot \frac{(c)_{n+1}}{(a)_{n+1}} z^p \qquad (p \in \mathbb{N})$$

And

$$f_2(z) = z^{-p} + \frac{2\beta\gamma(p-\varphi)(1-2\lambda)}{p(1+2\beta\gamma-\beta)} \cdot \frac{(c)_{n+1}}{(a)_{n+1}} z^p \qquad (p \in \mathbb{N}).$$

Theorem 9. *Let the functions* $f_j(z)(j = 1,2)$ *defined by* (27) *be in the class* $M_{a,c,\lambda}[\alpha,\beta,\gamma,\lambda]$. *Then the function* $h(z)$ *defined by*

$$h(z) = z^{-p} + \sum_{n=0}^{\infty} (a_{p+n,1})^2 (a_{p+n,2})^2 z^{p+n}$$

belongs to the class $M_{a,c,\lambda}[\varepsilon,\beta,\gamma,\lambda]$, *where*

$$\varepsilon = p - \frac{4\beta\gamma(p-\alpha)^2(1-2\lambda)}{p(1+2\beta\gamma-\beta)} \cdot \frac{(c)_{n+1}}{(a)_{n+1}}.$$

This result is sharp for the functions $f_j(z)(j = 1,2)$ *defined by* (28).

Proof. We note that

$$\sum_{n=0}^{\infty} \left[\frac{(p+n)\left[1+\lambda\left(\frac{n}{p}\right)\right](1+2\beta\gamma-\beta)}{2\beta\gamma(p-\alpha)(1-2\lambda)} \cdot \frac{(a)_{n+1}}{(c)_{n+1}} \right]^2 (a_{p+n,j})^2$$

$$\leq \left[\sum_{n=0}^{\infty} \frac{(p+n)\left[1+\lambda\left(\frac{n}{p}\right)\right](1+2\beta\gamma-\beta)}{2\beta\gamma(p-\alpha)(1-2\lambda)} \cdot \frac{(a)_{n+1}}{(c)_{n+1}} a_{p+n,j} \right]^2 \leq 1 \qquad (j = 1,2),$$

for $f_j(z) \in M_{a,c,\lambda}[p,\alpha,\beta,\gamma,\lambda](j = 1,2)$, we have

$$\sum_{n=0}^{\infty} \frac{1}{2} \left[\frac{(p+n)\left[1+\lambda\left(\frac{n}{p}\right)\right](1+2\beta\gamma-\beta)}{2\beta\gamma(p-\alpha)(1-2\lambda)} \cdot \frac{(a)_{n+1}}{(c)_{n+1}} \right]^2 \left[(a_{p+n,1})^2 (a_{p+n,2})^2 \right] \leq 1.$$

Therefore, we have to find the largest ε such that

$$\frac{1}{p-\varepsilon} \leq \frac{(p+n)\left[1+\lambda\left(\frac{n}{p}\right)\right](1+2\beta\gamma-\beta)}{4\beta\gamma(p-\alpha)^2(1-2\lambda)} \cdot \frac{(a)_{n+1}}{(c)_{n+1}} \qquad (n \geq 0),$$

That is, that

$$\varepsilon \leq p - \frac{4\beta\gamma(p-\alpha)^2(1-2\lambda)}{(p+n)\left[1+\lambda\left(\frac{n}{p}\right)\right](1+2\beta\gamma-\beta)} \cdot \frac{(c)_{n+1}}{(a)_{n+1}} \qquad (n \geq 0).$$

Now, defining a function $\Phi(n)$ by

$$\Phi(n) = p - \frac{4\beta\gamma(p-\alpha)^2(1-2\lambda)}{(p+n)\left[1+\lambda\left(\frac{n}{p}\right)\right](1+2\beta\gamma-\beta)} \cdot \frac{(c)_{n+1}}{(a)_{n+1}} \qquad (n \geq 0),$$

We note that $\Phi(n)$ is an increasing function of n $(n \geq 0)$. Thus, we conclude that

$$\varepsilon \leq \Phi(n) = p - \frac{4\beta\gamma(p-\alpha)^2(1-2\lambda)}{p(1+2\beta\gamma-\beta)} \cdot \frac{(c)_{n+1}}{(a)_{n+1}},$$

This completes the proof of the Theorem 9. ■

References

[1] O. Altintas, S. Owa, Neighborhoods of certain analytic functions with negative coefficients, Internat. J. Math. Math. Sci. 19 (1996), 797–800.

[2] O. Altintas, O. Ozkan, H.M. Srivastava, Neighborhoods of a class of analytic functions with negative coefficients, Appl. Math. Letters 13 (2000), 63–67.

[3] O. Altintas, O. Ozkan, H.M. Srivastava, Neighborhoods of a certain family of multivalent functions with negative coefficients, Comput. Math. Appl. 47 (2004), 1667–1672.

[4] M. K. Aouf, A generalization of meromorphic multivalent functions with positive coefficients. Math, Japonica 35(1990) 609-614.

[5] M. K. Aouf, On a class of meromorphic multivalent functions with positive coefficients, Math. Japonica 25(1990)603- 608.

[6] M. K. Aouf, New criteria for multivalent meromorphic starlike functions of order alpha, Proc. Japan. Acad. 69(1993) 66- 70.

[7] M. K. Aouf and B. A. Frasin, Properties of some families of meromorphic multivalent functions involving certain linear operator, Filomat 24:3 (2010) 35-54.

[8] M. K. Aouf, H. M. Mossen, H. E.Elattar, A certain class of meromorphic multivalent functions with positive and fixed second coefficients, Punjab Univ. J. Math. 33(2000)115-124.

[9] M. K. Aouf, A. O. Mostafa, Properties of some families of meromorphic multivalent functions associated with generalized hypergeometric functions, Matematiqki Vesnik. 64, 3(2012), 173–189

[10] A.W. Goodman, Univalent functions and nonanalytic curves, Proc. Amer. Math. Soc. 8 (1957), 598–601.

[11] S. B. Joshi, H. M. Srivastava, A certain family of meromorphically multivalent functions, Clmput. Math. Appl. 38(3-4)(1999)201-211.

[12] A. R. S. Juma and Hazha Zirar. Some classes of meromorphic multivalent functions with positive coefficients involving certain linier operator. International Journal of Basic & Applied Sciences IJBAS-IJENS Vol:13 No:03(2013), pp. 56-78.

[13] J.-L. Liu, Properties of some families of meromorphic p-valent functions, Math. Japon. 52 (2000), 425–434.

[14] J.-L. Liu, H.M. Srivastava, A linear operator and associated families of meromorphically multivalent functions, J. Math. Anal. Appl. 259 (2000), 566–581.

[15] M. L. Mogra, Meromorphic multivalent functions with positive coefficients. I, Math. Japonica 35(1)(1990)1-11.

[16] M. L. Mogra, Meromorphic multivalent functions with positive coefficients. II, Math. Japonica 35(6)(1990)1089-1098

[17] S. Owa, H. E. Darwish, M. K. Aouf, Meromorphic multivalent functions with positive and fixed second coefficients, Math. Japonica 46(2)(1997)231-236.

[18] R. K. Rain, H. M. Srivastava, A new class of meromorphically multivalent functions with applications to generalized hypergeometric functions, Math Comput. Modelling 43(2006)350-356.

[19] S. Ruscheweyh, Neighborhoods of univalent functions, Proc. Amer. Math. Soc. 81 (1981), 521–527.

[20] A. Schild, H. Silverman, Convolution of univalent functions with negative coefficients, Ann. Univ. Mariae Curie-Sklodowska Sect. A 29 (1975), 99–107.

[21] H. M. Srivastava, H. M. Mossen, M. K. Aouf, A unified presentation of some classes of meromorphically multivalent functions, Comput. Math. Appl. 38(1999)63-70.

[22] B. A. Uralegaddi, M. D. Gannigi, Meromorphic multivalent functions with positive coefficients, Nepali. Math. Sci. Rep. 11(1986)95-102.

[23] B. A. Uralegaddi and C. Somantha, Certain classes of meromorphic multivalent functions, Tamkang J. Math. 23(1992), 223- 231.

[24] D. G. Yang, On a new subclasses of meromorphic p-valent functions, J. Math. Res. Exposition 15(1995)7-13.

Al-Mustansiriyah Journal of Science
Vol. 27, No 2, 2016

journal homepage:www.mjs-mu.com

On Partial Sums of Regular Functions

Shatha S. Alhily
Dept. of Mathematics, College of Sciences, Al- Mustansiriyah University, Baghdad, Iraq

Articleinfo

Received
1/9/2015
Accepted
3/1/2016

KEYWORDS:
Regular function,
Partial sum,
univalent function,
p-valent function.

ABSTRACT

Let $f(z)$be regular in the unit disk D $(|z| < 1)$ then each of its partial sums will have the same properties of function. For instance, if $f(z)$ be univalent in D, then each of its partial sums be univalent in the disk

$D_{1/4} = \left\{z \in D; |z| < \frac{1}{4}\right\}$(cf.[12]).

The purpose of this paper on the contrary to what the above, through putting a sharp condition on the partial sum of $f(z)$, that will make $f(z)$ belong to the certain class in theory of complex functions such as , a univalent function , p-valent function, p-valent function has p zeros at the origin in the unit disk , and p-valent and regular function in the punctured unit disk $|\zeta| > 1$ except for a pole at $\zeta = \infty$, which have been addressed in this paper.

الخلاصة

لتكن$f(z)$ داله منتظمه معرفه على قرص الوحدهD $(|z| < 1$ فكما هو معروف ان كل مجموع جزئي يمتلك نفس الخواص التي تمتلكها الداله $f(z)$. على سبيل المثال اذا كانت الداله $f(z)$ معرفه على قرص الوحده D احاديه التكافؤ فان كل مجاميعها الجزئيه ستكون احاديه التكافؤ في القرص $D_{1/4} = \left\{z \in D; |z| < \frac{1}{4}\right\}$. [12]

لذا فان الغرض من هذه الورقه البحثيه هو الاجابه على ما يحتويه المفهوم المعاكس لما جاء اعلاه من خلال وضع بعض القيود للمجاميع الجزئيه بغيه توليد دوال تنتمي الى فئه معينه ضمن نظريه الدوال المعقده كدوال احاديه التكافؤ , دوال متعدده القيم p , دوال متعدده القيم p وتمتلك p من الاصفار عند نقطه الاصل ودوال متعدده القيم p معرفه على قرص مثقوب $|\zeta| > 1$ ما عدا القطب الواقع عند $\zeta = \infty$. جميع تلك الدوال قد تم تناولها في هذا البحث من خلال ايجاد القيود اللازمه للمجاميع الجزئيه لتلك الدوال لتتمكن من نقل خواصها الى الدوال الاصليه .

INTRODUCTION

The theory of univalent and multivalent functions which is one of the ancient and modern topic in the theory of complex functions. As known, the power series of $f(z)$ in the unit disk convergent in such domain, and provides a mapping from the unit disk D onto some region through the sequence of coefficients $a_o, a_1, a_2, \ldots$ with a main effect of $f'(z)$ that give several geometric property of D.

More precisely, what the above mentioned is true for each partial sum $S_n(z)$ of $f(z)$, and its derivative plays a main role in this respect as A. Hurwitz observed,

$$\frac{S_n(z) - S_n(z_o)}{z - z_o} = 1 + \sum_{k=2}^{\infty} a_k Q_k(z, z_o) \ldots\ldots (1)$$

where $Q_k(z, z_o)$ be a polynomial of complex variables and $|Q_k(z, z_o)| < k$.

Indeed, the right side of (1) is never zero for $z, z_o \in D$.

Let $f(z)$ be an analytic function represented by the following power series

$$w = f(z) = \sum_{n=0}^{\infty} a_n z^n = a_o + a_1 z + a_2 z^2 + \ldots, \quad (2)$$

which maps the unit disk onto subdomain of a Riemann surface.$\{D: |z| < 1\}$. (c.f [9]).

If we normalize $f(z)$ under two conditions $f(0) = 0, f'(0) = 1$, then $f(z)$ is univalent function or in other word , $f(z)$ has never taken value more than once for z in D (c.f [11], [1]) that is why; its image will be formed as a simple region S, such that S is denoted as a set of all univalent functions in D, and has a geometric property about the sequence $\{a_n\}$ (c.f [3]).

It is familiar in univalent function theory that each the partial – sum

$$S_n(z) = \sum_{k=0}^{n} a_k z^k \quad (3)$$

of $f(z)$ in (3) is univalent in D, because $f(z)$ already is.

This kind of analytic function has a normal extension as p-valent function (multivalent of order p) in D, so that the generalization of a univalent function is much less than the theory of p-valent functions, which can be written in the form

$$f(z) = a_1 z + a_2 z^2 + \cdots + a_p z^p + \sum_{n=p+1}^{\infty} a_n z^n, \qquad (4)$$

Under the following condition

$$f(z_1) = f(z_2) = \cdots = f(z_{p+1}), \quad z_1, z_2, \ldots, z_{p+1} \in D. \qquad (5)$$

Gives $z_i = z_j$ for some $i \neq j$, that is $f(z)$ has no value more than $p$times in D [6].

Here, let $S(p)$ denote the set of all functions that are regular and p- valent in D with $f(0) = 0$.

Goodman's Conjecture [2] assumed that, if $p \geq 2$ be a fixed integer and let $f(z)$ be given by (4). then for each

$$n > p$$
$$|a_n| \leq \sum_{k=1}^{p} \frac{2k(p+n)!}{(p+k)!(p-k)!(n-p-1)!(n^2-k^2)} |a_k|, \qquad (6)$$

which established in order to study the large class of p-valent functions, when $f(z)$ has p zeros at the origin, then we have a subclass of $S(p)$ and can be represented in the following form

$$f(z) = z^p + \sum_{n=p+1}^{\infty} a_n z^n, \quad (p \in \mathbb{N} = \{1,2,3,\ldots\}) \qquad (7)$$

such that the magnitude of the coefficients of $f(z)$ is influenced in the number of zeros function [4] , hence there is a constant $C(p)$ for each $p \geq 1$; where $f(z)$ given by (7) such that,

$$|a_n| \leq C(p) \max\{|a_1|, |a_2|, |a_3|, \ldots, |a_s|\} n^{2p-1}$$
For $n > s$. (8)

As known

$|a_{p+1}| \leq 2p$, $|a_{p+2}| \leq p(2p+1)$

Respectively (cf.[5],[7])

In the following we have lemma A which has a key role in proof of the theorem 3.

Lemma A [8].

Suppose $p(z)$ is a polynomial in $\mathbb{C}$, m is a positive integer and w *is* a complex number *on* $\mathbb{T} = \partial D(D: |z| < 1)$. Then the number of roots of $R_m(z) = wz^m p(z) \pm p^*(z)$, where $p^*(z) = p\left(\frac{1}{z}\right)$ in the closed unit disk is greater than or equal to the number of roots of $S_m(z) = z^m p(z)$ in the same region.

Finally, we shall consider Σ_p ; class of p-valent and regular function (Meromorphic p-valent functions) of the form

$$f(z) = \frac{1}{z^p} + \sum_{k=0}^{\infty} a_{p+k} z^{p+k}; \quad a_{p+k} \geq 0 \qquad (9)$$

in the $|\zeta| > 1$ except for a pole at $\zeta = \infty$ (cf.[13]).

As known, the necessary and sufficient conditions on the coefficients of $f(z)$ for all types regular functions which have mentioned above so exciting, thus the condition will be sufficient condition for $f(z)$ to become in S, $S(p)$, $S(p)$ has p zeros in D , and Σ_p as we will see that soon by normalizing the partial sum of the function $f(z)$ in (2), (4) , (7) and (9) under a sharp conditions in order to make $f(z)$ be a univalent function , p-valent function, p-valent function has zeros at the origin in the unit disk , and p-valent regular function in the punctured unit disk $|\zeta| > 1$ except $\zeta = \infty$ respectively.

Now, we turn our attention to establish some theorems that will show how to normalize the partial sum under a specific condition in order to know the classification $f(z)$ for the regular functions theory as the follows.

Main Results.

Theorem (1).

$f(z)$ in (2) be a univalent function on the unit disk $D(|z| < 1)$, if its n^{th} −partial sum be univalent in; provided that

$$\left|\frac{S_n(z) - S_n(z_0)}{z - z_0} - S_n(z_0)\right| \leq S_n(z_0).$$

Proof.

Let $S_n(z) = z + \sum_{k=2}^{n} a_k z^k; \quad n \geq 2$ be a partial sum of $f(z)$ in (2).

$$S_n(z) = 1 + \sum_{k=2}^{n} k a_k z^{k-1}$$

Such that, $S_n(0) = 1$

Hence;

$$\frac{S_n(z) - S_n(z_0)}{z - z_0} = \frac{z + \sum_{k=2}^{n} a_k z^k - z_0 - \sum_{k=2}^{n} a_k z_0^k}{z - z_0}$$

$$= \frac{(z - z_0) + \sum_{k=2}^{n} a_k (z^k - z_0^k)}{z - z_0}$$

$$= 1 + \sum_{k=2}^{n} a_k (z^{k-1} + z^{k-2} z_0 + z^{k-3} z_0^2 + \cdots + z_0^{k-1})$$

$$\frac{S_n(z)-S_n(z_o)}{z-z_0}-1=\sum_{k=2}^{n}a_kQ_k(z,z_o);$$

Where,

$$Q_k(z,z_o)=z^{k-1}+z^{k-2}z_o+z^{k-3}z_o^2+\cdots+z_o{}^{k-1}.$$

We notice that

$$|Q_k(z,z_o)|=|z|^{k-1}<k.$$

Hence,

$|\frac{S_n(z)-S_n(z_o)}{z-z_o}-1|<\sum_{k=0}^{n}|a_k|\,|z|^{k-1}<\sum_{k=2}^{n}|a_k|\,k$

Well, one way to check the rest of this fact; is to let $S_n(z)=z+z^2+z^3$

be n^{th} −partial sum of the function in (2) such that $S_n(z)$ is not univalent in $|z|<r$; (r< 1) let us choose $r=\frac{\sqrt{3}}{2}$.

This implies to

$$|\frac{S_n(z)-S_n(0)}{z}-1|=|\frac{z+z^2+z^3}{z}-1|<1.61$$

That's why the fact above leads to be$\sum_{k=2}^{n}|a_k|\,k<1$ in order to keep the theorem right.

Example(1).

Let $f(z)=\sum_{n=1}^{\infty}\frac{z^n}{n}$. Define thenth- partial sum of it as follows

$$|\frac{S_3(z)-S_3(0)}{z}-1|<0.68,\qquad (z_o=0)$$

which is univalent in $|z|<\frac{\sqrt{3}}{2}$.

Theorem (2).

$f(z)$ in (4) be a p-valent function on the unit disk $D\,(|z|<1)$, if its n^{th} −partial sum are at most p-valent in ; provided that

$$|\frac{S_n(z)-S_n(z_o)}{z-z_0}-a_1|\le|a_2|+\cdots+M|a_p|+\sum_{k=p+1}^{n}|a_k|\,k$$

Proof.

Let $S_n(z)=a_1z+a_2z^2+\cdots+a_pz^p+\sum_{k=p+1}^{n}a_kz^k$.

$$S_n'(z)=a_1+2a_2z+\cdots+pa_pz^{p-1}+\sum_{k=p+1}^{n}ka_kz^{k-1};$$

$$where\ S_n'(z_o=0)=a_1.$$

Hence;

$$S_n(z)-S_n(z_o)=a_1(z-z_o)+a_2(z^2-z_o^2)+\cdots a_p(z^p-z_o^p)+\sum_{k=p+1}^{n}a_k(z^k-z_o^k).$$

$$\frac{S_n(z)-S_n(z_o)}{z-z_o}=a_1+a_2(z+z_o)+\cdots+a_p(z^{p-1}+z^{p-2}z_o+z^{p-3}z_o^2+\cdots)+\sum_{k=p+1}^{n}a_k(z^{k-1}+z^{k-2}z_o+z^{k-3}z_o^2+\cdots+z_o^{k-1}).$$

$S_n'(0)$ exists and does not vanish on the boundary of D $(|z|<1)$, that is

$S_n'(0)=a_1$, (a_1 is non-zero)

$$|\frac{S_n(z)-S_n(z_o)}{z-z_0}-a_1|\le|a_2(z+z_o)|+\cdots+M|a_p|\,|z|^p+\sum_{k=p+1}^{n}|a_k|\,k$$

$$\le|a_2|+\cdots+M|a_p|+\sum_{k=p+1}^{n}|a_k|\,k.\ \blacksquare$$

Theorem (3).

$f(z)$ in (7) be a p- valent function on the unit disk $D\,(|z|<1)$, has a zeros at the origin if its n^{th} −partial sums are at most p- valent in ; provided that

$|\frac{S_n(z)-S_n(z_o)}{z-z_o}|\le$

$P(p,m)\max\{|a_1|,|a_2|,|a_3|,\dots,|a_s|\}$ for $n>s$.

Proof. Let

$$S_n(z)=z^p+\sum_{k=p+1}^{n}a_kz^k.$$

$$S_n'(z)=pz^{p-1}+\sum_{k=p+1}^{n}ka_kz^{k-1}.$$

Here, $S_n'(z_o=0)=0$ that means ($z_o=0$) is a critical point of $f(z)$ denoted by C_o. The existence such as this point would destroy the univalence of $f(z)$, but may be $f(z)$ have an infinite number of a critical points such as $C_1,C_2,\dots,C_m$; j = 1,2, ... , m depends on the range of the partial sum.

Now, let us assume

$$S_n(z) - S_n(z_o) = (z^p - z_o^p) + \sum_{k=p+1}^{n} a_k(z^k - z_o^k).$$

$$\frac{S_n(z) - S_n(z_o)}{z - z_o} = (z^{p-1} + z^{p-2}z_o + z^{p-3}z_o^2 + \cdots) + \sum_{k=p+1}^{n} a_k (z^{k-1} + z^{k-2}z_o + z^{k-3}z_o^2 + \cdots + z_o^{k-1})$$

$$= Q_p(z, z_o) + \sum_{k=p+1}^{n} a_k\, Q_k(z, z_o),$$

where $Q_p(z, z_o) = z^{p-1} + z^{p-2}z_o + z^{p-3}z_o^2 + \cdots + z_o^{p-1}$,

$Q_k(z, z_o) = z^{k-1} + z^{k-2}z_o + z^{k-3}z_o^2 + \cdots + z_o^{k-1}$

Put $z_o = 0$, we have

$|Q_p(z,0)| = |z|^{p-1}$, $p \in \mathbb{N}$ .....(10),

$|Q_k(z,0)| = |z|^{k-1}$ .....(11)

$$\left|\frac{S_n(z) - S_n(z_o)}{z - z_o}\right| = |z|^{p-1} + \sum_{k=p+1}^{n} |a_k|\,|z|^{k-1}.$$

Suppose that z_o is one of the zeros of $S_n(z)$ lies in the open disk $D(0,1+B)$, so that $|z_o| < 1 + B$; $B = \max\{|a_1|, |a_2|, |a_3|, \ldots, |a_s|\}$ for $n > s$.

One can consider the polynomial $q(z) = (1 - z)\,p(z)$, where $q(z) = \left|\frac{S_n(z) - S_n(z_o)}{z - z_o}\right|$, see lemma A.

Let,

$$|q(z)| = |(1 - z)\,p(z)|$$
$$\geq |p(z)| - |zp(z)|$$
$$= |z|^{p-1} + \sum_{k=p+1}^{n} |a_k|\,|z|^{k-1} - |z|\left\{|z|^{p-1} + \sum_{k=p+1}^{n} |a_k|\,|z|^{k-1}\right\}$$
$$= (|z|^{p-1} - |z|^p) + \sum_{k=p+1}^{n} |a_k|\,(|z|^{k-1} - |z|^k)$$
$$= |z|^{p-1}(1 - |z|) + (1 - |z|) \sum_{k=p+1}^{n} |a_k|\,|z|^{k-1}$$
$$= (1 - |z|)\left[|z|^{p-1} + \sum_{k=p+1}^{n} |a_k|\,|z|^{k-1}\right].$$

From (10), (11), we obtain

$$< (1 - |z|)\left[p + \sum_{k=p+1}^{n} |a_k|\,k\right].$$

It's obvious that $|q(z)| > 0$ whenever $|z| \geq 1 + B$ which implies $1 - |z| \leq B$.

At once, we obtain

$$\left|\frac{S_n(z) - S_n(z_o)}{z - z_o}\right| < \max\{|a_1|, |a_2|, |a_3|, \ldots, |a_s|\}\left[p + \sum_{k=p+1}^{n} |a_k|\,k\right] \qquad (12).$$

But $f(z)$ has a critical points $C_j, j = 1,2,\ldots,m$ which influence on the coefficients of $f(z)$ such as its zeros. Now, if z_o is any one such zero, then at least one critical point of $p(z)$ lies on the disk $|z - z_o| < 1$ and , there exist a positive number $P(p,m)$, depends on p and m such that $|C_j| \leq P(p,m)$, $j = 1,2,\ldots,m$ (cf.[10]), at least one index j would be large enough to hold an inequality (12) (cf.[3]) as follows

$\left|\frac{S_n(z) - S_n(z_o)}{z - z_o}\right| < \max\{|a_1|, |a_2|, |a_3|, \ldots, |a_s|\}\,[p + |C_j|]$, $j = 1,2,\ldots,m$.

Finally,

$\left|\frac{S_n(z) - S_n(z_o)}{z - z_o}\right| \leq P(p,m)\max\{|a_1|, |a_2|, |a_3|, \ldots, |a_s|\}$, $j = 1,2,\ldots,m$. ■

Theorem (4). $f(z)$ in (9) be a meromorphic and p-valent function on the punctured unit disk $\{z: 0 < |z| < 1\}$, if its n^{th} −partial sums are at most regular and p- valent in ; provided that

$$\left|\frac{S_{p+n}(z) - S_{p+n}(z_o)}{z - z_o}\right| < \begin{cases} \frac{1}{p+1} + P(p,m), & for\ (z: |z| < \frac{1}{2}) \\ \frac{1}{p+1} + \sum_{k=1}^{p+n} (p+k)\,|a_{p+k}|, & for\ (z: \frac{1}{2} < |z| < 1). \end{cases}$$

Proof.

Let $S_{p+n}(z) = \frac{1}{z^p} + \sum_{k=1}^{p+n} a_{p+k} z^{p+k}$.

And,

$$S'_{p+n}(z) = -pz^{-(p+1)} + \sum_{k=1}^{p+n}(p+k)a_{p+k}z^{p+k-1}.$$

$$S'_{p+n}(z_o = 0) = 0.$$

Obviously , z_o is a critical point never lies in the given domain $\{z: 0 < |z| < 1\}$, so what about the nieghborhoods of z_o.

Part 1: First we have to check whether nieghborhoods of the critical point z_o affect or not on the partial sum which is chosen within the given domain.
Well, consider $H_{p+n}(z_1)$ be a partial sum at the certain critical point z_1 near z_o, so that $|H_{p+n}(z_1)| \le \frac{1}{2}$.
Suppose that, $S'_{p+n}(z_1) = 1 + H_{p+n}(z_1)$, and Koebe Distortion theorem (cf.[13]) gives

$$S'_{p+n}(z_1) \ge \frac{1}{4|z - z_1|}.$$

We have $S'_{p+n}(z_1) \ge \frac{|S_{p+n}(z) - S_{p+n}(z_1)|}{4|z-z_1|}$

In fact, $\frac{1}{4|z-z_1|} \ge \frac{1}{4|z_1|(1+|z||z_1|^{-1})}$, which implies to

$$4\left(1 + \frac{|z|}{|z_1|}\right) \ge 4\left(\frac{|z_1| + |z|}{|z_1|}\right) \ge 4\left(\frac{|z_1 - z|}{|z_1|}\right)$$

$$4exp\left(1 + \frac{|z|}{|z_1|}\right) \ge 4\, exp\left(\frac{|z_1 - z|}{|z_1|}\right)$$

to obtain

$$4\, exp\left(\frac{|z_1 - z|}{|z_1|}\right) \ge |S_{p+n}(z_1)| = 1 + H_{p+n}(z_1) \ge |z_1|.$$

As a result $|z_1| \le 4e^8$. Thus we have been examined that no critical points of $H_{p+n}(z)$ in $\{z: |z| > 4e^8\}$, means there is only a critical points in $\left\{z: |z| < \frac{1}{2}\right\}$.

Part 2: Let

$$S_{p+n}(z) - S_{p+n}(z_o) = \left(z^p - z_o^{-p}\right) + \sum_{k=1}^{p+n} a_{p+k}\left(z^{p+k} - z_o^{p+k}\right).$$

$$\frac{S_{p+n}(z) - S_{p+n}(z_o)}{z - z_o} = \left(z^{-(p+1)} + z^{-(p+2)}z_o + z^{-(p+3)}z_o^2 + \cdots\right) + \sum_{k=1}^{p+n} a_{p+k}\left(z^{p+k-1} + z^{p+k-2}z_o + z^{p+k-3}z_o^2 + \cdots + z_o^{p+k-1}\right).$$

Where

$Q_{p+k}(z, z_o) = z^{p+k-1} + z^{p+k-2}z_o + z^{p+k-3}z_o^2 + \cdots + z_o^{p+k-1}$, $Q_{-p}(z, z_o) = z^{-(p+1)} + z^{-(p+2)}z_o + z^{-(p+3)}z_o^2 + \cdots + z_o^{-(p+1)}$.

Indeed,

$|Q_{p+k}(z, 0)| = |z^{p+k-1}| < p + k$, and
$|Q_{-p}(z, 0)| = |z^{p+1}| < \frac{1}{p+1}$.

We obtain,

$$\left|\frac{S_{p+n}(z) - S_{p+n}(z_o)}{z - z_o}\right| < \frac{1}{p+1} + \sum_{k=1}^{p+n}(p+k)|a_{p+k}|.$$

Now, in part 1 we proved that there is only a critical points in $\left\{z: |z| < \frac{1}{2}\right\}$, hence , there exist a positive number $P(p, m)$, depends on p and m such that $|C_j| \le P(p, m)$, for each $j = 1, 2, \ldots, m$ (cf.[10]) such that

$$\left|\frac{S_{p+n}(z) - S_{p+n}(z_o)}{z - z_o}\right| < \frac{1}{p+1} + P(p, m)$$

As a result, the rest of the partial sums of the meromorphic and p- valent function $f(z)$ will be defined as follws

$$\left|\frac{S_{p+n}(z) - S_{p+n}(z_o)}{z - z_o}\right| < \frac{1}{p+1} + \sum_{k=1}^{p+n}(p+k)|a_{p+k}|, \quad for\ \left(z: \frac{1}{2} \le |z| < 1\right).$$

Finally,

$$\left|\frac{S_{p+n}(z) - S_{p+n}(z_o)}{z - z_o}\right| < \begin{cases} \frac{1}{p+1} + P(p, m), & for\ (z: |z| < \frac{1}{2}) \\ \frac{1}{p+1} + \sum_{k=1}^{p+n}(p+k)|a_{p+k}|, & for\ (z: \frac{1}{2} \le |z| < 1). \end{cases}$$ ■

REFERENCES

[1] J. B. Conway,"Functions of one complex variable II", Springer-Verlag, New York, 1996.
[2] A. W. Goodman, "On some determinants related to p- valent functions", Trans. Amer. Soc. 63 (1948), 175-192,M R 9, 421.
[3] A. W. Goodman, "Open problems of univalent and multivalent functions", Bull. Amer. Math. Soc., Vol.74, No. 6 (1968), pp. (1035-1050).
[4] A. W. Goodman, "An Invitation to the study of univalent and multivalent functions", J. Math.& Math. Sci. Vol. 2, No. 2(1979), pp.(163-186).
[5] W.K. Hayman, "Some applications of the transfinite diameter to the theory of functions", J. Analyse Math. 1(1951), pp. (155-179).

[6] W.K.Hayman,"Multivalent functions", Cambridge Univ. Press, Cambridge, 1958.
[7] J.A.Jenkins,"Univalent functions and conformal mapping", Springer-Verlag, Berlin, 1958; Russian transl., IL, Moscow,1962.
[8] P. Lakatos, "On a number theoretical application of Coxeter transformations", Riv. Mat. Univ. Parma (8) 3 (2000), 293–301.
[9] A. Lyzazik and D. Styer, " Goodman's conjecture and the coefficients of univalent functions", Proceedings of the American Mathematical Society, Vol. 69, No. 1 (Apr., 1978), pp. (111-114).
[10] M. Marden," Conjectures on the critical points of a polynomial ", J. American Mathematical Monthly, Vol. 90, No. 4 (Apr., 1983), pp. 267-276.
[11] CH. Pommerenke, "Univalent Functions", Vanderhoeck and Ruprecht, Gottingen, 1975.
[12] G.Gal. Sorin; "Shape Preserving Approximation by Real and Complex Polynomial", birkhauser Boston,a part of Springer Science, (pp. 219),2008.
[13] J. Zheng,"Value Distribution of Meromorphic Functions",Springer Heidelberg Dordrecht London New York, 1965.

Vol. 27
No.2
2016

مجلة علوم المستنصرية

تصدر عن كلية العلوم الجامعة المستنصرية

رئيس التحرير
أ.د. صاحب كحيط جاسم

مدير التحرير
أ.م.د.صلاح مهدي الشكري

الكادر الفني
ميساء نزار مصطفى
شذى جاسم محمد

www.mjs-mu.com
E-mail: mustjsci@yahoo.com
Mobile: 07711184399
رقم الايداع في دار الكتب والوثائق العراقية 278 لسنة 1977

مجلة علوم المستنصرية

مجلة علمية محكمة تصدر عن عمادة كلية العلوم في الجامعة المستنصرية بأختصاصات الكيمياء والفيزيا والرياضيات وعلوم الحياة وعلوم الحاسبات وعلوم الجو. تنشر المجلة البحوث العلمية التي لم يسبق نشرها في مكان آخر بعد إخضاعها للتقويم العلمي من قبل مختصين وباللغتين العربية او الانكليزية وتُصدر المجلة اربعة اعداد سنوياً على الاقل وبكلا اللغتين.

تعليمات النشر في المجلة

1. يقدم الباحث طلبا تحريريا لنشر البحث في المجلة ويكون مرفقا بثلاث نسخ من البحث مطبوعة على ورق ابيض قياس (A4, 21.6×27.9 cm) مع ترك حاشية بمسافة انج واحد لكل طرف من اطراف الصفحة ومطبوعة بأستعمال برنامج (Microsoft Word, 2007 او 2010) بصيغة (.doc) اضافة الى نسخة الكترونية لأصل البحث مخزنة على قرص (CD).
2. يرفق مع البحث ملخص باللغة الإنجليزية على ان لاتزيد كلمات الملخص عن (150) كلمة.
3. عدد صفحات البحث لاتتجاوز 10 صفحة بضمنها الاشكال والجداول على ان تكون الاحرف بقياس 14 نوع (Time New Roman) وبمسافة مزدوجة بين الاسطر. وينبغي ترتيب اجزاء البحث دون ترقم وبالخط العريض (Bold) كالاتي: صفحة **العنوان، الخلاصة باللغة العربية، الخلاصة باللغة الإنجليزية، مقدمة، المواد وطرائق العمل (الجزء العملي)، النتائج والمناقشة، الاستنتاجات وقائمة المراجع.**
4. يطبع عنوان البحث واسماء الباحثين (كاملة) وعناوينهم باللغتين العربية والانكليزية أضافة الى البريد الاليكتروني للباحث الرئيس وتطبع على ورقة منفصلة شرط ان لاتكتب اسماء الباحثين وعناوينهم في أي مكان اخر من البحث ، وتعاد كتابة عنوان البحث فقط على الصفحة الاولى من البحث.
5. ترقم الجداول والأشكال على التوالي حسب ورودها في المتن، وتزود بعناوين، ويشار إلى كل منها بالتسلسل ذاته في متن البحث.

6. يشار الى المصدر برقم يوضع بين قوسين بمستوى السطر نفسه بعد الجملة مباشرة وتوضع بين قوسين كبيرين مثلاً [1] وفي حالة وجود اكثر من مصدر وبتسلسل فيكتب من الراقم الاول الى الاخير مثلاً [1-4]. تطبع المصادر على ورقة منفصلة ، ويستعمل الاسلوب الدولي المتعارف عليه عند ذكر مختصرات اسماء المجلات.

7. يتبع الاسلوب الاتي عند كتابة قائمة المصادر على الصفحة الاخيرة كالاتي: ترقيم المصادر حسب تسلسل ورودها في البحث ، يكتب الاسم الاخير (اللقب) للباحث او الباحثين ثم مختصر الاسمين الاولين فعنوان البحث ، اسم المجلة ، المجلد ، العدد ، الصفحات الاولى والاخيرة ، سنة نشر. . وفي حالة كون المصدر كتابا يكتب بعد اسم المؤلف او المؤلفين عنوان الكتاب ، الطبعة ، الصفحات ، اسم دار النشر، الدولة واخيراً سنة النشر.

المـــحتـــويـات

مجلة علوم المستنصرية
المجلد 27، العدد 2، 2016

journal homepage:www.mjs-mu.com

عزل وتشخيص بعض انواع الخمائر من ثمار واوراق وتربة بعض النباتات

[1]بادية عبدالرزاق ملاعبيدة، [2]رافعة قادر جرجيس، [2]رعد حساني سلطان
[1] قسم علوم الحياة / كلية العلوم / جامعة الموصل، [2] قسم علوم الحياة / كلية التربية للعلوم الصرفة / جامعة الموصل

Articleinfo.

تقديم البحث:
2015/5/31
قبول البحث:
2016/1/3

الخلاصة

تضمنت الدراسة الحالية عزل 251 عزلة محلية من الخمائر خلال ثلاثة اشهر ابتداء من تاريخ 4 / 2 / 2013 من مصادر نباتية مختلفة في مدينة الموصل. وقد تم تشخيص العزلات بالاعتماد على الاختبارات المظهرية والمزرعية والكيموحيوية وجرى تأكيد التشخيص باستعمال اختبار الـ API 20C. واظهرت النتائج انها تعود الى 16 نوع مختلفا من الخمائر *Rhodotorula graminis*، *Candida magnolia*، *Kodamaea ohmeri*، *Kleockera apiculata*، *C. lusitaniae*، *R. mucilaginosa* 1، *R. mucilaginosa* 2، *C. albicans* 1، *Cryptococcus humicola*، *R. minuta*، *R. glutinis*، *C. pelliculosa*، *Crypto. albidus*، *Stephanoascus ciferrii*، *Saccharomyces cerevisiae*.

ABSTRACT

The present study includes a collection of 251 local yeast isolates during three months starting from 4/2/2013 from different plant sources in Mosul city.These isolates were identified depending on morphological, cultural characteristics and biochemical tests. And their identification was confirmed by API 20 C (Analytic Profile Index) test. The resuls revealed that isolates belonged to 16 different species from yeasts *Rhodotorula graminis*, *Candida magnolia*, *Kodamaea ohmeri*, *Kleockera apiculata*, *C. lusitaniae*, *R. mucilaginosa* 1, *R. mucilaginosa* 2, *C. albicans* 1, *Cryptococcus humicola*, *R. mucilaginosa*, *R. minuta*, *R. glutinis*, *C. pelliculosa*, *Crypto. albidus*, *Stephanoascus ciferrii* and *Saccharomyces cerevisiae*.

المقدمة

تعتبر النباتات (أسطح الثمار, الأزهار, الأوراق والحبوب) بيئات شائعة لنمو الخمائر، تنمو على أسطح أوراق النباتات و تحصل على غذائها من إفرازات هذه الأوراق [1-2]. ان تواجد الخمائر يتوقف على توفر المادة العضوية، الرطوبة والمصدر الكاربوني بصوره المتعددة (سكر، احماض دهنية، كحولات وكاربوهيدرات) وهذا يعني انها تبدي تخصصا نوعيا بالنسبة لإماكن تواجدها [3] أشارت العديد من الدراسات إلى إمكانية عزل الخمائر من الثمار, الأزهار والأوراق [4-5-6]. تستقبل التربة والماء كل أو معظم العناصر الغذائية من مصادر خارجية مثل النباتات والحيوانات والمواد الناتجة عن نشاط الإنسان والتي تعتبر مصدرا غذائيا للخمائر ولذلك فان مجموعة الخمائر التي توجد في التربة تتغير في أعدادها وأنواعها حسب كمية ونوع المواد الغذائية التي تصل إليها، غير أن هناك أجناس كثيرة من الخمائر التي تسود في التربة بصفة دائمة وتختلف الخمائر المعزولة من التربة تبعا لنوع التربة ونسبة الرطوبة وكذلك تبعا لنوع المحصول المزروع على التربة [1]، إذ عزلت العديد من أنواع الخمائر من التربة مثل *S. exigus*، *S. rosinii*، *R. minuta* [7] *Pichia segobiensis*، *Trichosporon porosum*، *Crypto. pdzolicus* [8] و*S. cerevisiae* [9]. الهدف من البحث عزل وتشخيص الخمائر المتواجدة في البيئة المحلية وتحديد البيئات التي يمكن الحصول منها على الخمائر المطلوبة في العديد من الصناعات التي تعتمد عليها التقنية الحيوية.

المواد وطرائق العمل:

جمع عينات المصادر النباتية

جمعت مصادر نباتية مختلفة تضمنت ثمار الفاكهة اوراقها وتربتها والتي تم الحصول عليها من الاسواق المحلية لمدينة الموصل وكذلك من الحدائق المنزلية وحدائق جامعة الموصل.

عزل الخمائر Isolation of Yeasts

عزلت الخمائر من ثمار نباتات مختلفة بالإضافة الى أوراقها وفقا لما متبع في عزل الخمائر [3-4-5].

الاختبارات التشخيصية Identification Tests

الصفات المظهرية للمستعمرات والفحص المجهري

زرعت العزلات بطريقة التخطيط على الوسط الغذائي وسط مستخلص الشعير المنقوع Malt Extract Agar Medium (MEA) وحضنت عند درجة 28°م لمدة 48 ساعة تم تسجيل الملاحظات المتعلقة بالصفات المظهرية، وفحصت تحت المجهر الضوئي عند القوى 40X لملاحظة شكل الخلايا الخميرية [6].

اختبار أزرق الديازونيوم Diazonium Blue B (DBB) Color test

تم اجراء هذا الاختبار بتنميت الخمائر المعزولة على الوسط الغذائي MY Agar وحضنت عند درجة حرارة 28°م لمدة 10 أيام لحين تكون الأكياس في الخمائر الكيسية [7].

اختبار النمو في درجة حرارة 25 و37°م
زرعت الخمائر على الوسط الغذائي الصلب MEA بطريقة التخطيط، حضنت عند درجة حرارة 25 و37°م ولمدة 3-7 أيام. تسجل النتيجة سلبية عند غياب النمو أو ايجابية وجود نمو [6].

اختبار قابلية الاستفادة من النترات كمصدر وحيد للنتروجين و تحديد القدرة على مقاومة حامض الخليك الثلجي
تم اجراء هذين الاختبارين بزراعة الخمائر على الوسط الغذائي الصلب MEA بطريقة التخطيط، حضنت عند درجة حرارة 25 و37°م ولمدة 3-7 أيام [6].

قابلية النمو في المستويات المنخفضة من الماء مع الارتفاع في مستوى الكاربوهيدرات وقابلية النمو في المستويات المنخفضة من الماء مع زيادة في مستوى كلوريد الصوديوم
بنقل جزء من مزرعة كل عزلة من الخمائر قيد الدراسة وزراعتها بطريقة التخطيط على سطح أطباق بتري معقمة تحتوي على الوسط الغذائي الصلب Czapek agar. حضنت عند درجة حرارة 28°م لمدة 3-7 أيام [6].

اختبار قدرة الخمائر على تشكيل المايسليوم Mycelium Formation Test
لتحديد وجود المايسيلوم وشكله سواء أكان حقيقيا True$Mycelium أم كاذبا Pseudomycelium [7].

اختبار نظام API 20C
اجري هذا الاختبار طبقا لتعليمات الشركة المجهزة Biomerieux .

النتائج والمناقشة :

العزل Isolation
أظهر نمو المستعمرات على الاوساط المستخدمة للعزل وجود 251 عزلة خميرة، إذ بلغ اعلى عدد من العزلات (23) ضمن ثمار التمر في حين كان اقل عدد (2) عزلة من ثمار كل من الكيوي، البرتقال الأمريكي والعرموط. في حين اظهر العزل من اوراق الاشجار وجود 28 عزلة تمثلت بعزلات اوراق الزيتون(السليمة والمصابة) 14عزلة، فضلاً عن 3 عزلات من اوراق اشجار التين. بينما كان عدد العزلات من التربة 8 والتي اشتملت على المنطقة المحيطة لجذور السعد (6) عزلات وعزلة لكل من جذور الزيتون والتين (الجدول 1). جاءت نتائج العزل هذه متفقة مع الكثير من الدراسات التي تشير إلى أن الخمائر تنتشر في الطبيعة انتشارا واسعا، إذ إنها تتواجد في التربة، على السطح الخارجي للفاكهة، أوراق النباتات، وجذوعها [15]. إن هذا الانتشار الكبير للخمائر في أوساط بيئية وغذائية مختلفة قد ثبت فيها على اختلاف أنواعها وأماكن تواجدها صفات مهمة منها تحمل الحرارة والتركيز السكري وتختلف الأغذية من حيث محتواها من الخمائر، إن للنشاط المائي تأثيراً كبيراً على وجود الخمائر، إذ إن انخفاض النشاط المائي إلى حد كبير يؤدي الى اختفاء الخمائر، إذ إنه من المعروف أن الخمائر تحتاج الى رطوبة عالية أو نشاط مائي عالي نسبيا [16].

الجدول (1): مصدر عزل الخمائر واعداد العزلات

مصدر العزل		اسماء العزلات	المجموع
ثمار		BA1، BA2، BA3، BA4، BA5، BA6، BA7، BA8، BA9، BA10، BA11، BA12، BA13، BA14، BA15، BA16، BA17، BA18، BA19، BA20، BA21، BA22، BA23	23
الاناس		BA24، BA25، BA26، BA27، BA28، BA29، BA30	7
فراولة		BA31، BA32، BA33، BA34، BA35، BA36، BA37، BA38، BA39، BA40، BA41، BA42، BA43، BA44، BA45	15
تفاح أحمر		BA46، BA47، BA48، BA49، BA50، BA51، BA52، BA53، BA54	9
يوسفي		BA55، BA56، BA57، BA58، BA59، BA60، BA61، BA62، BA63، BA64، BA65، BA66، BA67، BA68، BA69، BA70، BA71، BA72، BA73، BA74	20
تمر تين		BA75، BA76، BA77، BA78، BA79، BA80، BA81، BA82	8
سعوط		BA83، BA84، BA85، BA86، BA87، BA88، BA89، BA90، BA91، BA92، BA93، BA94، BA95، BA96، BA97، BA98، BA99	17
تارنج		BA100، BA101، BA102، BA103، BA104، BA105، BA106، BA107، BA108، BA109، BA110، BA111، BA112، BA113، BA114	15
ليمون حامض		BA115، BA116، BA117، BA118، BA119	5
موز		BA120، BA121، BA122، BA123، BA124، BA125، BA126	7
زيتون		BA127، BA128، BA129، BA130، BA131، BA132، BA133، BA134، BA135، BA136، BA137، BA138، BA139، BA140، BA141، BA142، BA143، BA144	21
كريب فروت		BA145، BA146، BA147، BA148، BA149، BA150، BA151	4
خوخ		BA152، BA153، BA154، BA155، BA156، BA157، BA158، BA159، BA160، BA161، BA162، BA163، BA164، BA165، BA166، BA167، BA168، BA169، BA170، BA171، BA172، BA173	22
برتقال		BA174، BA175، BA176، BA177، BA178، BA179، BA180، BA181، BA182، BA183	10

مصدر العزل		اسماء العزلات	المجموع
تفاح اصفر		BA184، BA185، BA186، BA187، BA188، BA189، BA190	7
كيوي		BA191، BA192	2
عنب		BA193، BA194، BA195، BA196، BA197، BA198	6
رمان		BA199، BA200، BA201، BA202، BA203، BA204، BA205، BA206، BA207، BA208، BA209، BA210، BA211	13
برتقال امريكي		BA212، BA213	2
عرموط		BA214، BA215	2
اوراق زيتون سليمة		BA216، BA217، BA218، BA219، BA220، BA221، BA222، BA223، BA224، BA225، BA226، BA227، BA228، BA229	14
اوراق زيتون مصابة		BA230، BA231، BA232، BA233، BA234، BA235، BA236، BA237، BA238، BA239، BA240	11
اوراق تين		BA241، BA242، BA243	3
تربة زيتون		BA244	1
تربة تين		BA245	1
جذور نباتات السعد		BA246، BA247، BA248، BA249، BA250، BA251	6
المجموع			251

التشخيص Identification

الصفات المزرعية Coltural Characteristies
اوضحت الصفات المظهرية للمستعمرات النامية على وسط MEA بالإضافة الى الفحص المجهري كتشخيص اولي وجود عدد من العزلات تعود لنفس النوع، لذلك وقع الاختيار على 16 عزلة (جدول2، الشكل1). وجاءت الصفات التشخيصية الاولية لهذه العزلات مطابقة لما ورد ذكره [13-14-17].

الجدول (2) : اختبارات الصفات المظهرية لمستعمرات الخمائر

العزلة	الصفات المظهرية							
	لون المستعمرة	شكل المستعمرة	قطر المستعمرة (ملم)	هيئة حافات المستعمرة	ارتفاع المستعمرة	قوام المستعمرة	لمعان المستعمرة	شكل سطح المستعمرة
R. graminis BA1	ارجواني	منتظمة	2.0	غير منتظمة	مسطحة قليلة التحدب	زبدية	معتمة	ناعم الملمس
C. magnoliae BA13	ابيض	زهرية الشكل	17.1	مهدبة	مسطحة مرتفعة المركز	غشائية قطنية	معتمة	خشن
Kod. ohmeri BA26	كريمي	مفصصة	3.0	مسننة	محدبة	زبدية	معتمة	خشن
Klo apiculata BA28	كريمي	دائرية	2.6	ناعمة كاملة	محدبة	زبدية	لامعة	ناعم الملمس
C. lusitaniae BA 32	كريمي	دائرية	2.4	ناعمة كاملة	مرتفعة	زبدية	معتمة	ناعم الملمس
R. mucilaginosa BA58	برتقالي	دائرية	3.2	ناعمة كاملة	محدبة	لزجة	لامعة	ناعم الملمس
R. mucilaginosa BA61	برتقالي	دائرية	1.9	ناعمة كاملة	محدبة	مخاطية	لامعة	ناعم الملمس
C. albican 1 BA69	ابيض	دائرية	2.8	ناعمة كاملة	محدبة	زبدية	معتمة	ناعم الملمس
Crypto. humicola BA73	كريمي	مفصصة	3.1	مسننة	مرتفعة	زبدية	معتمة	خشن
R. mucilaginosa BA75	برتقالي	دائرية	2.3	ناعمة كاملة	محدبة	جلدية	معتمة	مجعد
R. minuta BA78	برتقالي فاتح	مستطيلة متشعبة	9.9	مسننة	مسطح	مخملية	معتمة	خشن
R. glutinis BA83	ارجواني	دائرية	3.5	غير منتظمة	محدبة	زبدية	معتمة	ناعم الملمس
C. pelliculosa BA100	ابيض	غير منتظمة	17.1	مهدبة	مسطحة مرتفعة المركز	غشائية قطنية	معتمة	خشن
Crypto. albidus BA148	كريمي	دائرية	1.3	ناعمة كاملة	مرتفعة	زبدية	لامعة	ناعم الملمس
Steph. ciferrii BA163	كريمي	منتظمة	2	ناعمة كاملة	محدبة	طباشيرية	معتمة	خشن
S. cerevisiae BA179	كريمي	منتظمة	2.4	ناعمة كاملة	مرتفعة المركز	زبدية	لامعة	ناعم الملمس

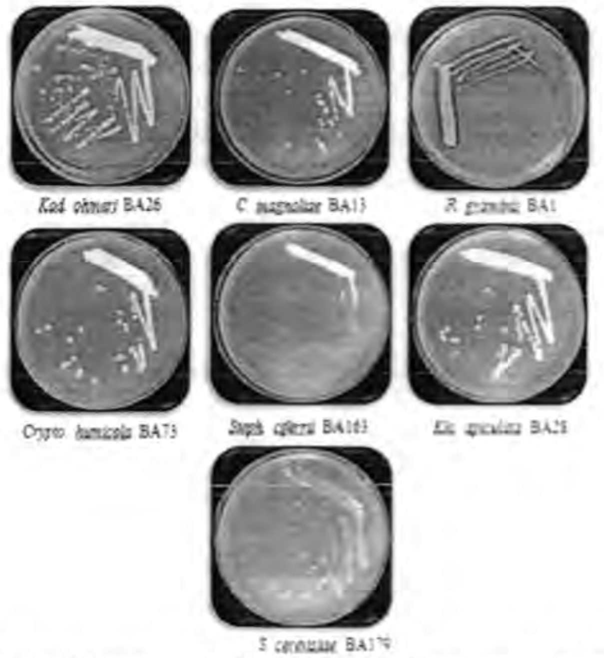

الشكل (1): الصفات المظهرية لمستعمرات الخمائر المعزولة والمنماة على وسط MEA وبعمر 48 ساعة

الفحص المجهري

اظهرت نتائج الفحص المجهري للعزلات تباينا واضحا فيما بينها (جدول 3) والتي كانت اشكال خلاياها متبرعمة، كروية، بيضوية او متطاولة ليمونية والبعض عصوي وبأحجام مختلفة. هذه النتائج جاءت متوافقة مع المعلومات الموثقة من قبل المصادر التصنيفية [13-14- 17].

اختبار قدرة الخمائر على تشكيل المايسليوم

بينت نتائج الدراسة الحالية قدرة 11 عزلة (68.75 %) على اعطاء المايسليوم الكاذب في حين أظهرت النتائج قدرة عزلتين (*C. albican* 1 BA69 و *Steph. ciferrii* BA163) وبنسبة 12.5% على تكوين المايسليوم الحقيقي، وتباينت عزلات اخرى *R. graminis* BA1 و *C. lusitaniae* BA 32 و *Kod. ohmeri* BA26 18.75% بقدرتها على اعطاء المايسليوم فبعضها كون مايسليوم حقيقي True Mycelium وبعضها الاخر كون مايسليوم كاذب Pseudomycelium. تعتبر هذه الخاصية متباينة لدى هذه الانواع من الخمائر وتوافقت هذه النتائج مع المصدر التشخيصي [14].

اختبار القدرة على النمو في درجات حرارية مختلفة

أوضحت نتائج هذا الاختبار قدرة جميع عزلات الخمائر 16 عزلة (100%) قيد الدراسة على النمو عند درجة حرارة 25°م في حين اظهرت النتائج قدرة 11 عزلة (68.75%) على النمو عند 37°م (الجدول 4)، إذ نمى بعضها وبشكل ضعيف 3 عزلات 18.75% (*C.* BA13 *magnolia*، *R. mucilaginosa* BA58، *R. mucilaginosa*1 BA75) والبعض الاخر 8 عزلات 50 % (*Kod. ohmeri* BA26، *C. lusitaniae* BA32، *R. mucilaginosa* BA61، *C. albicans* 1 BA69، *R. minuta* BA78، *Crypto. albidus* BA148، *Steph. ciferrii* BA163، *S. cerevisiae* BA17) أبدت استجابة واضحة من خلال النمو عند هذه الدرجة الحرارية. جاءت النتائج الحالية مقاربة لدراسة اخرى في هذا المجال لمجموعة من عزلات الخمائر ضمن درجات حرارية متنوعة [18].

قابلية الاستفادة من النترات كمصدر وحيد للنتروجين

لوحظ أن 14 عزلة (87.5%) استطاعت الاستفادة من النترات كمصدر وحيد للنتروجين رغم تفاوت القدرة على الاستفادة منه. اما العزلتان الباقية (12.5%) فكانت سالبة للاختبار (الجدول 4). وهذا يتفق مع ما توصل اليه دراسات اخرى لدى تشخيصهم مجموعة من الخمائر [15 -16].

الجدول (3): نتائج الفحص المجهري لعزلات الخمائر المدروسة

العزلة	نوع الفحص المجهري		
	شكل الخلية	ابعاد الخلية (مايكرومتر)	اختبار تشكيل المايسليوم
R. graminis BA1	كروية – ليمونية	13.9	+ / -
C. magnoliae BA13	بيضوية متطاولة	7.9×14.0	-
Kod. ohmeri BA26	كروية – ليمونية	9.6	+ / -
Klo. apiculata BA28	بيضوية صغيرة	8.8×15.6	-
C. lusitaniae BA 32	كروية – ليمونية	9.6	+ / -
R. mucilaginosa BA58	بيضوية	8.6×16.3	-
R. mucilaginosa BA61	بيضوية متطاولة (اسطوانية)	8.3 ×15.6	-
C. albican 1 BA69	ليمونية – بيضوية	7.7×15.2	+
Crypto. humicola BA73	بيضوية صغيرة	7.3 ×10.7	-
R. mucilaginosa BA75	كروية	9.0	-
R. minuta BA78	عصوية	9.4×19.5	-
R. glutinis BA83	كروية – ليمونية	9.4	-
C. pelliculosa BA100	بيضوية متطاولة	9.2–17.8	-
Crypto. albidus BA148	كروية	12.47	-
Steph. ciferrii BA163	عصوية صغيرة	7.0×11.8	+
S. cerevisiae BA179	كروية – ليمونية صغيرة	7.3	-

الخلايا الكروية والليمونية الشكل تم حساب قطر الخلية، اما الاشكال الاخرى من الخلايا فقد تم حساب الطول × العرض. (-): مايسليوم كاذب، (+): مايسليوم حقيقي، (- / +): بعضها تشكل مايسليوم كاذب وبعضها الآخر يشكل مايسليوم حقيقي.

تحديد القدرة على مقاومة حامض الخليك الثلجي

جاءت نتائج هذا الاختبار لتبين ان 11 عزلة (68.75 %) كانت موجبة لهذا الاختبار اما العزلات الباقية وعددها 5 عزلات (13.25%) أظهرت نتيجة سالبة لهذا الاختبار(الجدول 4) وهذا يتفق مع المصدر التشخيصي [13].

تحديد قابلية النمو في المستويات المنخفضة من الماء مع الارتفاع في مستوى الكاربوهيدرات

كشفت النتائج الحالية ان 11عزلة (68.75%) كانت سالبة للاختبار، بينما كانت 5 عزلات (13.25%) موجبة للاختبار(الجدول 4).

تحديد قابلية النمو في المستويات المنخفضة من الماء مع زيادة مستوى كلوريد الصوديوم

بينت النتائج ان 4 عزلات (25%) كانت سالبة للاختبار في حين كانت 12 عزلة (75%) موجبة للاختبار وذات نمو كثيف ماعدا الخميرة BA148 *Crypto. albidus* التي ابدت نمو ضعيف (الجدول 4). وجاءت هذه النتيجة مقاربة لما ذكره المصدر التشخيصي [13].

اختبار Diazonium Blue B (DBB) Color test

بينت النتائج أنه من بين 16 عزلة من الخمائر المختبرة كانت 8 عزلات (50%) موجبة لهذا الاختبار في حين كانت 8 عزلات سالبة (50%) كما موضح في الشكل (2). هذه الصفات متوافقة مع ما جاء في المصدر التشخيصي [14]، إذ ذكر ان هذا الاختبار يستعمل بشكل واسع في التمييز بين الخمائر الكيسية والبازيدية.

الجدول (4): نتائج اختبارات التشخيص الكيموحيوي لعزلات الخمائر قيد الدراسة

العزلة	نوع الاختبار: القدرة على النمو عند 25° م	عند 37° م	بوجود النتريت كمصدر (N)	بوجود حامض الخليك الثلجي	بمستوى ماء منخفض على الكاربوهيدرات	بمستوى ماء منخفض وعلى 5 NaCl	اختبار DBB
R. graminis BA1	+++	-	+	+++	-	+	-
C. magnoliae BA15	+++	+	+	+++	+	+++	-
Kod. ohmeri BA26	+++	+++	+++	+++	+	+++	-
Klo. apiculata BA28	+++	-	+	-	-	-	-
C. laitaniae BA32	+++	+++	++	+++	+	+++	-
R. mucilaginosa BA58	+++	+	++	-	-	-	-
R. mucilaginosa BA61	+++	+++	++	+++	++	+++	-
C. albicans BA69	+++	+++	+	+++	++	+++	-
Crypto. humicola BA73	+++	-	++	+++	-	+++	-
R. mucilaginosa BA76	+++	+	++	-	-	-	-
R. minuta BA78	+++	-	+++	+++	-	+++	-
R. glutinis BA83	+++	-	+	+++	-	+++	-
C. pelliculosa BA100	+++	-	-	+++	-	+++	-
Crypto. albidus BA148	+++	+++	++	-	-	+	-
Sugiy. ciferii BA151	++	+++	-	+++	-	+++	-
S. cerevisiae BA175	+++	+++	-	++	-	-	-

(-): لا يوجد نمو، (+): نمو ضعيف، (++): نمو متوسط، (+++): نمو جيد كثيف، (•): نتيجة ايجابية، (•): نتيجة سلبية

الشكل (2): نتائج اختبار ازرق الديازونيوم Diazonium Blue B Color (DBB) لمستعمرات الخمائر المعزولة والمنماة على وسط MY Agar لمدة 10 أيام

الاختبار التأكيدي الكيموحيوي باعتماد فحص API 20 C

النتائج التي تم الحصول عليها من خلال التغيرات اللونية والكيميائية لأنابيب الاختبار الدقيقة ميزت بين انواع الخمائر الـ (16) قيد الدراسة وشخص العزلة *R. mucilaginosa* BA75 و *R. mucilaginosa* BA61 الى 1 و 2، على التوالي بحسب هذا الاختبار. باستثناء الجنس *R. graminis* BA1 الذي لم يتم تحديده من خلال هذا الفحص. توافقت هذه النتائج مع ما جاء في دراسة مع دراسة اخرى [19- 20- 21-22-23].

الاستنتاجات

في ادناه اهم الاستنتاجات التي افرزتها الدراسة الحالية:

- ✓ بينت نتائج العزل ان البيئة المحلية (ثمار واوراق النباتات والتربة) تعد مصدرا غنيا لأنواع مختلفة من الخمائر.
- ✓ أظهرت العزلات تغايرا كبيرا في الصفات المظهرية للمستعمرات.

المصادر:

1- Pollock, T.J. Pullulan from polymorphic Aureobasidium pullulans SIM Ind. Microbial. News.,42: 147-155, (1992).

2- James, S.A.; Barriga, E.J.C.; Barahona, P.P.; Harrington, T.C.; Lee, C.F.; Bond, C.J. and Roberts, I.N. Wickerhamoyces arborarius f.a., -sp. No., an ascomycetous yeast species found in arboreal habitats in three different continents. International Journal of Systematic and Envolutionary Microbiology, 64: 1057-1061, (2014).

3- Maragatham, C. and Panneerselvam, A. Isolation, Identification and characterization of wine yeast from rotten papay for win production. Advances in Applied Science Research, 2(2): 93-98, (2011).

4- Mokhtari, M.; Etebarian, H.; Mirhendi, S.H. and Razavi, M. Identification and phylogeny of some species of the genera *Sporidiobolus* and *Rhodotorula* using analysis of the 5.8S RDNA gene and two ribosomal internal transcribed spacers. Arch. Biol. Sci., Belgrade, 63(1): 79-88, (2011).

5- El-Banna, A.A.; Abd-El-Razek, A.M. and El-Mahdy, A.R. Isolation, Identification and screening of carotenoid-producing strains of *Rhodotorula glutinis*. Food and Nutrition Sciences, 3: 627-633, (2012).

6- Yurkov, A. M.; Kachalkin, A. V.; Daniel, H. M.; Groenewald, M.; Libkind, D.; de Garcia, V.; Zalar, P.; Gouliamova, D. E.; Boekhout, T. and Begerow, D. Two yeast species *Cyctobasidium psychroaquaticum f.* a. sp. nov. and *Cystobasidium rietchieii f.* a. sp. nov. isolated from natural environments, and the transfer of *Rhodotorula minuta* clade members to the genus *Cystobsidium*. Antonie Van Leeuwenhoek Journal of Microbiology, 107(1): 173-185, (2015).

7- Ali, M.N. and Khan, M.M. Screening, identification and characterization of alcohol tolerant potential bioethanol producing yeasts. Current Research in Microbiology and Biotechnology, 2(1): 316-324, (2014).

Schulze, I.; Hansen, S.; Gro Bhans, S.; Rudszuck, T.; Ochsenrither, K.; Syldatk, C. and Neumann, A. Characterization of newly isolated oleaginous yeasts-*Cryptococcus podzolicus*, *Trichosporon porosum* and *Pichia segobiensis*. AMB Express, 4:24, (2014).

9- صوفي، بلقيس يحيى نجم. دراسة تشخيصية ووراثية جزيئية للخميرة من جنس الـ *Saccharomyces* المعزولة من مصادر مختلفة في مدينة الموصل، اطروحة دكتوراه، كلية التربية، جامعة الموصل، العراق، (2013).

10- Assis, S.M.P. and Mariano, R.L.R. Antagonism of yeasts to *Xanthomonas campestris* pv. Campestris on cabbage phylloplane in field. Rev. Microbiol., 30: 191–195, (1999).

11- Pan, L. X. ; Yang, D. F. ; Shao, L. ; Li, W. ; Chen, G. G. and Liang, Z. Q. Isolation of the oleaginous yeasts from the soil and studies of their lipid-producing capacities. Food Technol. Biotechnol., 47(2): 215-220, (2009).

12- بريشة، جابر زايد. الخمائر : تقنيات إنتاجها ودورها في الصناعة وفساد الاغذية وصحة الانسان (الطبعة الاولى)، 493 صفحة، جامعة الملك سعود، الرياض، المملكة العربية السعودية، (2010).

13- Pitt, J.I. and Hocking, A.D. Fungi And Food Spoilage. Springer Dordrecht Heidelbery London New York, (2009).

14- Kurtzman, C.P. and Fell, J.W. The yeasts, A Taxonomic Study.4th ed., Elsevier Science B.V., The Netherland, (1998).

15- صدقي، غازي سليم. مساهمة في تحديد الخمائر المنتشرة على بعض الفاكهة السورية. مجلة جامعة دمشق للعلوم الزراعية، 16(2):79-89، (2000).

16- الخفاجي، زهرة محمود ، سناء برهان الدين النعمة، الخفاجي وشذى سلمان العزواي. دراسة للخمائر الشائعة لمنطقة بغداد 2: منتجات الحبوب والبقول الجافة، المجلة العراقية للاحياء المجهرية، 4 (1 ،2): 54 -60، (1992).

17- Deák, T. Handbook of Food Spoilage Yeasts (second Edition). CRC Prees Taylor and Francis Group. Boca Raton London New York, (2008).

18-Kirsop, B. E. and Kurtzman, C.P. Living resources for biotechnology " Yeasts " Cambridge Univ. Press. Cambridge, (1988).

19- Willemsen, M. ; Breynaert, J. and Lauwers, S. Comparison of auxacolor with API 20 C Aux in yeast identification. Clinical Microbiology and Infection, 3(3): 369-375, (1997).

20- اليازجي، صباح ; الحاج علي، انور وهدال، احمد. تحري الخمائر والفطور الملوثة للبن الرائب المنتج في بعض المحافظات السورية وتشخيصها. مجلة جامعة دمشق للعلوم الزراعية، 26 (1): 261-275، (2010).

21- Csutak, O. and Vassu, T. Phylogenetic analysis and characterization of an alkane –polluted yeast strain isolated from oil – polluted soil. Turkish Journal of Biology, 38: 601-610, (2014).

22- مثلاء، روضة ; يازجي، صباح والحاج علي، انور. قياس فعالية الإنفرتاز في عزلات خمائر من مواد سكرية محلية مختلفة. مجلة جامعة دمشق للعلوم الزراعية، 40 (1): 239-251، (2014).

23- Nadăş, G. C.; Kalmár, Z.; Taulescu, M. A.; Chirilă, F.; Bouari, C. M.; Răpuntean, S.; Bolfa, P. and Fiţ, N. I. Comparative identification of *Candida* species isolated from animals using phenotypic and PCR-RFLP methods. Bull. Vet. Inst. Pulawy., 58:219-222, (2014).

مجلة علوم المستنصرية
المجلد 27، العدد 2، 2016

journal homepage:www.mjs-mu.com

دراسة تصميمية لأنعكاسية الحرارة للمرآيا الباردة العازلة (TiO_2/SiO_2)

الهام جاسم محمد
الجامعة المستنصرية, كلية العلوم, قسم الفيزياء

Articleinfo.

تقديم البحث:
2015/5/6
قبول البحث:
2015/9/7

الخلاصة

في هذا البحث تم أجراء دراسة نظرية لتصميم غشاء رقيق متعدد الطبقات للمرآة الباردة من خلال برنامج نظري تم فيه حساب الانعكاسية (R), الامتصاصية (A), النفوذية (T), تأخر المجموعة (GD), تشتت تأخر المجموعة (GDD), المجال الكهرياني, المخطط الدائري والسماحية البصرية.
المواد المستخدمة في هذا التصميم هي مادة ثاني أكسيد التيتانيوم (TiO_2) ومادة ثاني آكسيد السيليكون (السيليكا) (SiO_2), وبالاعتماد على مبدأ التناوب الترتيبي في معاملات الانكسار العالي والواطئ, حيث اعتمدت هذه المواد في تصميم المرآة الباردة ضمن نطاق الطول الموجي (300-1000) نانومتر وترسيب هذه المواد على ركائز من مادة الفيوزد سيليكا (Fused-silica).
في التركيب متعدد الطبقات المستخدم في هذا البحث، بدأت عملية التصميم مع طبقة واحدة رقيقة من ثاني آكسيد التيتانيوم ومن ثم تم زيادة سمك و عدد الطبقات في التصميم. وبعد اجراء عملية اعادة التشذيب (re-Optimize) للتصميم، تم التوصل الى التصميم المقبول والمؤلف من (21) طبقة. لكن الصعوبة القصوى التي تترافق مع هذا النوع من الطلاء, هو تصميم طلاء عاكس. وبعد اتمام تصميم عاكس مقبول، يمكن تحقيق وظيفة المرآة الباردة حيث انها تعكس الأطوال الموجية القصيرة وتسمح بمرور الاطوال الموجية الطويلة.

ABSTRACT

This research was studied the theory design of thin film multilayer cold mirror using a theoretical program to account the reflectivity (R), transmission (T), permeability, group delay (GD), group delay dispersion (GDD), electric field, circle diagram and optical permittivity.
Materials which used in this design is titanium dioxide (TiO_2) and silicon dioxide (silica) (SiO_2), was arranged as high and low refractive index. These materials were adopted in the cold mirror design within the wavelength range (300-1000) nm and deposition on Fused-silica substrates.
Multilayer which used in this research, the design process began with a thin single layer of titanium dioxide and then increased the thickness and number of layers in the design. After a re-optimization process, the design was reached unacceptable design which contend (21) layer. But the extreme difficulty with this coting type is the reflector coting design. After the completion of the reflector design was acceptable, it is usually easy to achieve the cold mirror function, where it's reflects the short wavelengths and transmits long wavelength.

المقدمة

تعتبر المرآة الباردة بشكل خاص مرآة عازلة، حيث تعمل على عكس طيف الضوء المرئي وتسمح للاشعة تحت الحمراء من النفوذ خلالها. ويمكن ضبط وضعية المرايا الباردة داخل المنظومة البصرية, بوضع يسمح لها بصنع زاوية (0^o) او (45^o) كما هو مبين في التصاميم الموضحة في الشكل (1) والشكل (2)، ويتم بناؤها مع الطلاء العازل متعدد الطبقات, حيث يتم ترتيب عدة طبقات طبقات من مواد مستقطبة وبشكل متتابع, بطريقة مشابهة لبناء مرشحات التداخل الضوئي [1].

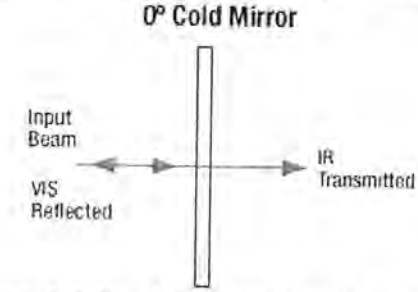

الشكل (1) مرآة باردة مصممة في حالة السقوط العامودي للضوء [1].

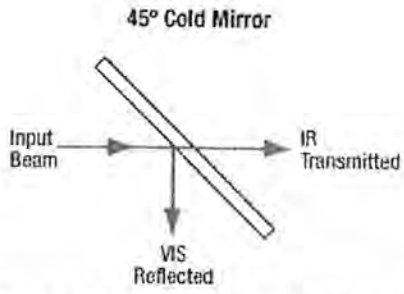

الشكل (2) مرآة باردة مصممة بزاوية سقوط (45^o) [1].

ويمكن استخدام المرآة الباردة في منظومة الليزر بهدف السماح بأنعكاس الضوء المرئي ونفوذ الاشعة تحت الحمراء دون حصول خسارة في الشدة [2].

وعلى سبيل المثال, لو اجرينا مقارنة بين المرآة الباردة نوع UV والمرآة الباردة نوع (CM-VS-STD) من خلال دراسة الرسم البياني لكلا المثالين. نلاحظ في الرسم البياني لعلاقة الطول الموجي والنفاذية للمرآة الباردة نوع UV والموضح في الشكل (3) أدناه:

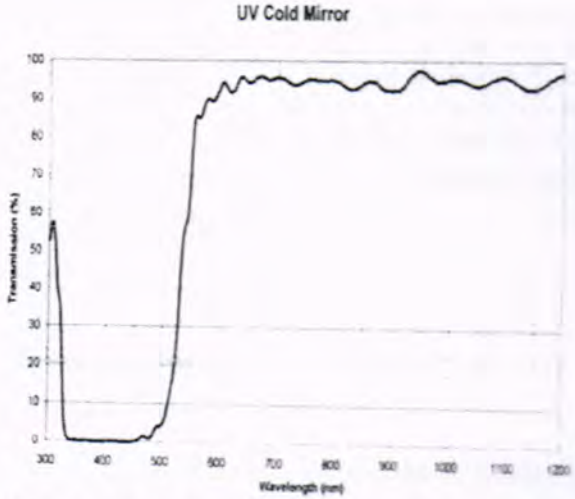

الشكل (3) علاقة الطول الموجي والنفاذية للمرآة الباردة نوع UV [1].

حيث تم ضبط وضعية المرايا الباردة داخل المنظومة البصرية, بوضع يسمح لها بصنع زاوية (45o) لتعكس أكثر من 95٪ من الأشعة فوق البنفسجية ضمن نطاق الطول الموجي (350-450) نانومتر، في حين تنفذ أكثر من 90٪ ضمن نطاق الطول الموجي (1200-550) نانومتر.
وهذا يعني أمكانية استخدام هذا الطلاء لتقسيم الشعاع والحصول على الاطوال الموجية الطويلة ضمن نطاق الطول الموجي (1200-550) نانومتر, وبالتالي امكانية عزل الحزم المطلوبة في التطبيقات العملية.
أما في المثال الثاني, المرآة الباردة نوع (CM-VS-STD) حيث تم ضبط وضعية المرايا الباردة داخل المنظومة البصرية, بوضع يسمح لها بصنع زاوية (45o)، ومن ملاحظة العلاقة البيانية الموضحة في الشكل (4) ادناه:

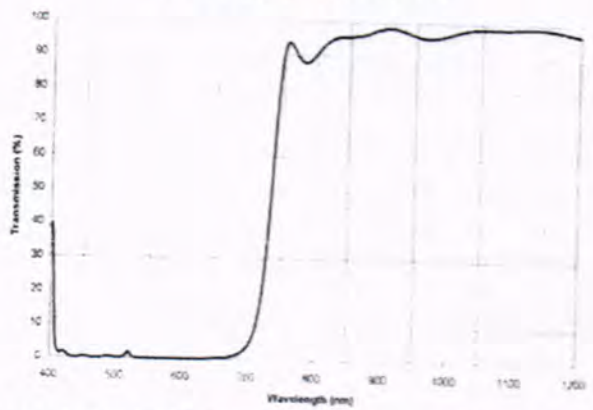

الشكل (4) علاقة الطول الموجي والنفاذية للمرآة الباردة نوع (CM-VS-STD) [1].

نرى ان متوسط الانعكاس أكبر من 95٪ ضمن نطاق الطول الموجي *(425-650)* نانومتر. ومعدل النفوذية أكثر من 85٪ ضمن نطاق الطول الموجي *(800-1200)* نانومتر.

الخصائص البصرية لتصميم المرآة الباردة

يتكون التصميم البصري من حزمة طبقات ذات السمك الفيزيائي *di (Physical Thickness)* ومعاملات الانكسار *ni* التي تشير الى معاملات الوسط الساقط ومعاملات وسط الخروج او القاعدة n_{inc} و n_{ex}، على التوالي.
ولحساب الخصائص البصرية، يتم تمثيل الطبقات *ith* بالمعادلة [3]:

$$M_i = \begin{bmatrix} \cos\varphi_i & i/\eta_i \sin\varphi_i \\ i\eta_i \sin\varphi_i & \cos\varphi_i \end{bmatrix} \quad (1)$$

حيث:

$$\eta_i = \begin{cases} n_i \cos\theta_i & s-polarization \\ n_i^2 / n_i \cos\theta_i & p-polarization \end{cases} \quad (2)$$

η_i يمثل معامل الانكسار الفعال *(Effective Refractive Index)* ويعتمد على الشعاع الساقط اذا كان مستقطب بشكل موازي او عمودي لمستوى السقوط.

ويمثل $\varphi_i = (2\pi/\lambda)N_i d_i \cos\theta_i$ سمك الطور *(Phase Thickness)*, و θ_i تمثل زاوية الانكسار، و λ هو الطول الموجي للضوء في فراغ. و وفقا للقانون سنيل فان n_i و $\sin\theta_i$، ثوابت. ويمكن حساب معامل الانكسار الفعال وفرق الطور باستخدام المعادلة [4]:

$$\eta_i = \begin{cases} \sqrt{n_i^2 - \alpha^2} & s-polarization \\ n_i^2 / \sqrt{n_i^2 - \alpha^2} & p-polarization \end{cases} \quad (3)$$

$$\varphi_i = \frac{2\pi}{\lambda}\sqrt{n_i^2 - \alpha^2}\, d_i \quad (4)$$

ان مصفوفة الخواص *(Characteristic Matrix)* التي تصف هذه الطبقات تعطى بالمعادلة:

$$M = \begin{bmatrix} m_{11} & m_{12} \\ m_{21} & m_{22} \end{bmatrix} = \prod_{i=q}^{1} M_i \quad (5)$$

حيث q هو عدد الطبقات، ويتم أخذ الناتج في ترتيب عكسي حيث المصفوفات للطبقات العليا يجب أن تضرب على اليسار. ان سعة الانعكاس r ومعاملات النفوذية t لمتعدد الطبقات تعطى بالمعادلة [5]:

$$r = \frac{\eta_{inc} m_{11} - \eta_{ex} m_{22} + \eta_{inc}\eta_{ex} m_{12} - m_{21}}{\eta_{inc} m_{11} + \eta_{ex} m_{22} + \eta_{inc}\eta_{ex} m_{12} + m_{21}} \quad (6)$$

$$t = \frac{2\eta_{inc}}{\eta_{inc} m_{11} + \eta_{ex} m_{22} + \eta_{inc}\eta_{ex} m_{12} + m_{21}} \quad (7)$$

حيث ان η_{inc} و η_{ex} هما معاملا الانكسار الفعال للوسط الساقط و وسط الخروج او القاعدة, على التوالي. والانعكاسية R والنفوذية T تعطى في المعادلات:

$$R = rr^* = |r|^2 \quad (8)$$

$$T = \frac{\mathrm{Re}\, n_{ex}}{\mathrm{Re}\, n_{inc}} tt^* = \frac{\mathrm{Re}\, n_{ex}}{\mathrm{Re}\, n_{inc}} |t|^2 \quad (9)$$

حيث ان, Re يشير الى الجزء الحقيقي و * تشير الى المرافق العقدي.
أن انعكاسية ونفاذية المرآة الباردة المصممة بزاوية سقوط (0^o او 45^o) تأخذ الاشكال الموضحة أدناه (الشكل (5) و الشكل (6)).
ونفاذية المرآة الباردة المصممة بزاوية سقوط (0^o او 45^o) تأخذ الاشكال الموضحة أدناه (الشكل (5) و الشكل (6)).

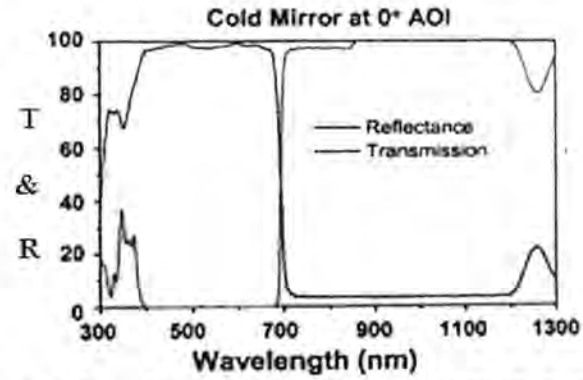

الشكل (5) الانعكاسية والنفوذية لمرآة باردة مصممة بزاوية سقوط (0^o) [1].

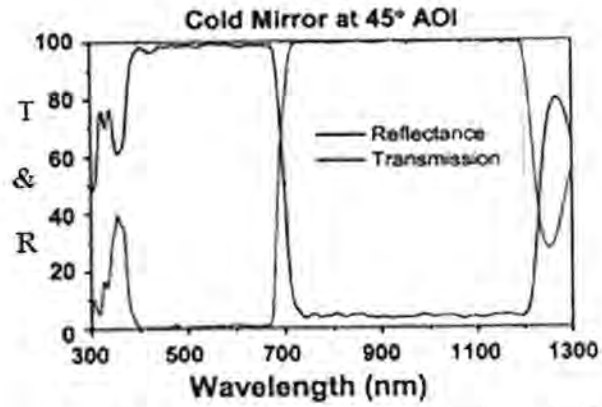

الشكل (6) الانعكاسية والنفوذية لمرآة باردة مصممة بزاوية سقوط (45^o) [1].

وعند التعامل مع رتل من النبضات *(Pulse Train)*، هنا يحتاج المرء الى التعرف على خصائص التشتت لمتعدد الطبقات. في مرحلة الطور الشامل *(Global Phase)* للانعكاسية والنفوذية، تكون 2π و ϕ_r زوايا تصنع بوجود r و t في مستو عقدي *(Complex Plane)* بحيث [5]:

$$\phi_r = \arg r = \arctan \frac{\mathrm{Im}\ r}{\mathrm{Re}\ r} \quad (10)$$

$$\phi_t = \arg t = \arctan \frac{\mathrm{Im}\ t}{\mathrm{Re}\ t} \quad (11)$$

حيث، Im هو الجزء الخيالي [5]. ان فرق الطور لا يوفر المعلومات الكافية عن سلوك التصميم. وعادة ولكثرة الاهتمام في عرض التأخر *(Delay)* عندما تنعكس او تنفذ النبضة, فأن تأخر المجموعة (*Group Delay (GD)*)، أو في تشوه عرض نبضة النطاق الترددي المحدود والناجم عن اختلاف GD مع الطول الموجي، وتشتت تأخر المجموعة (*Group Delay Dispersion (GDD)*). يتم تعريف تأخر المجموعة بأنه المشتقة السالبة للطور نسبة الى التردد [6] [7]، و GD، يعروف أيضا باسم "المغلف *(Envelope Delay)*" [8]. ان تشتت تأخر المجموعة يوجد في كل مكان، وهذه الظاهرة تنتشر في مختبرات الليزر فائق السرعة وغالبا ما تكون من الظواهر المزعجة جدا. حيث عندما تنتشر النبضات فائقة القصر خلال وسط التشتت، فأن مركبات التشتت تظهر في أوقات مختلفة بسبب GDD، مما تسبب السقسقة *(Chirped)* والكبس *(Stretched)* والحد من ذروة النبضة.

هذا التأثير يمكن أن يعمل له تعويض *(Compensated)* باستخدام ضاغط النبضات *(Pulse Compressor)*، والذي يعرض GDD سالب القيمة [9]. والطريقة المثالية لحساب GDD هي حساب معاملات الانعكاس المعقد *(Complex Reflection Coefficients)* باستخدام تقنية مصفوفة الانتقال *((Transfer Matrix (TM)* ثم أخذ الفرق الدقيق والمحدود الحاصل على التردد [10] [11]. ويتم الحصول على GD وGDD باستخدام:

$$GD = -\frac{d\phi}{d\omega} \quad (12)$$

$$GDD = -\frac{d^2\phi}{d^2\omega} \quad (13)$$

حيث، $\omega = 2\pi c / \lambda$ هو التردد الزاوي *(Angular Frequency)* و c هو سرعة الضوء في الفراغ.

النتائج والمناقشة

من الصعب غالبا، بل من المستحيل، تصميم مرشح لتطبيق جميع المواصفات في مجال ما. ومع ذلك، فمن الممكن برمجة المعادلات بطرق حسابية احترافية دقيقة للغاية والحصول على الحسابات النظرية واعتماد التشذيب *(Optimize)*, وعرض مواصفات المرشح باستخدام ال*(Refinement)* [12]. في هذه الطريقة، على المصمم أن يوفر تصميم ابتدائي حيث تكون خصائصه قريبة بما فيه الكفاية للمواصفات المطلوبة. ثم، يتم استخدام خوارزمية التشذيب *(Optimization Algorithm)* الأمثل لضبط سمك الطبقات، ومعامل الانكسار.
بالإضافة إلى التصميم الابتدائي، يجب على المصمم أن يوفر أهداف *(Targets)* لوصف المواصفات. يمكن للأهداف أن تكون أي من الخصائص الحسابية *(Property Computable)* للمعاملات *(Parameters)* الخاصة للمرشح, عادة، الانعكاسية، النفاذية، خصائص الطور, الاستقطاب وزاوية السقوط. واعتمادا على التطبيق، فإنه قد يكون من الضروري تحديد الهدف عند طول موجي واحد أو مجموعة من الأطوال الموجية. وفي الحالة الأخيرة، وبالنسبة للهدف, فأنه يجب تحديده في عدد محدود من الأطوال الموجية.
في هذه الدراسة النظرية، تم تصميم مرآة باردة باستخدام ثاني أكسيد التيتانيوم (TiO_2) وثاني أكسيد السيليكون (SiO_2). التصميم يتألف من (21) طبقة من TiO_2 (معامل الانكسار = 2.346) وSiO_2 (معامل الانكسار = 1.485) ضمن نطاق الطول الموجي *(300-1000)* نانومتر.
الشكل 7 يمثل العلاقة بين عمق التغلغل او عمق الاختراق *(Penetration Depth)* داخل طبقات الغشاء الرقيق ومعامل الانكسار للمرآة الباردة المصممة. حيث يبين الشكل تصميم (21) طبقة ضمن نطاق الطول الموجي *(300-1000)* نانومتر.

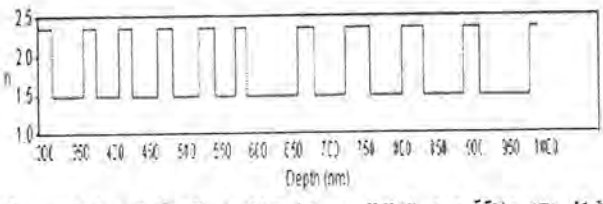

الشكل (7) علاقة عمق التغلغل ومعامل الانكسار للمرآة الباردة المصممة.

الشكل (8) يوضح سلوك الطور. ومن أجل دراسة خصائص المرآة الباردة، فإنه من الضروري دراسة فرق الطور كدالة للتردد الزاوي ω.

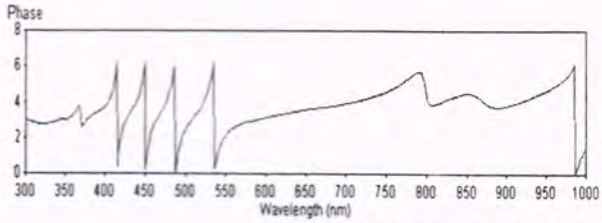

الشكل (8) يوضح ظاهرة التفريق.

ان المرآة الباردة تعكس الضوء المرئي وتسمح بمرور جميع ضوء الأشعة تحت الحمراء الضارة تقريبا من خلالها، وكما هو مبين في الاشكال (9) و (10). حيث يعكس الغشاء متعدد الطبقات أكثر من 98٪ من الضوء الساقط في المنطقة المرئية، ويسمح بنفوذ الإشعاع الحراري في مناطق الأشعة تحت الحمراء والأشعة تحت الحمراء القريبة. بمعنى اخر, ان هذه المرايا سمحت بمرور الحرارة والتبريد السريع. والاشكال (9) و (10) تمثل علاقة الطول الموجي مع النفاذية (T)، والانعكاسية (R), على التوالي, للمرآة الباردة المصممة.

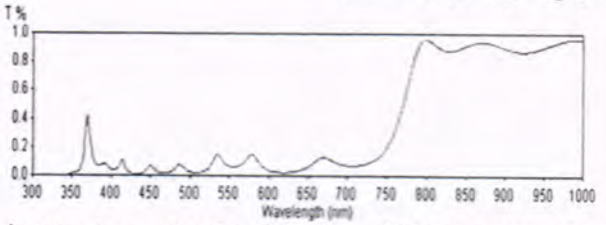

الشكل (9) يوضح العلاقة بين النفوذية والطول الموجي المستخدم في تصميم المرآة الباردة.

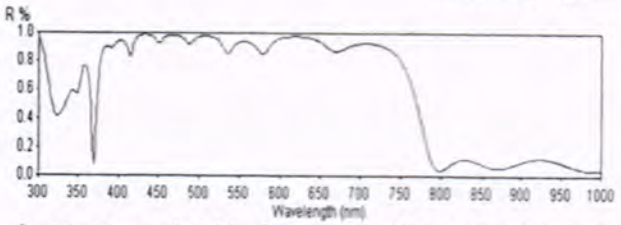

الشكل (10) يوضح العلاقة بين الانعكاسية والطول الموجي المستخدم في تصميم المرآة الباردة.

الشكل (11) علاقة تأخر المجموعة والطول الموجي. ومن الواضح انخفاض التذبذبات في منحني تأخر المجموعة عند منطقة الطول الموجي للتصميم (600) نانومتر.

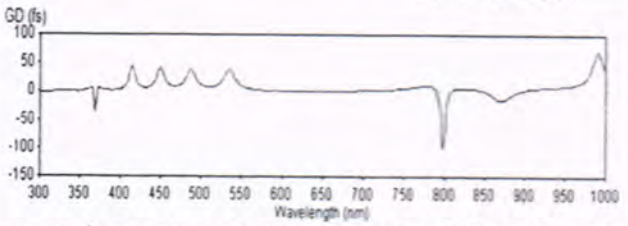

الشكل (11) علاقة تأخر المجموعة والطول الموجي المستخدم في تصميم المرآة الباردة.

الشكل (12)، تشتت تأخر المجموعة والطول الموجي. وبالطبع، نفس سلوك انخفاض التذبذب في المنحني يمكن العثور عليها في حالة ال *GDD* عند منطقة الطول الموجي للتصميم.

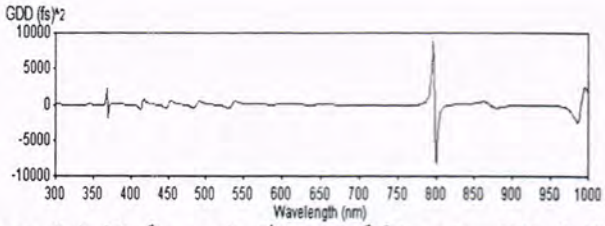

الشكل (12) يوضح علاقة تشتت تأخر المجموعة والطول الموجي المستخدم في تصميم المرآة الباردة.

عندما تضاء الأغشية الرقيقة بأستخدام الضوء، فأن أنماط الموجة الواقفة تتشكل والتي بدورها يمكن أن تظهر اختلافات كبيرة في سعة المجال الكهربائي سواء من حيث الطول الموجي ومن حيث الموقع داخل الطلاء. وفي هذا البحث تم رسم المنحني البياني لتوزيع المجال الكهربائي والموضح في الشكل (13) الناتج عن سقوط الإشعاع على غشاء متعدد الطبقات لتصميم المرآة الباردة, علما ان مخطط الدائرة ايضا تم عرضه في هذه الدراسة وموضح في الشكل (14) ادناه. حيث ان دراسة المجال الكهربائي تعتبر خطوة اساسية في احتساب السماحية. ومن الشكلين يمكن ملاحظة أن شدة المجال الكهربائي القوية وقعت في الطبقة الأولى وشدة المجال الكهربائي تبدأ تقل بعد أن اجتازت منطقة الطبقة.

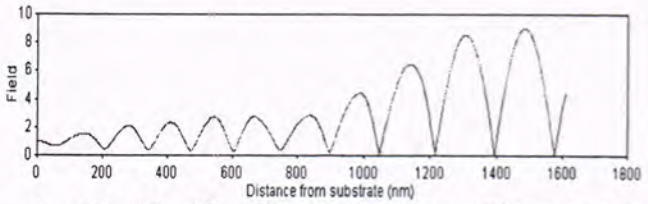

الشكل (13) علاقة المجال الكهربائي والمسافة نسبة الى القاعدة التي تم عليها ترسيب طبقات الطلاء المستخدم في تصميم المرآة الباردة.

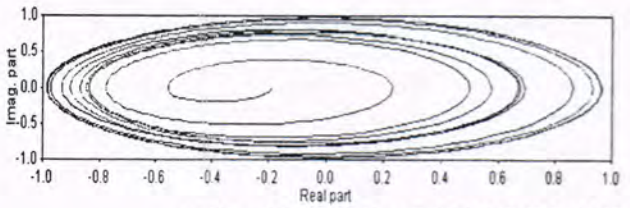

الشكل (14) المخطط الدائري للجزء الحقيقي والخيالي.

مخطط السماحية موضح في الشكل (15) حيث يعرض تقنية بسيطة لتقييم الاختلافات في السعة ومنه يمكن اجراء استقطاعات للخسائر. وفي هذه الدراسة أعتمدت حالة السقوط العامودي فقط.

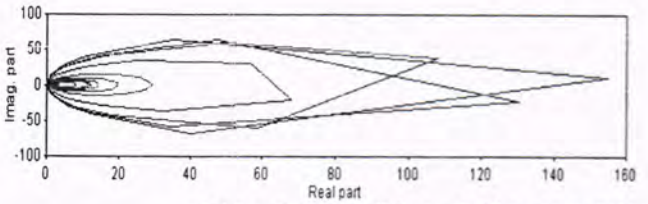

الشكل (15) مخطط السماحية للجزء الحقيقي والخيالي.

وأخيرا، علاقة الانعكاسية والنفاذية مع السمك البصري موضحة في الشكل (16) والشكل (17). ولقد تم الحصول على هذه النتيجة بعد عدة عمليات تشذيب *(Optimize)* واعادة التشذيب *(re-Optimize)* مستمرة.

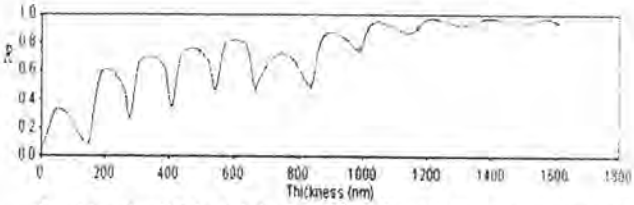

الشكل (16) تغير الانعكاسية دالة لسمك طبقات الطلاء المستخدم في تصميم المرآة الباردة.

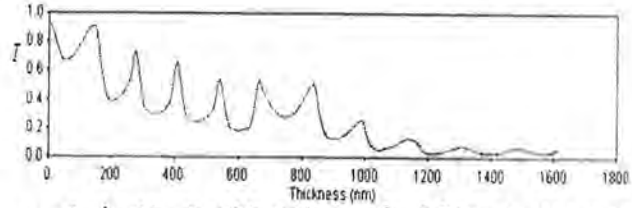

الشكل (17) تغير النفاذية دالة لسمك طبقات الطلاء المستخدم في تصميم المرآة الباردة.

الاستنتاجات

المرايا الباردة تمثل حالة خاصة لعرقلة الموجات القصيرة والسماح بعبور الموجات الطويلة. في هذا البحث، تمت عملية التصميم بأستخدام مادة TiO_2 وجرى زيادة سمك وعدد الطبقات في التصميم. المواد العازلة المستخدمة في تصميم المرآة الباردة هي TiO_2 وSiO_2 مع ضبط دقيق للنفاذية, الانعكاسية، السماحية البصرية، المجال الكهربائي والتشتت ضمن نطاق الطول الموجي *(1000-300)* نانومتر.

1. بأستعمال تركيب مؤلف من (21) طبقة, وكما موضح في الشكل (7), من مادتي *(TiO_2/SiO_2)* على قاعدة من زجاج *(Fused-silica)*, ومرتبة بحيث تبدأ وتنتهي بمادة ذات معامل انكسار عال, أمكن الحصول على انعكاسية عالية عند الطول الموجي المطلوب. حيث بلغ متوسط الانعكاس من خلال الطيف المرئي هو أكثر من 98٪.
2. ان الانعكاسية العالية لطبقة الطلاء ذي السمك البصري ربع الموجة ناتجة عن توافق طور الحزم المنعكسة عند السطحين.
3. أن زيادة الفرق في قيمة معامل الانكسار للمواد المستخدمة في التصميم وزيادة عدد الطبقات يؤدي بالتالي الى زيادة الانعكاسية, وان سمك الطبقات غير المتساوي والذي ظهر خلال عرض النتائج سببه اختلاف معامل الانكسار.
4. يمكن استخدام المرآة الباردة في زيادة الكفاءة الكمية للكشف عن الأشعة تحت الحمراء القريبة. وهي تستخدم عادة في أنظمة كاميرا الرؤية الليلية. وتستخدم أيضا في إضاءة الاجسام في منطقة الأشعة تحت الحمراء دون الحاجة الى الاضاءة باستخدام ضوء المنطقة المرئية. بمعنى, يمكن اضاءة جسم في المنطقة تحت الحمراء دون خلق أي أدلة واضحة على الإضاءة. ثم الكشف عن زيادة كسب أطياف الأشعة تحت الحمراء مع كاميرا الأشعة تحت الحمراء. وهذا ما يسمى النظام البصري السري المستخدم في الجيش. وبالإضافة إلى ذلك، فان عرقلة المرايا الباردة للأشعة فوق البنفسجية يمكن أن تستخدم للحفاظ على اللون الأصلي في الأعمال الفنية المرسومة. حيث ان هذه الفوتونات نشطة للغاية وتمتص في عمق طبقة الطلاء, وببطء تتدهور المواد التي تمتص مع مرور الوقت تاركة ظهور متلاشي السلوك.
5. مرشحات الحافة *(Long-Pass Edge Filters)* يمكن أن تستخدم في كثير من الاحيان كمرايا باردة لتقليل تراكم الحرارة التي تسببها الأشعة تحت الحمراء.

المصادر

[1] *Jiri G. D., "Radiation Technology for Polymers", Second Edition, CRC Press, Taylor & Francis Group, USA, (2010).*

[2] *Lemarchand F., "Application of clustering global optimization to thin film design problems", OSA, Vol. 22, No. 5, pp. 5166-5176, (2014).*

[3] *Abelès F., "Recherches sur la propagation des ondes électromagnétiques sinusoïdales dans les milieux stratifiés. Application aux couches mince," Ann. Phys. (Paris) 5, 596–640, 706–782, (1950).*

[4] *Furman Sh. A. and Tikhonravov A. V., "Basics of Optics of Multilayer Systems", Éditions Frontières, (1992).*

[5] *Larouche S. and Martinu L., "OpenFilters: open-source software for the design, optimization, and synthesis of optical filters", Appl. Opt., pp. 219- 230, Vol. 47, No. 13, (2008).*

[6] *Flanagan M., Brian C. J., Stone, Michael A., "Discrimination of Group Delay in Clicklike Signals Presented via Headphones and Loudspeakers", Journal of the Audio Engineering Society, pp. 593–611, (2005).*

[7] *Atkinson K., "An Introduction to Numerical Analysis", 2nd Edition, Wiley, New York, (1989).*

[8] *I. Shapir and Member S., "Suggestion for a new Formula to Calculate Group-Delay from Frequency Domain Measurements", Microwave Conference, 2006. 36th European, pp. 1233–1236, Manchester, (2006).*

[9] *Fowles R. G., "Introduction to Modern Optics", Pain American and International, pp. 13, New York, (1967).*

[10] *Birge J. R., Jirauschek C. and Kärtner F. X., "Efficient Analytic Computation of Group Delay Dispersion from Optical Interference Coatings", OSA, Interference Coating Top. Mtg. p. ThA6, Tucson, (2004).*

[11] *Jonathan R. Birge and Franz X. Kärtner, "Efficient analytic computation of dispersion from multilayer structures", Appl. Opt., Vol. 45, Issue 7, pp. 1478-1483, (2006).*

[12] *Baumeister P., "Design of multilayer filters by successive approximations", OSA, Vol. 48, pp. 955–958, (1958).*

مجلة علوم المستنصرية
المجلد 27، العدد 2، 2016

journal homepage:www.mjs-mu.com

تاثير الاشعاع الشمسي على الطاقة الحركية الاضطرابية (TKE) فوق مدينة بغداد

نغم عباس محمد
قسم علوم الجو/ كلية العلوم / الجامعة المستنصرية

Articleinfo.

تقديم البحث:
2015/10/8
قبول البحث:
2016/1/3

الخلاصة

في هذا العمل تم حساب الطاقة الحركية الاضطرابية (TKE) خلال فترة النهار من الساعة 7:00 الى الساعة 13:00فوق مدينة بغداد، وتم اختبار تاثير درجات الحرارة والاشعاع الشمسي على القيم المحسوبة للطاقة الحركية الاضطرابية . تم رصد البيانات لسرعة الرياح بمركباتها الثلاث (u،v،w) ودرجات الحرارة وذلك باستخدام جهاز قياس سرعة الرياح ذو الاستجابة السريعة (Ultrasonic). الفترة التي تمت فيها عملية الرصد امتدت على مدى عشرون يوما حيث تم اختيار رصدات منتخبة خلال اليوم امتدت من الساعة 7:00 الى الساعة 13:00 حسب التوقيت المحلي. ان عملية تسجيل بيانات الاشعاع الشمسي تمت باستخدام محطة الطقس الاوتوماتيكية ولنفس الفترة الزمنية. ان اعلى قيمة للطاقة الحركية الاضطرابية كانت ($5.1\ m^2/s^2$) في يوم 26/2/2015 ، واقل قيمة لها كانت ($0.06\ m^2/s^2$) في يوم 5/3/2015، وكذلك تم التوصل الى وجود علاقة طردية بين TKE والاشعاع الشمسي وبمعامل ارتباط يبلغ (0.7) وكذلك بين TKE ودرجات الحرارة وبمعامل ارتباط (0.73).

ABSTRACT

In this work the turbulent kinetic energy (TKE) on Baghdad city , as well we found a relation between the turbulent kinetic energy and temperature and solar radiation. The observations have been made for wind speed with three components (u,v,w) and temperature by using a fast response instrument. The rang scale of observations extended through the duration of twenty days. We choose a selected hour of the day from 7:00 to 13:00 in local time. The solar radiation has been measured by using the automatic weather station in the same rang scale with wind speed and temperature. Maximum turbulent kinetic energy value was ($5.1\ m^2/s^2$) on 26/2/2015, and minimum turbulent kinetic energy value was ($0.06 m^2/s^2$) on 5/3/2015.

المقدمة

الطاقة الحركية الاضطرابية Turbulent Kinematic Energy(TKE) هي من اهم المتغيرات في علم الانواء الدقيقة Micrometeorology لانها ترتبط بشكل مباشر بانتقال الحرارة والرطوبة والزخم خلال الطبقة المحادة كما ان الطاقة الحركية الاضطرابية يمكن ان تستخدم كنقطة بداية في حدوث الانتشار المضطرب[1].

ان حدود معادلة ميزانية الطاقة الحركية الاضطرابية TKE يمكن ان تستخدم في وصف العمليات الفيزيائية التي تولد الاضطراب، ان الموازنة النسبية لهذه العمليات تحدد قابلية الجريان ان يتحول الى مضطرب وهذا يشير الى ارتباط TKE بالاستقرارية ويمكن ان تستخدم معادلة الطاقة الحركية الاضطرابية في وضع بعض المعاملات والمقاييس الابعدية dimensionless groups التي تخص الاستقرارية مثل طول ابوكوف Obkhove Length وعدد ريجاردسون Richardson Nember وغيرها. وتكمن اهمية حساب الطاقة الحركية الاضطرابية في دراسة الاضطراب في الطبقة المحادة حيث يمكن تقييم حالة الجو في الطبقة المحادة (مستقر، غير مستقر ، متعادل)[2].

ان جريان الهواء أو ما تسمى بالرياح ممكن أن نقسمها إلى ثلاثة انواع, معدل سرعة الرياح ,الاضطراب والحركة الموجية ومن الممكن ان تاتي هذه الانواع بشكل منفصل أو مجتمع خلال الطبقة المحادة, فمثلا الرطوبة والحرارة والزخم والملوثات تنتقل أفقياً بواسطة معدل الرياح وعمودياً بواسطة الحركة الاضطرابية .

إن معدل سرعة الرياح هو المسؤول عن الانتقال الأفقي السريع أو ما يسمى Advection خلال الطبقة المحادة. حيث ان الاحتكاك يجعل من معدل سرعة الرياح تتباطأ بالقرب من سطح الأرض .إن معدل سرعة الرياح العمودية أقل بكثير وعادة تتراوح ما بين بضعة مليمترات إلى بضعة سنتمترات لكل ثانية .

اما الاضطراب فيساهم في حركة الرطوبة والحرارة والزخم والملوثات عموديا[3] ، ويعرف الاضطراب بانه عصفة ريح منطبقة على معدل سرعة الرياح ممكن ملا حضتها على انها تتكون من حركات دورانية غير منتظمة تسمى بالدوامات Eddies. ويتالف الاضطراب عادة من دوامات مختلفة الاحجام.

ان معظم الاضطراب في الطبقة المحادة يتولد بسبب تاثيرات سطح الارض فمثلا التسخين الشمسي لسطح الارض يولد كتلا او طرود هوائية ساخنة صاعدة. هذه الطرود الحرارية ما هي الا دوامات كبيرة. اما تاثير الاحتكاك على الهواء القريب من السطح فيسبب قص الرياح الذي يصبح اضطرابا ايضا.

ان فائدة الاضطراب تكمن في فعاليته في عملية النقل بالمقارنة مع الانتشار الجزيئي وهو الذي يسمح للطبقة المحادة بالاستجابة الى تاثيرات السطح[4].

اما الحركة الموجية فهي الحركة التي تلاحظ بشكل متكرر في الطبقة المحادة الليلية فإنها تنقل القليل من الحرارة والرطوبة وكذلك جزء من الملوثات لكنها فعالة في نقل الطاقة والزخم حيث تتولد الموجات موضعياً بسبب قص الرياح أو من جريان المانع فوق الحواجز وممكن أن تتقدم الموجات من مصدر بعيد مثل الزوابع الرعدية أو من الانفجارات الخ[5].

فاذا اخذنا نظام الاحداثيات الموضوعة باتجاه معدل الرياح وبافتراض ان هناك تجانس افقي ، واهملنا الترسيب فان معادلة الطاقة الحركية الاضطرابية تعطى بالعلاقة:

$$\frac{\partial \bar{e}}{\partial t} = \frac{g}{\bar{\theta}_v}\left(\overline{\dot{w}\dot{\theta}_v}\right) - \overline{\dot{u}\dot{w}}\frac{\partial \bar{u}}{\partial z} - \frac{\partial(\dot{w}e)}{\partial z} - \frac{1}{\bar{\rho}}\frac{\partial(\dot{w}\dot{p})}{\partial z} - \epsilon \ldots\ldots (1)$$

$$I \qquad II \qquad III \qquad IV \qquad V \qquad VI$$

I الحد الاول يمثل الخزن الموضعي local storage للطاقة الحركية الاضطرابية حيث ان $\bar{e}$:يمثل معدل الطاقة الحركية الاضطرابية لوحدة الكتل، t : الزمن.

II الحد الثاني يمثل تاثير الطفو لانتاج او تبدد الطاقة معتمدا على التدفق الحراري حيث يكون موجب في النهار (فوق اليابسة) وسالب في الليل حيث ان g : التعجيل الارضي، $\overline{\theta_v}$: معدل درجة الحرارة الجهدية الفعلية، $\dot{w}$: القيمة المضطربة لسرعة الرياح باتجاه w.*[6]*

III الحد الثالث يمثل التاثير الميكانيكي (قص الرياح) في انتاج او فقدان الطاقة (قص المركبات الافقية). ان فيض الزخم (momentum flux) اشارته دائما عكس معدل الرياح القصية ($\frac{\partial \bar{u}}{\partial z}$) لان الزخم دائما يفقد الى الاسفل باتجاه السطح حيث ان $\dot{u}$: القيمة المضطربة لسرعة الرياح باتجاه u ، z: الارتفاع.

IV الحد الرابع يبين الانتقال العمودي للطاقة الحركية الاضطرابية (*TKE*)

V الحد الخامس يبين علاقة الضغط في توزيع (*TKE*) خلال الطبقة المحادة حيث ان ρ: كثافة الهواء، $\dot{p}$: القيمة المضطربة للضغط.

VI الحد السادس ϵ يمثل معدل التبدد الجزيئي، وهذا الحد يتواجد دائما طالما قيمة الطاقة الحركية الاضطرابية لاتساوي صفر ، وفيزياويا يعني ان الاضطراب يتناقص او يتبدد مع الوقت الا اذا تولد موضعيا او ينتقل بواسطة معينة او بواسطة عمليات الضغط لذلك لاتعتبر *TKE* كمية محفوظة والطبقة المحادة يمكن ان تكون مضطربة فقط اذا كانت هناك عمليات فيزياوية تولد الاضطراب [7-9].

لقد جرت الكثير من المحاولات لدراسة الطاقة الحركية الاضطرابية منها ما قام به الباحث John D. Albertson وجماعته (1997) حيث تحدث عن الطاقة الحركية الاضطرابية وعلاقتها بفيض الزخم الناتج عن السطح والحرارة كما وحاول تصميم زوج من المعادلات من الدرجة الثانية والثالثة لحساب الفيض السطحي من خلال نسبة التبدد*[10]*. كما قام الباحث*Ewan J.O Connor* وجماعته *(2010)* بمحاولة ايجاد طريقة او صيغة لتقدير نسبة تبدد الطاقة الحركية الاضطرابية باستخدام جهاز *Doppler lidar* ومقارنة المعلومات الناتجة بنتائج استخرجت من اجهزة قياس سرعة الرياح ذو الاستجابة السريعة (التراسونك) المحمولة على بالون *[11]*. كما قام الباحث عقيل غازي (*2013*) بحساب وتقدير شدة اضطراب سرعة الرياح الافقية في مدينة بغداد باستخدام اجهزة قياس سرعة الرياح ذات الاستجابة البطيئة (الانيمومتر) في جو متعادل او قريب من التعادل حيث سجل اعلى شدة اضطراب على ارتفاع *7.5 m* اذ كانت قيمتها 5 في يوم *31/10/2010* عند الساعة *16:24* حسب التوقيت المحلي لمدينة بغداد *[12]*.

الجزء النظري

من المعروف ان الطاقة الحركية لجسم متحرك تعطى بالعلاقة :

$$KE = \frac{1}{2}mV^2 \dots\dots\dots (2)$$

حيث ان:

m: كتلة الجسم V: سرعة الجسم

وفي حالة التعامل مع الموائع (مثل الهواء) فان الطاقة الحركية KE تكون لوحدة الكتلة $\frac{KE}{m}$ فتكون المعادلة كالتالي:

$$\frac{KE}{m} = \frac{1}{2}V^2 \dots\dots\dots (3)$$

يمكن تقسيم الطاقة الحركية للجريان الكلي الى جزئين رئيسيين (جزء يرتبط بمعدل السرعة *MKE* وجزء يرتبط باضطراب السرعة *TKE*).

بالنسبة للطاقة الحركية لمعدل السرعة *MKE* تحسب كالتالي:

$$\frac{MKE}{m} = \frac{1}{2}(\bar{u}^2 + \bar{v}^2 + \bar{w}^2) \dots\dots\dots (4)$$

حيث ان : $\bar{w}$ ،$\bar{v}$ ،$\bar{u}$: تمثل قيم المعدل لسرعة الرياح باتجاه u،v،w على التوالي.

اما الطاقة الحركية الاضطرابية *TKE* فتحسب كالتالي:

$$e = \frac{1}{2}(\dot{u}^2 + \dot{v}^2 + \dot{w}^2) \dots\dots\dots (5)$$

حيث ان *e*: تمثل القيم الانية للطاقة الحركية الاضطرابية لوحدة الكتل .

$\dot{u}$،$\dot{v}$،$\dot{w}$: تمثل القيم المضطربة لسرعة الرياح باتجاه u،v ،w على التوالي.

لحساب الطاقة الكلية للجريان اقتضى الجمع بين الحالتين فباخذ المعدل للقيم الانية للسرعة نستطيع كتابة معادلة حساب معدل الطاقة الحركية الاضطرابية لوحدة الكتل بشكل اكثر تمثيلا للجريان الكلي وكالتالي [13]:

$$\bar{e} = \frac{\mathrm{TKE}}{\mathrm{m}} = \frac{1}{2}\left(\overline{\dot{u}^2} + \overline{\dot{v}^2} + \overline{\dot{w}^2}\right) \dots\dots\dots (6)$$

المواد وطرائق العمل

الموقع ورصد البيانات

تقع منطقة المستنصرية في الجزء الشمالي الشرقي من مدينة بغداد والتي تقع على ارتفاع 31.7m عن مستوى سطح البحر والواقعة على خط طول °44.20 شرقاً ودائرة عرض °33.14 شمالاً[14]. حيث كان مركز تسجيل البيانات في النقطة الواقعة على خط طول "44°24'70 شرقا ودائرة عرض "33°22'18 شمالا [15]، ان المنطقة هي منطقة حضرية تحيط بها بنايات متوسطة الارتفاع من جميع الجهات كما موضح في الشكل (1).

في هذا العمل تم استعمال بيانات سرعة الرياح ودرجات الحرارة الماخوذة من جهاز قياس سرعة الرياح ذو الاستجابة السريعة (التراسونك) التابع لقسم علوم الجو في كلية العلوم، الجامعة المستنصرية وهذا الجهاز من نوع Wind Master pro, Ultrasonic Anemometer UMG07914- 1189-PK-021 يقوم الجهاز بقياس سرعة الرياح بمركباتها الثلاثة (u،v،w) ودرجات الحرارة وبفاصلة زمنية قدرها ثانية واحدة لكل تسجيل ، كما تم الحصول على بيانات الاشعاع الشمسي من محطة الطقس الاوتوماتيكية التابعة لقسم علوم الجو في كلية العلوم، الجامعة المستنصرية وهذه المحطة من نوع Davis Vantage Pro(2) الامريكية الصنع.

امتدت فترة الرصد على مدى عشرون يوما من 22/2/2015 الى 13/3/2015 ابتداءا من الساعة 7:00 الى الساعة 13:00 حسب التوقيت المحلي لمدينة بغداد، وبعد عملية تبويب البيانات تم انتخاب 2520 رصدة والتي تمثل حالة الجو غير المستقر وتحتوي على بيانات خالية من الثغرات، اما الرصدة الواحدة فهي متكونة من 60 قراءة وبفاصلة زمنية مقدارها ثانية واحدة (مايمثل 151200 قراءة للفترة المدروسة)، حيث احتوت الرصدات على تسجيلات سرعة الرياح بمركباتها الثلاث ودرجة الحرارة، وقد تم حساب معدلات TKE لكل ساعة. اما قيم الاشعاع الشمسي فقد تم الحصول عليها من محطة الطقس الاوتوماتيكية والتي تعطي قيم ساعية للمتغيرات الانوائية ولنفس التوقيتات والفترة الزمنية للرصد.

الشكل (1): منطقة حي المستنصرية [16]

النتائج والمناقشة

1- الطاقة الحركية الاضطرابية

تم استخراج قيم المعدلات الساعية للطاقة الحركية الاضطرابية خلال فترة الدراسة، حيث تبين ان اعلى قيمة للطاقة الحركية الاضطرابية (5.1 m^2/s^2) في يوم 26/2/2015 ، واقل قيمة لها كانت ($0.06m^2/s^2$) في يوم 5/3/2015. ويبدو من خلال النتائج ان قيم TKE تبدا بالتزايد بالتدريج من الساعة 7:00 لتصل الى اعلى قيمة لها في الساعة 13:00 على امتداد ايام الرصد. حيث ان الشكل (2) يمثل نموذجا لاحد ايام الرصد وهو يوم 1/3/2015.

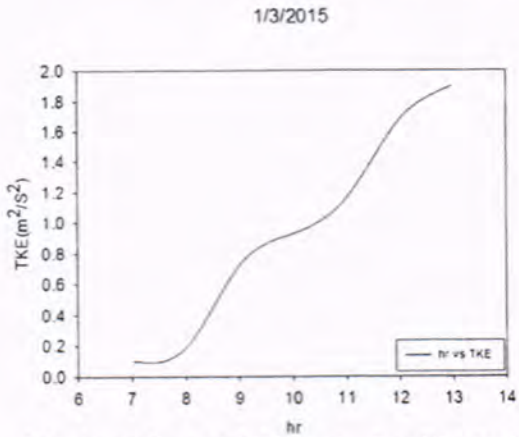

الشكل (2): التغير الساعي للطاقة الحركية الاضطرابية في يوم 1/3/2015

2- التغيرات الساعية لكل من الطاقة الحركية الاضطرابية والاشعاع الشمسي

يوضح الشكل (3) طبيعة التغير الساعي لكل من TKE و الاشعاع الشمسي لفترة الدراسة، اذ يتضح ان هناك علاقة واضحة بين الطاقة الحركية الاضطرابية والتغيرات الساعية للاشعاع الشمسي، اذ تبدا قيم الاشعاع الشمسي بالتزايد بالتدريج من الساعة (7:00) لتصل الى اعلى قيمة لها في الساعة (13:00) وهذا ما يتناغم بشكل جيد مع التغيرات الساعية للطاقة الحركية الاضطرابية . ويتضح من خلال الشكل ايضا ان معدلات الاشعاع الشمسي الساعية لفترة الدراسة تقع تقريبا مابين (728-5 w/m^2) ، اما معدلات TKE تقع تقريبا مابين ($0.06-5.1\ m^2/s^2$) .

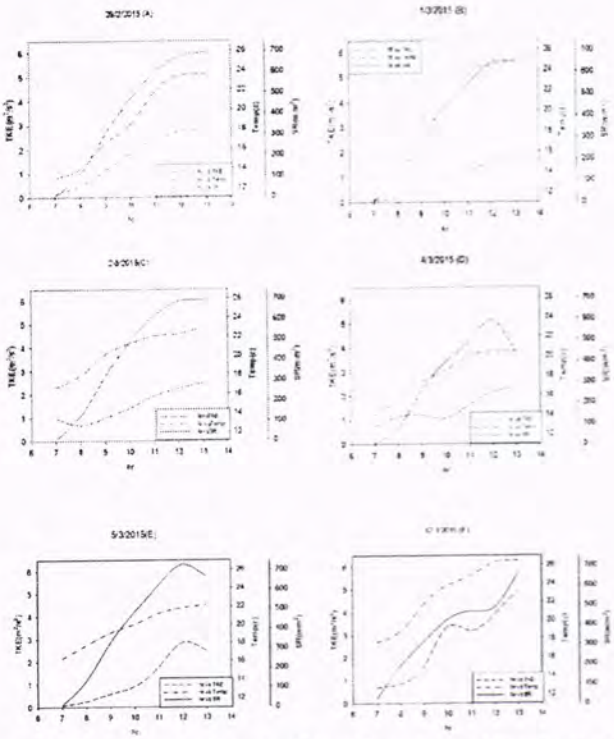

الشكل (3): التغيرات الساعية للطاقة الحركية الاضطرابية و الاشعاع الشمسي ودرجات الحرارة

SR: الاشعاع الشمسي **Temp: درجة الحرارة**

ان العلاقة بين الاشعاع الشمسي و TKE يمكن ان تبين في الشكل (4):

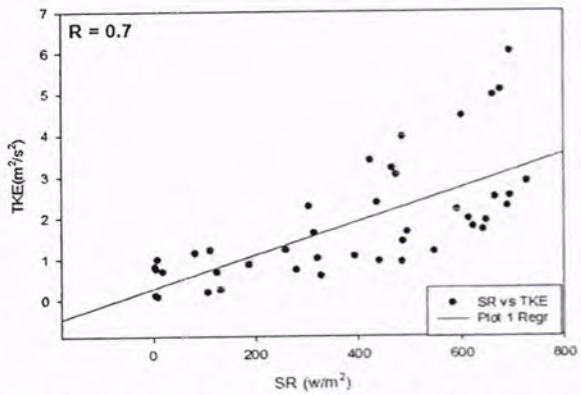

الشكل (4): علاقة الارتباط الخطية بين المعدل الساعي للطاقة الحركية الاضطرابية والاشعاع الشمسي

ان الصيغة الرياضية الناتجة عن الارتباط الخطي بين TKE والاشعاع الشمسي كالتالي:

$$TKE = 0.276 + 0.00407 * SR \ldots\ldots\ldots (7)$$

ان معامل الارتباط R هو (0.7) وتشير هذه القيمة الى ارتباط جيد بين المتغيرين.

3- التغيرات الساعية لكل من الطاقة الحركية الاضطرابية و درجة حرارة الهواء

يوضح الشكل (3) طبيعة التغير الساعي لكل من TKE و درجة حرارة الهواء لفترة الدراسة، اذ يتضح ان هناك علاقة واضحة بين الطاقة الحركية الاضطرابية والتغيرات الساعية لدرجات الحرارة اذ تبدا قيم درجات الحرارة بالتزايد بالتدريج من الساعة (7:00) لتصل الى اعلى

قيمة لها في الساعة (13:00) وهذا ما يتناغم بشكل جيد مع التغيرات الساعية للطاقة الحركية الاضطرابية . ويتضح من خلال الشكل ايضا ان معدلات درجات الحرارة الساعية لفترة الدراسة تقع تقريبا بين (11.3-26.4^{0}c) درجة مئوية، اما معدلات TKE تقع تقريبا مابين (0.06-5.1 $(m^2/s^2$.

ان التناغم الواضح بين قيم التغير في قيم الطاقة الحركية الاضطرابية ودرجات الحرارة مع الزمن وعلى امتداد ايام الرصد مهمة الى ايجاد صيغة رياضية تصف العلاقة بين TKE ودرجات الحرارة من خلال الارتباط الخطي بين المتغيرين وان معامل الارتباط البالغ (0.738) يشير الى وجود ارتباط جيد وعلى هذا الاساس تم استنتاج صيغة رياضية تصف العلاقة بين المتغيرين وكما هو موضح بالمعادلة (8) والشكل (5).

$$TKE = -4.055 + 0.272 * Temp \dots\dots\dots (8)$$

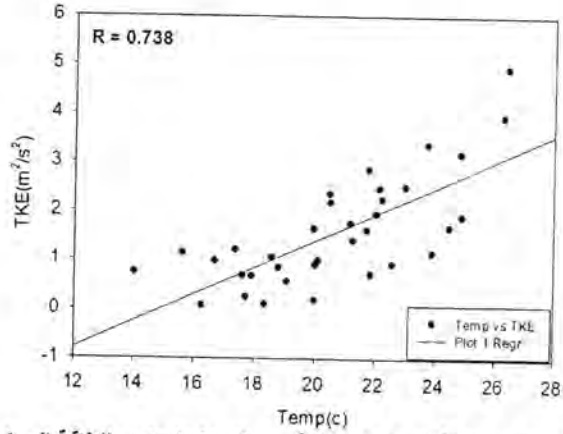

الشكل (5) : علاقة الارتباط الخطية بين المعدل الساعي للطاقة الحركية الاضطرابية مع درجات الحرارة

الاستنتاجات:

1- اعلى قيمة للطاقة الحركية الاضطرابية كانت ($5.1m^2/s^2$) في يوم 26/2/2015 واقل قيمة لها كانت ($0.06m^2/s^2$) في يوم 5/3/2015 خلال فترة الدراسة.

2- تراوحت قيم درجات الحرارة خلال فترة الدراسة بين (11.3-26.4 ^{0}c)، في حين تراوحت قيم الاشعاع الشمسي بين (5-728 w/m^2) خلال فترة الدراسة.

3- هنالك ارتباط بين الطاقة الحركية المضطربة ودرجة الحرارة ، حيث كان معامل الارتباط بين المتغيرين (0.73) وهذا يؤشر ارتباطا جيدا حيث تم التوصل الى صيغة وضعية بين المتغيرين خلال فترة الدراسة.

4-- هنالك ارتباط بين الطاقة الحركية الاضطرابية والاشعاع الشمسي ، حيث كان معامل الارتباط بين المتغيرين (0.7) وهذا يؤشر ارتباطا جيدا حيث تم التوصل الى صيغة وضعية بين المتغيرين خلال فترة الدراسة.

المصادر:

1- Bean, B.R. and T.P Repoff " A study of Turbulent Energy Over Complex Terrain". Bound Layer Meteor. 25, 17-23, 1983.

2- Roland B. Stull" Introduction to Boundary Layer Meteorology" Kluwer, Acadecmic Publishers, London, 1989.

3- الشمري، حسين علي حاتم "خصائص الطبقة المتاخمة لسطح مدينة بغداد وتحديد طول الخلط" رسالة ماجستير مقدمة لقسم علوم الجو_كلية العلوم، الجامعة المستنصرية, 2006 .

4- Lumly J. L, H. A. Panofsky "The Structure of Atmospheric Turbulance. Monographsand Texts Physics and Astronomy" vol XII, Inter Science Puble, john wider and Sons, NY, 1964.

5- Gossard,E.E., W. H. Hooke " Wave in the Atmosphere, Atmospheric Infra sound Gravity Wares-their Generation and Propagation", Elsevier Scientific publ, Co, NY, 1975.

6-Yamada,T. and G. Mellor: A Simulation of The Wangara Atmospheric Boundary Layer Data. J. Atmos. Sci. 32, 2309-2329, 1975.

7-Pennell, W.T. and M.A. Le Mone: An Experimental Study of Tarbulence Structure in The Fair-Weather Trade Wind Boundary Layer. J. Atmos. Sci. 31, 1308-1323, 1974.

8.Therry, G. and P. Lacarrere: Improving The Eddy Kinetic Energy Model For Planetary Boundary Layer Description. Bound Layer Meteor. 25, 63-88, 1983.

9. Lenschow, D.H: Model of The Height Variation of The Tarbulance Kinetic Energy Budget in The Unstable Plantary Boundary Layer. J. Atmos. Sci. 31, 465-474, 1974.

10- John D. Albertson, Mare B. Parlange, Gerard Kiely, and William E. Eichinger" The average dissipation rate of turbulent kinetic energy in the neutral and unstable atmospheric surface layer "JOURNAL OF GEOPHYSICAL RESEARCH, VOL 102,NO.D12,PAGES 13,423-13,432,JUNE 27, 1997.

11- EWAN J.O'CONNOR, ANTHONY J. ILLINGWORTH, IAN M. BROOKS,CHRISTOPHER D.WESTBROOK, ROBIN J. HOGAN, FAY DAVIES AND BARBARA J. BROOKS, ,:" A method for estimating the turbulent kinetic energy dissipation rate from a vertically-pointing Doppler lidar, and independent evaluation from ballon- borne in-situ measurements" J. Atmos. Ocean. Technol. 18 January, 2010.

12- مطر,عقيل غازي"حساب شدة اضطراب سرعة الرياح الافقية في مدينة بغداد" مجلة الهندسة والتكنولوجيا, المجلد31. الجزء(B) العدد.5. 2013.

13- Deardorff, J.W: Prediction of Convection Mixed-Layer Entrainment for Redistic Capping Inversion. structure. J. Atmos. Sci .36, 424-436, 1979.

14- مطر، عقيل غازي و محمد، نغم عباس "حساب قيمة دالة الخشونة السطحية والاستقرارية الجوية (P) في ظروف جوية مختلفة فوق مدينة بغداد" كلية الهندسة والتكنولوجيا المجلد (32) الجزء (B) العدد (6) 2014،.

15- الغبان، زهراء محمد محمد صالح " تقييم تاثير بعض العوامل الانوانية على تراكيز جسيمات PM10و TSP في مدينة بغداد"، رسالة ماجستير، قسم علوم الجو، كلية العلوم، الجامعة المستنصرية، 2014.

[16]Baghdad Map Picture,2013.http://www.google.iq.

مجلة علوم المستنصرية
المجلد 27، العدد 2، 2016

journal homepage:www.mjs-mu.com

تأثير زاوية السمت على قيم مركبات الاشعاع الشمسي الساقط على السطوح المائلة ولزوايا مختلفة

مروه مزهر حسن، سعدي عبد الرزاق عبد الوهاب
قسم علوم الجو، كلية العلوم، الجامعة المستنصرية

Articleinfo.

تقديم البحث:
2015/2/16
قبول البحث:
2015/5/18

الخلاصة

تعد الطاقة الشمسية من افضل مصادر الطاقة الاخرى لما تتميز به من حيث كونها مصدرا هائلا للطاقة الكامنة ومجانية الحصول عليها ولانها طاقة لاتنضب ولاتسبب تلوثا في البيئة كباقي المصادر وكذلك لامكانية تحويلها الى اشكال اخرى من الطاقة. ومن اهم تطبيقات الطاقة الشمسية هي استخدامها في تكنلوجيا الالواح الشمسية التي تعمل الى تحويل الطاقة الشمسية الى طاقة كهربائية. ومن اهم العوامل التي تعتمد عليها هذه التقنية هي زاوية ميل السطح وكذلك زاوية السمت حيث يجب مراعاة ذلك في اوقات مختلفة معتمدا على موقع الارض بالنسبة للشمس خلال اشهر وفصول السنة. لهذا وجد من الضروري دراسة وتحليل مركبات الاشعاع الشمسي الساقط على السطح لزوايا ميل وزوايا سمت مختلفة. حيث تم في هذا البحث تحليل ودراسة المجموع الشهري للقيم الساعية لمركبات الاشعاع الشمسي الكلي والمباشر والمنتشر وكذلك المنعكس لمدينة بغداد ولسنة2005 على السطوح المائلة بزوايا 20، 25، 30، 35 و40 درجة عندما تكون زاوية السمت 45، 135 و270 درجة على التوالي، اظهرت النتائج انه عند زاوية سمت 45 درجة فان قيم مركبات الاشعاع الشمسي تتخذ السلوك الطبيعي، حيث تبدا القيم بالزيادة من الشهر الاول وتصل الى اعلى القيم في منتصف السنة ثم تبدا بالانحدار الى نهاية السنة، اما عند زاوية سمت 135 درجة فان سلوك القيم يكون شاذا، اما عند زاوية سمت 270 درجه فاننا نلاحظ عودة التوزيع الطبيعي

ABSTRACT

Solar energy is considered as the best energy source than other sources for being as a tremendous source of potential and free energy, because it is an endless energy and cause no environmental pollution like other sources and the possibility to convert it into another forms of energy, the most important applications of solar energy is by using it in Solar panels technology that convert the solar energy into the electrical energy, the most important factors that this technique bases upon is the inclination angel of surface and Azimuth, where shall take this into consideration at different times depending on the position of earth relative to the sun during the months and seasons of the year. Thus, it was founded that it is necessary to study and analysis the components of the solar radiation fallen on the surface for different angles of inclination and Azimuth. This Research includes the analysis and the study of Total monthly values Hourly of solar radiation components direct, diffuse and reflected for the city of Baghdad for the year 2005 falling on the inclined surfaces. when the Tilt angle at 20°, 25°,30°, 35° and 40° at Azimuth angle 45°, 135° and 270°, research's results showed at azimuth 45° that the value of these components starts to increase from the beginning of the year and reaches to the highest degrees in the middle, then it decreased till reaching the end of the year as normal active, the case may be reversed for this values Identified when the azimuth angle 135°, At azimuth 270° we notice the normal active come back again.

المقدمة

الاشعاع الشمسي هو الطاقة الشمسية الساقطة على وحدة المساحة من السطح الافقي، وهي شكل من اشكال الطاقة التي تنبعث على شكل موجات كهرومغناطيسية يتراوح طولها الموجي بين(0.15-4) مايكرون، وان اقصى شدة للاشعاع الشمسي هي عند الطول الموجي (0.47) مايكرون وهي حزمة الطيف المرئي[1].

يتأثر الإشعاع الشمسي أثناء اختراقه الغلاف الجوي بعدة عمليات توهين معقدة تؤدي بالنتيجة إلى التقليل من شدته التي تصل إلى سطح الأرض، وهذه العمليات هي: التشتت والانعكاس والامتصاص، وتحدث عملية التشتت نتيجة وجود جزيئات الهواء والهباء والغبار، أما عملية الامتصاص فتحدث نتيجة وجود الغازات مثل النتروجين والأوكسجين وبخار الماء وثاني أوكسيد الكربون، أما عملية الانعكاس فتحدث بفعل الغيوم وسطح الأرض والملوثات[2].

ويمكن تمييز عدة مركبات للاشعاع الشمسي وهي [3] وهي:

- مركبة الاشعاع الشمسي المباشر: ويعرف بانه الشعاع المنطلق من الشمس والساقط على السطح الذي يعترضه مباشرة من دون حدوث اي تغيير في اتجاهه.
- مركبة الاشعاع الشمسي المنتشر: يمثل الاشعاع الذي يعترض طريقه اجسام تعمل على انتشاره مما يحول دون وصوله مباشرة الى السطح.
- مركبة الاشعاع الشمسي الكلي: يمثل مجموع الاشعاع الشمسي الساقط سواء كان مباشرا او منتشرا.
- مركبة الاشعاع الشمسي المنعكس: وهو الاشعاع الشمسي المنعكس من الاسطح الساقطة عليه.

يعتبر الإشعاع الشمسي احد أهم مصادر الطاقات المتجددة إذ يكون مكملا للطاقات الأخرى، ففي الفترة الأخيرة وبسبب ارتفاع أسعار الوقود الاحفوري فضلا عن الآثار السلبية الناتجة عنه من تلوث وزيادة في تركيز الغازات الدفيئة (الاحتباس الحراري) كذلك نضوب طبقة الأوزون، لذلك كله أصبح البحث عن مصادر جديدة للطاقة هو الشغل الشاغل لدى المهتمين. كذلك فان للإشعاع الشمسي تأثيراته المباشرة على المناخ، ومن

أهم هذه التأثيرات تسخين سطح الأرض (يابسة ومياه)، والغلاف الجوي، وذلك نتيجة لامتصاص جزء من الاشعاع الشمسي مسببا ارتفاع درجة حرارة السطح والذي يؤدي بدوره الى صعود الهواء الساخن الى الاعلى وانتقال الحرارة بطريقة الحمل، اذا كان الهواء محملا ببخار الماء فان درجة حرارته تنخفض كلما ارتفع للاعلى ويتكثف ليكون الغيوم، وأيضا إن الإشعاع الشمسي هو العامل الرئيسي في عملية البناء الضوئي للنباتات، أي إن له دور في إنتاج الأوكسجين للتنفس حيث يدخل في سلسلة من العلميات التي تقوم بها النباتات لانتاج الاوكسجين[4].

الزوايا الشمسية

ان معرفة اتجاه الشمس عند اي نقطة منطح الارض والتي تسمى بالموقع الشمسي ضرورية لاجل تحديد موقع الشمس بالنسبة للارض، وتشمل الزوايا الشمسية[5]:

1Solar Altitude Angle (h). زاوية ارتفاع الشمس

تمثل الارتفاع الزاوي الذي يقاس من افق الراصد الى موقع الشمس في السماء، شكل(1)، وهذه الزاوية مهمة في تحديد كمية الاشعاع الواصل الى سطح الاض، حيث تساوي هذه الزاويه صفر عند شروق الشمس وغروبها، وتساوي 90° عندما تكون الشمس فوق الراصد مباشرة.

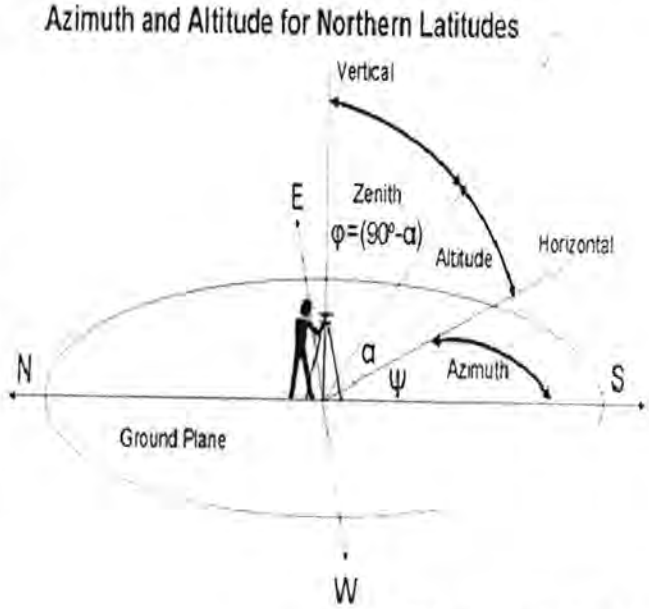

شكل(1) الزوايا الشمسية [6].

2Zenith Angle (z). زاوية سمت الراس

هي الزاوية المحصورة بين سمت الراصد وموقع الشمس، بمعنى اخر هي الزاوية التي يصنعها الشعاع الشمسي مع العمود المقام على السطح الافقي مجموع زاوية السمت وزاوية ارتفاع الشمس ويساوي 90°. اي انة :

$$h + Z = 90^{\circ}$$

3Solar Azimuth Angle (A). زاوية البعد الافقي للشمس

هي الزاوية التي يصنعها مسقط شعاع الشمس على مستوى افق الراصد مقاسة نسبة للشمال وقيمتها تتراوح بين الصفر و180 درجة وتحسب من العلاقة التالية :

$$A = \cos^{-1}\left[\frac{\sin(h)\sin(\varphi)-\sin(\delta)}{\cos(h)\cos(\varphi)}\right]$$

حيث φ خط العرض الجغرافي لموقع الراصد.

4Solar Declination (δ).زاوية ميلان الشمس

هي الزاوية المحصورة بين الشمس وخط الاستواء السماوي,تتغير زاوية ميلان الشمس من قيمة عظمى (23.5+) درجة الى الشمال من خط الاستواء السماوي في 21 حزيران الى قيمة صغرى (23.5-) درجة الى الجنوب من خط الاستواء السماوي 21 كانون الاول ,اما عند الاعتداليين الربيعي 21 اذار والخريفي في 22 ايلول تكون قيمتها صفرا,يوضح الشكل (2) تغير زاوية ميلان الشمس كدالة لتسلسل اليوم في السنة .

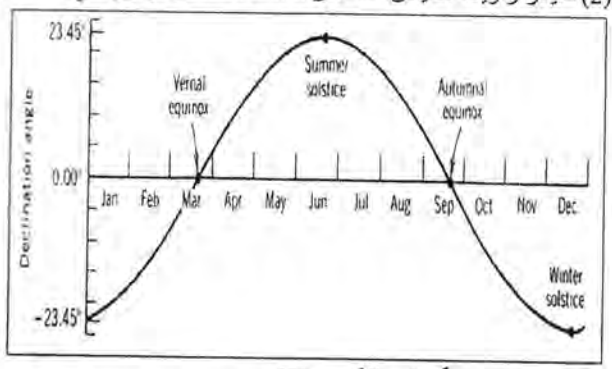

شكل(2) تغير زاوية ميلان الشمس [7].

4Hour Angle (W).الزاوية الساعية

هي القياس الزاوي للوقت وتساوي 15 درجة لكل ساعة,وتقاس بالنسبة الى موقع الشمس وقت الظهر، ويمكن استخراج قيمتها لاية ساعة من ساعات النهار من العلاقة التالية :

$$W = \frac{360}{24}(12 - t)$$

معدل الزمن بالساعات مقاسا من وقت الظهر لذا فالزاوية الساعية تكون موجبة قبل الظهر وt اذ ان سالبة بعده وتكون قيمتها صفرا عند الظهر[8].

البيانات المستخدمة

تم استخدام بيانات الاشعاع الشمسي من الموقع الفرنسي (خدمات الطاقة الشمسية للمتخصصين) Solar energy for professionals(Soda)، والذي يعتمد على اعادة تحليل البيانات من الموقعين (Mihes paris Tech,Transvalor s.a mougins,france).

الجزء العملي

تحليل مركبات الاشعاع الشمسي الساقط على السطوح المائلة

تعتمد قيم الاشعاع الشمسي الواصل الى السطح على زاوية ميل السطح والتي تؤثر على قيم مركبات الاشعاع الشمسي الكلي والمباشر والمنتشر وكذلك المنعكس , حيث ان تغير زاوية ميل السطح احد العوامل الرئيسية المؤثرة على كمية الاشعاع الشمسي ,اي تعتمد قيم هذه المركبات على مقدار هذه الزاوية , ونظرا لاهمية العلاقة بين زاوية ميل السطح ومركبات الاشعاع الشمسي في التطبيقات العلمية والنظرية فقد تم تحليل ودراسة المجموع الشهري للقيم الساعية لمركبات الاشعاع الشمسي عند زوايا ميل سطح مختلفة ولعدة زوايا سمت.

النتائج والمناقشة

مركبة الاشعاع الشمسي الكلي

عندما تكون زاوية السمت (45°)

تسلك قيم مركبة الاشعاع الشمسي الكلي سلوك التوزيع الطبيعي مع بعض التغيرات البسيطة عند (شهر اذار) عند فترةالاعتدال الربيعي، وكانت اعلى قيمة مسجلة في شهر حزيران ($21.3x10^4 Wh/m^2$) عندما تكون زاوية الميل (20°) واقل قسمة ($3.5x10^4 Wh/m^2$) عند زاوية ميل (40°)، كما في الشكل(3).

عندما تكون زاوية السمت (135°)

يبين الشكل (4) ان السلوك الشاذ للقيم يظهر من هذه الحالة، حيث تبدا القيم بالزيادة من الشهر الاول للسنة وتكون اعلى القيم عندما تكون زاوية ميل السطح (40°) واقل القيم عندما تكون زاوية ميل السطح (20°)، وتستمر القيم بالزيادة والتقارب من بعضها الى شهر (اذار) اي عند فترة الاعتدال الربيعي حيث تنقلب الحالة وتصبح القيم الاعلى عند زاوية ميل (20°) والقيم الاقل عند زاوية ميل (40°)، وتكون شبه مستقرة المسار الى ان تصل الى شهر (نيسان) حيث تبدا بالزيادة من جديد لتصل الى اعلى القيم، ثم تنحدر وتستمر الى شهر (ايلول) اي عند فترة الاعتدال الخريفي حيث نلاحظ عودة القيم للتقارب ولحين التطابق مع بعضها، وتعود القيم لحالتها الاولى اي القيم الاعلى عند زاوية ميل (40°) والاقل عند زاوية ميل (20°)، وتستمر القيم بالنزول متقاربة وتبدا بعدها بالتباعد والتوضح عند وصولها لشهر (كانون الاول)، وكانت اعلى قيمة في شهر حزيران ($21.8x10^4 Wh/m^2$) عند زاوية ميل(20°) اما اقل القيم فكانت عند شهر كانون الثاني ($11.4x10^4$ Wh/m^2) ايضا عند نفس زاوية الميل (20°).

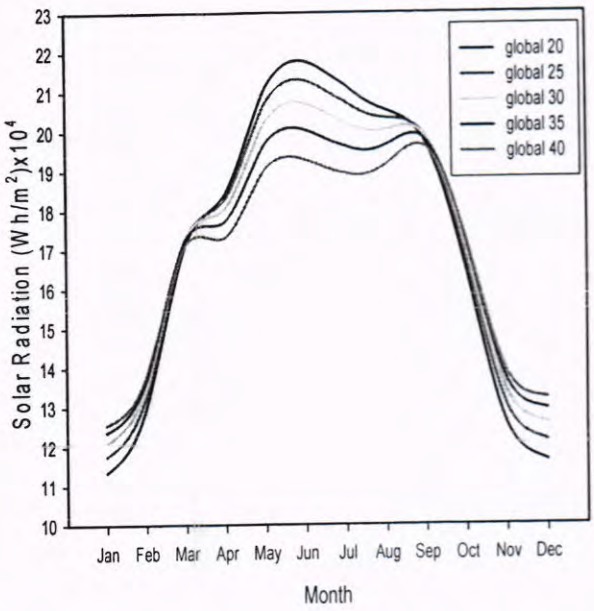

شكل (4) المجموع الشهري للقيم الساعية لمركبة الاشعاع الشمسي الكلي عندما تكون زاوية السمت (135°) .

عندما تكون زاوية السمت (270°)

يبين الشكل (5) عودة التوزيع الطبيعي لقيم مركبة الاشعاع الشمسي الكلي , حيث تبدا القيم بالزيادة طبيعيا من الشهر الاول وتكون متقاربة قليلا لكن واضحة، وبعد فترة الاعتدال الربيعي تتوضح اكثر وتصل الى قمتها في اشهر منتصف السنة ثم تنحدر وتستقر في اشهر نهاية السنة حيث تتقارب القيم من بعضها من جديد , وكانت اعلى القيم عند شهر حزيران ($21.8x10^4 Wh/m^2$) عند زاوية ميل (20°)، واقل القيم ($7.5x10^4 Wh/m^2$) عند زاوية ميل (40°) .

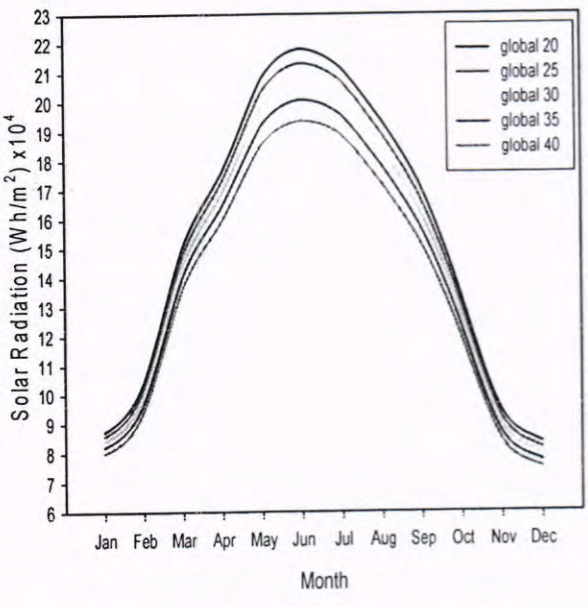

شكل (5) المجموع الشهري للقيم الساعية لمركبة الاشعاع الشمسي الكلي عندما تكون زاوية السمت (270°) .

مركبة الاشعاع الشمسي المباشر

عندما تكون زاوية السمت (45°)

مازالت القيم في هذه الحالة تسلك السلوك الطبيعي ويكون توزيع القيم مشابه للحالة السابقة مع بداية لتعرجات بسيطة عند شهر (اذار)، وكانت اعلى القيم في شهر حزيران ($15.05x10^4 Wh/m^2$) عند زاوية ميل (20°) واقل القيم في شهر كانون الاول ($1.3x10^4 Wh/m^2$) عند زاوية ميل (40°) .

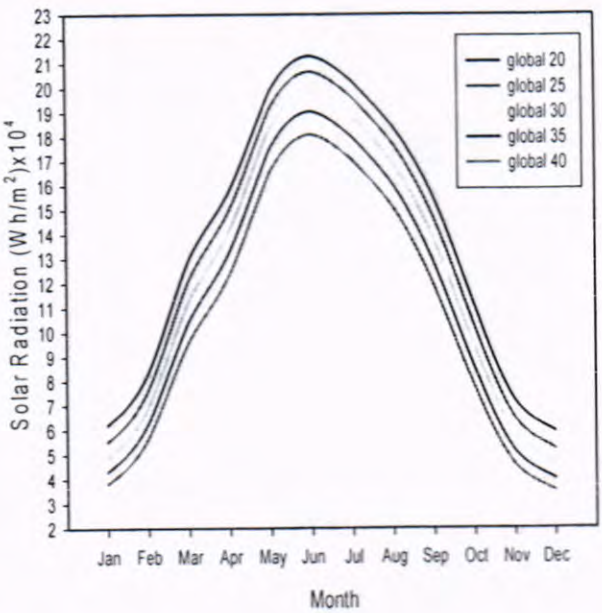

شكل (3) المجموع الشهري للقيم الساعية لمركبة الاشعاع الشمسي الكلي عندما تكون زاوية السمت (45°) .

عندما تكون زاوية السمت (135^o)

يبين الشكل (7) بداية لتغير السلوك الطبيعي وشذوذ سلوك القيم , حيث تبدا القيم بالزيادة الى الاعلى وبتقارب والقيم الاعلى تكون عند زاوية ميلان (40) والقيم الاقل عند زاوية ميل (20)، الى ان تصل القيم الى فترة الاعتدال الربيعي اي عند شهر (اذار) حيث تنقلب الحالة وتصبح القيم الاعلى عند زاوية ميل (20) والاقل عند زاوية ميل (40) وتستمر بالصعود الى الاعلى مع تعرجات في المسار حيث كانت اعلى القيم في اشهر منتصف السنة، ثم تبدا القيم بالتناقص ولحين فترة الاعتدال الخريفي (شهر ايلول) حيث يتغير التوزيع الزمني لهذه القيم وتصبح القيم الاعلى عند زاوية ميل (40) واقل القيم عند زاوية ميل (20) خلال اشهر تشرين الاول وتشرين الثاني، وكانت اعلى القيم في شهر حزيران ($21.8x10^4$ Wh/m^2) عند زاوية ميل سطح 20^o، اما اقل القيم فكانت في شهر كانون الثاني ($11.4x10^4$ Wh/m^2) عند نفس زاوية الميل 20^o.

عندما تكون زاوية السمت (270^o)

يبين الشكل (8) عودة التوزيع الطبيعي لقيم الاشعاع الشمسي المباشر وكما هو واضح في الشكل، حيث كانت اعلى قيمة عند شهر حزيران ($15.5x10^4 Wh/m^2$) واقل قيمة عند شهر كانون الاول ($4.6x10^4 Wh/m^2$) .

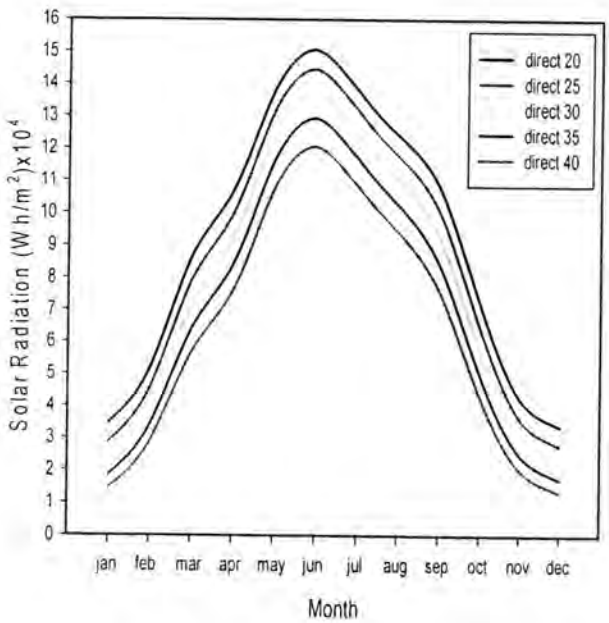

شكل (6) المجموع الشهري للقيم الساعية لمركبة الاشعاع الشمسي المباشر عندما تكون زاوية السمت (45^o) .

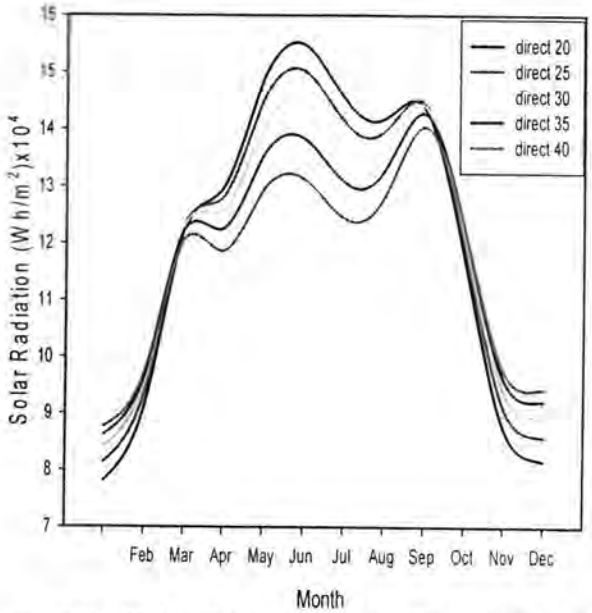

شكل (7) المجموع الشهري للقيم الساعية لمركبة الاشعاع الشمسي المباشر عندما تكون زاوية السمت (135^o)

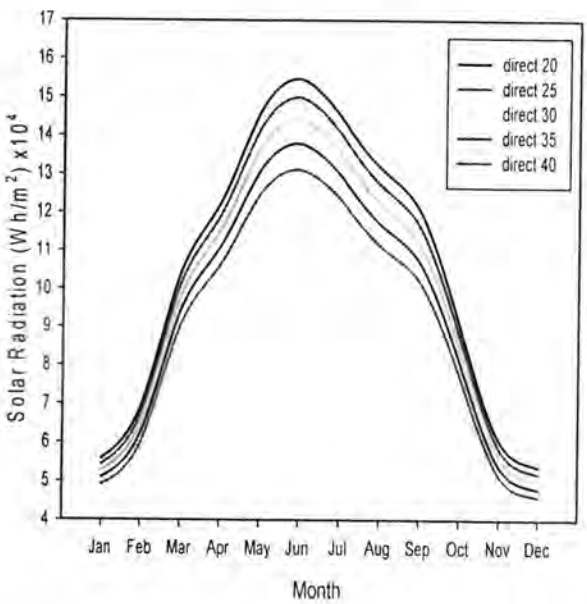

شكل (8) المجموع الشهري للقيم الساعية لمركبة الاشعاع الشمسي المباشر عندما تكون زاوية السمت (270^o)

مركبة الاشعاع الشمسي المنتشر

عندما تكون زاوية السمت (45^o)

مازال السلوك طبيعي وواضح كما في الحالة السابقة، وكانت اعلى القيم في شهر تموز ($6.4x10^4$ Wh/m^2) عندما كانت زاوية الميل (20^o)، واقل القيم ($1.9x10^4 Wh/m^2$) عندما كانت زاوية الميل (40^o)

عندما تكون زاوية السمت (135^o)

يتوضح من الشكل (10) انقيم مركبة الاشعاع الشمسي المباشر تسلك سلوكا شاذا عن الحالات السابقة حيث تكون اقل القيم عند زاوية ميل (20^o) واعلى القيم عند زاوية ميل (40^o)منذ بداية السنة و لحين وصولها الى

فترة الاعتدال الربيعي في شهر اذار، وبعد ذلك يعود سلوك القيم للحالة الاولى حيث تكون القيم الاعلى عند زاوية ميل (20^{o}) والاقل عند زاوية ميل (40^{o}) لحين الاعتدال الخريفي، ومن ثم تسلك القيم السلوك الشاذ مرة اخرى حيث تصبح القيم الاعلى عند زاوية ميل (40^{o}) والاقل عند زاوية ميل (20^{o})، وكانت اعلى القيم عند شهر تموز($6.5x10^{4}Wh/m^{2}$)، واقل القيم عند شهر كانون الاول ($3.4x10^{4}Wh/m^{2}$) عند نفس زاوية الميل (20^{o}).

عندما تكون زاوية السمت (270^{o})

نلاحظ ان في هذه الحالة عودة القيم للسلوك الطبيعي، حيث تبدا القيم بالزيادة من الشهر الاول وحتى اشهر منتصف السنة لاعلى القيم لتبدا بعدها بالانحدار الى الاسفل ، وكانت اعلى القيم في شهر تموز($6.6x10^{4}Wh/m^{2}$) عند زاوية ميل (20^{o})، واقل القيم في شهر كانون الاول ($2.7x10^{4}$ Wh/m^{2}) عند زاوية ميل (40^{o}) كما في الشكل(11) .

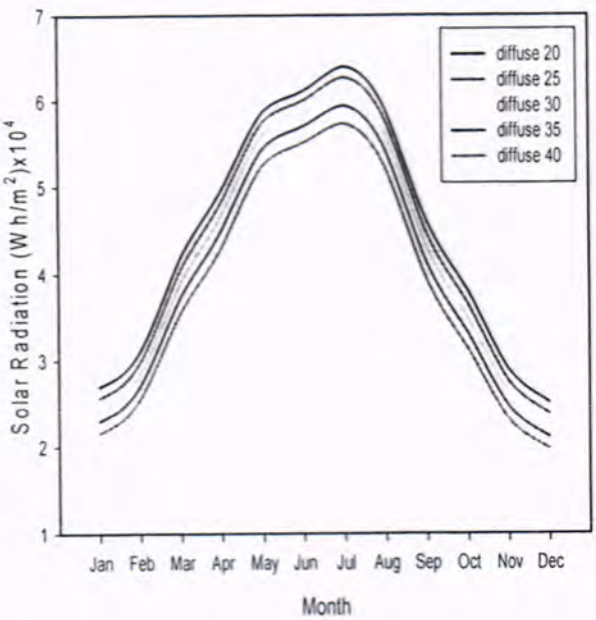

شكل (9) المجموع الشهري للقيم الساعية لمركبة الاشعاع الشمسي المنتشر عندما تكون زاوية السمت (45^{o}) .

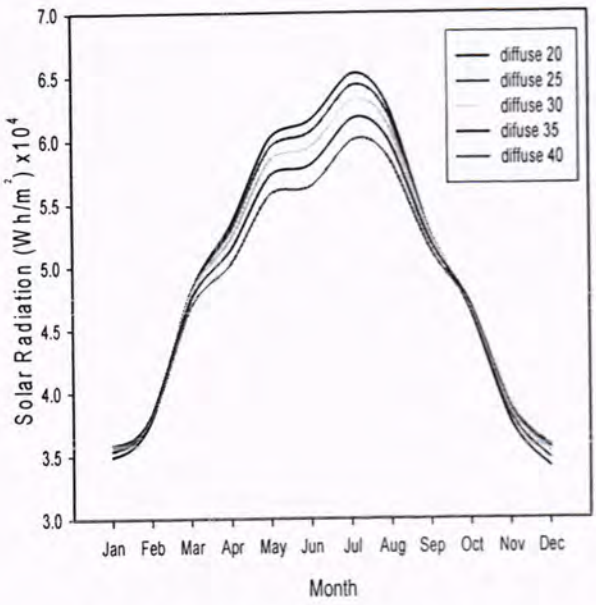

شكل (10) المجموع الشهري للقيم الساعية لمركبة الاشعاع الشمسي المنتشر عندما تكون زاوية السمت (135^{o}) .

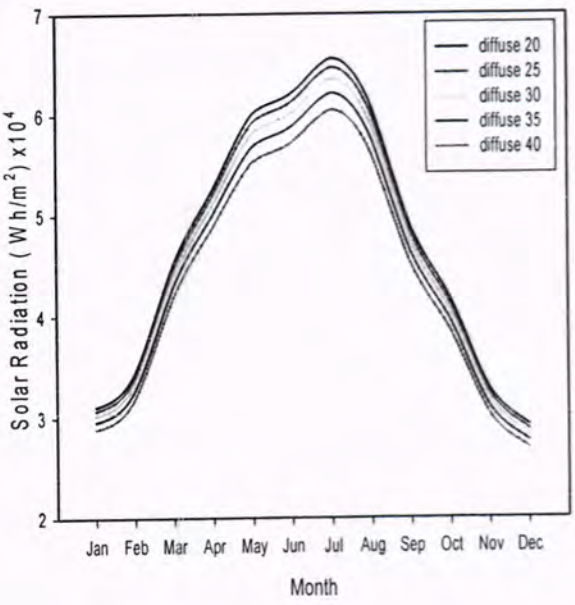

شكل (11) المجموع الشهري للقيم الساعية لمركبة الاشعاع الشمسي المنتشر عندما تكون زاوية السمت (270^{o}) .

مركبة الاشعاع الشمسي المنعكس

في هذه الحالة نلاحظ ان جميع قيم الانعكاس للاشعاع الشمسي المنعكس تكون متماثلة وفي جميع الحالات، اي حتى مع تغيير قيمة زاوية السمت باي اتجاه كان فان القيم تبقى كما هي بدون اي تغيير، وكانت القيم الاعلى عندما تكون زاوية ميل السطح (40^{o}) واقل القيم عند زاوية ميل (20^{o})، اي كلما تزداد زاوية الميل تزداد قيم الاشعاع الشمسي المنعكس معه، وكانت اعلى قيمة عند شهر حزيران ($5.3x10^{3}Wh/m^{2}$)، واقل القيم عند شهر كانون الاول ($0.5x10^{3}Wh/m^{2}$) عند زاوية ميل (20^{o}) كما في الشكل(12) .

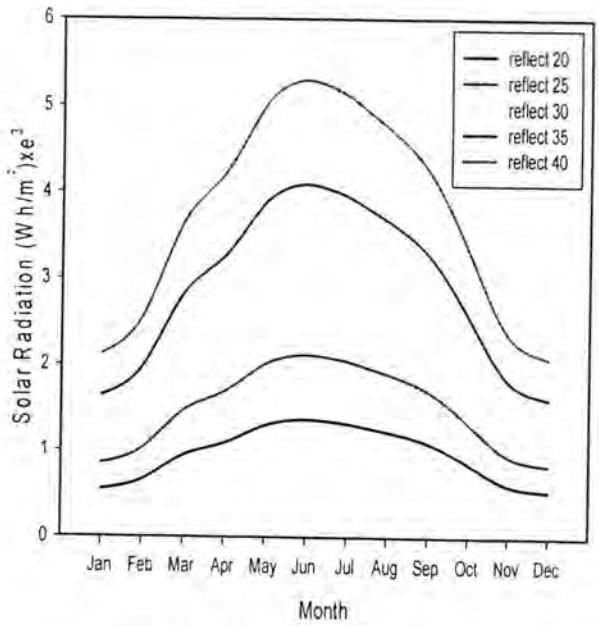

شكل (12) المجموع الشهري للقيم الساعية لمركبة الاشعاع الشمسي المنعكس .

الاستنتاجات

1. عندما تكون قيم زاوية السمت 45، درجة فان قيم مركبات الاشعاع الشمسي (الكلي والمباشر والمنتشر) الساقط على السطوح المائلة تتغير عكسيا مع زاوية ميل السطح اي كلما تزداد قيمة زاوية الميل تقل قيم المركبات ولجميع اشهر السنة بشكل عام .

2. عندما تكون زوايا السمت 135، درجة يكون تاثير زاوية ميل السطح على قيم مركبات الاشعاع الشمسي معكوسا في بداية السنة ولحين الاعتدال الربيعي في شهر اذار وكذلك من الاعتدال الخريفي في شهر ايلول ولحين نهاية السنة حيث تزداد القيم في هذه الحالة مع زيادة زاوية ميل السطح.

3. تعود العلاقة بين قيم مركبات الاشعاع الشمسي وزاوية ميل السطح عندما تكون زاوية السمت 270، علاقةعكسية حيث كلما تزداد زاوية الميلان للسطح تقل قيم المركبات.

المصادر

1. Roger G.Barry ,and Richard,(2003), "Atmosphere, Weather and Clamate",8th edition, J.Chorly Route ledge Tyler and Francies group London and USA.

2. Vardavas, I. M., and Taylor, F. W. , 2007, "Radiation and Climate", International Series of Monographs on Physics, No. 138, Oxford University Press, Oxford, 1–512

3. رسول ، رعد احمد (1986) ، دراسة الاشعاع الشمسي في العراق، رسالة ماجستير (غير منشورة) ، قسم العلوم التطبيقية، الجامعة التكنولوجية، ص13.

4. AL-Salaymeh. A, (2005),"Modeling of Global Daily Solar Radiation on Horizontal Surfaces for Amman City", Emirates Journal for Engineering Research,Vol,No.1,pp 49-56.

5. Vignola.F , Michalsky.J, Stoffel.T,(2012),"Solar and Infrared Radiation Measurment", by Taylor & Francis Group, LLC,pp 14-16.

6.http://www.srrb.noaa.gov/highlight/unrise/azelzen.gif.

7. ppt, cited by http://www.engr.sjsu.edu/mae/faculty/rongere/Solar_2008 Rongére FX. "Solar Energy" San Jose State University.

8. الشاعر ، هديل مجيد عباس،(2009) ، علاقة الاشعاع الشمسي والاشعاع الارضي بدرجات الحرارة في العراق من (1990-2007)، كلية التربية للبنات ، جامعة الكوفة, ص 66-67.

مجلة علوم المستنصرية
المجلد 27، العدد 2، 2016

journal homepage:www.mjs-mu.com

تكرار التطرف في قيم درجات الحرارة للاشهر الانتقالية في العراق

حسين جبر وسمي الشمري
قسم الجغرافية، كلية الاداب، جامعة بغداد

Articleinfo.

تقديم البحث:
2015/11/15
قبول البحث:
2016/1/3

الخلاصة

يظهر تكرار عالي للتطرف في درجة الحرارة يختلف من محطة الى اخرى من محطات الدراسه يتضح من الدراسه ان اعلى تكرار شهري للتطرف في محطة الموصل سجل خلال شهر (ايار - تشرين الاول - تشرين الثاني) ، اما محطة بغداد فان اعلى تكرار شهري للتطرف فوق الدرجه العظمى فقد سجل خلال الاشهر (ايلول -تشرين الاول -تشرين الثاني) ، بالنسبه لمحطه البصره ان اعلى تكرار شهري فوق العظمى قد سجل خلال شهري ايلول وتشرين الاول .

ABSTRACT

During the study Clearer repeat extremism in temperature from station to another station in study repeat extremism in Mosul station its repeat up to maximum during months may ,October and November, station of Baghdad was record up to top repeat overdo to degree maximum during months September, October and November.
So station of Basra overdo recorder was during months September and October.

المقدمة

يتميز مناخ العراق بالتطرف الكبير في درجات الحرارة سيما خلال فصلي الربيع والخريف اذ ان مناخ العراق مناخ قاري بعيد عن المؤثرات البحريه باستثناء البحر المتوسط الذي ينشط المنخفضات الجويه الموثرة على العراق شتاءا في هذه الدراسه سيتم التركيز على تكرار حالات التطرف في دراجات الحرارة للعظمى والصغرى ، زمانيا" تم تحديد الدراسه بالمدة الزمنية (1990 – 2000) ومكانيا تشمل الدراسة العراق بحدوده الجغرافية اذ يقع العراق في الجزء الجنوبي الغربي من قارة أسيا يمثل الجناح الشمالي الشرقي من الوطن العربي، يمتد مابين دائرتي عرض ($^{-}$5. 29°) و($^{-}$22. 37°) شمالاً، وبين خطي طول ($^{-}$45. 48°) و($^{-}$45. 38°) شرقاً وتم تحليل المعدلات اليومية وانحرافاتها عن المعدل الشهري للعظمى والصغرى بعد استخراج المعدلات الشهرية لدرجات الحرارة ولثلاث محطات مناخية (الموصل ، بغداد ، البصرة).

ظهرت دراسات حول موضوع الانخفاض والارتفاع في درجات الحرارة لكنها اهتمت بظاهرة انخفاض او ارتفاع درجات الحرارة دون او فوق الصفر المئوي دون الاخذ بنظر الاعتبار التباين اليومي حول المعدل الشهري، ان معظم الدراسات المناخية التي تناولت مناخ العراق انصب تركيزها حول جميع اشهر السنة فمثلا بعض الدراسات حددت السنة في العراق على انها سنة تقويمية تبدا من الشهر كانون الثاني وتنتهي الى شهر كانون الاول والبعض قام بتحديد المدة الزمنية على اساس السنة المطيرة او البعض يسميها السنة الغيمية واحيانا تسمى السنة المائية وتبدا من تشرين الاول وتستمر لغاية ايار وبهذا لاتوجد دراسة ركزت على الاشهر الانتقالية ، وهناك دراسات تناولت درجات الحرارة يمكن ايجازها باختصار وهي .

دراسة (احلام عبد الجبار، 1991 ، ص174) اشارت الى تاثير الكتل الهوائية القطبية القارية في انخفاض درجة الحرارة في العراق دون الصغرى المنوية واعتبرت هذة الكتل الهوائية المسؤل عن الانخفاض الشديد في درجات الحرارة. **اما دراسة (السامرائي وزملائة ،1995 ، ص 78)** اوجد الباحث ان هنالك موجات برد تؤثر على القطر بشكل عام واخذ مقياس اعتبر ان الانخفاض في درجة الحرارة 5° م دون المعدل العام الشهري وان يستمر لمدة ثلاثة ايام متتالية او اكثر على انة موجة برد.

اختيرت ثلاث محطات مناخية في العراق منتشرة بشكل جيد من الشمال إلى الجنوب وهي (الموصل ، وبغداد، والبصرة)، وجرى اختيار هذه المحطات بهذا الشكل لتمثل الأقاليم المناخية في العراق، كذلك لتغطي معظم أشكال السطح في العراق من المنطقة المتموجة المرتفعة إلى المناطق السهلية المنخفضة ، ينظر الجدول (1) .

جدول (1)الموقع الاحداثي والارتفاع لمحطات الدراسة

المحطة	دائرة العرض	خط الطول	الارتفاع عن مستوى سطح البحر (الأمتار)
الموصل	36° 32	43° 15	223
بغداد	33° 23	44° 23	34
البصرة	30° 57	47° 78	2.4

مشكلة الدراسة

تباين كبير لدرجات الحرارة اليومي خلال الاشهر الانتقالية يفوق التباين خلال فصلي السنة البارد والحار في العراق ويظهر هذا التباين خلال اشهر (اذار نيسان ايار ايلول تشرين الاول تشرين الثاني

فرضية الدراسة

يفترض الباحث ان اعلى تكرار للتباين اليومي في درجة الحرارة يظهر في محطة الموصل ومحطة البصرة وينخفض في محطة بغداد.

الجزء العملي من البحث:

تم تحديد المعدل الشهري لدرجات الحراره (العظمى والصغرى) بالاعتماد على ارشيف سجلات البيانات المناخيه المعتمده في الهيئة العامه للانواء الجويه العراقيه من اجل مقارنه الدرجه اليوميه للعظمى وللصغرى مع المعدل الشهري وتحديد عدد تكرار القيم المتطرفه اعلى من العظمى واقل

من الصغرى ولثلاث محطات (الموصل- بغداد- البصرة) مناخيه ولدورة مناخيه صغرى امدها 11 سنه من سنه (1990-2000).

1_ محطة الموصل

يتضح من الجدول (2) ان اكبر معدل شهري لتباين درجات الحرارة عن معدل العظمى هو خلال الاشهر(ايار – تشرين الاول _ تشرين الثاني) اذا بلغ المعدل اكبر من 16 تكرار في حين اقل الاشهر هي (اذار، نيسان ، ايلول) اذ بلغ المعدل حوالي 15 تكرار والسبب في زيادة المعدل في شهر ايار وتشرين الاول وتشرين الثاني في شهر ايار تكون بداية تاثير منخفض الهند الموسمي على العراق والذي يسبب ارتفاع في درجات الحرارة اما في تشرين الاول وتشرين الثاني بسبب تاثير المرتفع المداري الذي يسيطر على طبقات الجو العليا في العراق وفي هذة الاشهر يكون امتداده على العراق وغير منسحب جنوبا اذ يبداء انحسارة ابتداء من كانون الاول.

الجدول (2) التكرا رالشهري والمجموع السنوي لحالات التطرف في درجات الحرارة فوق العظمى لمحطة الموصل للمدة (1990-2000)

الاشهر السنوات	اذار	نيسان	ايار	ايلول	تشرين الاول	تشرين الثاني	المجموع
1990	15	15	15	15	17	17	93
1991	16	13	16	13	18	16	91
1992	17	14	16	16	17	15	94
1993	8	15	18	15	21	17	93
1994	20	17	13	18	17	13	97
1995	19	14	15	14	17	12	90
1996	16	14	22	15	16	15	97
1997	15	17	19	18	16	20	105
1998	20	15	17	17	15	17	100
1999	16	15	15	14	14	17	90
2000	14	20	17	18	13	17	99
المعدل	15	15	16	15	16	16	1049

اما بالنسبة للمجموع السنوي فان اعلى معدل تباين كان سنة 1997 بلغ مجموع التكرار 105 واقل تكرار خلال سنتين 1995-1999 اذ بلغ المجموع 90 على التوالي.

اما بالنسبة لدرجة الحرارة الصغرى فقد تقارب المعدل الشهري في التباين اذ تراوح التكرار لكل الاشهر مابين 15-16 والسبب في ذلك ان المحطة تقع تحت تاثير الانخفاض عن مستوى سطح البحر وان تكوينات تضاريسية تحيط بها في جميع الجهات الامر الذي يعدل خصائص الكتل الهوائية الموثرة عليها ينظر الى الجدول (3).

جدول (3) التكرار الشهري والمجموع السنوي لحالات التطرف في درجة الحرارة دون الصغرى لمحطة الموصل للمدة (1990-2000)

الاشهر السنة	اذار	نيسان	ايار	ايلول	تشرين الاول	تشرين الثاني	المجموع
1990	14	17	12	13	13	16	84
1991	17	18	15	15	15	17	96
1992	15	20	18	15	18	14	99
1993	7	15	17	14	17	15	84
1994	18	17	19	19	17	12	102
1995	17	15	14	14	24	15	99
1996	16	17	17	17	18	19	103
1997	15	15	17	16	16	16	94
1998	20	15	19	13	14	16	96
1999	15	16	15	14	16	15	90
2000	16	17	12	15	16	17	93
المعدل	15	15	15	15	16	15	1040

اما بالنسبة للمجموع السنوي اذ بلغ اعلى مجموع سنوي لعدد الحالات سجل سنة 1996 اذ بلغ 103 حالة بعدها سنة 1994 102 حالة و 1995 بلغ 99 حالة على التوالي اما السنوات الاخرى فقد تراوحت مابين 84 حالة كاقل مجموع سنوي مسجل سنة 1990.

2- محطة بغداد

يتضح من جدول (4) ان اكبر معدل شهري لتباين درجة الحرارة عن معدل العظمى هو خلال تشرين الثاني اذ بلغ معدل التباين 16 اما اقل قيمة سجلت خلال شهر نيسان اذ بلغ 13 اما الاشهر الاخرى فقد استمرت بالارتفاع خلال الاشهر ايلول وتشرين الاول ولم تنخفض عن 16 كمعدل للحالات في حين الاشهر الاخرى اذار ايار كان معدل التباين هو 13 على التوالي.

جدول (4) التكرار الشهري والمجموع السنوي لحالات التطرف في درجة الحرارة فوق العظمى لمحطة بغداد للمدة (1990-2000)

السنوات\الاشهر	اذار	نيسان	ايار	ايلول	تشرين الاول	تشرين الثاني	المجموع
1990	13	16	18	17	16	17	96
1991				13	18	13	43
1992	15	16	14	16	18	19	97
1993	11	12	17	15	22	20	36
1994	15	15	14	19	17	14	93
1995	19	15	15	17	13	18	99
1996	19	13	15	15	15	14	90
1997	19	16	17	20	13	15	99
1998	15	13	14	14	15	17	87
1999	12	15	15	11	14	20	87
2000	13	17	14	20	14	16	93
المعدل	13	13	13	16	16	16	920

يتضح من هذا الكلام ان هناك رتابة خلال الاشهر اذار ونيسان وايار وارتفاع في عدد حالات التباين خلال ايلول وتشرين الاول وتشرين الثاني والسبب في ذلك تاثير خصائص الصيف على اشهر الخريف والمقصود هنا بخصائص الصيف المنظومات الضغطية التي تفرض خصائصها على العراق مثل المرتفع المداري ومنخفض الهند الموسمي.

اما بالنسبة للمجموع السنوي اعلى قيمة سجلت كانت سنة 1995 اذ بلغ المجموع السنوي لعدد حالات التباين لدرجة الحرارة العظمى 99 حالة اما اقل قيمة سنوية سجلت كانت سنة 1991 اذ بلغ 43 حالة اما السنوات الاخرى فقد تراوحت مابين 87 حالة سنة 1998 واستمرت سنة 1999 على نفس الوتيرة اما بقية السنوات فقد سجلت مابين 90 حالة سنة 1996 ومابين 97 حالة سنة 1992 نستنتج مما سبق ان هناك تباين في عدد حالات التباين عن معدل العظمى السنوي وقد يكون هناك اسباب تتعلق بعدد مرات تكرار المنظومات الضغطية المختلفة على العراق والتي تفرض الخصائص الحرارية على المنطقة.

اما بالنسبة للصغرى فيتضح من الجدول (5) ان اعلى معدل شهري لعدد حالات التباين عن معدل الصغرى كان خلال الاشهر (اذار ،ايلول، تشرين الاول ،تشرين الثاني) اذ بلغ عدد الحالات 15 حالة كمعدل شهري اما الاشهر الاخرى فقد سجلت 14 حالة خلال شهري نيسان وايار ايضا السبب في ذلك يعود الى تاثير المنظومات الضغطية المسيطرة على العراق.

اما بالنسبة للمجموعة السنوي حيث يختلف بين سنة واخرى فاعلى مجموع سنوي لعدد الحالات سجل سنة 2000 اذ بلغ 114 حالة جاءت بعدها سنة1990 سجلت 103 حالة وكذلك سنة 1998 سجلت 102 حالة اما السنوات الاخرى فقد تراوحت مابين 48 حالة كاقل مجموع سنوي مسجل سنة 1991 ومابين 97 المسجلة خلال 1994 ايضا السبب في هذا التباين الكبير في حالات الانحراف عن معدل الصغرى يعود الى نوع الكتل الهوائية خلال هذة السنوات ونوع المنظومات الضغطية التي سيطرت على محطة الدراسة.

جدول (5) التكرار الشهري والمجموع السنوي لحالات التطرف في درجة الحرارة دون الصغرى لمحطة بغداد للمدة (1990-2000)

الاشهر / السنوات	اذار	نيسان	ايار	ايلول	تشرين الاول	تشرين الثاني	المجموع
1990	15	20	17	20	19	13	103
1991				14	17	18	48
1992	18	16	17	16	15	13	94
1993	7	14	16	15	15	11	78
1994	17	14	15	15	25	12	97
1995	17	15	13	15	18	11	88
1996	16	17	16	8	7	19	82
1997	15	11	15	14	11	16	81
1998	21	16	16	18	13	19	102
1999	16	16	16	15	17	16	96
2000	14	16	19	18	13	19	114
المعدل	15	14	14	15	15	15	983

3-محطة البصرة

يتضح من جدول (6) ان اكبر معدل شهري لتباين درجة الحرارة عن معدل العظمى هو خلال شهر ايلول اذ بلغ معدل التباين 16 اما اقل قيمة سجلت هي خلال شهر تشرين الثاني، اذ بلغت 15 اما الاشهر الاخرى فقد استمرت بالارتفاع خلال شهري اذار وتشرين الاول ولم تنخفض عن 16 كمعدل للحالات في حين الاشهر الاخرى اذار ، تشرين الاول وكان معدل التباين 15 ، 16 على التوالي، يتضح مماسبق ان هناك تباين واضح والسبب في ذلك يعود الى تاثير المسطح المائي الخليج العربي حيث يقوم بتزيد الكتل الهوائية بالرطوبة .

جدول (6) التكرار الشهري والمجموع السنوي لحالات التطرف في درجة الحرارة فوق العظمى لمحطة البصرة للمدة (1990-2000)

الاشهر / السنوات	اذار	نيسان	ايار	ايلول	تشرين الاول	تشرين الثاني	المجموع
1990	18	16	16	16	19	13	97
1991	13	12	14	15	17	14	84
1992	16	15	15	22	17	17	119
1993	11	12	12	17	21	21	93
1994	17	16	14	19	18	12	96
1995	16	17	17	21	12	18	100
1996	14	14	13	15	13	14	82
1997	19	18	19	18	18	14	105
1998	16	16	13	13	15	11	48
1999	19	15	16	13	13	17	93
2000	14	18	19	18	18	14	99
المعدل	15	15	15	16	16	15	1016

اما بالنسبة للمجموع السنوي فان اعلى معدل لتباين كان سنة 1997 اذ بلغ مجموع التكرار 105 اما اقل تكرار خلال سنة 1998 اذ بلغ 48 حالة اما السنوات الاخرى فقد تراوحت 100 حالة سنة 1995 ومابين 93 حالة سنة 1999 .اما بالنسبة لحالات التطرف في الدرجة الصغرى يتضح من الجدول (7) ان اعلى معدل شهري لعدد حالات التباين عن معدل الصغرى كان خلال شهر تشرين الاول اذ بلغ 16 وتقارب المعدل خلال شهري نيسان وايار 15 على التوالي. اما بالنسبة للمجموع السنوي اذ بلغ اعلى معدل التباين 468 حالة لسنة 2000 اقل تكرار كان سنة 1995 اذ بلغ 72.

جدول (7) التكرار الشهري والمجموع السنوي لحالات التطرف في درجة الحرارة دون الصغرى لمحطة البصرة للمدة (1990-2000)

الاشهر / السنوات	اذار	نيسان	ايار	ايلول	تشرين الاول	تشرين الثاني	المجموع
1990	15	15	14	14	15	15	87
1991	16	16	18	16	17	17	99
1992	14	14	21	10	17	12	87
1993	8	17	16	14	17	16	87
1994	14	18	18	17	17	14	97
1995	13	12	3	11	19	14	72
1996	19	14	13	4	8	7	64
1997	16	11	13	16	13	17	85
1998	15	15	13	13	20	19	94
1999	16	17	17	14	14	16	93
2000	17	16	10	14	19	13	89
المعدل	12	15	15	13	16	14	954

الاستنتاجات:

1- يتضح من الدراسه ان اعلى تكرار شهري للتطرف في قيم الدرجه العظمى سجل خلال شهر (ايار - تشرين الاول - تشرين الثاني) وان اعلى مجموع سنوي سجل خلال السنوات 1997 و1998 على محطة الموصل اما بالنسبه لتكرار القيم اقل من الصغرى فقد سجل خلال شهر تشرين الاول وان اعلى مجموع سنوي للتكرار فقد سجل سنه 1996

2- بالنسبه لمحطة بغداد ان اعلى تكرار شهري للتطرف فوق الدرجه العظمى فقد سجل خلال الاشهر (ايلول -تشرين الاول -تشرين الثاني) وان اعلى مجموع سنوي فقد سجل خلال السنه 1997

اما بالنسبه للصغرى فقد سجل اعلى تكرار للتطرف خلال الاشهر (اذار- ايلول-تشرين الاول -تشرين الثاني) وان اعلى مجموع سنوي سجل سنه 2000

3-بالنسبه لمحطه البصره ان اعلى تكرار شهري فوق العظمى قد سجل خلال شهري ايلول وتشرين الاول وان اعلى مجموع سنوي قد سجل سنه 1992

بالنسبه للدرجه الصغرى فقد سجل اعلى تكرار شهري خلال شهر تشرين الاول وان اعلى مجموع سنوي سجل سنه 1991

المصادر

1- غالم ، علي احمد ، الخفرافية المناخية ، الطبقة الاولى ،دار الميسرة للنشر والتوزيع والطباعة ، عمان ، 2007 ، ص 183

2- كاظم ، احلام عبد الجبار ، الكتل الهوائية ، تصنيفها ، خصائصها دراسة تطبيقية على مناخ العراق ، اطروحة كتوراة ، غير منشورة كلية الادب ، جامعة بغداد ،1991 ،ص 174

3- السامرائي ، قصي واحلام عبدالجبار وهدى علي صالح ، موجات البرد في العراق ،دراسة تطبيقية على مناخ العراق ،مجلة الجمعة الجفرافية العراقية ، العدد 29 ، 1995 ،ص 78

4- الهيئة العامة للانواء العراقية ، قسم المناخ ، بيانات درجات الحرارة للمدة (1971- 2000)

5- الشمري ، حسين جبر ، تكرار ظاهرة الصقيع وطول مدة بقائة على العراق ، العدد 91 ، 2009 ، (ص 178 – 198)

6- الهيئة العامة للانواء الجوية العراقية، اطلس مناخ العراق، (1961-1990) بغداد – العراق، ص (5)

7- الهيئة العامة للانواء الجوية العراقية ، قسم المناخ ،تحليل بيانات يومية ، غير منشورة